PREDICTIVE MODELLING AND CHARACTERIZATION OF LAND SUBSIDENCE DUE TO GROUNDWATER AND PETROLEUM EXTRACTION IN AND AROUND MEHSANA, GUJARAT

A thesis submitted to the
University of Petroleum and Energy Studies

For the Award of
Doctor of Philosophy
in
Geo-Informatics Engineering

BY
Ashish Aggarwal

December 2020

SUPERVISOR(s)

Dr. Pankaj Kumar Srivastava
Dr. Dharmendra Kumar Gupta
Dr. R.S Chatterjee

UPES
UNIVERSITY WITH A PURPOSE

Department of Petroleum Engineering and Earth Sciences
School of Engineering
University of Petroleum & Energy Studies
Dehradun-248007:Uttarakhand

PREDICTIVE MODELLING AND CHARACTERIZATION OF LAND SUBSIDENCE DUE TO GROUNDWATER AND PETROLEUM EXTRACTION IN AND AROUND MEHSANA, GUJARAT

A thesis submitted to the
University of Petroleum and Energy Studies

For the Award of
Doctor of Philosophy
in
Geo-Informatics Engineering

BY
Ashish Aggarwal
(SAP ID: 500032953)

December 2020

Supervisor
Dr. Pankaj Kumar Srivastava
Professor, Department of Petroleum Engineering and Earth Sciences,
University of Petroleum & Energy Studies, Dehradun, India.

Co-Supervisor
Dr. Dharmendra Kumar Gupta
Professor, Department of Health, Safety, Environment & Civil Engineering,
University of Petroleum & Energy Studies, Dehradun, India.

External Supervisor
Dr. R.S Chatterjee
Scientist-G & Head, Geosciences Department,
Indian Institute of Remote Sensing, Dehradun, India.

UPES
UNIVERSITY WITH A PURPOSE

Department of Petroleum Engineering and Earth Sciences
School of Engineering
University of Petroleum & Energy Studies
Dehradun-248007:Uttarakhand

July 2021

DECLARATION

I hereby declare that the thesis entitled **"PREDICTIVE MODELLING AND CHARACTERIZATION OF LAND SUBSIDENCE DUE TO GROUNDWATER AND PETROLEUM EXTRACTION IN AND AROUND MEHSANA, GUJARAT"** has been prepared by me under the guidance of Dr. Pankaj Kumar Srivastava, Professor of Dept. of Petroleum Engineering and Earth Sciences, UPES, Dr. Dharmendra Kumar Gupta, Professor, Department of HSE & Civil Engineering, UPES and Dr. R.S Chatterjee, Scientist G & Head, Geosciences Department, IIRS. No part of this thesis has formed the basis for the award of any degree or fellowship previously.

(Ashish Aggarwal)

Department of Petroleum Engineering and Earth Sciences

University of Petroleum & Energy Studies

Energy Acres Building, Bidholi,

Dehradun-248007

Uttarakhand, India

Date:

THESIS COMPLETION CERTIFICATE

This is to certify that the thesis titled **"PREDICTIVE MODELLING AND CHARACTERIZATION OF LAND SUBSIDENCE DUE TO GROUNDWATER AND PETROLEUM EXTRACTION IN AND AROUND MEHSANA, GUJARAT"** submitted by **ASHISH AGGARWAL (SAP ID: 500032953)** in fulfilment of the requirements for the award of the degree of Doctor of Philosophy is an original work carried out by him under our joint supervision and guidance.

It is certified that the work has not been submitted anywhere else for the award of any diploma or degree of this or any other University.

<table>
<tr><td>(Thesis Supervisor)</td><td>(Thesis Co-Supervisor)</td></tr>
<tr><td>

Dr. Pankaj Kumar Srivastava
Professor
Department of Petroleum Engg.
& Earth Sciences,
UPES, Dehradun-248007, India.
Email: pksrivastava@ddn.upes.ac.in

</td><td>

Dr. Dharmendra Kumar Gupta
Professor
Department of HSE & Civil Engg.,
UPES, Dehradun-248007, India.
Email: dkgupta@ddn.upes.ac.in

</td></tr>
</table>

THESIS COMPLETION CERTIFICATE

This is to certify that the thesis titled **"PREDICTIVE MODELLING AND CHARACTERIZATION OF LAND SUBSIDENCE DUE TO GROUNDWATER AND PETROLEUM EXTRACTION IN AND AROUND MEHSANA, GUJARAT"** submitted by **ASHISH AGGARWAL (SAP ID: 500032953)** in fulfilment of the requirements for the award of the degree of Doctor of Philosophy is an original work carried out by him under my external supervision and guidance.

It is certified that the work has not been submitted anywhere else for the award of any diploma or degree of this or any other University.

(Thesis External Supervisor)

R.S.Chatterjee

Dr. R. S Chatterjee
Scientist 'G' & Head
Geosciences Department,
Indian Institute of Remote Sensing (IIRS),
4 Kalidas Road, Dehradun-28001,
Uttarakhand, India.
Email: rschatterjee@iirs.gov.in

A THESIS

DEDICATED TO MY PARENTS

ABSTRACT

Land subsidence due to fluid withdrawal has been recognized as a serious geohazard worldwide owing to its disastrous socio-environmental implications. The Kutch-Sabarmati basin that hosts the city of Mehsana is facing serious decline in groundwater levels. Water in this region is being extracted from the deeper confined aquifers leading to aquifer compaction and land subsidence. The current groundwater scenario in the area calls for a critical review and investigation into the situation of the groundwater levels and develop remedial strategies to tackle the groundwater and land subsidence challenges. The present study is an attempt to investigate the relationships between groundwater extraction and land subsidence in the region through different modelling techniques. Aquifer modelling, geostatistical and differential interferometric techniques were utilized to examine the spatial and temporal patterns of groundwater resources in Kutch-Sabarmati basin and characterize the land subsidence phenomena because of groundwater abstraction and petroleum extraction in Mehsana and the surrounding oil fields. Aquifer modelling results which were based on ground recorded piezometric levels and the observed lithological and hydrogeological data were used to correlate and validate the space borne DInSAR derived deformation rates.

To gain a spatio-temporal understanding of groundwater level trends at a regional/ basin scale, statistical analysis of seasonal groundwater levels in piezometric wells was carried out using the non-parametric Mann-Kendall (MK) method and Sen's slope estimation from 2005 to 2017 at various locations in Kutch-Sabarmati basin. The groundwater trends were correlated with the rainfall trends to analyze their relationship with climatic changes. Identification and mapping of regional hotspots of groundwater recharge and depletion were also carried out using the Kalman Filter geostatistical approach. The results suggested that the Kutch and Saurashtra basin of the composite Kutch-Sabarmati basin are facing pronounced declining groundwater levels, while the depletion levels have improved on the west towards the Sabarmati basin. The results also suggest that increased agricultural practices have resulted into falling groundwater levels that leads to land subsidence.

To quantify and estimate land subsidence at local scale, modelling of aquifer system compaction was undertaken. The elastic aquifer

compaction and inelastic compaction of confining layers were computed independently for selected piezometric wells using one-dimension consolidation equations. The results indicated that there had been a gradual increase in total aquifer compaction from the period 2005-2011 to 2012-2017. The average rate of aquifer compaction during 2005-2017 ranged from 0.22 to 1.71 cm/ yr. in Mehsana-V and Mewad wells of Mehsana taluk, while the rates were still higher Modhera-II and Karalli-II wells of Visnagar and Unjha taluks. The higher compaction rates especially in Modhera-II was because of large variations in piezometric heads recorded in the observation well.

DInSAR technique that is capable of detecting and quantifying the ground displacements with high precision was employed for estimating local land subsidence in Mehsana and the surrounding oil fields. ALOS PALSAR-1 and ALOS PALSAR-2 InSAR data was utilized to study the deformation patterns in the area. The DInSAR observations also reveal land subsidence in the area that have been gradually increasing over the years. The mean land subsidence rate was 2.49 cm/yr. from 2007 to 2011 which increased to 2.78 cm/yr. during 2015-2018. RADARSAT-2 images of 2017-2018 were also processed to compare the deformation patterns obtained from ALOS PALSAR 1/2 images and both substantiated that deformation fringes have developed over the Mehsana city particularly in the vicinity of Mehsana airstrip.

The investigations from the regional patterns of the observed groundwater variability and comparable subsidence rates obtained from local scale predictive modelling of aquifer compaction and DInSAR modelling provide a good picture of the groundwater extraction and land subsidence scenario in the study area. The extended extractions of groundwater to support irrigation practices mainly controlled the differential patterns of elastic and inelastic compaction and the resulting land subsidence in the regional aquifers. The identification of the zones of excessive groundwater pumping and incumbent subsidence can thus be readily used to predict future land subsidence scenarios, mitigate the socio-economic losses occurring due to land subsidence, manage ground water resource allocation programs and support future infrastructural development plans.   .

Keywords: Land Subsidence, Groundwater, Mann Kendall, Kalman Filter, Aquifer Compaction, DInSAR.

ACKNOWLEDGEMENTS

TABLE OF CONTENTS

LIST OF FIGURES

LIST OF TABLES

CHAPTER 1.   INTRODUCTION

1.1 Background

Land subsidence is a natural hazard that causes gradual settling or sudden sinking of the Earth's surface due to the subsurface movement of earth materials (Galloway et al., 1999). It is essentially a vertical downward movement of the land surface with little or no horizontal movement and results in loss of surface elevation compared to the surrounding areas. Every year, the phenomenon influences many areas globally causing huge economic, social and environmental losses. It has become a major problem worldwide threatening the viability, sustenance and economic development for millions of people, with total losses amounting to many billions of dollars every year, including the loss of human lives and several menacing environmental damages.

Subsidence occurs because of certain mechanical and chemical processes acting on the surface or subsurface, with its magnitude depending upon the type of the process involved and the geologic environment of the area. The fundamental causes of land subsidence could be both natural as well as anthropogenic. While natural causes are slow and gradual processes, and include factors such as tectonic movements causing earthquakes, glacial movements, volcanic activities, landslides; soil compaction, drainage of sub surface soils, hydro compaction of naturally occurring sediments, natural sinkholes and thawing permafrost; the anthropogenic causes are rapid and are linked to factors like over exploitation of groundwater, vibrations on the land surface, sub surface mining and excavations, extraction of geothermal fluids, oil and gas withdrawals etc, they affect the holding capacities of aquifers and reservoirs, and result in system compactions leading to land subsidence (Whittaker, 1989, Leake, 2004, Galloway et al., 2011). The risk impact of land subsidence varies over different time periods and can produce surface deformations ranging from few millimetres to several meters extending from local to regional levels.

Both natural or human induced subsidence has a number of implications on human societies. Natural subsidence caused by tectonic movements and isostatic adjustments are the geological hazards such as earthquakes, faulting, folding and landslides which cause serious impacts on life, economy and environment and have been a matter of study for many decades now. Other natural causes of land subsidence like soil compaction, permafrost and sinkholes are gradual processes and do not pose imminent danger to the societies. However human induced land subsidence due to extraction of groundwater, oil and gas or mining activities have caught attention of the scientists and public owing to its quick repercussions. Land subsidence due to fluid withdrawal has been reported worldwide in countries like United States, Italy, Iran, China, India, Mexico, Indonesia, Thailand and many others. The impact of large-scale withdrawal of subsurface fluids namely water, gas or oil, pose a much severe socio-environmental hazard if the resulting subsidence occurs in locations of human inhabitation or industrial establishments where it leads to extensive damages including sinking of ground surface, reduction in the yield capacity of the reservoirs, development of cracks in buildings and infrastructure, damage to the underground water, power and sewer pipelines, increased probability of floods, water logging and others (Huang et al., 2012). Land subsidence in coastal areas which support many mega cities globally may face problems of sea level rise, tidal inundations, sea water intrusions into the agriculture land apart from loss of human lives and infrastructure as was seen in Houston-Galveston area in U.S where the combined effect of land subsidence and global sea level rise and land subsidence had made the coastal areas more vulnerable to flooding. Such human induced land subsidence is especially a growing problem in the developing world where growing cities and increasing population has resulted in overdemand and uncontrolled extraction of water and hydrocarbons without strict pumping regulations and enforcement.

Subsurface fluid withdrawal due to human activities generally takes place in three forms namely withdrawal of groundwater, withdrawal of oil and gas and associated water, and the withdrawal of subsurface hot water or steam. The sub surface fluid withdrawals where the rate of extraction is more than the rate of its replenishment have caused noticeable land subsidence in

various parts of the world. Land subsidence due to groundwater exploitation was observed in San Joaquin valley in California (Poland and Lofgren, 1984), where a maximum cumulative subsidence of 9 m was recorded in shallow aquifers during the period 1930-1975. An average subsidence rate of 9 cm/yr. was observed in Mexico City between 1965 to 1985 due to over extraction of groundwater around the urban centres (Figueroa-Vega, 1977). Oil and gas withdrawal induced land subsidence had been observed at Wilmington Long beach California during 1926-1968 (Poland and Davis, 1969, Mayuga and Allen., 1969) and Ekofisk, North sea (Zaman et al., 1995, Hermansen et al., 2000) where maximum subsidence of 9 m and 6m respectively were reported from deep reservoirs ranging in depths of 1000 to 3000 m. Land subsidence in the range of 9 to 14.5 meters was reported in Wairakei, New Zealand (Allis et al, 2009) during 1952 to 2009, where geothermal fluids were extracted from depths of 250-800 m.

Principally, the mechanism of land subsidence due to withdrawal of subsurface fluids whether it is water or natural oil and gas or geothermal fluids follow the basic relations between head, stress, fluid pressure and compressibility (Galloway, 2016). Withdrawal of the fluids from a hydrocarbon reservoir or an aquifer reduces the pore pressure and results in the increase in effective stress, leading to compaction of rocks or aquifer material. To balance the overburden pressure, the overlying formations and the land starts subsiding. The process of subsidence is very slow and starts from the beds lying immediately over the reservoir or aquifer from which the fluids are extracted. At this point of time, the land surface or the top layers do not show any signs of subsidence. Gradually the deformations extend their effect upwards and may even take years to show as surface expressions of subsidence (Khilyuk et al., 2000).

Most of the historical cases of land subsidence due to groundwater withdrawal have been reported in semi confined to confined aquifers made up of highly permeable and less compressible water bearing horizons of sand and gravel, with confining interbeds of clay having high compressibility and low vertical hydraulic conductivities. The withdrawal of

groundwater led to a decline in the hydraulic head inducing more effective stress on the coarse-grained aquifers, and the increase in pore pressure in the fine-grained confining beds led them to compact, thereby inducing land subsidence in the area. Because the confining units are highly compressible in comparison to the water bearing clastic and gravel sediments, the thickness and number of these confining units control the extent to which they can sustain the increased stress due to water extraction determines the net susceptibility of aquifer to compaction (Poland and Davis, 1969). In contrast to groundwater aquifers, hydrocarbon reservoirs are seated much deeper in the earth's subsurface. The land subsidence histories due to oil and gas extractions have been related to significant increase in the fluid pressures causing a decrease in the porosity and considerable increase of effective intergranular stress on the fluid bearing formations. In deeper reservoirs, the increased stress gets transferred from the fluid to the adjacent rock formations which start compacting and bending due to subsidence and result in compression, extension, and shear, which lead to fracturing of rocks and rock collapse. Deformations occur mostly on the vicinity of the subsiding basin and damage the wellbores and sometimes induce minor earthquakes. The net subsidence is dependent on the thickness, volume, porosity and the reservoir/aquifer compressibility. The amount and spread of surface subsidence depend on compressibility of unconsolidated or semi-consolidated rocks, confinement of the reservoir, presence of interbedded less permeable clays (in case of aquifers) or shales (in reservoirs) and porosity (Khilyuk et al., 2000).

While, land settlement above a hydrocarbon field is usually less than the reservoir compaction due to the larger depths of petroleum reservoirs, and spreads over a larger area than the reservoir horizontal compaction; the subsidence is much more widespread and shows up at a regional level in case of aquifers systems that are usually shallower than the hydrocarbon reservoirs (Gambolati et al., 1986). Another major distinction between aquifer system compaction and reservoir compaction is that in most of the aquifer systems that experience land subsidence the overdraft of groundwater is lot more than the rate of its recharge. However, in case of most hydrocarbon reservoirs, as the

production continues there is a significant drop in reservoir pressure due to withdrawal of hydrocarbons which gradually reduces the outward flow of hydrocarbons and reduces the rate of production. To maintain the reduced pressure in the reservoir and increase the flow of oil towards producing wells, the wells are injected with water through injection wells as part of secondary recovery. The process increases the oil production levels but also enhances the vulnerability of reservoir rock to compaction and collapse.

1.2 History and Techniques

The first evidence of land subsidence due to extraction of oil and gas was witnessed in in the Goose Creek Oil field near Houston, Texas (Pratt and Johnson,1926), where the researchers observed that the land subsided by around 1 m during the period of 1918 to 1926. They suggested that accelerated exploitation rate of hydrocarbons and associated water from shallow unconsolidated reservoirs in the area has caused lowering of the land surface which can cause minor earthquakes and activate faults in the periphery of the producing fields. A larger magnitude of land subsidence was later noticed in the Wilmington Field in Long Beach, California (Poland and Davis, 1969), where large volume extraction of hydrocarbons at depths of 600 to 1200 m caused compaction of sand and unconsolidated sediments resulting in land subsidence of around 9m during the period between 1926 and 1968. Another important area in United States that is a host to land subsidence due to subsurface fluid withdrawals is the Houston-Galveston region that hosts more than 110 oil and gas fields covering an area of more than 12,000 square kms. The land in the region had subsided almost 3 m because of extraction of groundwater for commercial uses from shallow aquifers (Gabrysch, 1984), as well as due to oil and gas withdrawal from deeper reservoirs (White et al., 1985). The infrastructure located near the subsidence bowl incurred huge losses with damage to houses, roads and pipelines. The combined effect of global sea level rise and land subsidence in the region has made the coastal areas more vulnerable to flooding. Subsidence caused by oil and gas extraction was mostly local and restricted to the areas around the production fields, while the major contribution to regional scale subsidence was attributed to the over exploitation

5

of groundwater (Coplin and Galloway, 1999). The decline in ground water levels was later halted when the Harris-Galveston Coastal Subsidence District passed an order to the industry in 1976, to switch from ground water use to supplies from the local surface water reservoirs. The subsidence phenomenon was also localized in the Gulf coast region (White and Morton, 1997), where the subsidence patterns coincided with the fault planes. The decline in pore pressure due to the extraction of oil and formation water led to an increase of stress near the faults and the surface expression of subsidence was observed around 2 km away from the production sites where the fault plane intersected with the land surface.

The Po River delta in Italy is another interesting case study of land subsidence where large withdrawal of methane rich groundwater during 1950-1957 revealed subsidence rates up to 30 cm/yr. in areas hosting the main pumping stations. Large scale withdrawal of groundwater in the Po valley after the second world water accelerated the groundwater pumping through deep pumping wells to satiate the need of the population and the growing industry, which resulted in land subsidence with a significant retreat in the shoreline, increase in the near shore slope and periodic flooding, restructuring of lagoons and modification in land use patterns in the valley. With the closure of production wells in the area through a law enactment in 1960, there was a substantial decrease in the subsidence rates. Although lesser as compared to the past, the subsidence is still happening today in range of 1 to 15 mm per year. Although, the subsidence due to human activities is much lower than in the past, but still it is much higher than the natural processes (Teatini et al., 2011).

Mexico City, with a population of more than 20 million is also facing subsidence since many decades mainly due to over dependence on groundwater for urban and commercial uses. Large scale pumping of groundwater in the core of the city has resulted in pressure decline and consolidation of aquitards in the regional aquifer system (Carrillo, 1947). The effects to infrastructure damage have been tremendous along with the development of fractures. In Mexico City, subsidence rates have reached up to 40 cm/yr. because of the compaction of clay deposits in the areas. The

compaction of the aquitard layers is mostly in areas with huge buildings and extensive infrastructure. Decline in piezometric levels upto a tune of 30 m has resulted in significant subsidence in parts of the city (Marie-Pierre et al., 2010). Over exploitation of groundwater has led to soil compaction in the Mexico Basin aquifer. The aquitard layer of the basin plays a crucial role in the subsidence process due to the extremely high compressibility of its clay deposits separated by a less compressible sand layer where the biggest buildings of the city are anchored. The aquifer over-exploitation leads to a large scale 30m depression of its piezometric level, inducing water downwards flow in the clays, yielding compaction and subsidence.

The case studies are numerous with human induced land subsidence happening worldwide ranging from groundwater induced regional level subsidence at places like Mashhad valley in Iran (Motagh et al., 2008), Latrobe valley in Australia (Gloe 1984, Alex et al., 2015) etc to hydrocarbon induced subsidence over Bolivar coast of Vietnam (Leal J., 1989, Finol et al., 1995), Groningen gas field in Netherlands (Ketelaar, 2009) etc., to urban subsidence like in Jakarta (Chaussard et al., 2013), Shanghai (Xue et al., 2005; Wu et al., 2012), Las Vegas (Burbey, 2002), Bangkok (Phien et al, 2006), Kolkata (Chatterjee et al., 2006) and many others. But the key issue of subsidence related deformations, its measurement and risk assessment remain the foremost.

The development of subsidence monitoring techniques has progressed from conventional topographic surveys, bedrock and layering mark surveying, to the instrumental methods such as extensometers and global positioning systems (GPS) to space borne remote sensing techniques, that provide precise measures of the ground deformations. Though the terrestrial techniques such as Levelling campaigns and GPS have been available since many decades and provide precise measurements of land subsidence, they are limited to a local scale with few locations and measurements within a few square kilometres because of non-feasibility of widespread installations and involve huge requirements of man-power and time. Land subsidence that takes place on a regional/basin scale rather than on a local scale as in the case of sinkholes,

requires information on the spatial and temporal evolution of land subsidence and is a resource-intensive task to be accomplished by using these traditional ground-based techniques.

Predictive modelling techniques for measurement and analysis of aquifer system compaction and associated land subsidence have been formulated and used by many researchers worldwide, to understand the inherent framework of the aquifers and the properties of confining units. Land subsidence due to ground-water withdrawal occurs because of the decrease of pore water pressure in the productive aquifers owing to drop in hydraulic head and are modelled using the basic relations between head, stress, fluid pressure and compressibility. The techniques tend to model the current and future scenario of land subsidence due to fluid extraction and help take preventive and remedial measures to counteract the adverse effects of land subsidence. Based upon on the geo-technical properties of the area and groundwater extraction practices various methods are implemented for predicting land subsidence due to excessive ground water exploitation and have been categorized into three approaches (Helm, 2003).

(1) Empirical approach: Empirical Methods derive the future trends of land subsidence using the available data.

(2) Semi-theoretical approach: Semi-theoretical methods are based on the empirical relations between the subsidence and its related phenomenon.

(3) Theoretical approach: The theoretical methods use the relationship between compressibility and decline in fluid pressure to model the land subsidence.

Mathematical solutions have been proposed for calculation of the compaction resulting from changes in hydraulic head. One-dimensional and three-dimensional consolidation theories proposed by Terzaghi (1925) and Biot (1941) respectively are generally used for analysis of compaction. While the three-dimensional consolidation theory can predict horizontal displacements as well as vertical ones, one-dimension theory assumes that the displacement is taking place only in the vertical direction. Though horizonal deformations can

be important in an aquifer system (Helm, 1994), most of the authors have neglected it, as large amount of uncertainties in assessing the soil parameters like Poisson's ratio, anisotropy, etc. are likely to offset the expected accuracy from a three-dimensional model (Okuyan, 2000). Another reason for neglecting the horizontal deformation is the geometrical distribution of the aquifer material. The compacting layers of an aquifer are mostly contained in sub horizontal layers having higher lateral extensions than vertical. The compacting layers cannot move freely in the horizontal direction as they are sandwiched between the over and underlying sediments which restrict them from undergoing significant deformations horizontally. The major confining units in an aquifer system are the clay and silt layers and have low vertical hydraulic conductivities. The pressure gradient in these layers is almost exactly vertical which suggests more relevancy of one-dimension model of compaction. (Hoffman, 2003). Higher values of hydraulic conductivity are generally associated with unconfined aquifers that yield water to water wells or springs, whereas lower values of hydraulic conductivity are largely associated with confining units which separate unconfined aquifers from deeper confined aquifers (Fryar and Mukherjee, 2019).

Amongst the various studies worldwide, utilizing the one-dimension model of compaction, in India Sikdar et al., 1996; Chatterjee et al., 2006; Bhattacharya, 2011; Sahu and Sikdar, 2011, Khorrami et al.,2020, used the one-dimension consolidation theory to assess land subsidence in Kolkata. The mechanism uses the information on aquifer piezometric head changes along with other hydrogeological aspects of the aquifer such as aquifer thickness, porosity, storativity, bulk modulus and the properties of the confining units, to give an insight into the magnitude and extent of aquifer compaction (H.Sun et al., 1999; Galloway et al., 1999; Teatini 2005; Sahu and Sikdar, 2011).

Since the late 1990's, the development in space-borne radar interferometry techniques such as Interferometric synthetic aperture radar (InSAR) and differential interferometric SAR (DInSAR) have introduced new perspectives in the detection and measurement of subtle vertical displacements (cm to mm levels) at a regional scale, and have proved to be an efficient and

cost effective technique for monitoring and quantifying the land subsidence phenomena over large areas with high precision spatially continuous measurements (Strozzi et al., 2001; Ding et al., 2004; Chatterjee et al., 2006, 2013; Ge et al., 2007; Chaussard et al., 2014; Castellazzi et al., 2016; Pepe and Calo 2017, Othman et al., 2019, Shahzad et al. 2020, Chabbani et al., 2020). The DInSAR based measurements are complementary to ground-based measurements such as levelling and global positioning system (GPS) and precisely detect the ground displacement with a large spatial coverage.

The D-InSAR technique which is based on the principles of Interferometric Synthetic Aperture Radar was first introduced by Gabriel et al. in 1989 for measuring very small surface movements with accuracies up to 1 cm over large swaths. This method was applied to SEASAT data of Imperial Valley, California where ground swelling and shrinking was caused due to water absorbing clays in the area. During the last two decades, D-InSAR has been used to study a wide range of surface displacements related to active faults, volcanoes, land subsidence, landslides and glaciers, at a spatial resolution of less than 100 m with cm to sub-cm level precision. DInSAR takes advantage of the phase component of reflected radar signals to measure apparent changes in the range distance of the land surface (Gabriel et al., 1989), and contains information about relative topography changes between two acquisition times. The analysis of phase differences in repeated orbits from several years evaluates the ground deformation projected along the sensor Line of Sight (LOS) and are used together to generate deformation time series in the area. The technique has proven to be quite effective particularly in areas that show deformations with a predominant vertical component, as in the case of subsidence and sinkholes. DInSAR can give a millimetre level of accuracy and shows well developed fringes in the subsidized area enabling very precise measurements of land deformation. Different radar sensors are available for various land applications including land deformations. Some of them include ALOS PALSAR-1/2 which are microwave sensors onboard ALOS satellite developed by Japan Aerospace Exploration Agency (JAXA) and are capable of taking measurements in multiple observation modes with different polarizations, resolution and variable

swath width. Sentinel-1 is a radar imaging mission by European Space Agency (ESA) and is equipped with dual polarization C-band SAR instruments to provide images of earth's surface every six days under all weather conditions. Terra Sar-X is a SAR satellite mission from Germany providing very high resolution data in different modes. The satellite has a temporal resolution of four days and can provide data of earth's surface for a variety of scientific applications. The deformations monitored is a function of radar sensor wavelength for example the wavelength 24 cm of L-band in ALOS PALSAR-1/2, 5.5 cm of Sentinel-1 C-band, or 3.1 cm in case of X-band on Terra Sar-X satellite, as each interferometric cycle represents half of the sensor's wavelength. The radar wavelength influences the precision of deformation measurement; the sensitivity of C-Band data is higher for detecting areas with slow rates of subsidence in comparison to L-Band (Chatterjee et al., 2013). However, a major limitation in using DInSAR is that it may get affected by numerous factors like orbital, topographic and atmospheric noise thus influencing the accuracy of the results. Hence, corrections such as pixel level phase variations, orbital trajectories, topographic and atmospheric corrections need to be applied to obtain more precise results (Massonnet and Feigl, 1998).

While major studies on anthropogenic land subsidence before in the last century, concentrated mostly on theoretical and predictive modelling of reservoir compaction involving the use of traditional methods of levelling surveys, hydrogeological and geomechanical concepts and fluid dynamics at local scales and were often limited by the availability of data, the advent of radar interferometric techniques since the beginning of 21st century has shifted the paradigm to more precise satellite-based regional level land subsidence measurements. The state-of-the-art interferometric techniques when integrated with regional aquifer studies and modelling gives a good perception and knowledge towards understanding the mechanism and cause for such subsidence in a more robust and accurate way, than ever before on a very large and multi temporal scale. In the current work, I have tried to correlate the aquifer compaction rates with the DInSAR derived rates at selected locations around Mehsana to get an insight on the ongoing land subsidence process.

1.3 Research Motivation

With more than 150 cities worldwide facing serious threats of land subsidence due to excessive ground water overdraft (Hu et al., 2004), the studies on land subsidence induced by excessive fluid withdrawals from the subsurface have caused attention of geologists, environmentalists and various public stakeholders. Though numerous studies on subsidence due to groundwater overdraft have been carried out in various parts of the world, the studies on hydrocarbon related subsidence have mostly been limited to the Americas and subsidence studies in oil and gas fields outside the United States are very few. Though, the consequences of groundwater withdrawals have more socio-economic impacts than hydrocarbons, where the implications are localized near the producing wells and the surface expressions of land subsidence are weaker than those from groundwater, nevertheless studies on both groundwater and hydrocarbon induced subsidence are critical for investigating and assessing their impacts on our society and the environment.

Land subsidence studies due to fluid withdrawal have been very limited in India. In India, much of the research work on groundwater induced land subsidence has been limited to areas in and around Kolkata, West Bengal (Sikdar et al., 1996; Chatterjee et al., 2006; Bhattacharya (2008, 2011); Sahu and Sikdar, 2011; Bhattacharya and Kumar, 2012; Ganguli M., 2011; Suganthi et al., 2017, 2020). A few DInSAR based land subsidence studies have also been carried out in Delhi (Malik et al., 2018); Rudrapur in Uttarakhand (Tripathi et al., 2018); Jagadhri city in Haryana (Gupta et al., 2019); Chandigarh (Tripathi et al., 2019); Mohali and Chandigarh (Kadiyan et al., 2021). Table 1 below lists the major work done on groundwater induced land subsidence in India.

Table 1.1: Previous studies on Groundwater induced Land subsidence in India.

References	Study Period	Location	Research Technique	Land Subsidence
Sikdar et al. (1996)	1956-1993 1956-1994 1958-1993	Selected locations in Kolkata and Howrah Municipal corporation zone.	One-dimension consolidation theory	3.33 mm/yr. to 13.78 mm/yr.
Chatterjee et al. (2006)	1992-1998	Selected locations in Kolkata city	D-InSAR using ERS InSAR data	5 to 6.5 mm/yr.
Bhattacharya (2008)	1956-2000 1958-2000 1956-2005	Selected locations in Kolkata city	Linear and Logarithmic Theory	10.56 mm/yr. to 20.46 mm/yr.
Sahu and Sikdar (2011)	1956-2005	Salt Lake City in Kolkata and the east Kolkata wetlands	One-dimension consolidation theory	13.53 mm/yr.
Ganguli M. (2011)	1998-2002	Singur block, Hooghly district, West Bengal	One-dimension consolidation theory	6.13 mm/yr.
Bhattacharya and Kumar (2012)	1956-2000	Selected locations in East Kolkata	Linear and Logarithmic Theory	7.50 mm/yr.
Suganthi et al. (2017)	2003-2007 2007-2010	Selected locations in Kolkata city	D-InSAR using ENVISAT ASAR data	12 mm/yr. 18 mm/yr.
Malik et al. (2018)	Sept. 2011 – Nov. 2013	Delhi NCR	PSI using TerraSAR-X data	10 to 32 mm/yr.
Tripathi et al. (2018)	Dec. 2014 - Dec. 2015	Rudrapur city, Uttarakhand	PSInSAR using TerraSAR-X data	2.46 mm
Gupta et al. (2019)	2017-2019	Jagadhri city, Haryana	D-InSAR using Sentinel-1 data	4.98 cm/yr.
Tripathi and Tiwari (2019)	2018-2019	Chandigarh	D-InSAR using Sentinel-1 data	0.5 cm-1.7 cm
Suganthi and Elango (2020)	2003-2010	Salt Lake City in Kolkata	SBAS-InSAR using ENVISAT ASAR data	8 mm/yr.
Kadiyan et al. (2021)	2005-2018	Mohali-Chandigarh	DInSAR using ALOS PALSAR -1/2 and RADARSAT data	4-7.5 cm/yr.

Though areas such as Mehsana district in Gujarat, Coimbatore district in TamilNadu, Kolar district in Karnataka, Bikaner and Jodhpur districts in Rajasthan, Delhi, Chandigarh and other parts of Haryana have been the

subject of recent research, but scientific documentation of these research is not readily available. Although site specific information is available, but still the paucity of funding and precise time series scientific data particularly in public domain, has resulted into lack of measurements on land subsidence and consequently many Indian cities have still not been reported. For hydrocarbon induced subsidence no notable work has yet been carried out in India, to study the impact of hydrocarbon extraction on surface subsidence.

In Kutch-Sabarmati basin of Gujarat where the productive aquifers are deep and tubewell remains the primary source of groundwater extraction, serious decline of groundwater levels have been reported. Aquifer compaction and consequent land subsidence studies are thus very important in the area. The Kutch-Sabarmati basin also hosts several oil fields with many producing wells. The Mehsana oil fields are one of the biggest oil producing asset of Oil and Gas Corporation (ONGC) in India. With respect to the notable reservoir thickness, significant pressure drop due to extraction and high areal extent of the Mehsana oil field there is a high subsidence potential in this field. In view of the current Indian situation, it is therefore a critical research requirement to understand & characterize the nature of ground deformation due to groundwater and petroleum over exploitation to foresee the future scenario of land subsidence.

1.4 Research Hypothesis

Water is one of the most vital necessity for sustenance of human life. Fresh water supplies in whole world depends solely upon groundwater. Groundwater is amongst the most important natural resource as it provides drinking water to the human communities, sustains irrigation and agriculture, supplies water to municipal and industry establishments, sustains the flow of streams and rivers during precipitation free periods and maintains the ecological integrity of wetland and riparian ecosystems. Being an agrarian society, India depends heavily on groundwater. In India, groundwater contributes approx. 62% in irrigation, 85% in rural water supplies and 45% in urban water consumption (Saha and Ray, 2019). The country is facing severe stress on water availability primarily because of high population density and increased usage of groundwater resources for agriculture and commercial sectors to sustain the demand of the growing population. The dependence on the groundwater has increased drastically over the years leading to over exploitation of the aquifers.

According to a report by NASA's Goddard Space Flight Centre, groundwater in northern India is being depleted at a rate of 19.2 gigatons per year (NASA, 2019). Overexploitation of groundwater has led to decline in ground water tables in most parts on northern India. Therefore, proper identification, monitoring and assessment of groundwater level scenarios are imperative to counteract and reverse any potential significant trend in the groundwater levels for efficient management of groundwater resources especially in arid regions. In Kutch-Sabarmati basin of Gujarat, where the productive aquifers are deep and tubewell remains the primary source of groundwater extraction, aquifer compaction and consequent land subsidence studies are thus very important to support infrastructural development plans and ground water resource allocation programs. The condition of the ground water table in district Mehsana, on the west of the basin has attracted a lot of attention of the geologists and hydrologists. The district with moderate to limited aquifers with withdrawals much larger than they could sustain has resulted in serious decline in ground water levels as well as yields of all aquifers, whether phreatic, semi-confined or confined over the past 25-30 years. According to a district report by CGWB (Sinha 2014, District Groundwater Brochure, Mehsana district, CGWB), piezometric heads of deep confined aquifer in the district have declined sharply due to over exploitation of groundwater. The report categorized eight talukas in the district as Over exploited and one under Critical stage of exploitation. Since declining groundwater levels have been reported in many parts of Gujarat including the Mehsana district (Bhatia 1992; Kumar 1995; Dinesh M., 2000; Sinha, 2014, CGWB annual report), the present work tries to estimate the relative risk of land subsidence associated with groundwater withdrawal in the region. Though studies on aquifer system compaction and related subsidence has been theoretically described and studied for many decades now, but lack of available scientific data and investigations have hindered the exploration into the phenomenon of land subsidence due to groundwater draft in the region. It is thus the prime objective of our study to apply satellite DInSAR observations to identify, characterize and analyse surface displacements caused by aquifer system compaction. The present work integrates detailed geological and hydrogeological data with differential SAR interferometry monitoring with the aim to better understand subsidence processes due to extraction of groundwater and hydrocarbons in and around Mehsana. Such studies would be useful for groundwater administration at the regional and local levels as well as in mitigating the effects of land subsidence in the region.

1.5 Study Area

The study area comprises of the composite Kutch and Sabarmati Basin lying in the western states of Gujarat and Rajasthan of India. Majorly, the study area covers the state of Gujarat with little hilly areas of Aravalli mountain range in Sirohi and Udaipur districts of Rajasthan, that act as the origin for the rivers draining the area. The composite basin has an area of 87582.37 sq. km., and the bounding coordinates are 22° N to 25° N and 68°15' E to 73°45' E. The study area map below shows the location of the study region along with the approximate location of major oil fields in and around Mehsana city (Fig. 1.1).
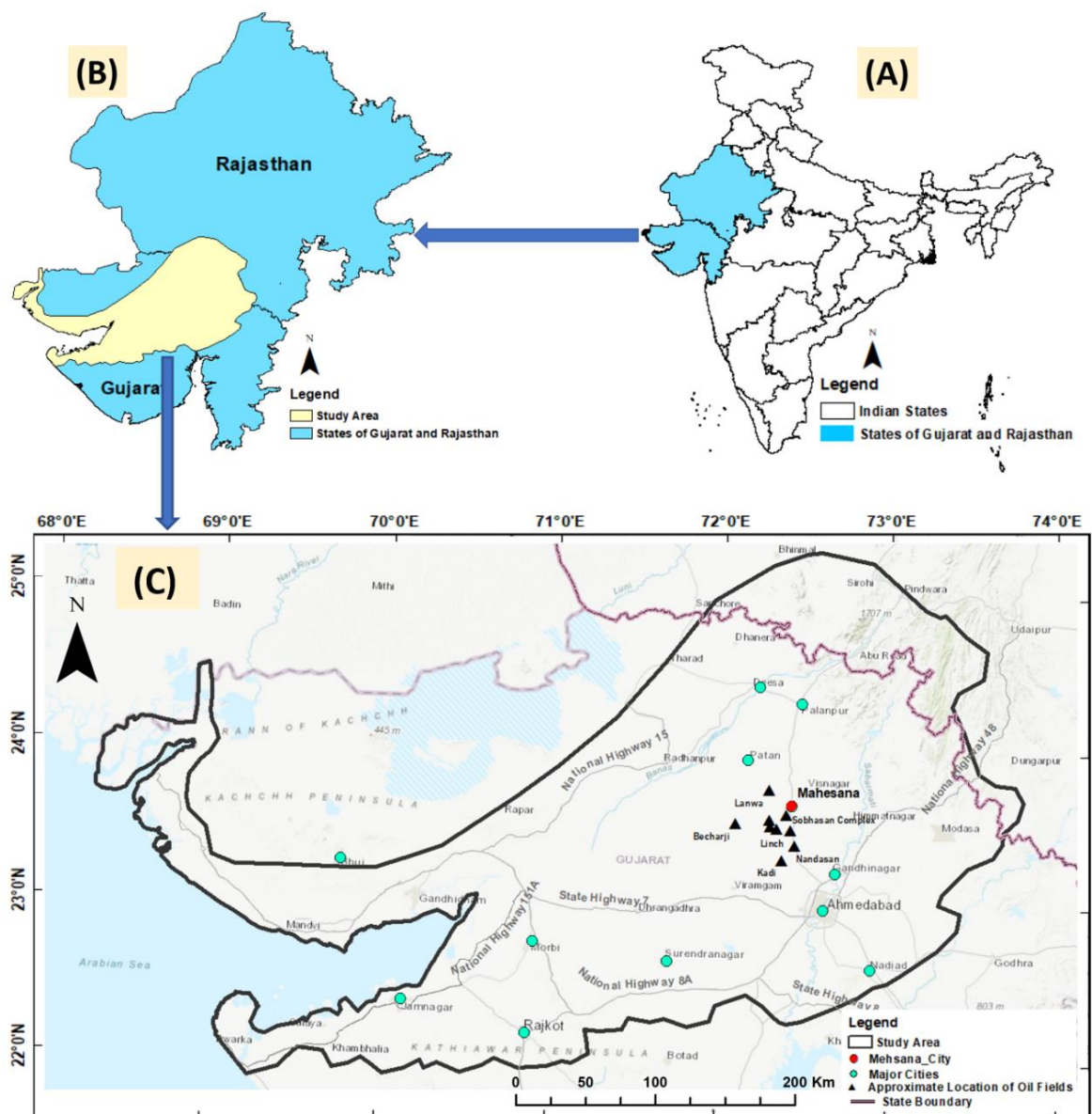
Fig 1.1: Study Area map. (A) India (B) Study Area encompassing the states of Gujarat and Rajasthan (C) Study Area which is a composite of both Kutch and Sabarmati basins.

The Kutch sedimentary basin lies between 22°30' and 24°30' North latitude and 68° and 72° East longitudes and covers the entire Kutch district of Gujarat extending upto the western part of Banaskantha district till the Santalpur taluk. With a total area of around 71,000 sq. km, the basin has 43,000 sq km. inland area and 28,000 sq km. offshore area within 200m water depth. Mesozoic sediments fill the major part of the basin with a thickness of over 2400m. So far, a good number of exploratory wells have been drilled by ONGC and other private companies in both offshore and onshore part of the basin, but hydrocarbon could be established only in few wells. The wells drilled in the inland part of the Kutch Basin reveal abundant sandstones developed in Jhuran and Bhuj formations and form extensive and excellent reservoirs for hydrocarbons with good permeability and porosity ranging upto 34%. The department of Directorate General of Hydrocarbons, Govt. of India has classified Kutch basin under category-II and has established it as a proven petroliferous basin yet to be exploited commercially (Khatri et al., 2015).

The Sabarmati river basin stretches between 72º 15' to 73º 49' East longitude and 22º 15' to 24º 53' North latitudes. The basin is bounded by Aravalli hills on the north and north-east, Rann of Kutch on the west and by Gulf of Khambhat on the south. The basin extends over states of Rajasthan and Gujarat with main parts of the basin lying in Gujarat, draining an area of 21,565 km^2, of which17,441 km^2 lies in the state of Gujarat and 4,124 km^2 in Rajasthan. The drainage area of the Sabarmati basin covers parts of Dungarpur, Jalor, Sirohi and Udaipur districts in Rajasthan, and includes parts of Banaskantha, Sabarkantha, Mehsana, Gandhinagar, Ahmedabad, Anand and Kheda districts in Gujarat (online resource).

1.5.1 Physiography and drainage

The state of Gujarat has been broadly divided into four physiographic regions. The arid to semi-arid North Gujarat, semi-arid to dry sub humid South Gujarat, dry sub-humid Saurashtra Peninsula and the arid Kutch Peninsula. The Kutch-Sabarmati basin covers four of these physiographic divisions. North Gujarat includes the districts of Sabarkantha, Mehsana,

Banaskantha, and Patan, Central Gujarat covers Kheda, Anand, Ahmadabad, Gandhinagar and Panchmahals districts, Saurashtra Peninsula includes Jamnagar, Rajkot and Surendranagar and the Kutch peninsula encloses the Kutch district (Gujarat State Environmental Information System (ENVIS) report [n.d.]).
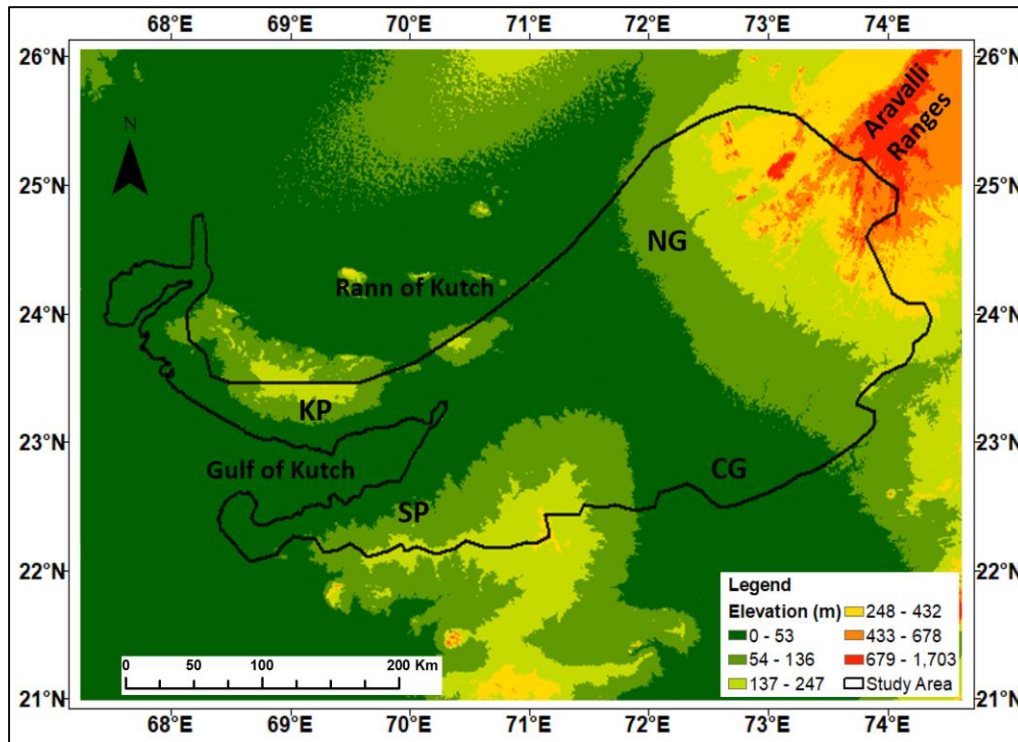
Fig 1.2: The physiographic features and divisions in the study area shown along with SRTM elevation. NG: North Gujarat, CG: Central Gujarat, KP: Kutch Peninsula, SP: Saurashtra Peninsula.

Major topographical features of the basin include the Aravalli mountain ranges and Gujarat plains towards east, Thar desert on the north and the Arabian Sea on the south and the west. The Gulf of Kutch is bounded by the Kutch Peninsula on the north-west, and the Saurashtra or Kathiawar Peninsula towards the west. Fig 1.2 shows the topography in the study region.

The area represents varied topography with shallow wetlands of Rann of Kutch on the western side and consists of grasslands, sparse vegetated areas, dry river beds, network of creeks, mangrove swamps, flat barren lands dominated by dry salt waste and a long coastline; mountainous terrain of Aravalli's and Sabarmati river on the north-east; the Luni river on the north which mostly flows through Rajasthan before it drains into the Rann of Kutch

and southern part represented by other important smaller rivers as Shetrunji, Machhu, Saraswati, Rupen, Banas and Bhadar. The Shetrunji river drains into the Gulf of Khambhat, Bhadar drains into the Arabian Sea, while Machhu, Rupen, Saraswati and Banas rivers culminate into the Little Rann of Kutch which is a sedimentary sub basin in the Kutch region. Rising in the central uplands and flowing northwards either to the Rann of Kutch or southwards towards the Gulf of Kutch, none of the rivers in the region are perennial. The basin receives its major part of rainfall from the South-West monsoon between June to September with peak months of July and August. Figure 1.3 shows the drainage pattern in the study area.
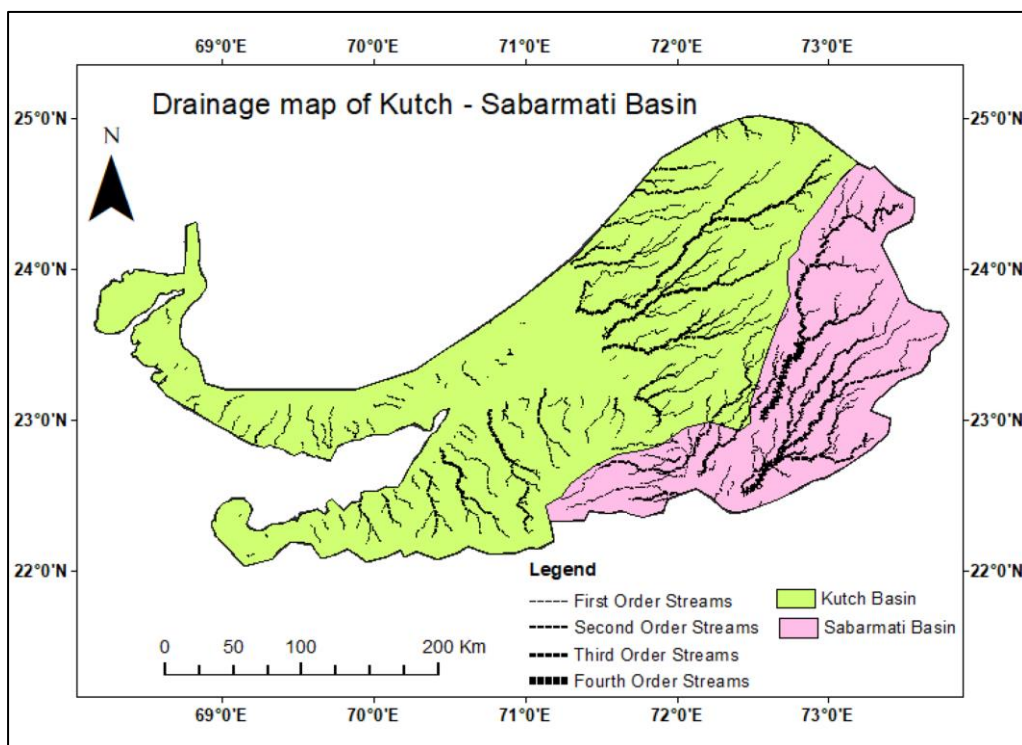
Fig 1.3: Drainage map of the Study area.

The Sabarmati basin is delimited by Aravalli hills in the North and North-East and separates the minor streams flowing into the Rann of Kutch on the west side from Sabarmati river draining into the Gulf of Khambhat on the south. The Sabarmati river originates from the Aravalli hills in Rajasthan at latitude 24°40' N and longitude 73°20' E at an elevation of 762 m above mean sea level. The total catchment area of the basin is around 21,565 sq.km with a drainage area of approx. 4,124 sq.km in Rajasthan and 17,441 sq.km in Gujarat. The total length of Sabarmati river is about 371 km with the river traversing

around 48 km through Rajasthan and 323 km through Gujarat before falling into the Arabian sea through the Gulf of Kambhat. Mean annual rainfall of the basin is around 727 mm.

1.5.2 Rainfall and Climate

The Kutch basin covers the entire Kutch district, the southern highlands of Saurashtra upto the western part of Banaskantha district. The district of Kachchh, western parts of Banaskantha and Mehsana, the northern fringe of Saurashtra (Jamnagar) and its western part have arid climate and the rest of the Kutch Sabarmati basin has semi–arid climate The Kutch district is characterized by hot summer and dryness in the non-rainy season. The higher evaporation from salty flatlands of Rann of Kutch and Little Rann of Kutch influences the climate of the mainland and makes it arid while the coastal region experiences a mild weather due to the cool sea breezes from the Arabian sea. The months of March to May are the hottest when the temperature rises to more than 40°C. The winter months are from December to February and experience temperatures of around 20°C. Winds are light to moderate with. Average annual rainfall in the area is around 380 mm with major part of the rainfall (about 345 mm) received from south-west monsoon between the months of June and September. The relative humidity in Kutch varies between 41.5% during March and 77% during August. (Groundwater Brochure, Kachchh district, CGWB, 2013). The rainfall in southern highlands of Saurashtra is around 630 mm while the other parts of Saurashtra receive lesser rainfall. The temperatures in the Saurashtra region range from 28° C to 38° C during summers and 10° C to 25° C in the winter months. The mainland of Gujarat which consists of North Gujarat, Central Gujarat and South Gujarat receive a rainfall between 500-1000 mm and generally fall under semi-arid climate with rainfall mostly received from south west monsoons as in other parts of the state. The average annual rainfall of the Sabarmati basin is around 690 mm and the average annual mean temperature is around 26 °C. The mean rainfall map of the study area for the period 2005 to 2017 (Fig. 1.4 below) was created using the 0.25 X 0.25 gridded rainfall data available from the Indian Meteorological department and was classified using Jenks natural breaks classification method to show the inherent natural groupings in the rainfall data.
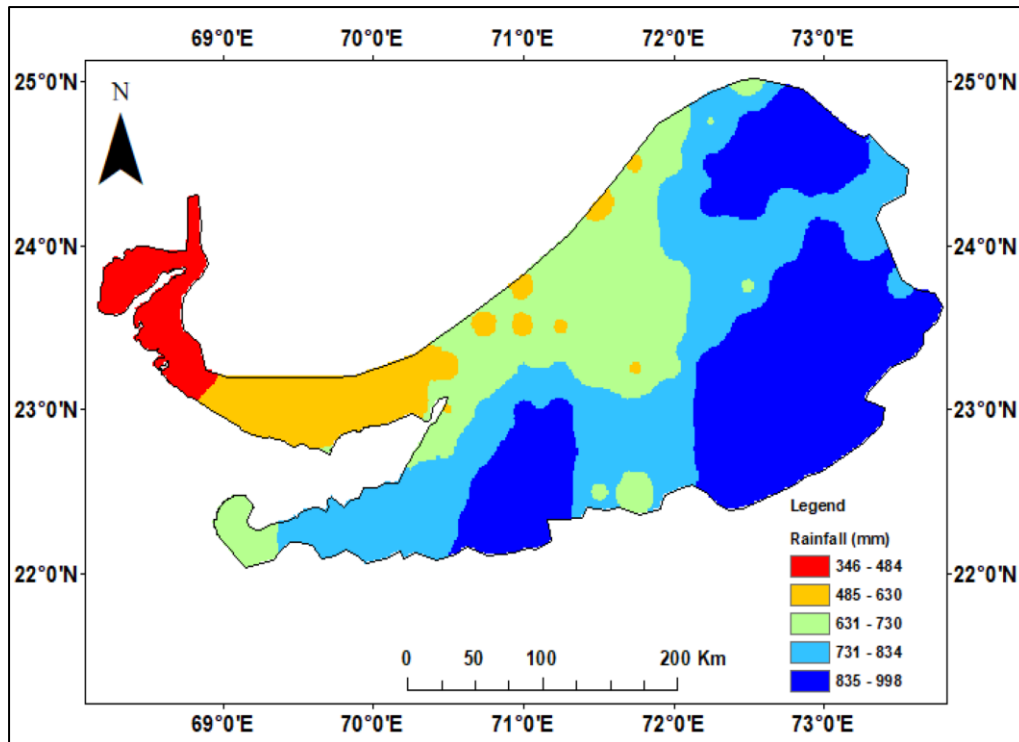
Fig 1.4: Mean Annual rainfall map of the Study area (2005-2017)

1.5.3 Geomorphology

The mainland of Kutch is an undulating country with rugged hilly terrain, extensive broad plains, gently sloping coastal erosional plains, alluvial or mud and salt flats (Rann) and grassy undulations (Banni). The Kutch basin is characterized by highlands that represents uplifts and lowland plains lying between the uplifts. These lowlands represent structural basins and are composed of alluvium, mud or clays. Geomorphologically, the region is divided into five broad areas:

i)   The Great Rann of Kutch which mainly comprises of marshy land and salt/mud flats. The Rann having an area of around 25,000 sq km. is majorly devoid of vegetation with extreme environmental conditions. The little Rann of Kutch, immediate inland of the Gulf of Kutch is a salt marsh with scanty vegetation. It is about 110 km in length and covers an area of around 5,000 sq km.

ii) Banni Plains covers an area of about 2000 sq. km. with majority of the area having the similar arid conditions of Rann of Kutch while about 777 sq. km of Banni plain is grassland. The maximum height of the Banni Plains is 458

m with regional elevation varying from 16 m to 232 m above mean sea level. The northern part of the region is hilly with dendritic drainage patterns.

iii) Central upland consisting of planes, hills and dry river beds. Several small streams flowing northwards across the Kutch Mainland culminating into the Great Rann-Banni plain forming semi-conical alluvial fans in the piedmont area. There are three hill ranges in the main land namely Dhinodhar, Jura and Vavar with elevations of 187m and 274m above mean sea level.

iv) The Southern coastal plains along the Arabian Sea. The coastal plain is about 15-45 km wide with a maximum elevation of 80 m above mean sea level and

v) Creeks and mangroves in the west. The coast is generally flat and is broken by small and big creeks Kori, Boacha and Godia. The geomorphic zones are flanked by the Nagar Parker fault in the north and the North Kathiawar fault in the south.

Geomorphologically, the Sabarmati basin is divided into three distinct units:

i) Gentle to moderate sloping rock outcrops, undulating dissected hills, elevated hills and sharp slopes. The northern part of the basin is endowed with such physiography mainly towards the north east highlands of Sabarkantha district lying on the foothills of Aravalli ranges which lie towards the north-east of the basin.

ii) Sabarmati Upper sub basin with gently sloping alluvial plains and pediments mainly between Khedbrahma to Ahmedabad. The alluvial plains are drained by some major tributaries like Sei, Wakal, Harnav, Hathmati, Watrak and

iii) The Lower Sabarmati basin with nearly flat alluvial plains. located between Ahmedabad-and Gulf of Cambay drained by major tributaries Bhogavo, Goma, Bhadar River, Limbadi- Bhogavo, Umai, Salva and others. Fig 1.5 below shows the geomorphological map of the study region.
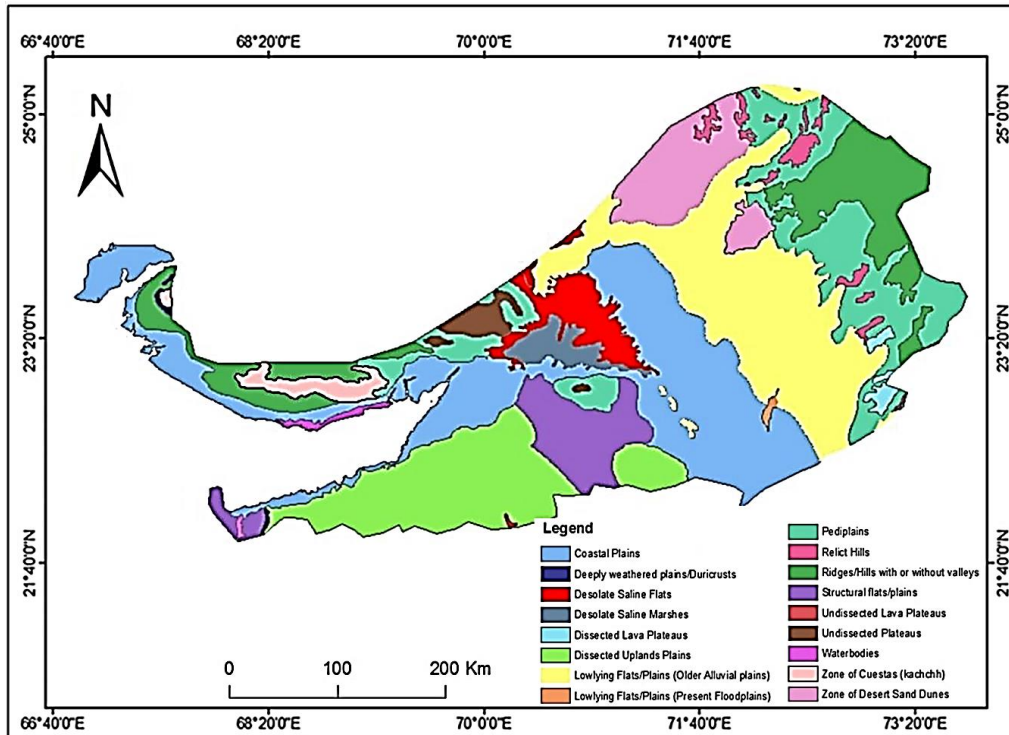
Fig 1.5: Geomorphological map of the Study area (Source: Geological Survey of India).

1.5.4 Hydro-Geological Settings

Kutch Basin was formed under fluvio-deltaic environmental conditions with intermittent marine invasions. The Kutch basin is reported to be filled by Mesozoic, Tertiary and Quaternary sediments with sediment thickness from 500 m northwards to around 4000 m on the southern side. The thickness varies from 200 m in the east to 2500 m on the west side. Mesozoic rocks are exposed in the upland areas with gently sloping Coenozoic rocks towards the coastal plains. Geologically, the Kutch district comprises of old lower Jurassic formation to recent alluvial formation. The northern part of the district is characterized by the salt marshy Rann. The southern part which is represented by coastal plains is formed of alluvial formations while the Tertiary formations are conspicuous on the western side of the district (Mukherjee et al., 2012). Being a highly arid region, the groundwater development in the district is very limited. Groundwater is developed in the central, eastern and western parts of the district, and the southern area yields normal to saline water from confined aquifers. The central and southern part of the district is occupied by the basaltic

23

deccan traps and yield limited quantity of drinkable water from shallow unconfined aquifers. The average depth of groundwater ranges in the district ranges from 75 and 125 m towards east and west part and in central part the average depth ranges between 135 and 180 mbgl. Four major hydrogeological units are identified in the Kutch region characterised by the sedimentary rocks formed under marine and non-marine environmental conditions during Jurassic to recent period; and volcanic and intrusive rocks of Deccan traps formed during middle Cretaceous to lower Eocene. 1) Mesozoic formations 2) Deccan Trap 3) Tertiary formations and 4) Quaternary sediments.

Mesozoic formations occupy about 60 percent of the area. Patcham, Chari and Katrol formations belong to Jurassic period while Umia and Bhuj formations represent lower Cretaceous. The Patcham formation is characterized by yellow and greyish coloured sandstone, shale, and fossiliferous limestone and represent marine sedimentary sequence. It occupies largely the island belt of Patcham, Khadir and Bela and small area in northern part of Kutch mainland. The ground water occurs under confined conditions in the sandstone-shale sequence of this group. The semi-consolidated sandstone exposed in the lower reaches forms unconfined aquifers aquifer and are tapped locally for drinking and agricultural purposes. The dug wells tapping this aquifer ranges in depth from 10 to 24 mbgl whereas the depth to water level during summer varies from 15 to 20 meters. The Chari formations constitute hilly topography and are composed of hard oolitic limestone, sand stone and shale representing marine facies, because of which there is no ground water development in this formation. Katrol formations is exposed in the upland and mainland of the Kutch district. It is formed by alternate sandstone and shale sequences with minor bands of limestone. The ground water in this formation occurs under unconfined to confined conditions with the depth of dugwells ranging from 10 to 25 m and dug com bore wells ranging from 25-60 m. Few tubewell, ranging in depth from 40 to 140 m also tap the fractured zones in the aquifer. Bhuj Formation exposed in the central part of the district form the major productive aquifers in the region. The sandstones of Bhuj formations are soft, highly porous and permeable and form the major groundwater reservoirs in the region. Bhuj

sandstone comprises of fine to coarse grained sandstone interbedded with siltstone, shale and limestone. Groundwater is extracted through deep and medium depth tubewell ranging in depth from 80 to 250 m with thickness of granular zones ranging from 30 to 100 mbgl.

Deccan Trap occurs as almost one continuous belt from Anjar to Lakhpat taluka but shows a lateral dislocation near the junction of Nakhatrana, Abdasa and Mandvi talukas. The deccan traps are characterized by extensive flows of basalt and dolerite. Groundwater development in the areas underlain by deccan trap is very less due to poor water bearing characteristics and is limited to a few weathered zones where the groundwater is highly saline (Groundwater brochure, Kachchh district, CGWB, 2013).

Tertiary Formations belong to Eocene to Miocene period are mainly of marine sediments which are mostly argillaceous and calcareous and hence water quality is quite meagre in the formation series. The formation is divided into Laki series which comprise of up to 160 m thick red & mottled clays and carbonaceous shale with thin seams of lignite & pockets of unconsolidated fine-grained sand beds at the bottom of the series. The water from dugwells in phreatic zones is brackish to saline while the confined aquifers yield large quantities of saline water. Kirthar series is about 325 m thick and is mainly composed of Nummulitic limestone with occasional thin beds of calcareous shale and yield little quantities of poor-quality water. Manchhar series is characterized by grey and mottled sandstone which forms yielding aquifers at places and calcareous grits. Wells range from 7 to 24m in depth with depth to water in the range of 3 to 15 m below the ground level.

Quaternary sediments are the recent formations. The hill slopes and faulted plains of the formation towards the north are characterized by Milliolite limestone, which do not yield any groundwater. Alluvium comprising of brown loamy, kankary. silt, clays, sand, gravel, loam and kankar occurs in channels of large ephemeral streams and coastal plains. The alluvium yields little quantities of saline water while the coarser sediments may yield small to moderate supplies of brackish water. There is no groundwater development at

Lakadiya and Kumbhariya where no aquifer bearing horizons have been met even at a depth of 450 and 305 mbgl. The dugwells range from 4 to 22 m depth between Bidada and Bhadreshwar with depth to water varying between 3 to 16 mbgl. Few tubewells tap aquifers upto a depth of 129m.

The Sabarmati basin is characterized by the hard rocks of Pre-Cambrian and the Decan trap and consists of discontinuous aquifers where water circulates through the open fractures and the secondary porosity. Water is also gathered in the weathered zones. The hard bedrock is poor water yielding formation and is not exploited from water. The water supplies in the area is thus mainly dependent on the surface water or dugwells in the weathered zones (Jain et al., 2019). The geology of Sabarmati Basin area ranges from Pre-Cambrian to recent alluvial deposits. The Pre-Cambrian formations are mainly igneous and metamorphic rocks. The oldest rock formations are meta-sediments and consist of calcareous rocks (marble and calc-gneiss), argillaceous rocks (micas, schists and phyllite), and arenaceous rocks that are mainly quartzite. Phyllites constitute the major aquifer type in the basin and occupy close to 30% of the basin area. Schist formed aquifers are around 9% of the area and few acquires are formed in Quartzites (Hydrogeological Atlas of Rajasthan, Sabarmati basin, 2013). The deposition of sediments was followed by the igneous activity. Deccan traps of cretaceous to lower Eocene cover these formations. The thickness of the sediments in the lowest ranges of the basin is up to 5000m, with the thickness of quaternary alluvium increasing from north east to south west direction. The hard basement is overlain by quaternary alluvial deposits consisting of gravel, sand and clay. The gravel and sand act as the major water bearing horizons with clay acting as aquitards in-between. Three aquifer zones are identified in the Sabarmati basin with 300 m depth. Aquifer "A" forms the upper unconfined aquifer and consists of sand and gravel. The Aquifer "B" lies underneath the first unconfined aquifer and occurs in confined conditions with a sandy layer of 80-160 m thickness. The second confined aquifer named as Aquifer "C" is found at depths of 154-274 m in sandy layers (Jain et al., 2019).

The multi layered aquifer system in Mehsana district is formed by the hard rocks of Precambrian, semi consolidated formations of Mesozoic

and unconsolidated Quaternary alluvial deposits. The groundwater occurs in both phreatic and confined conditions. While the unconfined aquifers in the alluvium formations are suitable for dug wells and tube wells with low yield, in confined aquifers, the depth of tube wells with adequate yield range from 120 m to 300m. Hydrogeologically, two major aquifer units have been identified in the Mehsana region upto a depth of 600m. The upper system consisting of coarse-grained sediments is phreatic and is termed as Aquifer A, while the lower unit with alternating beds of sand and clay is confined and is subdivided into four aquifers namely Aquifer B, C, D and E in Post Miocene and Aquifer F and G in the Miocene formations. Aquifer H of older cretaceous formation is in the form of a local aquifer in the north eastern part of the district. (Sinha 2014, District Groundwater Brochure, Mehsana district, CGWB). Due to sparse rainfall and a seasonal river system, the area depends heavily on ground water for its domestic, agriculture and commercial requirements.

1.5.5   Hydrocarbon Prospects

The study area comprises of the petroliferous fields of Mehsana that form a part of the Cambay sedimentary basin which is a major NW –SE trending rift graben extending from Gulf of Cambay in south to Barmer Basin of Rajasthan in North. The proven area of Cambay basin is around 53500 sq km. Cambay basin has been structurally divided into five tectonic blocks:

i) Patan-Sanchor Block

ii) Ahmedabad-Mehsana Block

iii) Cambay-Tarapur Block

iv) Jambusar-Broach Block

v)   Narmada-Tapti Block

The location of the blocks is shown in Fig. 1.6 below.

Mehsana Asset that hosts many pricing oil wells in the region is the northern segment of Ahmedabad-Mehsana block of North Cambay Basin. NNW-SSE trending Mehsana horst, subdivides the Mehsana sub-block into two depressions. Majority of the oil fields except Becharji lie to the east of Mehsana horst, in the Mehsana-Ahmedabad tectonic block of the Cambay Basin (Fig. 1.7) The basin was formed during rifting along N-S to NNW-SSE trend in Late Jurassic to early Cretaceous.
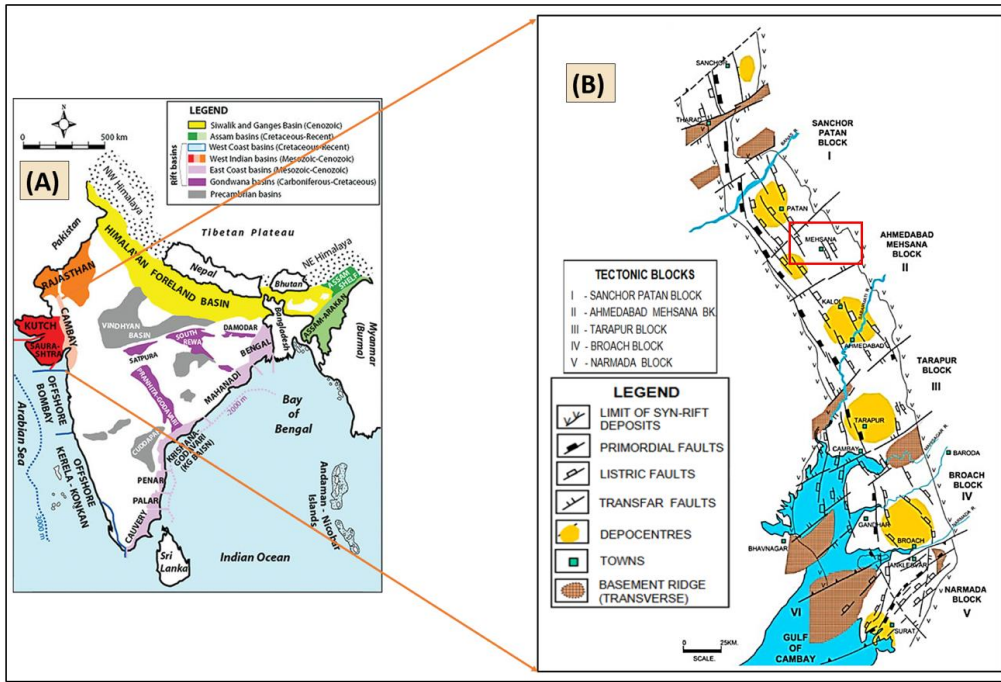
Fig 1.6: Tectonic map of Cambay Basin. (A) Sedimentary basins of India (B) Tectonic blocks and their distribution in Cambay basin. (Source: Hasan et al., 2013)

Mehsana Asset of Ahmedabad-Mehsana block is one of the largest onshore assets of Oil and Natural Gas Corporation of India and covers an area of around 6000 sq km with 27 oil fields and 1777 drilled wells.
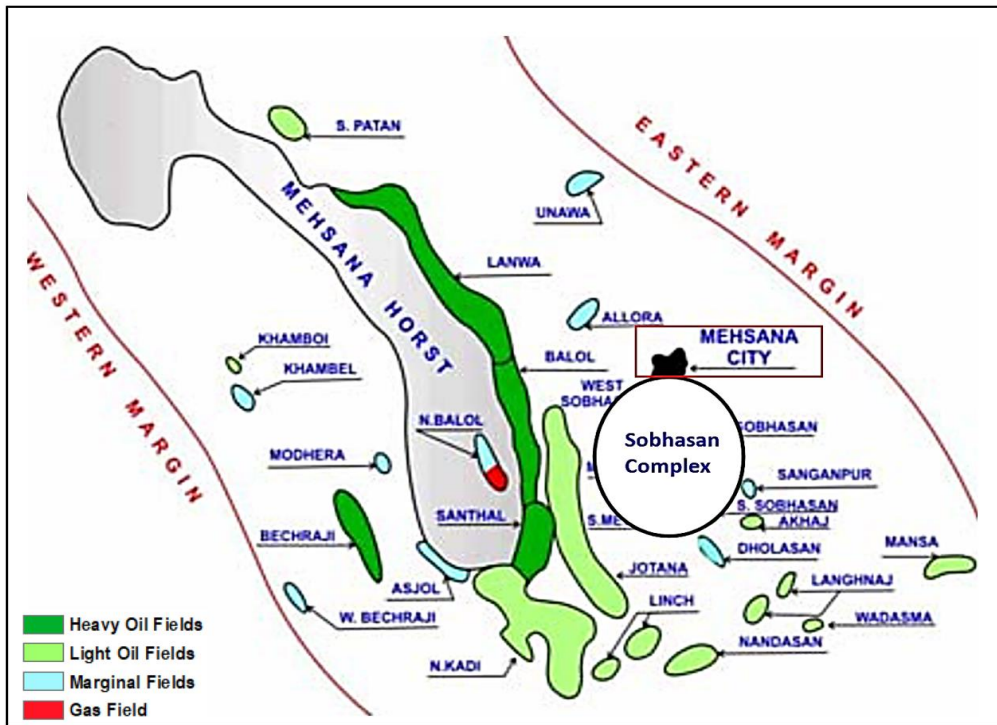
Fig 1.7: Location of Mehsana-Ahmedabad Tectonic block and oil fields of Mehsana Asset. (Source: Tiwari et al., 2011)

The major oil fields of the Asset have been divided into nine major areas for ease of administration and better control on conduct of scientific studies and filed development. The major areas are North Kadi, Sobhasan, Santhal, Balol, Jotana, Nandasan, Lanwa, Linch and Becharji (Fig. 1.7 above). The oilfields of Mehsana Asset have multi-layered pays belonging to Paleocene to middle Miocene age and form part of Mehsana-Ahmedabad Tectonic block. Oil & gas accumulation in these fields ranges in age from Upper Paleocene in the Olpad formation in Khamboi field to Miocene in the Babaguru in Lanwa and North Kadi field.

Mehsana oil fields are characterised by heavy oil and in-situ combustion is carried out in many wells for oil recovery. The primary oil recovery rate ranges from 6.5 to 15.8%. The Sobhasan complex which is just 7 km south of Mehsana city produces oil from sandstone reservoir belonging to Eocene age. The Complex comprises of six producing oil fields namely Sobhasan, West-Sobhasan, South-Sobhasan, Mewad, South-Mewad and Kherwa Hydrocarbons have been established in four different reservoir sand units – Kalol, Sobhasan, below Coal Sand (BCS) and Mandhali from top to bottom (Subir Das et al., 2006). Major lithological units are Sandstone, Shale, Carbonaceous Shale and Coal. The thickness of sandstone varies from 2 mts. to 50 mts. A brief illustration of different formations of Shobhasan complex along with their lithological descriptions and the approximate thickness of the different formations is shown in the table below (Table. 1.2).

Table 1.2: Generalized stratigraphic column showing the Lithological description showing the lithological description in Sobhasan Complex (Mehsana Asset). (Source: Subir Das et al., 2006)

AGE	FORMATION	PAY HORIZON	APPROX. THICKNESS (m)	BRIEF LITHOLOGICAL DESCRIPTION
Upper Eocene to Oligocene	Tarapur Shale	-	60-100	Greenish, with little sand
Middle Eocene	Kalol	Kalol Pays (Kalol I to VI)	150-300	Alterations of coal, shale and sand stone.

AGE	FORMATION	PAY HORIZON	APPROX. THICKNESS (m)	BRIEF LITHOLOGICAL DESCRIPTION
Early Eocene	Kadi	U. Tongue Mehsana (Sobhasan Pays Ia, Ib, II, III)	10-100 50-200	Dark gray shale, Sand with intercalations of coal and shale (Sandwiched between two coal beds namely top Coal and bottom Coal).
		Lr. Tongue Mandhali (MP-I to MP-VIII)	10-40 50-350	Dark gray shale, Alterations of shale and fine grained sandstone, and/or siltstone with some coal seams in between).
	Older Cambay Shale	-	2100	Dark gray shale (occasionally carbonaceous and silty).
Palaeocene	Olpad	-	20-1500	Trap conglomerates with occasional claystone.
Upper Cretaceous	Deccan Trap	-	-	Basalt

1.6 Research Objective

- To understand and map the spatio-temporal patterns of groundwater decline in Kutch-Sabarmati basin.
- To assess the extent of potential land subsidence by predictive modelling approach by estimating aquifer system compaction due to groundwater over-extraction.
- Generation of subsidence time series maps from temporal SAR images using DInSAR techniques.
- Comparison and Correlation of satellite derived mean deformation velocity with model-based aquifer system compaction and decipher the deformation history of land subsidence in relation to groundwater.

1.7 Research Questions

- How far is groundwater depletion responsible for land subsidence?
- Can time series analyses of advanced DInSAR technique efficient enough to detect the trend of ground water depletion and how far are they comparable to the subsurface aquifer system compaction data ?
- Can DInSAR based subsidence mapping detect deformations over the petroleum basins?

1.8 Datasets Used

The following datasets were used in the present work for predicting and characterizing land subsidence in and around Mehsana.

Table 1.3: Datasets Used

Type of Data	Dataset	Data type	Specifications *	Purpose
Optical Data	**Digital Elevation Model (DEM)** Source: Earth Explorer	SRTM (1 arc second data)	n20_e071, n21_e070, n21_e071, n21_e072, n22_e070, n22_e071, n22_e072, n22_e073, n23_e069, n23_e070, n23_e071, n23_e072, n23_e073, n24_e068, n24_e069, n24_e070, n24_e071, n24_e072, n24_e073).	Watershed Delineation
Optical Data		Cartosat-1 stereo pair	- Path-0506, Row-0288, 01 May 2010, Orbit no-26999. - Path-0505, Row-0288, 07 March 2010, Orbit no-26184.	- Generation of precise DEM - Terrain Analysis
Optical Data	**Landsat - 8 OLI data** Source: Earth Explorer	LC81490432017277LGN00	Path 149, Row 43, DOA: 2017-03-29	LULC preparation
Optical Data		LC81490442017277LGN00	Path 149, Row 44, DOA: 2017-03-29	
Optical Data	**Rainfall Data** Source: IMD, Pune	IMD Gridded Rainfall (0.25 x 0.25) data	Data from 2005 to 2017	Trend Analysis of Rainfall
Microwave Data	**SAR data**	ALOS PALSAR-1 Fine beam polarization (FBS) L-Band data	- ALPSRP051590460-20070112 - ALPSRP058300460-20070227 - ALPSRP111980460-20080301 - ALPSRP118690460-20080416 - ALPSRP158950460-20090117 - ALPSRP165660460-20090304 - ALPSRP273020460-20110310	DInSAR based deformation modelling (2007-2011)
Microwave Data		ALOS PALSAR-2 Fine beam Dual polarization (FBD) L-Band data	- ALOS2019470460-141002 - ALOS2029820460-141211 - ALOS2040170460-150219 - ALOS2083640460-151210 - ALOS2093990460-160218 - ALOS2116760460-160721 - ALOS2127110460-160929 - ALOS2147810460-170216 - ALOS2170580460-170720 - ALOS2180930460-170928 - ALOS2199560460-180201	DInSAR based deformation modelling (2015-2018)
Microwave Data		RADARSAT-2 C-Band data	Image Acquisition Date: 09-12-2017, 19-02-2018 08-04-2018, 19-06-2018	DInSAR based deformation modelling (2017-2018)

Type of Data	Dataset	Data type	Specifications *	- Purpose
Ancillary Data	**Groundwater Data**	Piezometric data	Obtained from Central Ground Water Board, India (2005-2018)	- Trend Analysis of Groundwater - Geostatistical modelling - Aquifer compaction modelling
	Thematic Data	Administrative boundaries, roads, cities	Obtained from State portals and open source data	- Preparation of Thematic maps.
	Lithologs	Lithologs	Obtained from Central Ground Water Board, India	- Aquifer compaction modelling - Lithological modelling
	Aquifer data	Porosity and Aquifer compressibility data	Obtained from published scientific reports	- Aquifer compaction modelling.
	Geological data	Geological and Geomorphological maps, Subsurface geology	Obtained from published scientific reports of Geological Survey of India	- Preparation of Thematic maps.

* The nomenclature of SRTM images is through Origin Latitude and Origin Longitude. For e.g. in n20_e071 image, origin latitude is 20^0N and origin longitude is 71^0 E. ALOS PALSAR 1/2 images are read by scene ID followed by date of acquisition. For e.g. in ALPSRP051590460-20070112, ALPSRP05159046 is the scene id and 20070112 is the image acquisition date.

Table 1.4: Specifications of Microwave data

Orbital Parameters of ALOS PALSAR-1		
ALOS PALSAR-1	**FBS**	**FBD**
Spatial Resolution	Strip map: 10 m ScanSAR: 100 m	
Altitude	691.65 km (above equator)	
Inclination	98.16 degree	
Orbital Period	98.7 min	
Recurrent Period	46 days	
Polarization	HH	HV
Incidence angle (deg.)	7.9-60.0	7.9-60.0
Swath Width (km)	40-70	40-70

Orbital Parameters of ALOS PALSAR-2		
ALOS PALSAR-2	**FBS**	**FBD**
Spatial Resolution	Strip map: 3 m /6 m /10 m ScanSAR: 100 m Spotlight: 1 m x 3 m	
Altitude	628 km (above equator)	
Inclination	97.9 degree	
Orbital Period	97.33 min	
Recurrent Period	14 days	
Polarization	HH	HV
Incidence angle (deg.)	7.9-60.0	7.9-60.0
Swath Width (km)	40-70	40-70
Orbital Parameter of RADARSAT-2		
Spatial resolution	3-100 m	
Altitude	798km above the equator	
Inclination	98.6 degree	
Orbital Period	100.7 min	
Recurrent Period	24 days	
Imaging frequency	C-band at 5.405 GHz	
Polarization	Single, Dual or Quad	
Swath Width	18 km – 500 km, depending on operation mode	

1.9 Methodology

An overall simplified methodology used in the present work is discussed here. The methodology progresses from regional to local studies in the study area. To gain a Spatio-temporal understanding on the groundwater scenario at a regional/ basin scale statistical analysis of seasonal groundwater levels in piezometric wells was carried out using the non-parametric Mann-Kendall (MK) method and Sen's slope estimation from 2005 to 2017 at various locations, in Kutch and Sabarmati basin of Gujarat, with an aim of detecting and mapping the groundwater level trends present at the study locations, and identifying the probable factors behind the observed trends. Then a similar statistical analysis of average rainfall time series data in the area was done to see the impact of rainfall trends over the fluctuating ground water levels.

Further, to observe the change in falling or rising level due to depletion or recharge of groundwater, spatio-temporal modelling of post-monsoon and pre-monsoon time series groundwater data level fluctuations was done. Standard statistical interpolation techniques of Inverse Distance Weighted Interpolation (IDW) and Kriging were used to create the groundwater

fluctuation interpolated maps for every year which were later weighted using the Kalman filter algorithm that gives a more robust prediction though a statistical comparison of the new set of predicted values to the original set of observations. The Kalman filter weighted product was computed by summing the product of respective correlation coefficient of both IDW and Kriging with their predicted outputs, and then dividing by the sum of correlation coefficients. The process was repeated for every year to find the depletion rates of groundwater levels in Kutch-Sabarmati basin. Fluctuation maps were produced for both pre-pre and post-pre monsoon seasons for every year and Average fluctuation maps and Standard deviation maps were made to understand the changes in regional groundwater levels during the study period.

An understanding of the regional groundwater scenario in the Kutch-Sabarmati basin, was followed with estimating subsidence at a local level. The microwave data subsidence rates as inferred after pre-processing and phase unwrapping of available microwave ALOS PALSAR-1 images (2007 to 2011), ALOS PALSAR-2 (2015-2018) and RADARSAT-2 (2017-2018) images were compared to the elastic and inelastic compaction rates calculated from the Ground-based piezometer (water level) data and aquifer parameters at selected observation wells, to obtain a grounded result on the undergoing land subsidence at the study locations. The DInSAR processing was carried out in ENVI SARSCAPE 5.1 environment. The DInSAR derived subsidence rates were analysed over the petroleum oil fields of Mehsana Asset to monitor the deformations over the oil fields. The overall methodology is shown graphically in the flowchart below (Fig. 1.8).
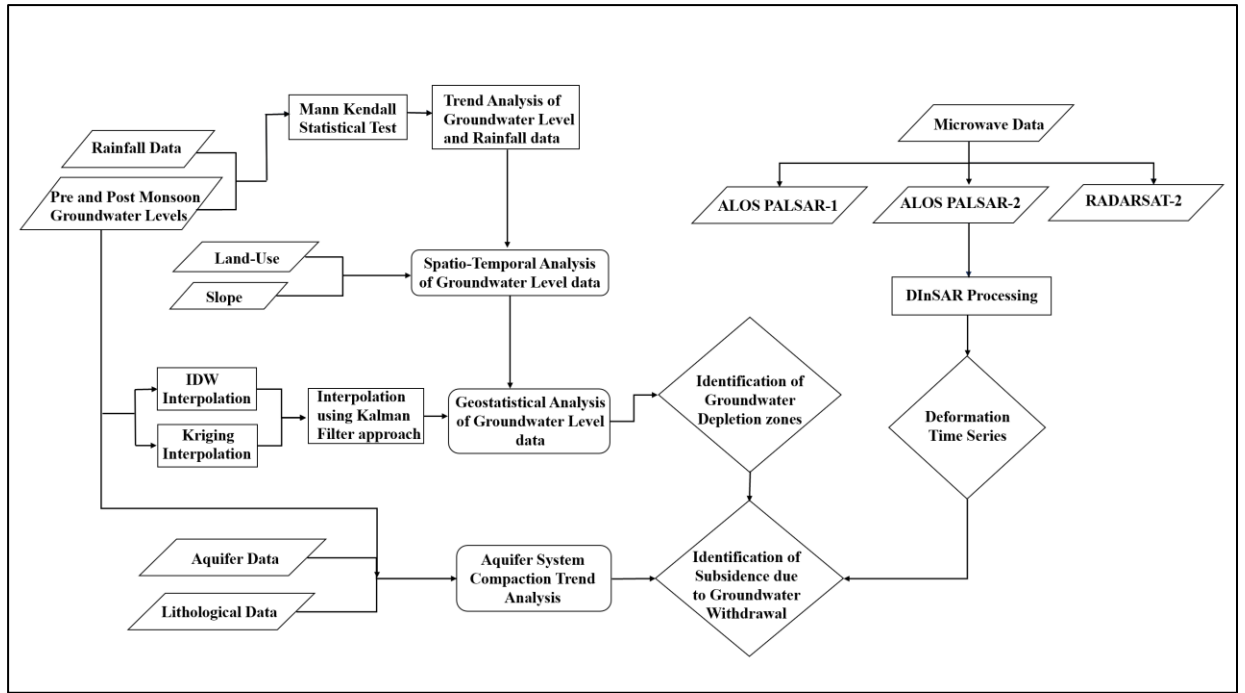
Fig 1.8: Flowchart for Overall Methodology for Estimation of Land subsidence

1.10 Structure and Outline of the Thesis

The thesis is outlined into six chapters and each chapter presented by Section, subsection and paragraphs.

CHAPTER 1: Introduction

This chapter briefly talks about the phenomenon of land subsidence and its consequences. It explains the probable causes, importance and history of land subsidence and the required motivation for study of groundwater induced subsidence. The chapter highlights the importance and applications of aquifer modelling as well as space borne techniques in studying, monitoring and mapping land subsidence at a regional and local scale with an unprecedented accuracy of millimetres to centimetres. The chapter describes in detail the Indian challenges in groundwater sustainability and provides a rationale for the research. A brief description of the study area along with the climate and hydrogeology is presented. Then the chapter comes up with the key objectives followed by research questions. At last, the chapter describes the datasets used for the study and the overall methodology used to accomplish the research work.

CHAPTER 2: Theoretical Background and Literature Review

Chapter 2 introduces all important concepts and theories adopted in predictive modelling of land subsidence. The chapter progresses from regional studies to localized studies. A brief description of groundwater studies at regional level and its correlation to land subsidence is presented. The regional studies include the nonparametric Mann Kendall Trend analysis along with Sen's slope estimation method, and the geostatistical methods of Interpolation. The latter part of the chapter focuses on the subsidence modelling at a local level and provides an overview of the conceptual framework for modelling aquifer-based Elastic and Inelastic compaction through an understanding of hydrogeological characteristics, and then provides a detailed description of advanced space borne Interferometry and Differential Interferometric SAR techniques for land subsidence mapping and monitoring. This includes the sensor and orbital information, baseline estimations, process techniques and the displacement mapping methods. Then the chapter explains the major field-based instrumentation techniques employed in subsidence measurements. Relevant research studies and literature review is presented throughout the chapter. The last part of the chapter discusses some of the significant previous studies carried out by various researchers and highlights their key findings.

CHAPTER 3: Regional Trend Analysis and Geostatistical Modelling of Groundwater levels.

Chapter 3 describes the methodological approach utilized for the study. The chapter discusses the regional and local characterization of groundwater in the study area and identifies the spatial extent as well as provides an estimate on the magnitude of the land subsidence due to over exploitation of groundwater. The application of Mann Kendall geostatistical trend analysis and Interpolation techniques with an emphasis on the more robust Kalman Filter based interpolation method at a regional scale is outlined. The understanding of recharge and depletion scenarios at a regional level gives a more precise input for studying land subsidence due to groundwater withdrawal at a local scale. Ancillary studies of rainfall, land use statistics and elevation parameters provide an insight into the observed spatial patterns of groundwater recharge and

depletion. The results and discussions are presented along with the respective work done.

CHAPTER 4: Aquifer Compaction and DInSAR Modelling of Land Subsidence due to Groundwater and Petroleum Extraction.

In Chapter 4 the detailed methodology and processing for estimating aquifer compaction-based land subsidence due to loss in piezometric head though the use of well-established Domenico's and Lohman's equations is illustrated with the computations of each of the input hydrogeological characteristics required for modelling. And finally, the DInSAR based subsidence modelling using ALOS PALSAR-1, ALOS PALSAR-2 and RADARSAT-2 InSAR data is highlighted with complete methodology, results and discussions. DInSAR based subsidence results due to groundwater and hydrocarbon extraction are shown with relevance analysis.

CHAPTER 5: Results and Discussions

Chapter 5 discusses the correlation of the results from aquifer compaction modelling and DInSAR modelling and provides a reasonable answer to the main research questions put forward for the present study. An analysis of Spatio-temporal subsidence rates over petroleum oil fields is made towards the last of the chapter.

CHAPTER 6: Conclusion

In Chapter 6 the main achievements and insights from the research of this thesis are presented, with possible future research directions proposed.

CHAPTER 2.   THEORETICAL BACKGROUND AND LITERATURE REVIEW

2.1 Introduction

Land subsidence is the gradual sinking of land in response to the excessive subsurface fluid withdrawal over the limit of its replenishment. The phenomenon is of great importance owing to its serious socio-environmental concerns such as damage to infrastructure, waterlogging, flooding, decreased aquifer yield, degradation of groundwater quality, increase in soil salinity and many others. Land subsidence occurs when there is a loss of aquifer pressure with the decline in the piezometric head and may vary seasonally and can be affected by climatic changes such as variability of rainfall patterns. To delineate and measure subsidence of land forms due to excessive drawdown of groundwater it is thus critical to investigate the spatial variability of groundwater level variations. The nonparametric Mann-Kendall test and the Sen's slope estimator is a useful statistical technique to estimate the Spatio-temporal trend of groundwater levels. The Mann Kendall test can statistically assess if there is an upward or downward trend of groundwater levels over time and can provide reliable indications to the regional variability of piezometric levels affecting aquifer compaction. Geo-statistics is an effective technique that is used to map groundwater variability in the region. Specifically, Inverse distance weighted (IDW), Kriging and Kalman Filter techniques provide information on regional variability of groundwater by performing spatial interpolation of measured groundwater observations obtained at various locations of the study area. An understanding on the spatial variability of piezometric head in the study area can be used to characterize the aquifer compaction at the local levels. The loss of piezometric head due to excessive withdrawal of groundwater leads to aquifer compaction causing the land to subside. Aquifer-System compaction is a function of the piezometric head, the depth of the total aquifer system and the hydrogeological characteristics such as

porosity and storativity of the aquifer. Changes in both elastic and inelastic aquifer compaction occur due to the decline of the piezometric heads coupled with the hydrogeological characteristics of the aquifers and provides an estimate of the magnitude of land subsidence. State of the art remote sensing techniques such as Differential Interferometric SAR techniques have been developed to monitor spatial and temporal patterns of ground deformation and provide highly precise measurements on land subsidence. The current chapter discusses the theoretical background of the regional and local methods employed for investigating groundwater levels and monitoring of land subsidence through aquifer compaction and DInSAR based techniques. Relevant literature review of the methods is presented throughout with a discussion on some of the previous case studies towards the end of the chapter.

2.2 Mann-Kendall Trend Analysis

The detection of trends in groundwater levels is very important for constant monitoring of ground water table fluctuations as well as to understand its response to other climatic parameters like rainfall and/or temperature. Time series analysis of the groundwater levels help in detecting the pattern, its conduct, and in identifying the causes of water level decline. Several statistical methods have already been designed and implemented to identify and quantify monotonic trends in hydrological time series data and have been divided into parametric and nonparametric tests. While parametric methods require that the data be normally distributed, and the sample size is sufficiently large, it provides a limitation in studying hydrological data as most of these data are usually not normally distributed (Yue et al., 2003; Kocsis, 2017). On the other hand, non-parametric methods, which are distribution-free, make no assumption on the population distribution or sample size, can be computed even if there are missing values or outliers, have been widely used to detect the existence of trend in a hydrological time series for groundwater monitoring applications.

One of the most widely used non-parametric trend detection tests is the Mann-Kendall (MK) test also known as Kendall's τau test or the Mann-Kendall trend test (Mann 1945, Kendall 1975, Gilbert 1987). MK test is

considered more suitable as its statistic are based on + and – signs instead of the values of the random variable, and hence the computed trends are less affected by the outliers present in the data series (Helsel et al., 1992). The MK statistical trend analysis is a hypothesis-testing process where null hypothesis (H_0) states that there is no trend and the alternative hypothesis (H_a) states that there is a trend and statistically assesses whether the variable of interest shows a monotonic upward or downward trend over the given time series.

Numerous studies have been conducted worldwide using the non-parametric Mann-Kendall test in hydrological time series data. Some examples of research studies and their key findings for detecting trends in groundwater time series using MK tests are briefly discussed in the subsequent texts. Rivard et al., (2009) conducted statistical trend analysis of historical series of baseflow and groundwater levels in Canada and found out that though most of the available groundwater time series showed significant trends, the base flow series did not show such trends. However, for slope estimates the groundwater level series showed smaller values than the baseflow series. Mair and Fares (2010), analyzed the spatio-temporal relationships between streamflow, rainfall, and groundwater for a small Hawaiian watershed using long-term data by employing MK tests. They also studied the influence of groundwater pumping on streamflow using multiple linear regression analysis. Their results suggested that though the rainfall did not show any significant trend over the years, the stream base flow as well as the total flow have gradually decreased, and that increased pumping has captured considerable amounts of groundwater that could have contributed to the stream flow. Tabari et al. (2012), used the MK test and the Sen's slope estimator to investigate the temporal trends in annual, seasonal and monthly groundwater levels using the in Iran. The statistical tests detected a significant increasing trend in more than 28% of the wells with significant positive trends during summer and spring months rather than autumn and winter. Their analysis also revealed that downward trends in relative humidity and increasing trends of temperature can be attributed to the fluctuations in the groundwater levels in the study area. Panda et al. (2012), utilized the Mann Kendall Slope test and linear regression to observe the

patterns in groundwater level, rainfall and temperature extremes for the western Indian state of Gujarat. They concluded that the groundwater withdrawal resulting in water table decline has happened due to droughts and increase in temperature in the arid areas and that the extreme events of rainfall have not been able to counteract this decline in the water table. Narjary et al. (2014) studied the temporal trends of rainfall and its variability on pre and post monsoon groundwater levels in Karnal district, India, using MK and Sen's slope approach. Their results indicated significant declining trend and emphasized the need of artificial groundwater recharge for the region. Ribeiro et al. (2015) combined the Mann-Kendall test, Sen slope test and principal component analysis to detect and map the monthly trends of piezometric time series. He found that most of the wells in his study area showed significant decreasing trends mainly due to the decrease in streamflow of the Elqui river derived mainly from snowfall rather than rainfall. Patle et al. (2015) worked on time series modelling of groundwater levels for forecasting the pre- and post-monsoon ground water levels in Karnal district of Haryana, using Mann-Kendall test and Sen's slope estimator. The ARIMA model results showed considerable decline in groundwater levels during their study period. They also quantified the average water level decline rate during the study period. Stasik et al. (2016) investigated the Trends in groundwater level changes in small forest catchments located in Wielkopolska region of Poland using the Mann-Kendall test. They found out that changes in groundwater level determined using the MK test were varied significantly between the forest habitats studied. A statistically insignificant increase in groundwater level was observed in moist mixed broad-leaved forest while a decreasing trend was seen in swamp and fresh mixed coniferous forest. Kumar et al. (2017) performed the Mann-Kendall trend, Sen's slope and regression slope analysis for annual and monthly rainfall data in five districts of south Gujarat and highlighted the spatio-temporal variability if rainfall in the area. Pathak et al. (2019) investigated the trends in groundwater levels and the regional groundwater drought characteristics of Ghataprabha river basin, India. MK test was employed to analyze the annual and seasonal groundwater-level trends and Standardized Groundwater level Index (SGI) was used to evaluate groundwater drought. A decreasing trend was

revealed in a large number of wells observed and the rate of decline was estimated. Their results from SGI analysis suggested that the recurrent droughts were attributed to the decreasing rainfall and increased groundwater exploitation.

The initial assumption of the MK test is that the null hypothesis (no trend) is true and that the data must be quite convincing before the null hypothesis is rejected and alternate hypothesis of existence of trend is accepted. The data values to be used in a MK test should be in an ordered time series. The test evaluates every value to every value preceding it in the time series, giving a total of n (n − 1) / 2 pairs of data, where "n" is the number of observations in the series and then computes the Mann-Kendall statistic (S) which measures the trend in the data. While, positive values of S indicate an increasing or upward trend, negative values give an indication towards a decreasing or downward trend in the time series. Larger values of S denote a stronger magnitude of trend and vice versa.

The first step in Mann Kendall computation is to determine the sign for all possible differences x_j - x_k, where $j > k$ for all n (n − 1) / 2 pairs of data. Sign (x_j - x_k) is an indicator function that results in the values of 1, 0, or -1 in accordance to the sign of x_j - x_k where $j > k$.

The function is calculated as follows in eq. (1)

$$\text{Sign}(x_j - x_k) = \begin{bmatrix} 1 & \text{if } xj\text{-}xk & > 0 \\ 0 & \text{if } xj\text{-}xk & = 0 \\ -1 & \text{if } xj\text{-}xk & < 0 \end{bmatrix} \qquad (1)$$

As an example, if (x_j - $x_{k)}$ > 0, it means that the observed data at time j, denoted by x_j, is greater than the observation taken at time k, denoted by x_k. Then the Mann-Kendall statistic (S) is assessed which is defined as the sum of the number of positive differences minus the number of negative differences in the time series x_1, x_2…. x_n, and is calculated in eq. (2) below.

$$S = \sum_{k=1}^{n-1} \sum_{j=k+1}^{n} sign(x_j - x_k) \qquad (2) \qquad [\text{from Gilbert, 1987}]$$

Where, n is the number of points, and x_j and x_k are the data values in time series j and k (j > k), respectively.

"If S is a positive number i.e. S>0, then the observations obtained later in time tend to be larger than observations made earlier and shows an upward trend and if S is a negative i.e. S<0, then the observations made later in time tend to be smaller than observations made earlier and indicates a downward trend" [3]. A value of 0 for S indicates that there is no trend.

Kendall's τ is a rank statistic that estimates the strength and direction of relationship existing between two variables that have been measured on an ordinal scale. The Tau correlation coefficient gives a value between 0 and 1, where 0 indicates that there is no relationship between the variables, and 1 indicates a good association. Kendall's τ is closely related to the S statistics and is given by eq. (3) below.

$$\tau = S / D \tag{3}$$

Where, D is the maximum possible value of S which occurs when $x_1 < x_2 < \ldots x_n$. [Renato et al., 1998].

The p value assesses the presence of a statistically significant trend. If the p value is less than a pre-specified value (α, acceptable type I error) set for the analysis, the null hypothesis is rejected. In our study, the trend was statistically evaluated at a significance level of $\alpha = 0.05$. At 5% significance levels p-values smaller than 0.05 indicate that there is a significant upward or downward trend in the time series and that we can reject the null hypothesis pertaining to no trend [2]. The trend is said to be decreasing if S is negative and the p value is greater than the level of significance, and if the S value is positive and the p value is also greater than the level of significance, the trend is considered to be increasing. If the computed p value is less than the level of significance there is no trend.

The final step of the time series analysis is the quantification or estimation of the magnitude of trend if detected. To quantify the rate of change per unit time, of an existing trend the Sen's estimator method is employed (Sen,

1968). This method has been used widely by various researchers to determine the magnitude of the trend in hydrological time series and firstly computes the slopes for all the n pairs of time points Q_i using the eq. (4) below.

$$Q_i = \frac{x_j - x_k}{j - k} \qquad \text{for i = 1,2,3 ……..n} \qquad (4)$$

Where, x_j and x_k are data values at time j and k (j>k) respectively. Then the overall slope Q is calculated using the median of these slopes in eq. (5).

$$Q = Q(n+1)/2 \qquad \text{if n is odd,} \qquad (5)$$

$$Q = [Qn/2 + Q\,(n+2)/2)]/2 \qquad \text{if n is even}$$

A positive value in the magnitude of Sen's slope shows an increasing trend and a negative value suggests a decreasing trend during the given time series. An important consideration here is that since the groundwater levels are measured relative to the ground surface, it implies that higher values of groundwater levels relate to deeper water table and vice-versa. Therefore, in Mann-Kendall results, a positive value of S indicates a decrease in groundwater level and a negative S value indicates its increase.

The present study tries to assess and estimate the groundwater level trends during pre and post monsoon months and investigate the effect of variability of rainfall on groundwater levels using the Mann Kendall, Sen's Slope estimator and linear regression methods, thereby understand the response of groundwater systems to rainfall stresses in Kutch Sabarmati basin of Gujarat.

2.3 Statistical Interpolation of Groundwater Level (GWL) Data

Statistical interpolation methods are the advanced geostatistical techniques used for interpolation of groundwater data and play an important role in management of groundwater resources. Understanding the spatio-temporal patterns of groundwater recharge and depletion is a crucial aspect of groundwater sustenance studies. The importance of geostatistical tools in groundwater studies stem from the limitation in availability of groundwater

monitoring data at all locations. Geostatistical methods not only provide accurate estimates of values at locations where samples were not taken but also give information on estimation errors for the corresponding interpolation technique. Interpolation techniques are classified under two main groups: deterministic and geostatistical. While the deterministic interpolation techniques such as Inverse Distance Weighted (IDW) method use the extent of similarity in measured data to create raster surfaces, geostatistical interpolation techniques such as Kriging utilize the statistical properties of the measured data to evaluate the spatial correlations considering the covariance and variogram functions (ArcGIS resources).

Groundwater levels are measured throughout India by the Central Ground Water Board (CGWB), four times every year through an extensive network of monitoring wells in the months of January, May (Pre-monsoon), August and November (Post monsoon). Based upon the Groundwater level change, monitored specifically during pre-monsoon and post-monsoon periods a time series analysis spatio-temporal modelling of groundwater level data can be done using the standard geostatistical techniques of Inverse Distance Weighted Interpolation (IDW) and Kriging, to observe the change in falling or rising groundwater level due to depletion or recharge of groundwater. To obtain much better estimates of the variables from inaccurate measurements Kalman Filter algorithm can be used. The Inverse Distance Weighted Interpolation (IDW) and Kriging methods can be weighted using the Kalman filter algorithm that gives a more robust prediction though a statistical comparison of the new set of predicted values to the original set of observations.

2.3.1 Inverse Distance Weighted Interpolation

The Inverse Distance Weighted (IDW) interpolation is one of the most widely used spatial interpolation methods in geoscience applications due to the simplicity of method and fast computations of predictions at unknown locations. The IDW technique is based on Tobler's first law of geography (Tobler 1970), which states that "everything is related to everything else, but near things are more related than distant things". IDW assumes that sampled

values closer to the prediction location have more influence on the predicted values. As such, in the IDW algorithm, the assigned weights are inverse of the distance from the interpolation point, with higher weights assigned to the locations closet to the prediction location. The inverse of the distance is raised to a mathematical power which controls the significance of surrounding points on the interpolated values based on their distance from the output point. A higher power values gives more weightage to the nearest points (ArcGIS resources). This IDW interpolation is an exact interpolator i.e. the interpolated surface passes through all measured points and the interpolated surface never crosses the minimum and maximum values in the input. The IDW uses the following equation to predict values at unknown points eq. (6)

$$z_p = \frac{\sum_{i=1}^{n}(\frac{z_i}{d_i{}^p})}{\sum_{i=1}^{n}(\frac{1}{d_i{}^p})} \tag{6}$$

The Sigma notation signifies that the total number of points to be interpolated are added, Z_i is the measured value and z_p is the predicted values, d_i is the distance between the observed values and p is the power.

2.3.2 Kriging Interpolation

Kriging is another interpolation technique used in geosciences to interpolate values at unknown location from measured points. The algorithm not only creates a prediction surface but also provides a measure of the uncertainty or accuracy of the predictions through estimation errors. Kriging considers both the distance between known and the predicted locations, as well as the variance between sample points to estimate values at unknown locations. The technique assumes that distance and direction between sample points show a spatial correlation that could explain the surface variations. It is commonly used when there is a spatially correlated distance or directional bias in the data. The most important thing in kriging is the variogram, which describes the relationship between distance and the spatial variability of the parameters and shows the possible existence of anisotropy in different directions of the variable. The variogram and covariance estimate the statistical relationship or spatial

autocorrelation between values depending on the type of fitted model. The modelling of spatial autocorrelation using a variogram makes Kriging different from IDW where the algorithm assumes a direct linear relationship with the separation distance between the input points. In Kriging the weights are determined depending on the values of variance and covariance between the pairs of points and the points with high covariance gets more weight in comparison to the point with low covariance.

The kriging interpolation method generates an interpolated surface through a three step process: 1) Determination of empirical variogram which measures the spatial variation and autocorrelation for the variable of interest, 2) Fitting the variogram with a theoretical model (such as spherical, gaussian, circular or exponential) to provide the necessary input parameters for the algorithm to compute values; and 3) Create a interpolated surface using the fitted model. Kriging uses the following formula to predict values at unknown points (eq. 7).

$$\hat{Z}(x_0) = \sum_{i=1}^{n} \lambda_i Z(x_i) \qquad (7)$$

where $\hat{Z}(x_0)$ is the predicted value at location x_0, $Z(x_i)$ is the measured value at location x_i, n is the number of measured values within the search neighbourhood, and λ_i is the weight for the measured value at the ith location. The weight being based on the parameters of the fitted model.

2.3.3 Kalman Filter

The Kalman filter developed by Rudolph Kalman in 1960 is another estimation algorithm that provides much better estimates of the variables from inaccurate measurements. The Kalman filter is used because it minimizes the variance of the estimation error (Rajan 2014). The technique can estimate the temporal dependence as well as the spatial correlation between variables and can provide statistical results both in terms of parameter estimation and prediction at unknown locations (Bernardo et al., 2019). To generate estimates of true and calculated values, the algorithm follows three steps in a recursive process: 1) Predicts a value 2) Calculates the uncertainty in

the predicted values 3) Calculates a weighted average of both the predicted and measured values (UmaMageswari et al., 2012). The weights are calculated from the covariance of the estimated uncertainty of the predicted values from the original values and produces a new set of point values where statistical comparison can be made from the new set of predicted values to the original set of values. The results obtained by the Kalman method gives estimates that are closer to the true values. For the present study, groundwater depletion maps for every year were prepared using the Kalman filter approach.

2.4 Aquifer System Compaction and Land Subsidence

An aquifer system generally comprises of flat lying aquifers interbedded with aquitards or aquicludes that confine fluid pressures in the underlying layers. When groundwater is being over extracted from such aquifer systems, the consolidation of these confining units or aquitards which are mostly clay and silt layers, results in aquifer compaction.

In a confined aquifer, compaction occurs when the piezometric head declines, which decreases the support for overlying sediments and results in an increase in the total vertical effective stress on the aquifer system. Therefore, the decline in the piezometric head is a direct measure of the increase in stress on the aquifer framework. However, in an unconfined aquifer, the decline in the water level however leads to a decrease in the buoyancy and loss in the support to the aquifer matrix. Land subsidence occurs when large amounts of groundwater that is partly responsible for holding the induced geostatic stress on the aquifer framework, is withdrawn from the fine-grained sediments such as silt and clay. Excessive withdrawal of groundwater leads to a decline of water table or piezometric surface and consequent drop in the pore pressure, thereby increasing the effective stress exerted by the overlying solid matrix and tends to deform the intergranular structure of the aquifer framework by creating more stress on the granular pores of the aquifer (Bouwer 1977). Initially the effective stress on the aquifer system is supported by the solid matrix of the aquifer and the fluid pressure within the system (Jacques, 1999; Quanlong, 2006). As the water is being is being pumped out of the aquifer there is a drop in the pore

48

pressure and the porosity thereby increasing the effective stress exerted by the solid matrix above. Consequently, the matrix compresses, and aquifer compaction takes place. Conversely, if the water is pumped into the aquifer through natural or artificial methods, the fluid pressure is restored and the effective stress decreases (Jacques, 1999). Also, during the heavy withdrawal of ground water the fall in piezometric pressure head produces a reverse hydraulic gradient between the aquifer and overlying confining layers. resulting into the leakage of pore water from the overlying confining layers leading to inelastic compression of confining layer materials. The deformation of the aquifer skeleton in turn results in the vertical compaction of the subsurface materials. The amount of aquifer compaction is essentially equivalent to the subsidence of the land surface (Carpenter, 1987).

Hydraulic conductivity is an important and crucial parameter useful for understanding the concept of movement of groundwater in an aquifer. The time required for a given amount of aquifer compaction to occur is dependent on the hydraulic conductivity, storage, and thickness of the aquitard (Epstein, 1987). Aquifer compaction is controlled by a number of parameters, including the patterns of water level decline, as well as the aquifer compressibility, porosity, storage coefficient, and the thickness of the compacting layers. The rate of aquifer compaction relies on the subsurface soil properties and clay and mud compacts more as compared to sand and rock (Ganguli, 2011).

Changes in aquifer compaction may be both elastic and inelastic. While elastic compactions are reversible and could be recovered after the induced stress is removed, inelastic compactions are irreversible or permanent and occur due to the decline in water levels in the confining layers of the aquifers having low vertical hydraulic conductivity and where regain of fluid pore pressures is slow due to the presence of clay or silty clay interbeds (Poland et al., 1972). Because of water over draft there is a fall in the piezometric pressure head between the aquifer and the overlying confining layers and the water is released from the confined layers into the aquifer below and undergo inelastic compaction (Chatterjee et al., 2013; Boni et al., 2016). Inelastic

compaction plays a major role in land subsidence in comparison to elastic compaction due to its irreversible nature.

2.4.1 Aquifer System Characteristics

Aquifer compaction is controlled by a number of aquifer system characteristics including the patterns of piezometric head decline, as well as the aquifer compressibility, porosity, storage coefficient, and the thickness of the compacting layers. The key aquifer parameters involved in aquifer compaction are discussed below.

i. **Pore-Pressure:** Pore water pressure is the pressure exerted by groundwater within the rock or soil particles, in gaps between the pores. The water present in the voids of the rock or soil particles is under pressure either because of the physical location of the particles or because of the geostatic pressure and is measured relative to the atmospheric pressure. The pore water pressures below a phreatic or fully saturated zone is measured with the help of piezometers.

ii. **Piezometric head:** Piezometric head also known as Hydraulic head is one of the most important parameters while describing a groundwater system and is a measure of fluid pressure above a vertical datum. In situ measurements of piezometric or hydraulic head are carried out by measuring the water level elevations in wells and are accomplished using piezometers (Ge and Gorelick, 2015). In a confined aquifer, it is calculated from the depth to water in a piezometric well and information of the piezometer's elevation and screen depth. The piezometric head measured at the surface of the well is obtained by subtracting the elevation of the bottom of the well from the elevation of the water surface. The piezometric or hydraulic head is represented as h = hp+hz, where hp denotes the pressure head and hz is the elevation head. The pressure head represents the energy due to pore fluid pressure, and the elevation head represents the gravitational potential energy arising from elevation. All three parameters have length dimension [L]. Groundwater flows from regions of higher hydraulic head to regions of lower hydraulic head. And this change in hydraulic head along the direction of

groundwater flow is known as hydraulic gradient. The figure below shows how hydraulic head is measured in a well. The water rises in the well from point "A" in the figure to the measured water level because of pressure energy (Fig. 2.1).
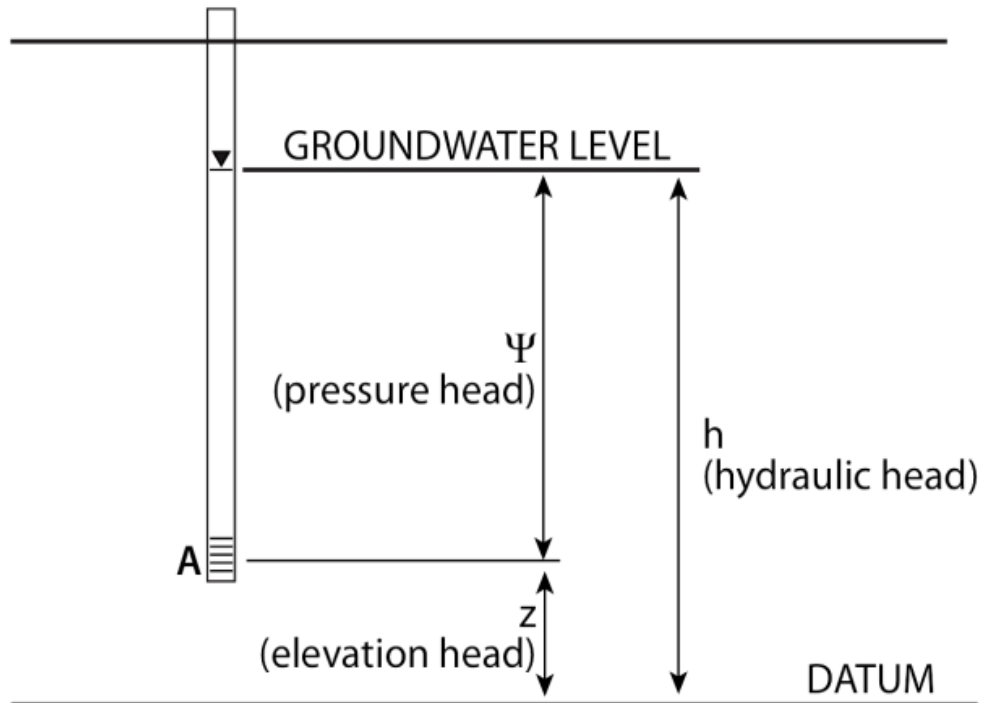
Fig 2.1: Diagram showing the components of Hydraulic Head measured at point "A" where the well is screened and connected to the subsurface formation. (Source: Maureen Feineman, Pennsylvania State University).

iii. **Compressibility of Water:** Compressibility is defined as the relative change in volume per unit increase in pressure. Fluids are compressible and an increase in pressure (*dP)* will lead to a decrease in the volume of a given mass of water (V_w). The compressibility of water is represented by the coefficient β (m^2/N) and is given by eq. (8) below.

$$\beta = \frac{-(dV_w)/V_w}{dP} \qquad (8)$$

where *dVw* is the change in the volume of the water, V_w is the original volume of the water, the *dP* is the change in pressure. The negative sign is necessary to ensure a positive β and that an increase in the applied external pressure will result in a decrease in the volume of the water. The Compressibility of

an aquifer is more dominant in case of a completely saturated confined aquifer.

iv. **Effective Stress:**

The weight of overlying rock and water creates a downward stress (σT) on a saturated aquifer. This stress is borne by the porous aquifer skeleton and the fluid pressure p of the water in the pore spaces. The relationship which is based on theory given by Terzaghi K. (1925) is defined as eq. (9) below.

$$\sigma e = \sigma T - p_w \tag{9}$$

where σe is the effective stress, σT is the total stress (the total overburden load or geostatic pressure) and p_w is the fluid or pore water pressure. Effective stress cannot be measured directly by any instrument but can only be calculated after measuring total stress and pore pressure.

v. **Aquifer Compressibility:**

When the water is pumped out from a confined aquifer the pressure head reduces causing an increase in the effective stress increases. The change in stress regime causes compaction of the aquifer due to the compression of the confining units. Aquifer Compressibility (α) can be expressed as eq. (10).

$$\alpha = -\left(\frac{db}{b}\right)/d\sigma e \tag{10}$$

Where b represents the original aquifer thickness, db is the variation in aquifer thickness and $d\sigma e$ is the change in effective stress. The negative sign implies that the increase in effective stress leads to decrease in aquifer thickness or compaction. It may be elastic compaction or inelastic compaction depending upon the effective stress; if the value of effective stress is smaller than the previous maximum effective stress which can be recovered than the elastic compaction occurs and if its value is more than inelastic compaction occurs which leads to permanent deformation (Galloway et al., 1998).

vi. **Specific Storage:**

The specific storage (Ss) of a saturated aquifer is one of the aquifer properties that characterizes the capacity of an aquifer to release groundwater from storage in response to a decline in hydraulic head. It is defined as the volume of water released from the storage per unit volume of the aquifer per unit

decline in hydraulic head. Water may be released from the storage due to three mechanisms i) either due to a decrease in the hydraulic head (h) ii) due to the expansion of the water caused by decreasing fluid pressure (p) iii) because of the compaction of the aquifer induced by the increasing effective stress (σe). Specific storage of a confined aquifer Ss depends on both the compressibility of water (β) and the compressibility of the aquifer (α) and is given by eq. (11) below.

$$Ss = \rho g(\alpha + n\beta) \tag{11}$$

Specific storage has the units of length [L-1].

vii. **Storativity (Storage Coefficient):** Storativity (S) of a confined aquifer of thickness *b* is the volume of water released from the storage per unit surface area of the aquifer per unit decline in hydraulic head or potentiometric surface. and is given by eq. (12) below.:

$$S = Ssb \tag{12}$$

Storativity is a function of the compressibility of water (β) and aquifer material and is proportional to the aquifer thickness and thus can also be given as eq. (13) below.

$$S = \rho g b(\alpha + n\beta) \tag{13}$$

Storativity is a dimensionless quantity, with values always greater than 0. The storativity values for confined aquifers vary from 0.00005 to 0.005 while for unconfined aquifers the values for are much higher in the range of 0.02 to 0.30 (Murthy, 2002). Therefore, for the same decline in hydraulic head, the total volume of water released from an unconfined aquifer will be much greater than the volume of water released from a confined aquifer.

2.4.2 Relationship Between Piezometric Head, Pore Pressure and Effective Stress

Land subsidence occurs when there is a loss of aquifer pressure with the decline in the piezometric head resulting in increase in total effective stress. The relationship between piezometric head, pore pressure and effective stress is summarized below.

The principle of effective stress as proposed by Terzaghi K. (1925), which states that effective stress σe of soil can be expressed by eq. (14) below.

$$\sigma e = \sigma T - pw \qquad (14)$$

where σT is the total stress (the total overburden load or geostatic pressure) and pw is the fluid or pore water pressure.

In a confined aquifer, the geostatic pressure changes negligibly with changes in fluid pressure in the confined aquifer, so that σT =0 and the change in the effective stress is due to the change in pore water pressure (Poland et al., 1972) and is given by eq. (15) below.

$$\Delta\sigma e = -\Delta pw \qquad (15)$$

which implies that with the increase in fluid pressure, the effective stress decreases by an equal amount.

The change in pore water pressure, Δpw is in turn caused by the change in groundwater level and is expressed as eq. (16).

$$\Delta pw = \rho wg\Delta h \qquad (16)$$

where ρw is the water density, g is gravitational constant and Δh is the change in groundwater level. From eq. (15) and (16),

$$\Delta\sigma e = -\rho wg\Delta h \qquad (17)$$

Eq. (15) above implies that as the water is being pumped out from the confined aquifers, the pressure head reduces and hence increases the effective stress in the depleting and intermediate layers leading to sediment compaction. Eq. (17) implies that in a saturated aquifer the change in the hydraulic head at a known position completely determines the change in effective stress at that point.

2.5 Predictive Modeling

Mathematical solutions have been proposed for calculation of the compaction resulting from changes in hydraulic head. One-dimensional and three-dimensional consolidation theories proposed by Terzaghi (1925) and Biot (1941) respectively are generally used for analysis of compaction. While the

three-dimensional consolidation theory can predict horizontal displacements as well as vertical ones, one dimension theory assumes that the displacement is taking place only in the vertical direction.

Though horizonal deformations can be important in an aquifer system (Helm, 1994), most of the authors have neglected it, as large amount of uncertainties in assessing the soil parameters like Poisson's ratio, anisotropy, etc. are likely to offset the expected accuracy from a three-dimensional model (Okuyan, 2000). Another reason for neglecting the horizontal deformation is the geometrical distribution of the aquifer material. The compacting layers of an aquifer are mostly contained in sub horizontal layers having higher lateral extensions than vertical. The compacting layers cannot move freely in the horizontal direction as they are sandwiched between the over and underlying sediments which restrict them from undergoing significant deformations horizontally. The major confining units in an aquifer system are the clay and silt layers and have low vertical hydraulic conductivities. The pressure gradient in these layers is almost exactly vertical which suggests more relevancy of one-dimension model of compaction. (Hoffman, 2003). Higher values of hydraulic conductivity are generally associated with unconfined aquifers that yield water to water wells or springs, whereas lower values of hydraulic conductivity are largely associated with confining units which separate unconfined aquifers from deeper confined aquifers (Fryar and Mukherjee, 2019).

Amongst the various studies worldwide, utilizing the one-dimension model of compaction. Chatterjee et al., 2006; Bhattacharya, 2011; Sahu and Sikdar, 2011; Sikdar et al., 1996 and Sahu and Sikdar, 2011 used the one-dimension consolidation theory to assess land subsidence in Kolkata, India. The present work uses one-dimensional elastic theory and Terzaghi's consolidation theory for studying the aquifer compaction in the study area.

To assess the cause of land subsidence due to compaction of aquifer system due shortening of the confining layer estimated by predictive modelling, using various parameters such as decline in the piezometric head in a year, bulk modulus of compression of aquifer grain structure, the thickness of

aquifer, capillary rise the porosity of the aquifer. (Chatterjee et al., 2013).

2.5.1 Elastic Compaction

The elastic consolidation of an aquifer refers to the compaction that can be recovered after the induced stress is lifted. The elastic consolidation of the confined aquifer is related to the storativity and compressibility. Lohman (1961) developed an equation to compute the amount of elastic compaction in aquifers to due to extraction of groundwater. To calculate the land subsidence due to elastic compaction in confined aquifers at our study locations, we used the Lohman's equation based on the subsurface lithology and change in hydraulic head during pre and post monsoon which is expressed as eq.(18) below.

$$\Delta b = \Delta p \left(\frac{S}{\gamma_w} - nb\beta\right) \tag{18}$$

The Storage coefficient was calculated from the Jacob (1940) equation and is expressed as eq. (19) as given below.

$$S = \gamma_w * b(\alpha + n\beta) \tag{19}$$

Where, Δb is the land subsidence (m), Δp is the reduction in piezometric pressure (N/ m^2) which is given by unit weight of water γ_w times the piezometric head, eq. (19) above; S is the Storage coefficient, γ_w is the specific weight of water (9810 N/ m^3), n is the porosity of aquifer (in decimal fraction), b is the saturated thickness of aquifer (m), $\beta = 1/ K_w$, inverse of the bulk modulus of elasticity of water $K_w = 2.1 * 10^9$ N/ m^2 and α is the compressibility of the aquifer material and is calculated by the reciprocal of the bulk modulus of elasticity of aquifer skeleton i.e. $\alpha = 1/ E_s$.

The saturated thickness of aquifers (b) was calculated from the lithologs, and the values of E_s were taken from the tables as provided by (Domenico and Mifflin, 1965, Table 2.1). The porosity values of the aquifer materials were taken from the values provided by (Brassington, 1998, Table 2.2). The piezometric head decline used to calculate the reduction in piezometric pressure

Δp was calculated by subtracting the pre-monsoon water level from post monsoon water level.

Table 2.1: Specific storage values adopted from Domenico and Mifflin (1965)

Material	Modulus of Elasticity $E_{s\,(N/m^2)}$	Specific Storage (γ_w/E) $S_s\,(m^{-1})$
Plastic Clay	$4.78 * 10^5 – 3.82 * 10^6$	$2.03 * 10^{-3} – 2.56 * 10^{-}$
Stiff Clay	$3.82 * 10^6 – 7.65 * 10^6$	$2.56 * 10^{-3} – 1.28 * 10^{-}$
Medium hard clay	$7.65 * 10^5 – 1.43 * 10^7$	$1.28 * 10^{-3} – 9.19 * 10^{-}$
Loose Sand	$9.56 * 10^5 – 1.91 * 10^7$	$1.02 * 10^{-3} – 4.92 * 10^{-}$
Dense Sand	$4.78 * 10^7 – 7.65 * 10^7$	$2.03 * 10^{-4} – 1.28 * 10^{-}$
Dense sandy gravel	$9.56 * 10^7 – 1.91 * 10^8$	$1.02 * 10^{-4} – 4.92 * 10^{-}$
Rock, fissured, jointed	$1.43 * 10^8 – 2.99 * 10^9$	$6.89 * 10^{-5} – 3.28 * 10^{-}$
Rock, sound	Greater than $2.99 * 10^9$	Less than $3.28 * 10^{-6}$

Table 2.2: Porosity values adopted from Brassington (1998)

Material	Porosity (%)	Specific Yield (%)	Fraction of Porosity producing specific yield
Coarse Gravel	28	23	0.80
Medium Gravel	32	24	0.75
Fine Gravel	34	25	0.73
Coarse Sand	39	27	0.69
Medium Sand	39	28	0.7
Fine Sand	43	23	0.53
Silt	46	8	0.17
Clay	42	3	0.07
Dune Sand	45	38	-
Loess	49	18	0.37
Peat	92	44	0.48
Till (mainly silt)	34	6	-
Till (mainly sand)	31	16	-
Till (mainly gravel)	-	16	-
Fine-grained sandstone	33	21	0.54
Medium-grained	37	27	0.64
Limestone	30	14	0.47
Dolomite	26	-	-
Siltstone	35	12	-
Mudstone	43	-	-
Shale	6	-	-
Basalt	17	-	-
Tuff	41	21	0.51

Schist	38	26	-
Gabbro (weathered)	43	-	-
Granite (weathered)	45	-	0.80

2.5.2 Inelastic Compaction

The subsidence due to Inelastic compaction is calculated from the equation given by (Domenico, 1972) which is expressed as eq. (20) below.

$$\Delta b_c = \frac{\gamma_w}{E_c} * \Delta h * m_c \qquad (20)$$

Where, Δb_c is the amount of inelastic compaction (m) or the amount of change in thickness of the confining layers; γ_w = specific weight of water (9810 N/m^3), E_c is the bulk modulus of compression of confining beds, Δh is the piezometric head decline (m) and m_c is the thickness of the confining bed (m).

Δh for inelastic compaction was calculated by subtracting the recent pre-monsoon water level from the preceding year's pre-monsoon water level. The thickness of the confining beds (m_c) was calculated from the lithologs and the values of E_c. were taken from the tables as provided by (Domenico and Mifflin 1965).

2.6 Interferometry

2.6.1 Synthetic Aperture Radar (SAR)

Synthetic Aperture Radar (SAR) imaging, is a technique that allows remote mapping of the reflectivity of objects or environments with a very high spatial resolution, through the emission and reception of electromagnetic signals (Laurent F.F. et al., 2016). The different frequency domains available in Synthetic Aperture Radar (SAR) devices, make them capable of producing very high-resolution images day and night and the sensing is not impacted in any weather condition. SAR systems can be mounted on airborne and/or satellite sensors and can scan vast areas of land surface and environments that may be inaccessible or difficult to reach and have proved to be very useful in many remote sensing applications. Mostly, a synthetic aperture radar is side-looking which means that the sensor looks at the earth's surface at an angle rather than

looking completely down at Nadir. The coherent measurements taken by Synthetic Aperture Radar (SAR) helps in synthesizing EM maps with a much higher resolution than fixed radar systems. They are an improvement over fixed radar systems as they use small antennae and relatively long wavelengths to achieve good azimuth resolution independent of the slant range to the target. The distance between the two satellites (or orbits) in the plane perpendicular to the orbit is called the interferometer baseline and its projection perpendicular to the slant range is the perpendicular baseline (Ferretti et al., 2001) and is shown in fig. 2.2. A synthetic aperture is produced by using the forward motion of the radar. As the radar passes over a scatterer many pulses are reflected in a sequence. By recording and then combining these individuals signals, a "synthetic aperture" is created electronically providing a much-improved azimuth resolution (ESA Radar Courses, 2019). These reflected pulses from each individual target are received by the SAR antennas and are utilized to reconstruct imaging scenes of the surface and forms the basis of SAR processing. The capacity of providing very precise measurements on land displacement with or without the aid of ground-based measurements make SAR data a perfect approach in studying land subsidence phenomenon.
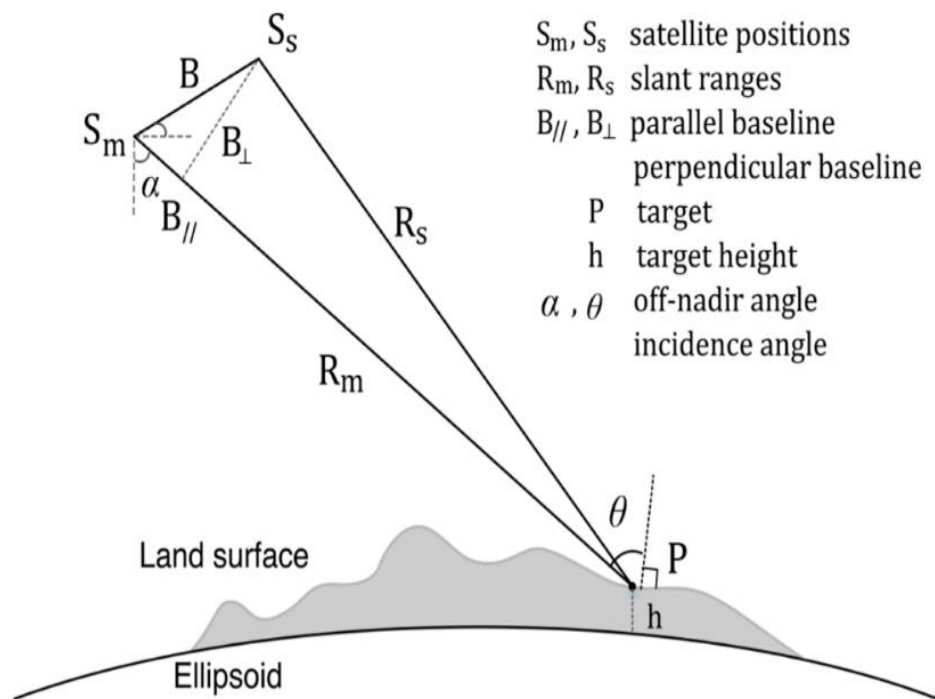
Fig 2.2: SAR Imaging Geometry. Subscripts m and s denote the Master and Slave Images of SAR Image pair.

2.6.2 SAR Interferometry

The SAR interferometry technique uses two SAR images of the same area acquired at different times and "interferes" (differences) them, resulting in maps called interferograms that show ground-surface displacement (range change) between the two time periods" (Laurent F.F. et al., 2016). SAR Interferometry is based on the fact, that by using two images of the same area it is possible to calculate an Interferogram capable of sensing changes in the position of the scatterer within the ground pixel. SAR images are acquired independently and record the amplitude and the phase information of the surface in the image pixels, with the phase information of major interest while doing interferometry for deformation modelling. Two SAR images whose phases are not aligned can thus be combined to observe the interference pattern of the surface. The Interferogram can be generated by cross-multiplying one image by the complex conjugate of the other image on a pixel by pixel basis (Massonnet, 1998). The reference image which is usually the earlier period is called a 'Master' Image and the other image is called as 'Slave' Image. Interferometric Synthetic Aperture Radar (InSAR) uses the differences in these reflected radar signals acquired from nearly the same antenna position (viewing angle) but at different time intervals (Rosen et al., 2000). This ability of SAR systems to extract the phase difference between two coherent measurements, enables them to derive the distance information (Woodhouse, 2006). In SAR interferometry technique, the amplitudes of the corresponding pixels are averaged, and the phase values are differenced for every point of the image. The interference between the phases of two SAR images of the same area generates an interferogram with several interference fringes. Each interference fringe that corresponds to the phase difference is given in the range of $-\pi$ to $+\pi$ and is called modulo 2π (Liang et al., 2021). The fringes are colour coded to show the phase differences.

Interferogram formed is a complex product of two component SAR images which can be taken simultaneously by an aircraft with two antennae separated by a distance known as the baseline and is known as "Single Pass or Single-Track Interferometry." However, if the images are acquired by

60

the satellite in two different passes of the same satellite, it is called as "Repeat Pass Interferometry." While single pass interferometry is generally used for rapidly changing surfaces, repeat pass interferometry is preferred over slowly varying terrains (Zhou et al., 2009).

An InSAR interferogram is formed by coregistration of two SAR phase image of the same area. The quality of the interferogram generated depend on the coherence if the images which is the amount of resemblance of radar phase between multiple (two) SAR images of the same area. Coherence is a useful measure to infer the quality of the interferograms produced and is an important parameter for applying efficient phase unwrapping procedures (Rodriguez and Martin, 1992; Zebker et al., 1997, Agram et al., 2015). InSAR has applications in many fields such as monitoring of land use changes, producing high quality digital elevation models, measuring and mapping earth surface deformations like seismic, volcanic and crustal deformations, monitoring of natural hazards and many others. The technique can also reveal surface deformation response induced by volumetric changes (through time and space) resulting from withdrawal of subsurface fluids (Bell et al., 2008).

InSAR measurements are often limited due to decorrelation issues which arise due to changes either in the characteristics of the surface or the image over time. Decorrelation tends to degrade the interferometric coherence in individual interferograms and can produce errors in phase and displacement measurements. Therefore, an optimal value of coherence should be maintained to acquire correct phase measurements (Woodhouse, 2006). Major sources of decorrelations that pose limitations to InSAR are geometric, temporal and atmospheric decorrelations. Geometric decorrelations occur when the geometries of master and slave images do not match and need to be taken care of during the initial selection of master and slave images as improper selections can cause significant coregistration errors which will propagate through the entire process resulting in degraded quality of final products. As the baseline between two different satellite observations increase away from near zero, the geometric decorrelation increases. A baseline closer to zero will produce a higher geometric correlation while a baseline greater than 300 m

significantly increases the geometric decorrelation between the Single look complex (SLC) pairs. InSAR uses pairs of Single look complex (SLC) images having the same illumination area to make interferometric phase measurements and measure height displacements using interferometry. Therefore, a baseline as close as possible to zero is recommended, though a baseline between 100 m to 300m also results in optimum correlation (Ferretti et al., 2007).
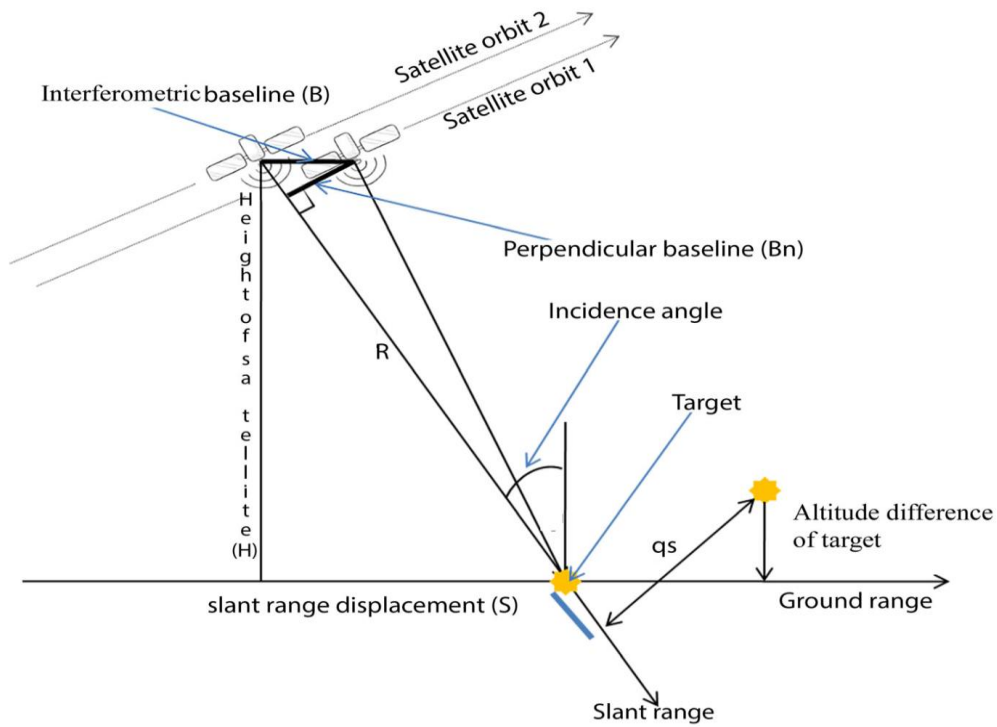
Fig 2.3: Geometric parameters of INSAR system.

The temporal decorrelation occurs due to physical or geometrical changes in the surface over the time between acquisition of master and slave images. It is a major issue in repeat pass interferometry where there is a loss of coherence due to time delay between the image acquisitions. Temporal decorrelations can happen due to changes in the vegetation over the area and can vary with seasons for e.g. the loss of coherence is more during the rainy seasons when the moisture absorbs the electromagnetic energy causing a reduction in the backscattered energy. Differential properties of various land cover types as well as temporal changes in surface roughness also leads to temporal decorrelation.

Atmospheric decorrelations occurring mainly in troposphere and ionosphere is another limiting factor in repeat pass InSAR measurements. Often significant errors are introduced due to time delay of electromagnetic waves while passing through the troposphere. Zebker et al. (1997) reported that spatial and temporal changes of 20% in relative humidity present in the troposphere can produce errors in the deformation measurements within a range of 10 to 14 cm's, and the errors in the deformation products can even propagate upto 100 cm's in derived topographic maps where pairs with optimum baselines are not acquired. While the troposphere slows down the electromagnetic waves, the ionosphere on the contrary accelerates the electromagnetic waves and can degrade the phase accuracy. The range error due to ionospheric effects is proportional to the total electron content (TEC) in the ionosphere (Ding et al., 2008).

2.6.3 Differential Interferometry

Differential SAR interferometry is one of the most popular techniques in SAR imaging studies and is used for mapping surface deformation from archived SAR data and can provide measurements of surface displacements ranging from several millimetres to a few dozen centimetres with a large spatial coverage (Gabriel, et al., 1989). The technique exploits the interferometric phase differences of two coherent SAR images and provides a measurement of the ground deformation projection along the Radar Line of Sight (LOS). The precision and feasibility of D-InSAR technique is largely controlled by the quality of InSAR data pairs, in terms of baseline and wavelength of the SAR signal. The displacement of the area observed occurring between the two SAR measurements of an interferometric pair, results in a phase anomaly, adding to the flat earth or topographic components, and helps to measure the topographic deformation very accurately. The phase difference is given by eq. (21) below.

$$\Delta \phi = \frac{4}{\lambda} * d \qquad \qquad (21)$$

Where d is the relative scatter displacement.

The D-InSAR technique was first introduced by Gabriel et al. in 1989 for measuring very small surface movements with accuracies up to 1 cm over large swaths. This method was applied to SEASAT data of Imperial Valley, California where ground swelling and shrinking was caused due to water absorbing clays in the area. During the last 15 years, D-InSAR has been used to study a wide range of surface displacements related to active faults, volcanoes, land subsidence, landslides and glaciers, at a spatial resolution of less than 100 m and cm level to sub-cm level precision. Various workers have used this technique for monitoring long term land subsidence phenomenon (Zebker et al., 1986, 1992, Goldstein et al., 1993, 1995; Galloway et al., 1998; Massonnet et al., 1998; Strozzi et al.,2001; Amelung et al., 1999; Franceschetti et al., 1999; Ferretti et al., 2000, 2001,2005; Rosen et al., 2000; Usai 2001; Colesanti et al., 2001,2005; Hanssen et al., 2001,2002,2005; Fruneau and Sarti, 2000; Berardino et al., 2002; Crosetto et al., 2005,2016; Mora et al., 2003; Lanari et al., 2004; Teatini et al., 2005; Chatterjee et al., 2006; Raucoles et al., 2007,2013; Hooper et al., 2007,2008).

Ideally, each interferogram should contain only the phase difference due to ground motion, but external factors cause imperfections in phase difference which must be preprocessed, and the non-deformation related components should be removed to correctly estimate the displacement phase. Hanssen (2001) expressed Phase as the sum of five different components: flat earth component (difference in range distance because of earth curvature assuming a flat surface), topographic phase (due to elevation changes), displacement phase (phase difference due to ground displacement), atmospheric phase (atmospheric contribution to the interferometric phase, and noise component (which may be caused due to different look angles, or change in scatterers and volume scattering).

From the interferometric phase of a repeat pass data pair (Hanssen, 2001; Strozzi et al., 2001; Mora et al., 2003), flat-earth and topographic phase components ($\delta\phi_{flat}$ and $\delta\phi_{topo.}$) can be removed and displacement phase component ($\delta\phi_{disp.}$) can be separated using the InSAR geometry and a reasonably high precision external DEM can be obtained as described as eq. (22) below.

$$\Delta\phi = \delta\phi_{flat} + \delta\phi_{topo.} + \delta\phi_{disp.} + \delta\phi_{atm.} + \delta\phi_{nois.} + n*2\pi \qquad (22)$$

Where,

$\Delta\phi$ = Interferometric phase

$\delta\phi_{flat}$ = flat earth component related to range distance differences in absence of topography and can be simulated from the satellite geometry.

$\delta\phi_{topo.}$ = topographic phase can be extracted from an external DEM and satellite geometry.

$\delta\phi_{disp.}$ = phase contribution due to ground displacement occurring between two SAR image acquisitions.

$\delta\phi_{atm.}$ = phase component due to atmospheric disturbances.

$\delta\phi_{nois.}$ = phase due to decorrelation noise.

$\delta\phi_{atm.}$ and $\delta\phi_{nois.}$ represent the atmospheric phase resulted from spatio-temporal variation in the atmosphere, and random noise resulting from radar instrument and temporal decorrelation between two images. In the last term of the equation ' n*2 π ', 'n' represents the number of phase cycles in the wrapped phase difference and is a whole number, such as 1,2, 3... including 0 (Chatterjee et al., 2006). From the stack of differential interferograms, subtle land subsidence can be detected on a regional scale.

The deformation observed by DInSAR is one dimensional along the Line of Sight (LOS) which is the direction from the sensor to the individual surface targets. Therefore, the LOS needs to be converted to the subsidence or vertical displacement denoted by "Z" and can be expressed as eq. (23) below.

$$Z = \frac{LOS\ Displacement}{Cos\ \theta} \qquad (23)$$

The diagram below shows the relationship between LOS displacement and vertical displacement (Z), fig. 2.4 below.
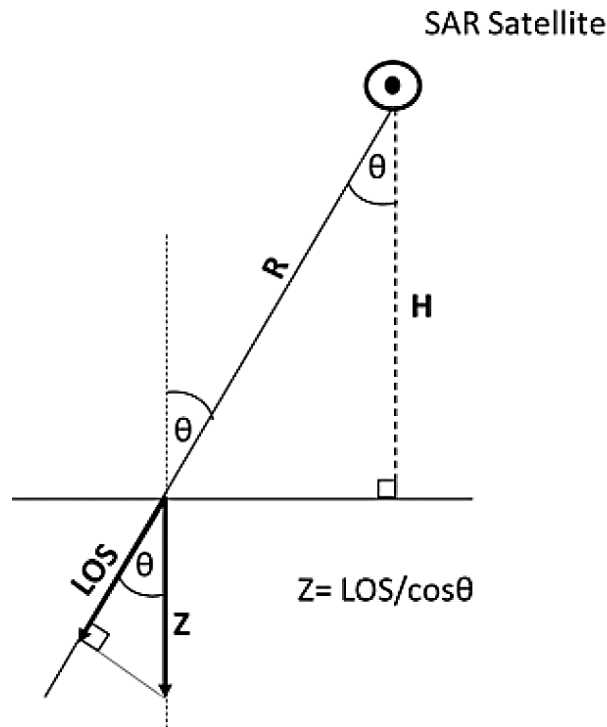
Fig 2.4: Relationship between Line of Sight (LOS) and Vertical displacement.

"θ" and "R" are the off-nadir angle and the slant range, respectively, and "H" is the altitude of the satellite   (Image Source: Yastika et al., 2016)

2.6.4   DInSAR Processing

The main steps involved in DInSAR processing comprise of pre-processing the raw data, SAR image process of stacking and coregistration, Differential interferometry process, Image filtering, phase unwrapping, and making measurements of vertical displacements.

1. **Baseline Estimation**

a) Two SAR images with small perpendicular baseline should be used not exceeding the critical baseline limit.

b) Pairs are chosen that show high coherence amongst them. The smaller the baseline, the greater is the coherence in the image pair.

The baseline, which is based on satellite's acquisition geometry and the characteristics of the radar sensor is one of the most important parameters in interferometry, as a higher baseline results in higher topographic

baseline. A very short perpendicular baseline results in two different views to the ground objects perpendicular to the SAR antenna and would limit the topographic accuracy. If the normal baseline is more than the critical baseline which is the threshold value of perpendicular baseline beyond which there is loss of coherence, the noise increases, and it affects the quality of the interferogram generated. Therefore, a spatial baseline more than the critical baseline should always be avoided (Sefercik et al., 2011).

2. **Co-registration**

For coregistration, one reference SAR image called as master and image and one slave image both with similar acquisition geometry should be overlapped to achieve sub-pixel accuracy in the slant range geometry. Coregistration which is the alignment of SAR images from two antennas, is an important step for the accurate determination of phase difference and for noise reduction. This is done to extract common feature in the SAR image pairs and a highly precise coregistration will lead to generation of high quality interferograms resulting in high coherence and will thereby generate accurate phase product for displacement calculations (Schreiber R. et al., 2000). Proper coregistration will produce better coherence that measures the similarity of the phase of two SAR images used in the coregistration process. Theoretically, coherence values range between 0 and 1, where 0 denotes no coherence, and 1 corresponds to perfect coherence. Phase information can be successfully retrieved when the correlation values are larger than 0.20, are difficult to get when the values are between 0.15 and 0.20 and cannot be retrieved when the correlation is below 0.15. A higher correlation of 0.20 or more can be seen in urban areas where surface conditions do not vary much over time and low correlation is seen in vegetated areas where the nature of the surface changes dynamically (Wei and Sandwell, 2010).

3. **Interferogram Generation**

a) Interferogram flattening: - The orbit attitude influences the flat earth phase which is the phase difference between the scattering elements on the same height level and needs to be removed from the resulting interferometric phase

to get the phase values only due to the unevenness in the topography and obtain accurate topographic and deformation information in the phase values. The flattened data set is obtained by deducting the phase of this simulated interferogram from the interferometric phase.

b) **Topographic Phase Removal**: - The DInSAR processing tries to separate the topographic and deformation components in an interferogram. To highlight the phase information of deformation, the topographic phase contribution which occurs due to variation in topography should be removed using a high-resolution external Digital elevation model like SRTM to avoid topography-based inconsistencies in the resultant interferogram (Raucoules et al., 2007).

4. **Interferogram filtering**

To enhance the signal to noise ratio of the interferometric phase, filtering is applied on the interferograms. Spatial and temporal baseline decorrelation as well as the atmospheric effects produce a large amount of noise in the interferograms and should be removed using filtering. Several filtering methods, such as non-Adaptive filtering, Adaptive filtering, Goldstein filtering and Multilooking filtering are available. Goldstein Filter is used largely in interferometry for reducing the interferogram noise. Alpha values are normally provided in a range of 0-1 to improve the performance of filter. Higher values of Alpha do a better task of noise filtering and gives enhanced results.

5. **Phase Unwrapping**

Interferogram filtering is followed by Phase Unwrapping and is the final step for extracting the phase information from the SAR images. Due to the wrapped nature of the phase signal (2π cycles), phase unwrapping must be applied to convert them to one complete cycle and correctly estimate the ground deformation. It involves getting the correct phase from the wrapped phase by removing 2π discontinuities. The interferometric phase of two SAR images at different times can only be measured modulo 2π. This ambiguous phase is known as the wrapped phase. To obtain the complete phase difference from the wrapped phase an integer number of 2π has to be added which can be achieved by adding an exact multiple of 2π to the interferometric phase for every pixel to

remove the 2π ambiguity and obtain sequential phase values across the entire image. This results in achieving the values of $-\pi$ or π is achieved depicting a phase jump from one end to the other end. Some of the common algorithms employed for phase unwrapping include Region growing, Minimum cost Flow and Phase decomposition algorithms. In the present study, Minimum Cost flow algorithm was used to perform phase unwrapping of the SAR data pairs.

2.7 Field Based Instrumentation

A piezometer is a device that is used to measure the fluid pressure in a system by measuring the height to which a column of the fluid rises against gravity. They are usually placed in boreholes to monitor the pressure or depth of groundwater and measure the piezometric head at a specified point. The piezometric head which is one of the most important measures for interpreting groundwater flow and quantifying aquifer properties is measured based on water level measurements in piezometers. The device consists of stand tubes that are inserted into the saturated zone. It has a screened opening at its lower end that allows water under positive hydrostatic pressure to enter the tube. The piezometric head is the water level measured to the screen at the bottom of the piezometer. Typically nests of locally distributed piezometers are installed at selected locations below the land surface with each piezometer representing a different depth. The measurements are made relative to a datum which may be mean sea level or a local datum. The total hydraulic head of the piezometer is the height to which the water level rises relative to the datum (William Bleam, 2017). Although different types of piezometers such as Standpipe units, Vibrating piezometers, Pneumatic piezometers are available in the market for various application requirements, the choice of piezometer depends upon the location, distance between the piezometers, the geology and structural aspects of the stratum, depth of the target and geotechnical aspects (Murthy, 2002). Apart from applications in hydrologic investigations, piezometers are also used in a variety of civil engineering and infrastructure projects such as tunnels, dams and buildings, where they are used for different geotechnical purposes like monitoring uplift pressures, observing seepage, estimating slope stability etc. Fig. 2.5 below shows the various components of a piezometer.
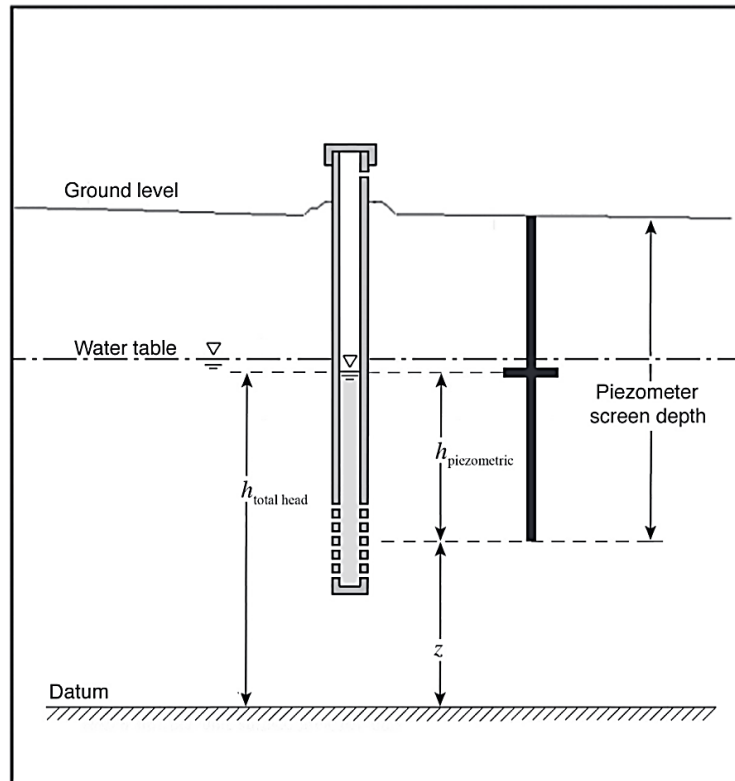
Fig 2.5: Components of a Piezometer used to measure piezometric head. The screen depth (black heavy line) and the water level (black crossbar) in the piezometer tube are shown. (From: William Bleam, 2017)

2.8 Previous Case Studies on Groundwater Induced Land Subsidence

Amelung et al. (1999), analyzed land subsidence rates in Las Vegas, Nevada, United States between April 1992 and December 1997 by using InSAR technique. Two European Earth Remote Sensing (ERS) images were utilized with a temporal baseline of one year were processed and the results indicated two major subsidence bowls in the study area with a maximum subsidence of 19 cm during the observed period of 5.75 yrs. The subsidence bowls were aligned with the fault location and the InSAR measured rates and the levelling measurements showed a good agreement. The comparison indicated that the reduction in the groundwater extraction decreased the subsidence rates in the area. They concluded that that the spatial extent of land subsidence was controlled by geological structures and sediment (clay) thickness.

Teatini et al. (2005), developed and used Subsidence Integrated Monitoring System (SIMS), which combined the usage of five different monitoring techniques of Spirit levelling, Differential Global Positioning System (DGPS), Continuous GPS (CGPS), Interferometric Synthetic Aperture Radar (InSAR) using ERS 1 and ERS 2 radar images from 1993 to 2000, and Interferometric Point Target Analysis (IPTA), to investigate land subsidence at the coastland of Venice City, Italy on a regional scale of 100 X 100 km. A very high resolution was achieved using this method. The results showed a general stability over the central lagoon which also included the city of Venice, while the northern and southern lagoon regions showed high subsidence rates of 3 to 5 mm/yr. The subsidence rates were even higher upto 10-15 mm/yr. towards the coastlands. Apart from the subsiding patters, small uplifts < 1 mm/year were detected towards the Alpine foothills. The contribution of natural processes of tectonics, seismicity, thickness of compressible clayey units, as well as contribution of human induced groundwater extraction in the measured vertical ground movements were highlighted in the study.

Chatterjee et al. (2006), utilized Differential Synthetic Aperture Radar Interferometry (D-InSAR) to assess the potential land subsidence at selected site of Kolkata city, India. ERS-1 and ERS-2 InSAR data pairs during 1992 to 1998 were utilized to study the deformation rates in the area. They highlighted that in slowly subsiding areas such as Kolkata, large temporal baselines generally in years should be used and that in such places the atmospheric fringes may be difficult to decipher due to significant temporal decorrelations. The atmospheric fringes however can be differentiated from subsidence fringes since they will not lie at the same location when seen in different interferometric pairs, whereas the subsidence fringes will remain at the same location due to similar conditions of land subsidence. Four InSAR data pairs with master image (previous time) acquired during post-monsoon season and the slave image (later period) acquired during pre-monsoon were processed. The piezometric decline causes the compression of clay units in the confined aquifer and leads to vertical compaction and land subsidence. The seasonal images were chosen considering the fact that the piezometric decline is

maximum between post-monsoon and pre-monsoon periods. The results estimated a subsidence rate of 5 to 6.5 mm/yr. at the selected locations of the city. They also highlighted the importance of GPS monitoring and levelling measurements to validate the DInSAR derived results.

Motagh et al. (2008), showed the association of groundwater extraction to land subsidence in and around Tehran, Iran. InSAR based vertical displacement rates were calculated and were correlated with the available piezometric data. The subsidence rates in Western Tehran were estimated to be around 14 cm for the 140-day time interval between 13 June and 31 October 2004. In Varamin area, a maximum subsidence of 9 cm was observed during June-October. In Rafsanjan plain within central Iran with extensive groundwater exploitation for agriculture, 10 cm of subsidence was seen between 17 May 2005 and 26 July 2005. The north east parts of Iran that include major cities like Mashhad and the Yazd-Ardakan plain in Iran's desert area also showed considerable subsidence during the study periods. The study highlighted the applicability of InSAR techniques for subsidence measurements at a regional level and pointed out the importance of acquiring detailed hydrological data such as well locations, pumping rates and lithostratigraphic maps to better comprehend the relationships between surface subsidence and the declining groundwater levels.

Sahu and Sikar (2011), carried out predictive modelling of aquifer system compaction in Kolkata city including the Salt Lake City and the east Kolkata wetlands. They estimated the inelastic compaction of the confined aquifer using the changes in piezometric heads and emphasized that the inelastic compression of highly compressible clay and silt layers of the confined aquifer system are more responsible for land subsidence in contrast to the elastic compaction. Available piezometric head data for the period 1956-2005 was analyzed sector wise and then land settlement was estimated using Domenico's one-dimension consolidation equation for each sector. The estimated land subsidence was in the range of 1.12 and 43.8 mm/yr. with a mean subsidence rate of 13.53 mm/yr. For every 1 m drop in the piezometric head, the land subsidence was found to be between 1.79 to 10 cm with an average of 3.28 cm.

Ganguly (2011) studied the land subsidence due to groundwater withdrawal in Singur block of Hooghly district in West Bengal. Only one observatory well was considered due to lack of data. The rate of land subsidence was calculated using Jacob's (1940) and Lohman (1961) equations and used data obtained from secondary sources. Pre monsoon water level was considered for calculation of land subsidence since the water levels are lowest in pre monsoon months due to less precipitation and more exploitation to cater to domestic, irrigation and commercial demands. The rainfall and the declining water levels due to groundwater overdraft were concluded to be the primary reasons for the land subsidence. He estimated an increate in rate of land subsidence from 0.92 mm/yr. during 1998-2002 to 8.7mm/yr. assessed during the period 2002-2006. The average rate of land subsidence was found out to be 6.13 mm/year for every 1 m drop of water table.

Chaussard et al. (2014), did a time series analysis on ALOS-InSAR data between 2007 and 2011 over the entire Mexico City. They identified subsidence over 21 areas including 17 cities, with a higher deformation rate of 30 cm/yr. in the Mexico City and 5-10 cm/ yr. at other locations. A small spatial baseline < 1.5 km and a temporal baseline of < 1 year were used to obtain interferograms with high coherence. Vertical displacement rates were calculated from the observed LOS (Line of sight) rates. The subsiding sites were categorized according to four criteria. 1) the rates of subsidence 2) spatial extent, 3) correlation between velocity gradients and locations of existing faults and 4) type of land use. The results identified areas with high velocity gradients that could result in potential faults or fracture developments and confirmed that the extensive extraction of groundwater from the aquifer–aquitard systems was the primary cause of land subsidence.

Calo et al. (2015), studied the land subsidence in Istanbul Megacity, Turkey using SBAS- InSAR approach, using images from TerraSAR-X satellite. 43 TerraSAR-X images between 30 November 2010 and 24 June 2012, with HH polarization, were used with each scene covering an area of approx. 30 km (width) $\times$ 50 km (length) and 3 m $\times$ 3 m spatial resolution. A spatial baseline of 400 m was used for selecting the image pairs. They

highlighted the importance of InSAR measurements in megacities like Turkey where deformation measurement is not possible with the use of conventional in-situ measurements and where ground measurements are often incomplete or inconsistent. They followed a two-scale approach of first mapping the hotspots of risk over a city scale and then analyzing the available geological and urban development data at local scale to understand the causes of deformations in the megacity. The major geological units in the area are composed of sand, gravel and silt, with highly compressible clay units interbedded by sand lenses and gravel. The InSAR results showed prominent subsidence patterns in two zones at an average subsidence rate of 3 cm/yr. Most of the observed subsidence was found to be occurring in the Quaternary layers both alluvial and man-made fills.

Rojas et al. (2015) investigated land subsidence rates in Mexico metropolitan area using SqueeSAR PS-InSAR approach. They analyzed ENVISAT-ASAR images between 2003 and 2010 and also compared it with GPS measurements. They found out that the sites with low subsidence gradients occurring in the lacustrine area had the highest subsidence rates and had vertical GPS velocities upto -273 mm/yr. They also examined the relationship between the estimated rates of land subsidence and groundwater decline using data from 180 well hydrographs. From the well hydrographs they revealed that there was a groundwater drawdown of upto 30 m in the region. Decline in groundwater levels were seen throughout the subsiding zones suggested that the aquifer system was under great stress. However, a low correlation between subsidence rates and groundwater decline suggested that apart from groundwater overdraft other hydrogeologic variables such as lithology, aquitard thickness and pore pressure also play an importance role in subsidence. They found out a positive correlation between the aquitard thickness and rate of land subsidence.

Ahmad et al. (2017), analyzed land subsidence due to groundwater extraction in Quetta valley, Pakistan using ESA Sentinel-1 C-band SAR images. They also related the spatial patterns of land cover obtained from ESA Sentinel-2 multispectral images with the land subsidence patterns in the region and concluded that land subsidence is related to groundwater extraction and varies with the differential patterns of land use. Through maps and graphs

they highlighted that urban and agricultural areas were more prone to land subsidence due to extended groundwater extraction, while barren and seasonally cultivated areas showed lesser magnitudes of land subsidence. Twenty nine Sentinel-1 images were used to form eight interferograms to study land subsidence between the period 16 Oct 2014 and 06 Oct 2016. PS-InSAR technique was utilized to derive the land subsidence maps of Quetta valley. Through their study the researchers observed that during the study period there was uneven patterns of land subsidence ranging in magnitude of 10 mm to 280 mm which were more pronounced in the urban and cultivation rich areas with increased level of groundwater usages.

Calo et al. (2017), studied land subsidence in groundwater overexploited areas of Koyna region, Turkey between the time period of Dec. 2002 to July 2010. The study area lied in the agricultural and industrial sectors where groundwater utilization was more pronounced. Small Baseline Subset (SBAS) DInSAR technique was used to evaluate the ENVISAT SAR images and was complemented with temperature, rainfall, geological, piezometric and land use data. Piezometric data recorded monthly from nine wells during 2003-2010 were used to correlate the changes in groundwater levels with SBAS derived time series surface deformations. The thickness of clay and silt layers were used to demarcate the incompressible layers that cause groundwater extraction induced land subsidence and were shown to have a spatial correlation with land subsidence. Land use cover maps were created using supervised classifications of Landsat 5 TM and Landsat 8 images with a major focus on irrigated lands with more water consumption. Modified Normalized Difference Vegetation Index (mNDVI) was calculated to assess the changes in vegetation cover. They showed that uncontrolled irrigation practices were mainly responsible for groundwater depletion. Analysis of long term temperature data revealed an increase of 0.75^o C during the study period and indicated towards rise in water needs for irrigational purposes. The analysis of rainfall data also revealed seasonal trends with dry and wet periods. Through SBAS analyses of two datasets of ENVISAT images, the researchers detected land subsidence in about 1200 sq. km of Koyna basin and observed a subsidence rate upto 1.5

cm/yr. during the study period 2002-2010.

Chen et al. (2018), investigated time series images of COSMO-SkyMed images from July 2011 to July 2012 and Sentinel-1A images both with HH polarization, from April 8th, 2015 to January 27th, 2017 using SBAS (Small Baseline) InSAR technique to map and analyze the Spatio-temporal variations and investigate the causes of land deformation in Changzhou City, China. The temporal gap between the two study periods i.e. July 2012 to April 2015, was filled with the average of the earlier period. SBAS method was used since it requires a smaller number of SAR images as compared to the PS (Persistent Scatterer) InSAR method. The SBAS-InSAR results were validated with the levelling observations and measurements of the groundwater level of the confined aquifer. To ensure the comparability between the levelling and InSAR measurements, the InSAR measurements were projected in a vertical direction. The comparison between InSAR and levelling measurements indicated a great agreement between the two, with a minimum and maximum difference of 1.2 mm/year and 3.0 mm/year, respectively. The error in InSAR derived annual subsidence results were within 2 mm. Groundwater level data was recorded for the period that coincided with the COSMO-SkyMED image acquisition period and a strong correlation between the land subsidence and groundwater depth was observed. The study showed the applicability of SBAS technique in successfully estimating the land subsidence due to groundwater extraction in the city.

Krishnan and Kim (2018), employed StaMPS PS-InSAR technique to investigate the land subsidence in Kathmandu basin during the period May 2015 to December 2017. Thirty four Sentinel-1 C-band images were studied to estimate time series deformation rates in the Kathmandu basin. A 30 m SRTM was used for topographic correction and displacement maps were produced using the PInSAR technique. Subsidence rate in the LOS direction was obtained with respect to a stable GPS station in the basin. They found out that the central part of Kathmandu basin subsided considerably in the LOS direction and the subsidence rate was estimated to be 8.06 cm/yr. with a maximum subsidence rate of 9.5 cm/yr. With the available information on past

groundwater trends and the geologic information they inferred that land subsidence was correlated with groundwater decline in the area.

Malik et al. (2018), used 68 TerraSAR-X images between the duration of September 2011 to November 2013 to assess land subsidence in Delhi NCR region. They used the Persistent Scatterer Interferometry (PSI) technique to estimate a land subsidence rate of 10 to 32 mm per year in the region. The satellite-based subsidence rates were compared with the IDW interpolated maps of groundwater depletion and it was shown that the trend in deformation from PSI closely followed the trend of groundwater depletion. A decline in groundwater level at the selected sites to a tune of 3.8 m during the two-year period indicated a link between groundwater depletion and subsidence. They also pointed out that the areas with ongoing construction activities in the region showed considerable deformations.

Edalat et al. (2019), investigated land subsidence in Aliabad plain of central Iran using DInSAR technique. Seventeen Sentinel-1A IW SLC SAR images which were acquired in ascending pass were investigated between the period from 24 March 2015 to 9 August 2016. Four interferograms were chosen and analyzed for land subsidence that minimized temporal decorrelations. The DInSAR studies were complemented with studies on groundwater level decline recorded from piezometer, alluvium thickness and transmissivity and their relationships with land subsidence were examined. Their results revealed that during the study period there was a continuous subsidence in the region with similar spatial patterns. A direct relationship was observed between the levels of groundwater decline and land subsidence and subsidence occurred on the same side of the basin where groundwater was depleting. Though they could not establish a relation between alluvium thickness and subsidence in the study area but found a similar and positive relationship of transmissivity to ground subsidence as was observed with piezometric decline. The litholog studies also suggested that grain size distribution also affected land subsidence in the region. The vertical displacement rate as calculated from the DInSAR processing of Sentinel images was estimated to be 178 mm/yr. Their study thus revealed a good correlation between land subsidence and groundwater depletion.

Othman and Abotalin (2019), estimated the regional subsidence rates in Saq aquifer in Saudi Arabia using SBAS interferometric techniques. SAR images from ENVISAT for the period between 2003 and 2004 were processed to estimate the land subsidence rates. They noticed a subsidence rate of 5 to 12 mm/yr. in the area which coincided with areas showing major drawdowns of groundwater and depletion of terrestrial water storage (TWS) obtained from GRACE data. The researchers also did an extensive field survey collecting information on surface features and infrastructure. The data collected showed that deformation features were more located in proximity to lands with agricultural practices and areas without proper sewage facilities. The deformation features mapped in the field were concentrated at the locations with maximum decline in the groundwater table. Interpolated maps of groundwater decline were correlated with time series variations in groundwater mass obtained from GRACE satellite. The terrestrial water storage values obtained from GRACE showed significant declines in the study aquifer which showed a good agreement with the declining groundwater trends and agriculture prone areas. The increased drawdown of groundwater and the presence of high plastic cay beds in the aquifer resulted in increase in the net effective stress leading to subsidence. The results from SBAS processing, TWS from GRACE, aquifer characteristics and groundwater levels sowed a good consensus on areas prone to land subsidence.

Gao et al. (2019), used Quasi PS-InSAR technique to monitor land subsidence in Beijing, China. The authors used 63 images from TerraSAR-X/TanDem-X that were acquired between 2010 and 2017 and generated time series deformation maps for the study area. The deformation rates estimated from QPS technique were compared with ground levelling measurements using linear regression analysis in order to evaluate the accuracy of the QPS-InSAR processing. A correlation coefficient of 0.96 with a standard error of 1.33 mm/yr. was found out between the InSAR measurements and ground levelling measurements which showed a good agreement between the two different types of measurements. A maximum value of −1174.1 mm for estimated for the vertical displacement in the area with an average sinking rate of 15. have been

estimated to have a maximum value of −1174.1 mm and the average sinking rate was found out to be 152.9 mm/year.

Gupta et al. (2019), estimated a land subsidence of around 4.98 cm/year in Jagadhri city, Haryana using six Single look images of Sentinel 1 SAR C band data for the months of January and April between 2017 to 2019. Images with minimum temporal and perpendicular baselines were chosen to minimize the decorrelation issues in the images. Perpendicular baselines of 110, 136, and 121 m and temporal baselines of 108, 102 and 120 days were chosen for processing during the study period. With an aerial extent of around 25 sq. km the consistency in the deformation fringes suggested that the subsidence was due to groundwater over draft rather than any sudden natural activity. The study of groundwater levels from borewells in the study area which showed that the decrease in water level in April was 1.2 times than November corroborated the conclusion that overexploitation of groundwater was mainly responsible for subsidence in the city.

Khorrami et al. (2020) investigated land subsidence in Mashhad city of Iran using SAR interferometry. They combined the InSAR studies with piezometric data to estimate aquifer specific storage and predict land subsidence in the area. PS-InSAR technique was deployed on sixty nine image acquisitions from Sentinel-1 SAR data in both ascending and descending modes and time series deformation rates were estimated between the period October 2014 and February 2017. They found out a maximum rate of subsidence to be 14.6 cm/yr. in the LOS direction and a maximum vertical deformation rate of 19.1 cm/yr. The PinSAR results were compared with observations at GPS locations and a good agreement in subsidence rates was observed in both of the techniques. Groundwater level data from 4 piezometric wells were also analyzed and compared with the PInSAR values and showed that groundwater level declines and land subsidence took place in similar areas showing their direct interrelationship. They also calculated specific storage using one dimensional theory and showed its usage to calculate land subsidence rates in areas with high alluvium thickness and increased rates of groundwater extraction.

Suganthi and Elango (2020), analyzed temporal ENVISAT ASAR multilook DInSAR images using SBAS technique to monitor and assess the rate of land subsidence due to groundwater pumping in Kolkata metro city between 2003 and 2010. With an observed decline of 6m in the piezometric head the rates coincided very well with the mean deformation rates from DInSAR. Maximum land subsidence rates were around 8 mm/yr. at Salt Lake City and near the eastern metro bypass of Science city. The consolidation of sediments in the confined aquifers to fill up the lakes and marshes in the Salt Lake City area was mainly responsible for the compaction. The comparison between the piezometric head declining rates and the DInSAR rates made them conclude that the subsidence could be attributed to the overdraft of groundwater from confined aquifers in the city and that the subsidence rate is increasing after 2007.

Khan et al. (2021), monitored land subsidence in Abbottabad city of Pakistan using PS-InSAR technique. Sentinel-1 C band images acquired between March 2017 and September 2019 were processed and it was observed that there was an increasing pattern of land subsidence from 2017 to 2019 with a mean increase of 60 mm/yr. The estimated subsidence was 30 mm/yr. in 2017 which increased to 85 mm/yr. in 2018 and further increased to 150 mm/yr. in 2019. The study also suggested that the central parts of the city were more affected with land subsidence in contrasts to the peripheral parts because of higher number of tube wells in the central part leading to over extraction of groundwater for domestic and commercial uses and has consequently led to ground subsidence. The variability of fluid pressure owing to groundwater extraction causes aquifer compaction and it was shown that the major subsiding areas from PS-InSAR occurred in the quaternary alluvium deposits.

CHAPTER 3. REGIONAL TREND ANALYSIS AND GEOSTATISTICAL MODELLING OF GROUNDWATER LEVELS

3.1 INTRODUCTION

Groundwater resources are one of the most vital requirements sustaining human lives. In the study area, there has been a widespread decline in the groundwater tables to fulfil the needs of domestic, agriculture and commercial sector. The depleting groundwater levels need to be adequately monitored and mapped to identify significant potential trends in groundwater levels and take counteractive measures. Trend analysis tests along with geostatistical techniques have proved to be useful techniques to map and analyze the spatio-temporal patterns of groundwater variability.

Mann Kendall statistical test along with Sen's slope estimator is a non-parametric statistical approach that can identify and quantify such trends in an area. The importance of Mann Kendall trend test for groundwater monitoring lies in the fact that the method makes no assumption on the population distribution or sample size and the statistics can be computed even if there are missing values or outliers. Groundwater time series data is often characterized by outliers and missing values therefore, Mann Kendall statistical test proves very useful in detecting the existence of trend in hydrological time series. The test can statistically assess whether the groundwater shows upward or downward trend over the given time period. Sen's slope estimator quantifies the magnitude of this trend by looking at the rate of change in groundwater levels per unit time. The groundwater variability can also be affected by climatic changes like changing rainfall patterns. The MK and Sen's slope methods can also be used to detect and assess the rainfall trends in the area of interest.

The present study employed these techniques to investigate and quantify the groundwater trends in Kutch-Sabarmati basin of Gujarat for both

pre and post-monsoon seasons for the period 2005–2017. The rainfall trends were also assessed using the above techniques to analyze the correlation between groundwater and rainfall over the study period. As some parts of the basin are highly agriculture dominated with large topographic gradients, the groundwater level trends need to be analyzed with the observed landuse and slope patterns to identify the cause of the observed patterns of groundwater trends. The identification of trends is an initial step towards identifying the hotspots of seasonal groundwater fluctuations which can suggest areas prone to excessive groundwater pumping.

To identify the hotspots of seasonal groundwater fluctuations and analyze the spatio-temporal patterns of groundwater recharge and depletion geostatistical techniques are employed. Geostatistics is a branch of statistics that considers the spatial availability and continuity of groundwater data in estimating values at unknown locations. The measurements of groundwater depth are often limited to a small number of locations due to non-feasibility of setting up monitoring stations at every place. To acquire the information on groundwater depth over a dense grid, statistical interpolation techniques are often employed that use algorithms to predict values at unknown locations where measurements are not available. The geostatistical methods not only provide interpolated values at the locations where samples were not taken, but also measure the uncertainty in those values.

Inverse distance weighted (IDW) and Kriging are two of the most commonly used methods for geostatistical interpolation of groundwater levels. While, in IDW method no statistical model is involved, and it uses the distance weights to estimate unknown values and does not take the spatial variability into account; the Kriging method considers the variance or spatial autocorrelation of the variables as a function of distance. The estimation variance in Kriging is determined by the variogram model and the spatial proximity to the sampling locations. Irrespective of the chosen technique, error analysis like Root mean square error (RMSE) or Mean error (ME) can be done to gauge the accuracy of the predicted results (Tziachris et al., 2017). The techniques have been widely used by many researchers worldwide to monitor the spatial variability of

hydraulic head, understand the uncertainty associated with the predictions and demarcate the zones of recharge and depletion in groundwater levels. The outputs have been successfully used to suggest measures and remedial policies for groundwater sustainability. Kalman Filter is another advanced algorithm that gives a prediction much closer to the true values by minimizing the estimation variance. The weights are calculated from the covariance of the estimated uncertainty of the predicted values from the original values and produces a new set of point values where statistical comparison can be made from the new set of predicted values to the original set of values. The present study uses the Kalman filter approach for geostatistical interpolation of groundwater depths in the study area that takes the weighted average of both IDW and Kriging outputs to generate a better interpolated result. Piezometric levels for both pre-pre and post-pre monsoon months in Kutch-Sabarmati basin were analyzed geostatistically for the period 2005-2017, to monitor the spatio-temporal hotspots of groundwater recharge and depletion in the study area.

3.2 MANN KENDALL TREND ANALYSIS OF GROUNDWATER

Statistical trend analysis of seasonal groundwater levels was carried out using the non-parametric Mann-Kendall (MK) method and Sen's slope estimation from 2005 to 2017 at 30 locations, in Kutch and Sabarmati basin of Gujarat, in order to identify and map the groundwater level trends present at the study locations. The entire trend analysis was evaluated at 5% significance level. Piezometric groundwater level seasonal data for pre and post-monsoon months for the years 2005 to 2017 were acquired from the Central Ground Water Board (CGWB). Considering the number of monitoring stations and the missing gaps in the data, only 30 monitoring wells in the study area was selected for statistical analysis, with the most complete time series of groundwater level measurements and which best represented the varied groundwater level variations at a regional scale. The Location details of groundwater level stations are illustrated in Table 3.1 below.

Table 3.1: Location details of Groundwater monitoring stations.

S No.	DISTRICT	BLOCK	STATION	Lat.	Long.
1	Ahmedabad	Daskroi	Ghuma2	23.03	72.45
2	Anand	Tarapur	Tarapur I	22.49	72.66
3	Banaskantha	Danta	Ambaji	24.34	72.85
4	Banaskantha	Danta	Danta	24.19	72.77
5	Banaskantha	Deesa	Rasna	24.22	72.25
6	Banaskantha	Dhanera	Dhanera I	24.51	72.23
7	Banaskantha	Palanpur	Palanpur	24.17	72.45
8	Jamnagar	Jamnagar	Jamnagar	22.47	70.5
9	Jamnagar	Jodiya	Amran	22.82	70.55
10	Jamnagar	Kalavad	Kalavad	22.22	70.39
11	Jamnagar	Kalyanpur	Bhatiya	22.09	69.27
12	Jamnagar	Lalpur	Lalpur	22.19	69.94
13	Kachchh	Abdasa	Naliya	23.26	68.84
14	Kachchh	Lakhpat	Lakhpat	23.82	68.77
15	Kachchh	Mandvi	Asambia mota	22.97	69.45
16	Kachchh	Mundra	Mundra	22.83	69.72
17	Kheda	Balasinor	Balasinor	22.96	73.34
18	Kheda	Matar	Matar II	22.71	72.67
19	Kheda	Nadiad	Nadiad	22.71	72.87
20	Kheda	Thasra	Thasra	22.79	73.21
21	Mahesana	Kadi	Vidaj	23.25	72.3
22	Mahesana	Visnagar	Bhandu V	23.7	72.37
23	Patan	Chanasma	Harij iii	23.69	71.9
24	Patan	Santalpur	Sidhada	23.81	71.3
25	Rajkot	Morvi	Morbi	22.83	70.86
26	Sabarkantha	Bayad	Bayad	23.22	73.23
27	Sabarkantha	Idar	Chandap	23.93	72.86
28	Surendranagar	Chotila	Chotila	22.43	71.18
29	Surendranagar	Halvad	Malaniyad	23.12	71.25
30	Surendranagar	Sayla	Sayala	22.53	71.48

The data sets of the piezometric wells in the study area were analyzed in individual time steps for pre-monsoon and post-monsoon months. Groundwater level trends for all the 30 stations were statistically computed and analyzed using the non-parametric Mann-Kendall trend test for both seasons and statistically significant trends in the groundwater time series at 5 % significance level were identified. The magnitudes of the trend were estimated using the Sen's slope estimator. GIS and remote sensing platforms were used to delineate the basin, analyze the spatial distribution of groundwater trends and

to correlate the variability of groundwater trends with the rainfall and existing landuse patterns in the study area. The Kutch and Sabarmati basins were delineated from SRTM 1 arc sec. elevation data using hydrologic modelling in ArcGIS environment. High resolution gridded daily rainfall data (0.25 X 0. 25 degree) was obtained from Indian Meteorological Department for the same period. The data was clipped for the study area and annual rainfall was extracted for the 30 monitoring stations. Similar trend analysis was conducted on annual rainfall in the study area at 5% significance level to analyze the correlation between rainfall and groundwater trends. AddinSoft's XLSTAT (2019) was used to explore potential trends in groundwater levels and rainfall, and to estimate the slope. A land use land cover map was created using pixel level classification of Landsat8 Image of 2015 in ERDAS environment, showing the variability of landuse patterns in the basin. District wise land use statistics were calculated from the classification results. Slope map was created form a 30 m resolution STRM DEM and was analyzed to investigate the relationship of slope and groundwater trends. Figure 3.1 below shows the methodology applied for trend analysis of groundwater.
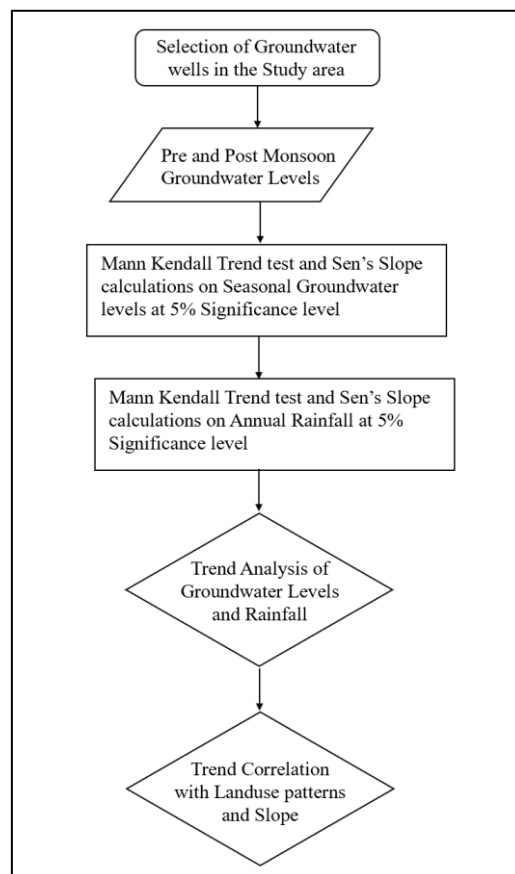
Fig 3.1: Methodology for Trend analysis of Groundwater

3.2.1 Results and Discussion

Seasonal groundwater and rainfall levels were analyzed at 5% significance level using Mann Kendall and Sen's Slope methods from 2005 to 2017 at 30 locations, in Kutch and Sabarmati basin. The locations were chosen in the study area that had the best time series groundwater level data. The spatial distribution of the selected monitoring wells for statistical analysis is shown in Fig. 3.2 below.
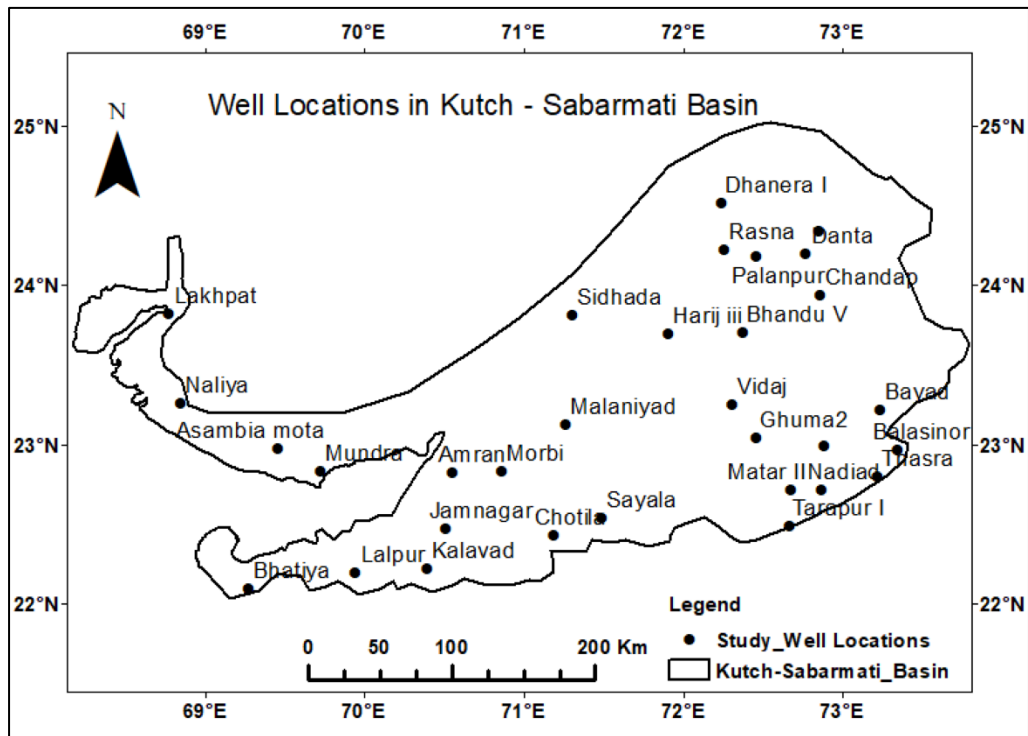
Fig 3.2: Spatial distribution of Groundwater Monitoring stations in Kutch-Sabarmati basin.

The results statistically highlight the stations which show increasing or decreasing trends in the time series data. A positive number of S i.e. S>0, shows an upward trend whereas if S is a negative i.e. S<0, it indicates a downward trend. A value of 0 for S indicates that there is no trend in the time series. The Kendall's τ gives a value between 0 and 1, where 0 indicates that there is no relationship between the variables, and 1 indicates a good association. Also, at 5% significance levels p-values smaller than 0.05 indicate that there is a significant upward or downward trend. Overall, the trend is said to be decreasing if S is negative and the p value is greater than 5%, and if the S value is positive and the p value is also greater than 5%, the trend is considered to be increasing. If the computed p value is less than 5% there is no trend. The

slope factor quantifies the observed trend. A positive value in the magnitude of Sen's slope shows an increasing trend and a negative value suggests a decreasing trend during the given time series.

Groundwater level data of pre and post monsoon months were analyzed along with the variability in mean annual rainfall and the regional land use patterns to understand the observed groundwater trends in the study area. Fig. 3.3 shows that the pre-monsoon water levels have gone up in most of the districts which is obvious as the maximum percentage of the annual rainfall falls in the monsoon period of August to October, except for the Banaskantha, Patan, Sabarkantha and Surendranagar districts with Patan showing a considerable decline in the groundwater levels even after the monsoon period.

Distribution of Mean Groundwater Levels during Pre and Post Monsoon Seasons and Annual rainfall in different districts of Kutch-Sabarmati Basin (2005-2017)

	Ahmedabad	Anand	Banaskantha	Jamnagar	Kachchh	Kheda	Mahesana	Patan	Rajkot	Sabarkantha	Surendranagar
Avg. Mean_PreMonsoon(mbgl)	3.74	7.62	32.26	9.48	8.42	26.90	16.55	9.05	8.36	13.83	5.25
Avg. Mean_PostMonsoon(mbgl)	8.34	3.40	43.95	6.98	9.36	9.40	17.12	18.19	5.37	9.20	9.95
Avg. Mean_AnnualRain(mm)	878.09	870.44	835.37	759.09	486.99	895.74	839.29	672.72	825.93	893.46	791.60

Fig 3.3: Distribution of Pre & Post-Monsoon Groundwater Levels & Annual Rainfall(2005-2017).

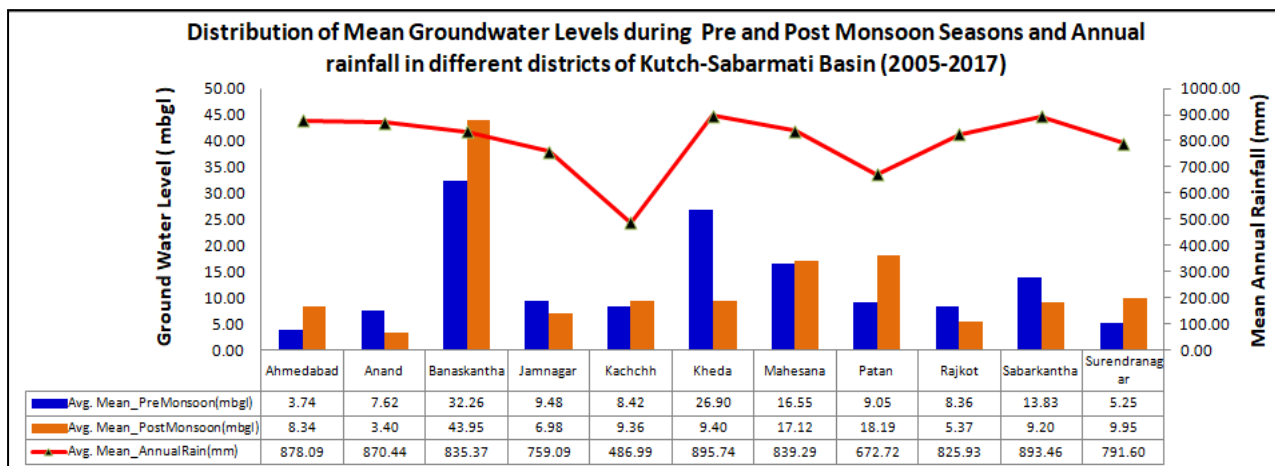The results obtained from the Mann Kendall groundwater trend test and Sen's slope in XLstat, are presented in Table 3.1 and Table 3.2 below. The tables highlight the locations showing positive and negative trends, based on the computed values of Tau, S and p-value. Also, the tables show the rate of change as Slope in m/yr.

Table 3.1: Pre-Monsoon Mann-Kendall Statistics (2005-2017)

Well No.	Station	District	Tau	S	p-Value	Slope (m/yr.)	Trend
1	Ghuma 2	Ahmedabad	-0.128	-10	0.59	-0.103	NO
2	Tarapur I	Anand	-0.128	-10	0.59	-0.157	NO
3	Ambaji	Banaskantha	0.769	60	**< 0.0001***	-2.228	Negative
4	Danta	Banaskantha	0.897	70	**< 0.0001***	-3.624	Negative
5	Rasna	Banaskantha	-0.452	-35	**0.032***	0.357	Positive
6	Dhanera I	Banaskantha	0.385	30	0.076	1.245	NO
7	Palanpur	Banaskantha	0.477	37	**0.024***	-2.747	Negative
8	Jamnagar	Jamnagar	0.077	6	0.765	1.032	NO
9	Amran	Jamnagar	0.077	6	0.765	0.018	NO
10	Kalavad	Jamnagar	0.026	2	0.952	0.073	NO
11	Bhatiya	Jamnagar	-0.769	-60	**< 0.0001***	0.568	Positive
12	Lalpur	Jamnagar	0.168	13	0.427	0.003	NO
13	Naliya	Kachchh	0.077	6	0.765	0.12	NO
14	Lakhpat	Kachchh	0.205	16	0.367	0.213	NO
15	Asambia mota	Kachchh	0.308	24	0.163	0.779	NO
16	Mundra	Kachchh	0.282	22	0.204	0.422	NO
17	Balasinor	Kheda	-0.41	-32	0.057	-2.12	NO
18	Matar II	Kheda	0.128	10	0.59	0.109	NO
19	Nadiad	Kheda	0.051	4	0.858	0.024	NO
20	Thasra	Kheda	-0.077	-6	0.765	-0.01	NO
21	Vidaj	Mehsana	-0.436	-34	**0.042***	0.78	Positive
22	Bhandu V	Mehsana	0.103	8	0.675	0.104	NO
23	Harij iii	Patan	0.462	36	**0.03***	-0.412	Negative
24	Sidhada	Patan	0.41	32	0.057	0.214	NO
25	Morbi	Rajkot	-0.684	-53	**0.001***	0.38	Positive
26	Bayad	Sabarkantha	-0.103	-8	0.675	-0.09	NO
27	Chandap	Sabarkantha	-0.103	-8	0.675	-0.09	NO
28	Chotila	Surendranagar	0.256	20	0.252	0.11	NO
29	Malaniyad	Surendranagar	0.077	6	0.765	0.099	NO
30	Sayala	Surendranagar	0.385	30	0.076	0.428	NO

Note: * Statistically Significant at 5% Level of Significance

Table 3.2: Post-Monsoon Mann-Kendall Statistics (2005-2017)

Well No.	Station	District	Tau	S	p-Value	Slope (m/yr.)	Trend
1	Ghuma 2	Ahmedabad	0.051	4	0.858	0.033	NO
2	Tarapur I	Anand	0.410	32	0.057	0.114	NO
3	Ambaji	Banaskantha	0.231	18	0.306	0.569	NO
4	Danta	Banaskantha	0.154	12	0.510	0.330	NO
5	Rasna	Banaskantha	0.513	40	**0.015***	-1.664	Negative
6	Dhanera I	Banaskantha	0.282	22	0.204	2.609	NO
7	Palanpur	Banaskantha	-0.426	-33	**0.044***	0.297	Positive
8	Jamnagar	Jamnagar	0.231	18	0.306	0.319	NO
9	Amran	Jamnagar	0.026	2	0.952	0.017	NO
10	Kalavad	Jamnagar	0.179	14	0.435	0.029	NO
11	Bhatiya	Jamnagar	-0.026	-2	0.952	-0.022	NO
12	Lalpur	Jamnagar	0.667	52	**0.001***	-0.568	Negative
13	Naliya	Kachchh	-0.103	-8	0.675	-0.081	NO
14	Lakhpat	Kachchh	0.231	18	0.306	0.347	NO
15	Asambia mota	Kachchh	-0.026	-2	0.952	-0.090	NO
16	Mundra	Kachchh	-0.039	-3	0.855	-0.041	NO
17	Balasinor	Kheda	0.026	2	0.952	0.006	NO
18	Matar II	Kheda	-0.128	-10	0.590	-0.161	NO
19	Nadiad	Kheda	0.154	12	0.510	0.276	NO
20	Thasra	Kheda	0.615	48	**0.003***	-0.094	Negative
21	Vidaj	Mehsana	-0.179	-14	0.435	-0.215	NO
22	Bhandu V	Mehsana	0.103	8	0.675	0.182	NO
23	Harij iii	Patan	0.154	12	0.510	0.661	NO
24	Sidhada	Patan	0.179	14	0.435	0.088	NO
25	Morbi	Rajkot	0.256	20	0.252	0.142	NO
26	Bayad	Sabarkantha	-0.026	-2	0.952	-0.011	NO
27	Chandap	Sabarkantha	0.051	4	0.858	0.017	NO
28	Chotila	Surendranagar	0.359	28	0.100	0.474	NO
29	Malaniyad	Surendranagar	0.154	12	0.510	0.241	NO
30	Sayala	Surendranagar	0.385	30	0.076	0.801	NO

Note: * Statistically Significant at 5% Level of Significance.

Similar Mann Kendall statistical trend analysis tests were conducted on time series rainfall data of 2005 to 2017. Results are presented in Table 3.3 below.

Table 3.3: Annual Rainfall Mann-Kendall Statistics (2005-2017)

Well No.	Station	District	Tau	S	p-Value	Slope (mm/yr.)	Trend
1	Ghuma 2	Ahmedabad	-0.308	-24	0.161	-22.17	NO
2	Tarapur I	Anand	-0.41	-32	0.059	-45.32	NO
3	Ambaji	Banaskantha	0.282	22	0.2	28.22	NO
4	Danta	Banaskantha	0.282	22	0.2	30.77	NO
5	Rasna	Banaskantha	0	0	1	1.35	NO
6	Dhanera I	Banaskantha	-0.128	-10	0.583	-20.56	NO
7	Palanpur	Banaskantha	0.051	4	0.855	2.88	NO
8	Jamnagar	Jamnagar	-0.359	-28	0.1	-33.64	NO
9	Amran	Jamnagar	-0.154	-12	0.502	-10.93	NO
10	Kalavad	Jamnagar	-0.333	-26	0.127	-30.99	NO
11	Bhatiya	Jamnagar	-0.128	-10	0.583	-12.23	NO
12	Lalpur	Jamnagar	-0.359	-28	0.1	-28.18	NO
13	Naliya	Kachchh	-0.077	-6	0.76	-12.23	NO
14	Lakhpat	Kachchh	-0.179	-14	0.428	-17.54	NO
15	Asambia mota	Kachchh	-0.282	-22	0.2	-16.60	NO
16	Mundra	Kachchh	-0.282	-22	0.2	-27.68	NO
17	Balasinor	Kheda	-0.256	-20	0.246	-25.88	NO
18	Matar II	Kheda	-0.41	-32	0.059	-41.82	NO
19	Nadiad	Kheda	-0.41	-32	0.059	-49.85	NO
20	Thasra	Kheda	-0.359	-28	0.1	-42.92	NO
21	Vidaj	Mehsana	-0.256	-20	0.246	-37.14	NO
22	Bhandu V	Mehsana	-0.205	-16	0.36	-17.17	NO
23	Harij iii	Patan	-0.205	-16	0.36	-13.98	NO
24	Sidhada	Patan	0.077	6	0.76	2.06	NO
25	Morbi	Rajkot	-0.179	-14	0.428	-31.56	NO
26	Bayad	Sabarkantha	-0.231	-18	0.3	-14.83	NO
27	Chandap	Sabarkantha	0.051	4	0.855	5.88	NO
28	Chotila	Surendranagar	-0.436	-34	**0.044***	-39.56	Negative
29	Malaniyad	Surendranagar	-0.308	-24	0.161	-36.38	NO
30	Sayala	Surendranagar	-0.333	-26	0.127	-46.55	NO

Note: ***** Statistically Significant at 5% Level of Significance.

An important consideration here is that since the groundwater levels are measured relative to the ground surface, it implies that higher values of groundwater levels relate to deeper water table and vice-versa. Therefore, in Mann-Kendall results, a positive value of S indicates a decrease in groundwater level and a negative S value indicates its increase. The MK statistics reveal that comparatively there are more number of wells with significant decline in pre monsoon as compared to the post monsoon season. Results from Table 3.1 and Table 3.2 indicate that Banaskantha and Patan district on an average showed a decreasing trend with a rate of 2.23, 3.62 and 2.74 m/yr. at Ambaji, Danta and Palanpur monitoring stations in Banaskantha district and 41 cm/yr. at Harji station in Patan district. The monitoring wells in Jamanagar and Rajkot districts however showed an upward trend with 56.8 cm/yr. and 38.2 cm/yr. at Bhatiya and Morbi and stations respectively. Rasna in Banaskantha also showed an increasing trend at a rate of 35.7 cm/yr. The strongest increase was witnessed at Vidaj in Mehsana district with a rate of 78 cm/yr. For post monsoon season during the same years only 4 locations showed significant trends with 3 locations showing downward trend and 1 location showing an increasing trend. The maximum declining rate witnessed was 1.66 m/yr. at Rasna in Banaskantha with an increasing rate of 29.7 cm/yr. at Palanpur. The test statistics for annual rainfall during 2005-2017 (Table 3.3) did not reveal any significant trend in the Kutch-Sabarmati basin, except for 1 location Chotila in Surendranagar district where a decline in rainfall was observed, at a rate of 39.6 mm/yr. during the study period (Figure 3.4). Though a cyclic pattern of rainfall is present, but no specific trend was observed over the years.
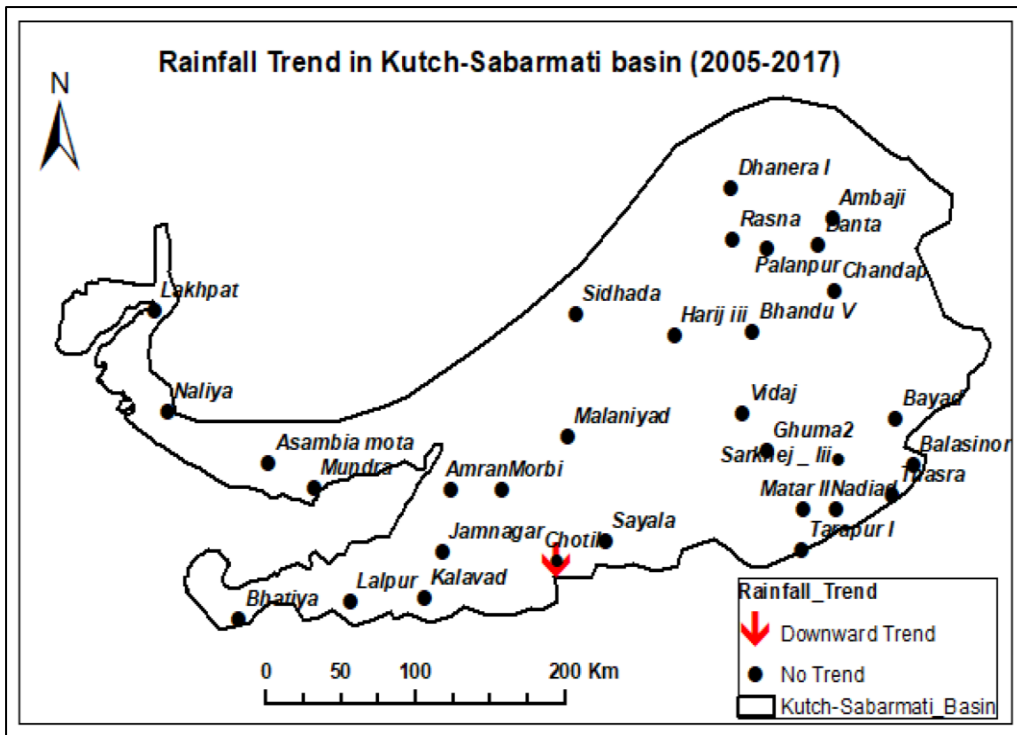
Fig 3.4: Spatial distribution of Rainfall Trend in Kutch Sabarmati basin

Figures 3.5 and 3.6 show the spatial distribution of groundwater level trends in the study area during pre and post monsoon seasons based on Mann Kendall results.
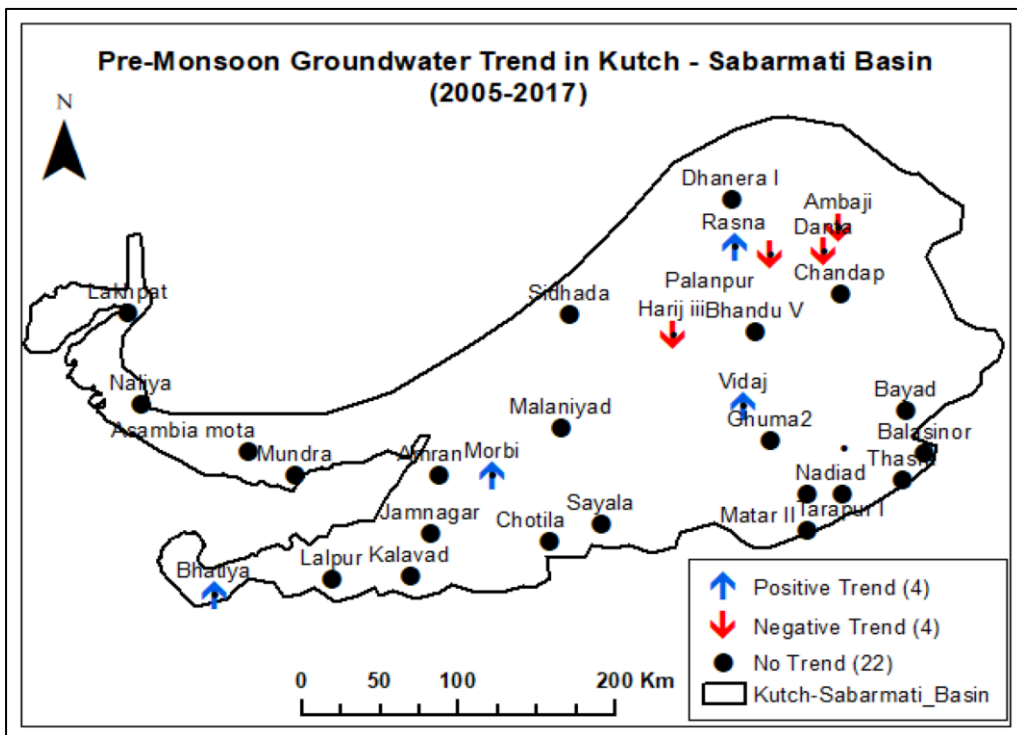

Fig 3.5: Spatial distribution of Pre-Monsoon Groundwater Trends in Kutch-
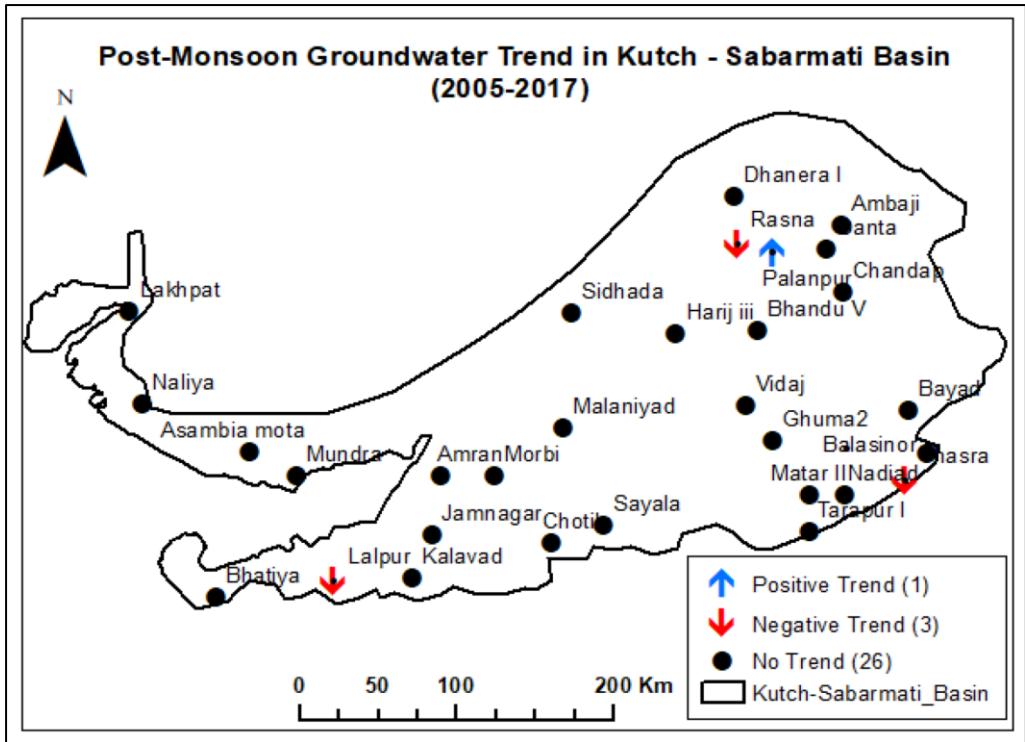Sabarmati basin

Fig 3.6: Spatial distribution of Post-Monsoon Groundwater Trends in Kutch
Sabarmati basin

Since, the pre monsoon ground water levels of May, also relate to the groundwater pumping amounts done after the post monsoon in the preceding year, i.e between the months of November to May; the declining results of pre monsoon trend analysis suggest that the amount of groundwater pumping is more in Banaskantha and Patan districts as compared to the other districts especially towards the Kutch basin on the west that show some increasing trends mostly of local nature. During the post monsoon season, lesser number of declining wells primarily in Banaskantha and Patan districts is due to the recharge of the aquifers from the monsoon rainfall. The higher percentage of agriculture and lesser percentage of water bodies in Banaskantha and Patan districts as compared to Jamnagar and Rajkot districts provide a reasonable explanation to the groundwater trends witnessed in these areas (Figure 3.7). The map was created using pixel level classification of LandSAT-8 image of 2017 in ERDAS Imagine and groundwater trends were overlaid on the Landuse-Landcover map.
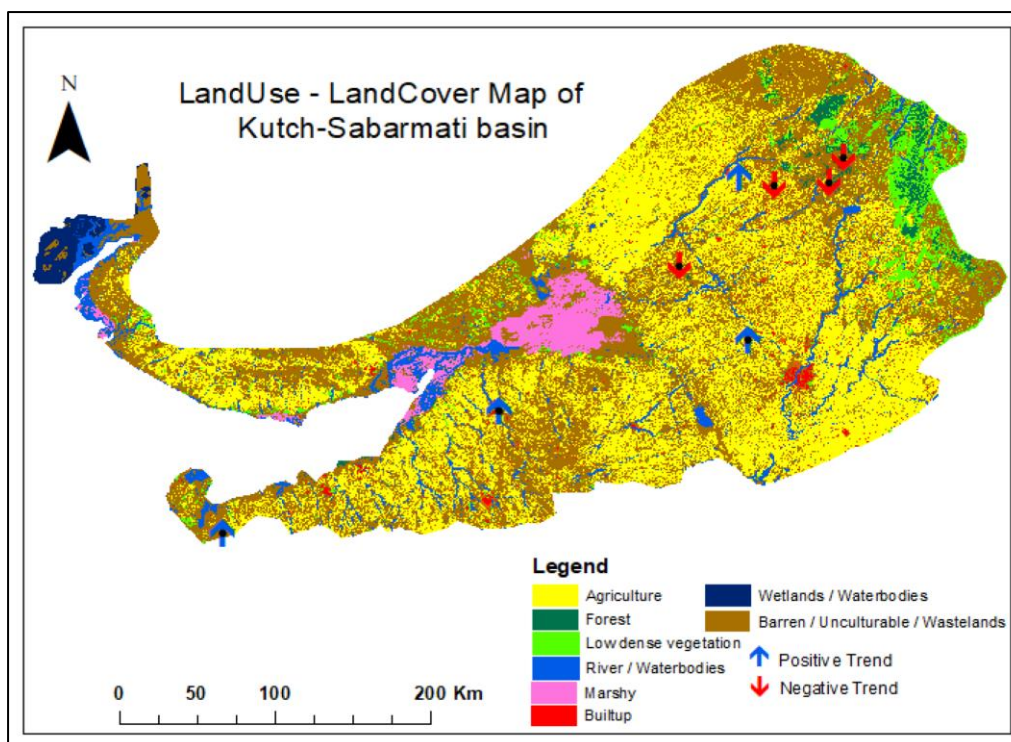
Fig 3.7: Landuse-Landcover map of Kutch-Sabarmati basin with pre-monsoon groundwater trends.

Table 3.4 below shows the percentage of each landuse class as observed in Kutch-Sabarmati basin.

Table 3.4: Percentage of Landuse classes in different districts of Kutch-Sabarmati basin.

District	Percentage of Land Use classes					
	Agriculture	Waterbodies	Urban	Forest	Low Dense Vegetation	Barren/Non Cultivable/ Wasteland
Banaskantha	58.51	1.07`	1.24	2.39	0.73	36.05
Patan	58.12	2.02	1.46	0.28	0.92	37.20
Jamnagar	43.76	3.71	1.99	1.40	1.55	47.59
Rajkot	44.87	2.26	2.64	0.03	1.04	48.79

During the post monsoon season, lesser number of declining wells primarily in Banaskantha and Patan districts is due to the aquifer recharge from the monsoon rainfall. The slope map of the basin (Figure 3.8) reveals that most of the significant declining trends in pre-monsoon groundwater levels are in the wells of Banaskantha district that lie towards the steeper slope areas where the slope is more than 15 degrees. Banaskantha is an arid to semi-arid district which is surrounded by Aravalli mountain ranges on the north east. The Aravalli

94

ranges receive high rainfall during the monsoons and the water flowing down from the mountains is a major source of feeding the ephemeral rivers of the district and also acts as major contributor to the groundwater recharge. However, the higher slope factor results in greater runoff thereby reducing the groundwater recharge due to less infiltration. Consequently, the wells in these areas are witnessing sharp declining trends in the groundwater levels.
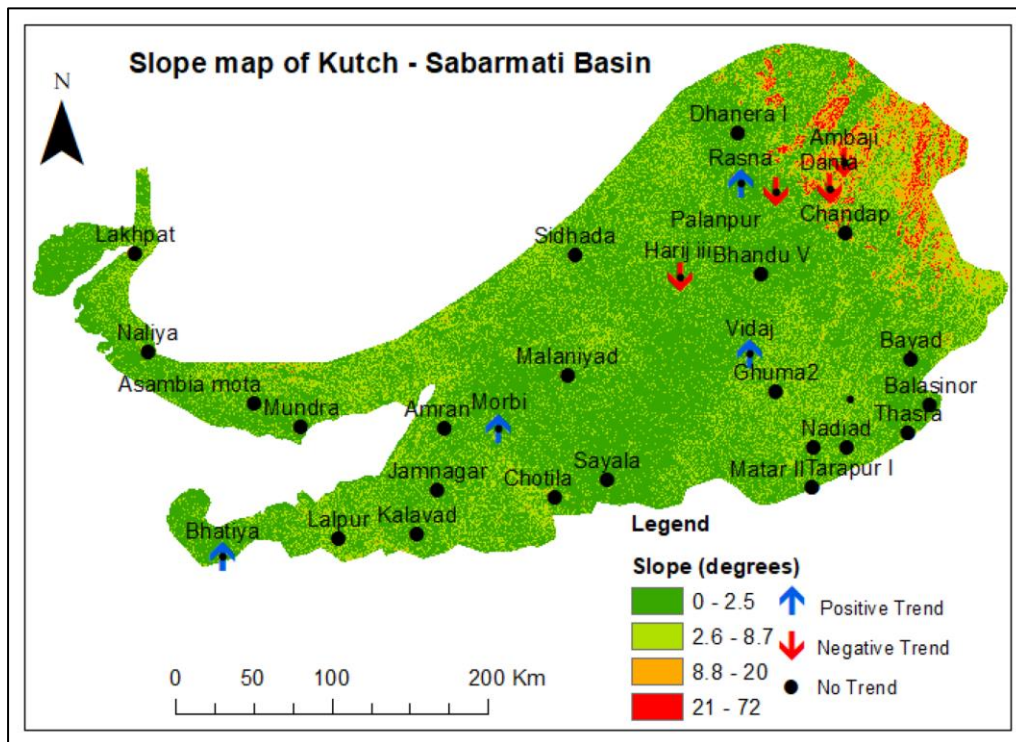

Fig 3.8: Slope map of Kutch-Sabarmati basin with pre-monsoon groundwater trends.

The overall analysis of trends for both pre and post monsoon groundwater level suggests that Banaskantha and Patan districts in the study area are more vulnerable to decreasing water levels and increased pumping as compared to other regions.

3.3 GEOSTATISTICAL ANALYSIS OF GROUNDWATER LEVELS

Geostatistical tools were used to analyze spatio-temporal pattern of groundwater depletion using field-based piezometric groundwater level data collected from CGWB. Based upon the Groundwater level change, monitored specifically during the pre-monsoon to pre-monsoon and during post-monsoon to pre-monsoon seasons, a time series spatio-temporal modelling is done to observe the change in falling or rising levels due to depletion or recharge of groundwater. Standard statistical techniques of Inverse Distance Weighted

Interpolation and Kriging were used to create the piezometric head fluctuation interpolated maps for every year which were later weighted using the Kalman filter algorithm that gives a more robust prediction though a statistical comparison of the new set of predicted values to the original set of observations. The Kalman filter weighted product was computed by summing the product of respective correlation coefficient of both IDW and Kriging with their predicted outputs, and then dividing by the sum of correlation coefficients. The process was repeated for every year to find the depletion rates of groundwater levels in Kutch-Sabarmati basin. Fluctuation maps were produced for both pre-pre and post-pre monsoon seasons for every year (2005-2017) and Average fluctuation maps and Standard deviation maps of the same period were made to understand the changes in regional groundwater levels during the study period. Hotspots of groundwater decline were identified from the seasonal maps. The methodology flowchart for geostatistical analysis of groundwater levels is given below in Figure 3.9.
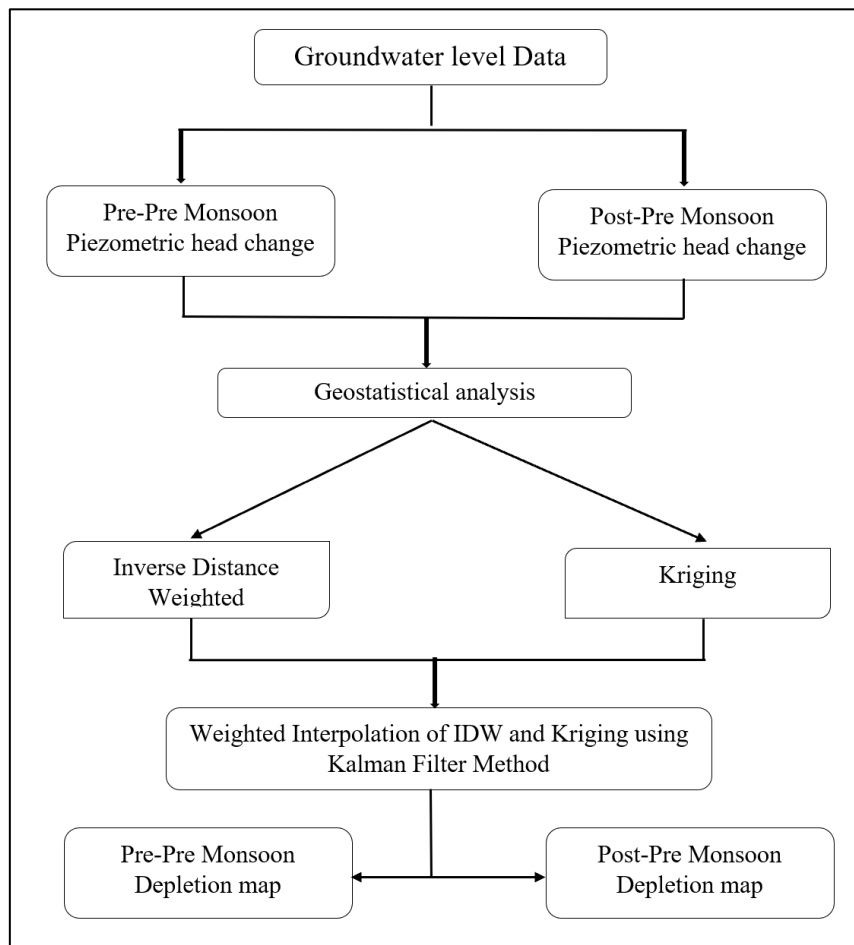

**Fig 3.9**: Flowchart for Statistical Interpolation of Groundwater Level.

3.3.1 Results and Discussion

The Fluctuation maps of Pre-Monsoon to Pre-Monsoon piezometric heads were created using Kalman Filter method which is based on Correlation coefficient values obtained from IDW and Kriging Interpolation techniques (Table 3.5).

Table 3.5: Correlation Coefficient of Pre to Pre Monsoon

Year	IDW	Kriging	Kalman
May 05_06	0.61	0.61	0.70
May 06_07	0.98	0.57	0.83
May 07_08	0.76	0.21	0.94
May 08_09	0.69	0.33	0.36
May 09_10	0.86	0.27	0.88
May 10_11	0.07	0.11	0.20
May 11_12	0.91	0.70	0.83
May 12_13	0.59	0.30	0.68
May 13_14	0.96	0.41	0.92
May 14_15	0.85	0.53	0.89
May 15_16	0.97	0.83	0.97
May 16_17	0.78	0.44	0.91

The groundwater fluctuation maps of pre-pre monsoon groundwater levels were created for every year, where the pre monsoon groundwater levels of succeeding year was subtracted from the pre monsoon groundwater levels in the preceding year (Fig. 3.10 a to l).
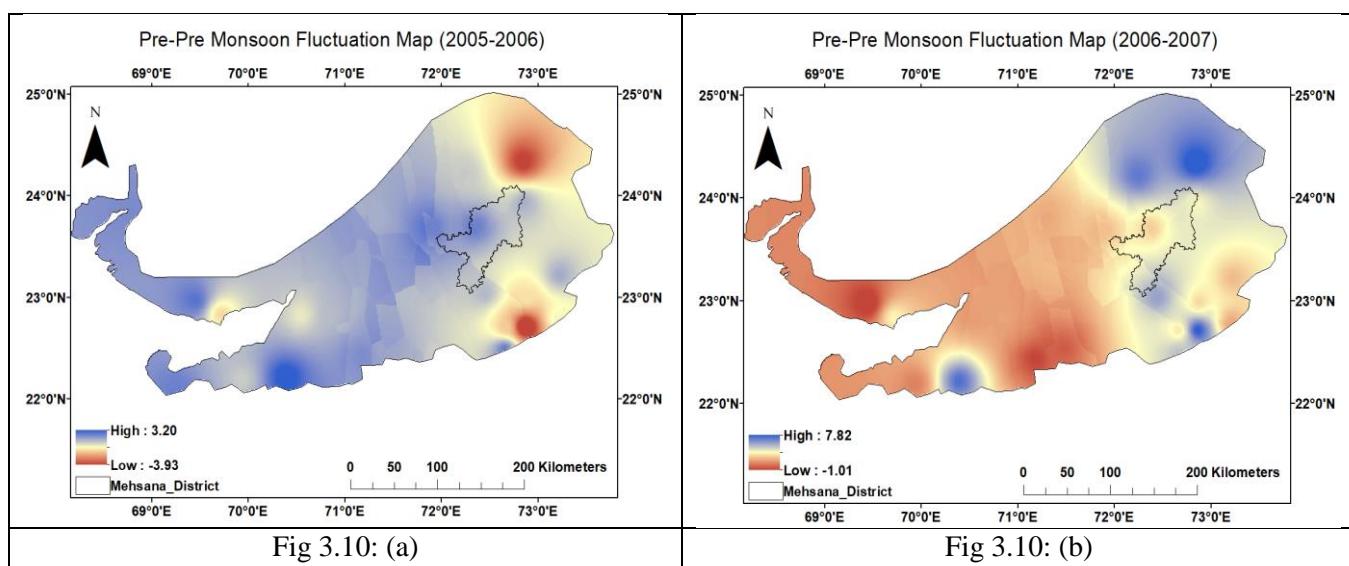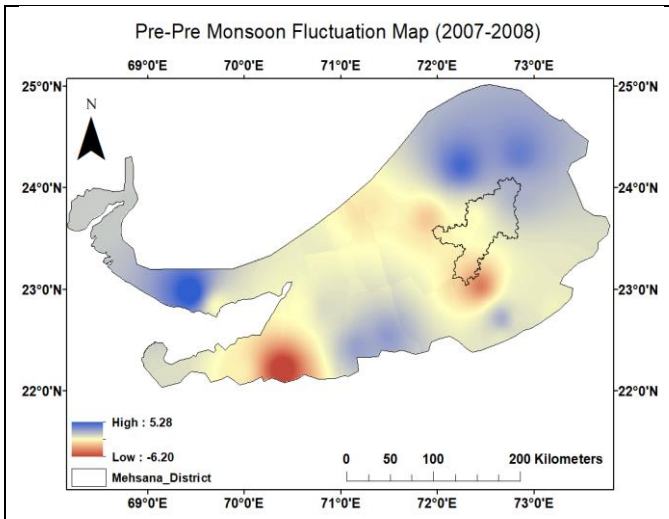

Fig 3.10: (a)	Fig 3.10: (b)
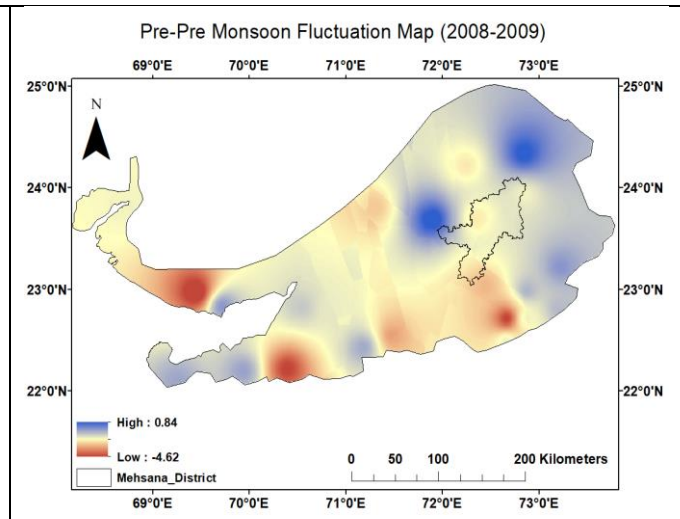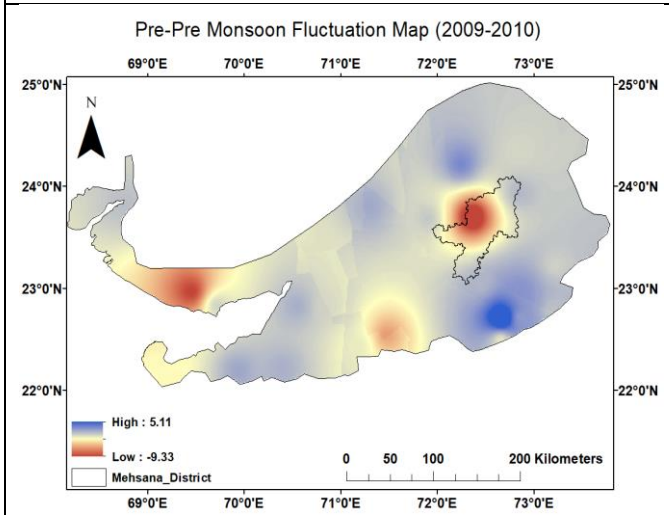
Fig 3.10: (c)

Fig 3.10: (d)

Fig 3.10: (e)
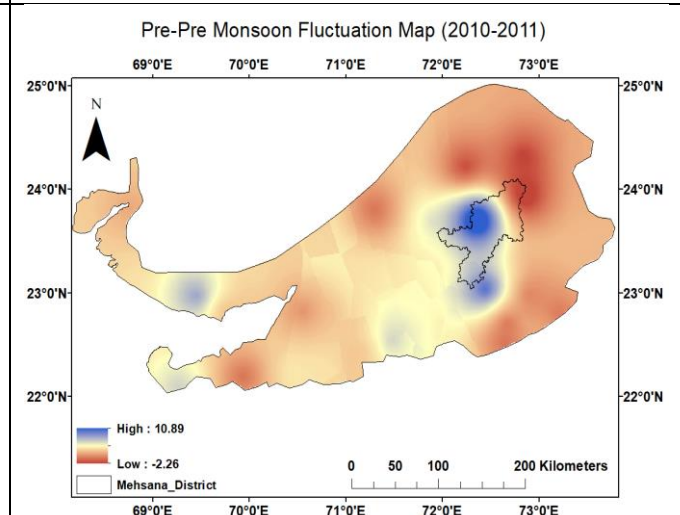
Fig 3.10: (f)

Fig 3.10: (g)

Fig 3.10: (h)
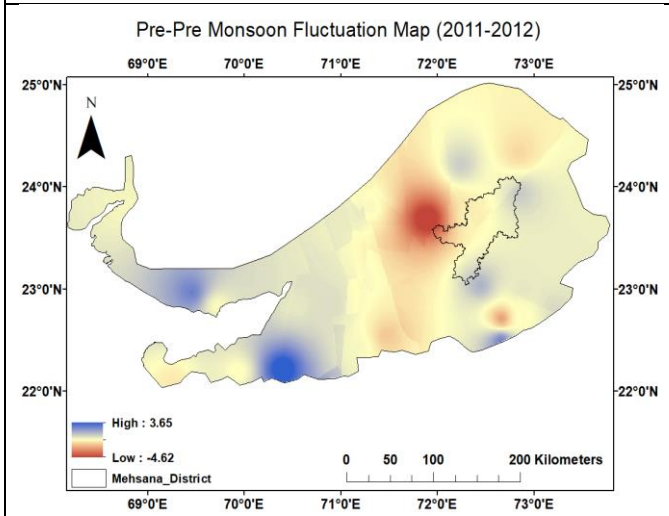
Fig 3.10: (i)
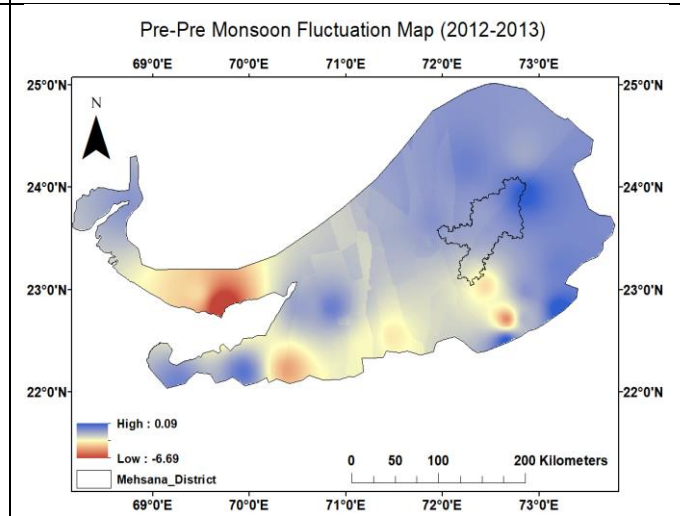
Fig 3.10: (j)
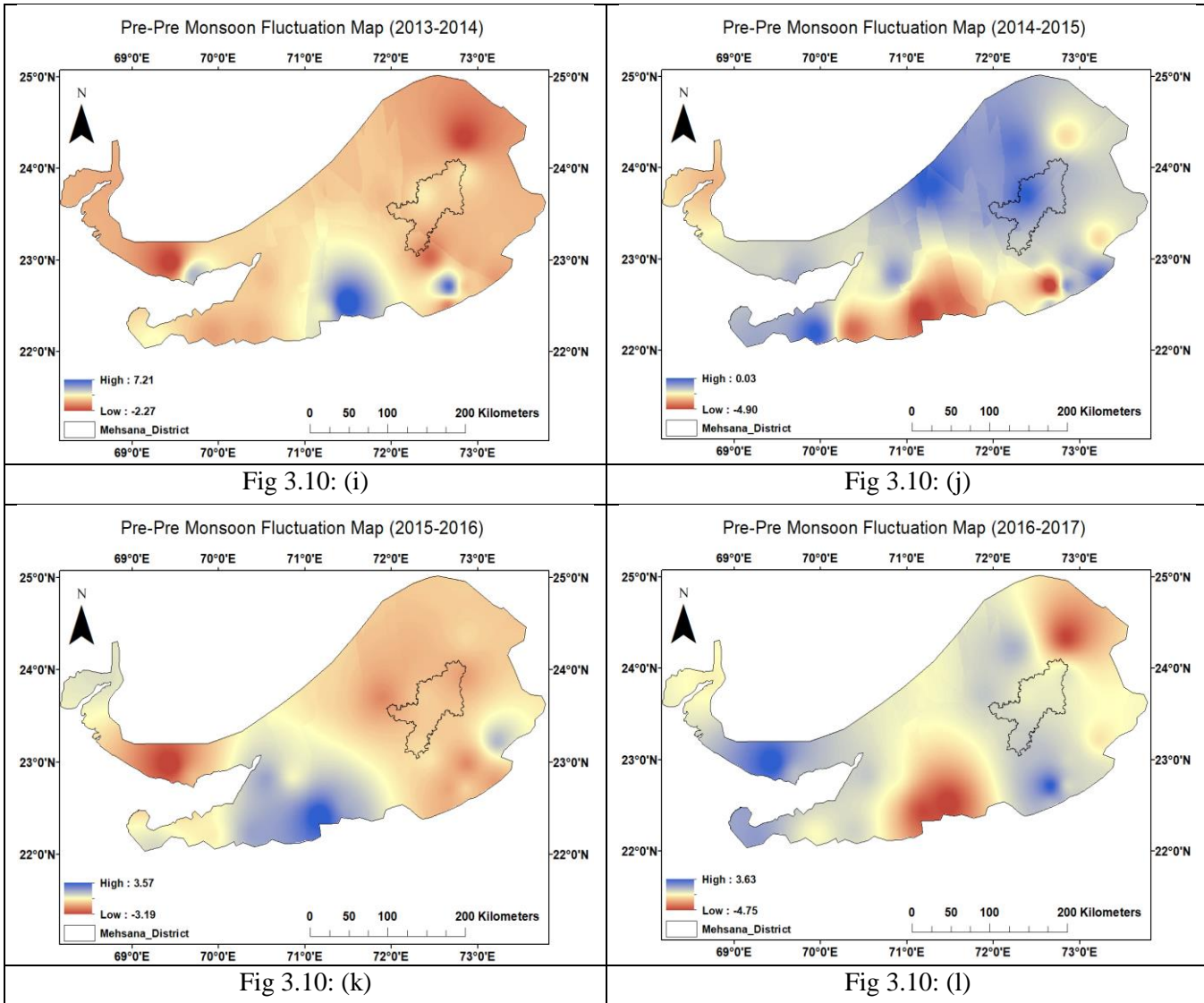
Fig 3.10: (k)

Fig 3.10: (l)

Fig 3.10 (a to l): Pre-Pre Fluctuation Maps for Individual years (2005-2017)

The average pre-pre fluctuation maps for the time periods 2005-2011, 2012-2017 and 2005-2017 are shown in Fig. 3.11 to 3.13 below. The standard deviation map for 2005-2017 also shown in Fig.3.14.

Fig 3.11 Average Map of Pre-Pre Fluctuation (2005-2011)

Fig 3.12 Average Map of Pre-Pre Fluctuation (2012-2017)

99

| **Fig 3.13**: Average Map of Pre-Pre Fluctuation (2005-2017) | **Fig 3.14**: Standard Deviation Map of Pre-Pre Fluctuation (2005-2017) |
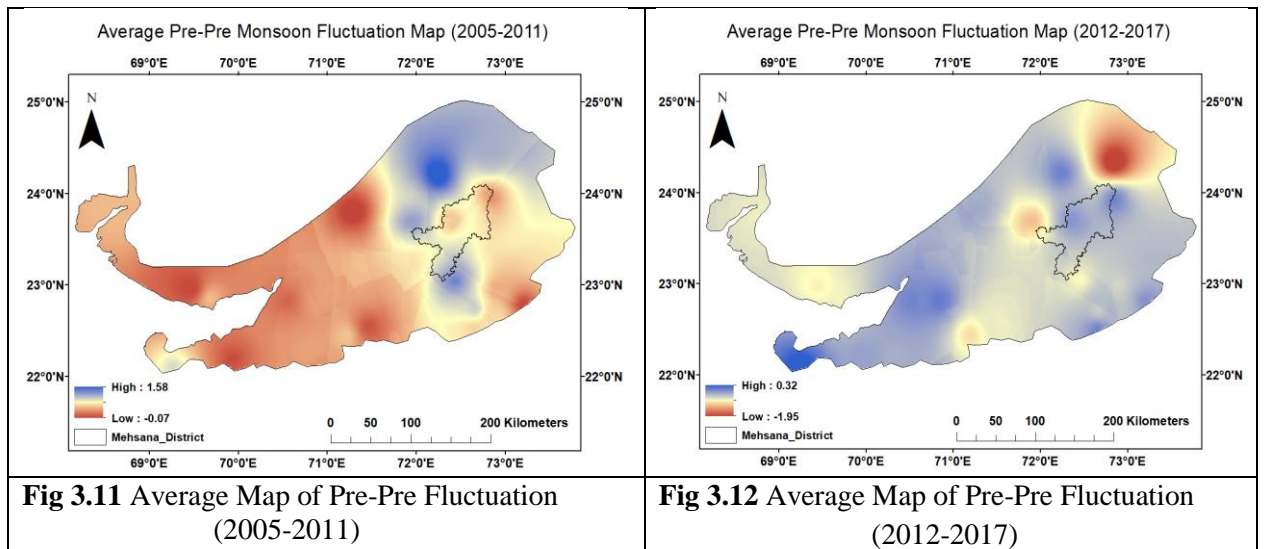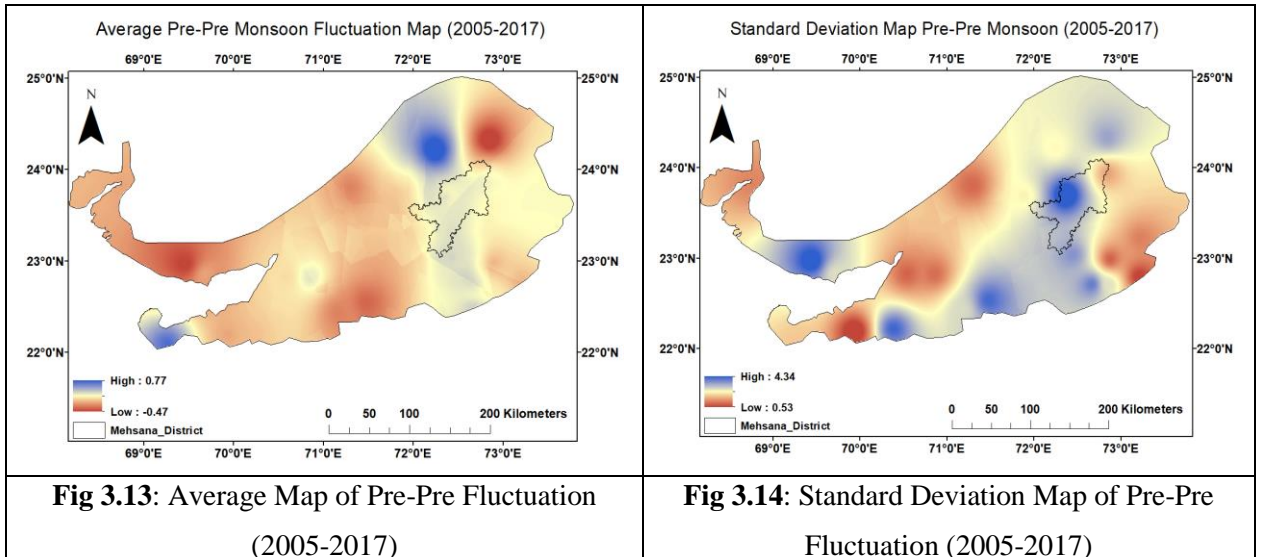
The mean rainfall recorded in Mehsana district during the period 2005 to 2017 is shown in Fig. 3.15 below.
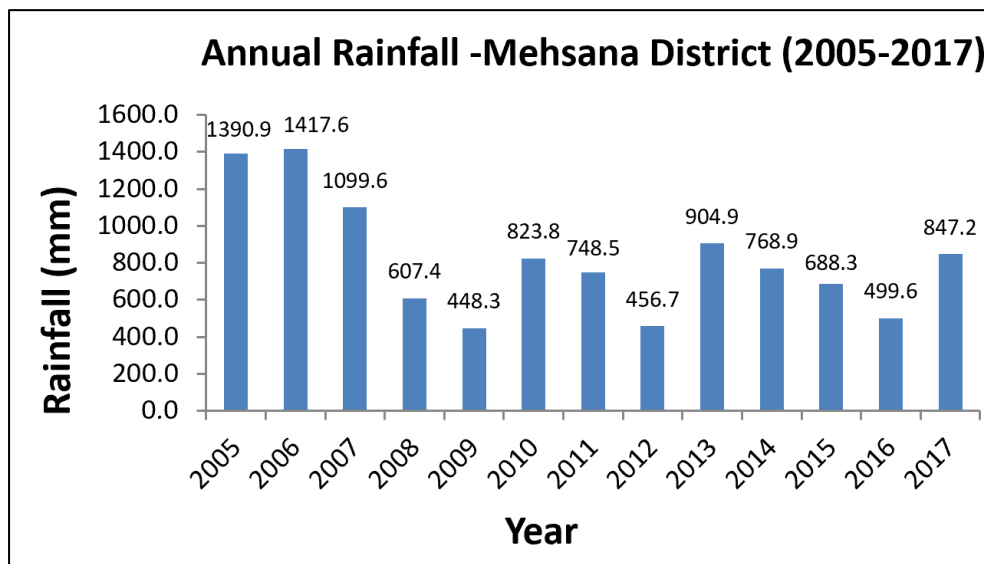
Fig. 3.15: Annual Rainfall in Mehsana district (2005-2017)

The results indicate that though there have been intermediate episodes of recharge and depletion of groundwater levels in Kutch-Sabarmati basin, but Kutch basin which is towards the west of the composite basin show high declining trends as compared to the Sabarmati basin on the east. Rainfall and rivers are the primary sources for recharging subsurface aquifers. Kutch basin receives very less rainfall (Figure 1.4) and is drained by very small seasonal river tributaries as compared to the Sabarmati basin which is drained by high flowing rivers like Sabarmati, Banas and Rupen. In pre-pre monsoon maps, positive values suggest recharge whereas negative values point towards depletion. Mehsana district along with some portions of Banaskantha, Deesa,

100

Palanpur and Patan districts also show gradual signs of depletion over the long term period from 2005 to 2017. Similar trends were also seen from Mann Kendall statistical test where some portions of Banaskantha and Patan were showing negative trends. Though there have been intermediate episodes of recharge and depletion, due to cyclical patterns of high and low rainfall in the area (Figure 3.15), the rate of depletion was observed to be higher in years prior to 2009 in and around Mehsana district, with more recharge episodes seen post 2009. From figures 3.11 and 3.12, it is evident that there has a been an improvement in the depletion scenarios in and around Mehsana district during the period 2012 to 2017 as compared to the earlier time period of 2005 to 2011. The average map of 2005 and 2017 shows that the rate of depletion during the pre-monsoon months is moderate in Mehsana district, with an average depletion rate of -0.54 m/year from 2005 to 2017. Depletion rate is also moderately high south of Mehsana towards Ahmedabad and Gandhinagar districts. Since, the pre-pre monsoon groundwater levels also relate to the groundwater pumping so the higher rates of depletion in Mehsana, Ahmedabad and Gandhinagar districts suggest that groundwater pumping is widespread in these parts of the basin.

Though there has an improvement in the second half of the study period but the overall analysis throughout the study period of 2005 to 2017 show gradual signs of reducing piezometric heads. The standard deviation map of pre-pre monsoon piezometric heads, show high value of deviation from the average in around Mehsana District which indicates that the groundwater head fluctuation is considerably more in these parts of the basin, especially around the Mehsana Taluk of Mehsana district, higher fluctuations are observed in the standard deviation maps. The improvement of groundwater levels after 2012 can also be attributed to the fact that that after the commissioning of Narmada canal in 2008, which passes through parts of South and North Gujarat, the dependence on groundwater for irrigation purposes have reduced thereby showing relative slowdown in the depletion scenario in the region. Also, the canal water recharges the underground aquifers which has also helped in the improvement of water levels. The Kutch Branch canal of Narmada Main canal that is supposed to supply water to the arid Kutch region is not fully functional as of now and it will take more time before we could see improvements in the groundwater levels of the Kutcha and Saurashtra regions.

The fluctuation maps of Post Monsoon to Pre Monsoon were created using Kalman Filter method (Fig. 3.16) which is based on Correlation coefficient values as obtained from IDW and Kriging Interpolation techniques and interpolated results using Kalman Filter approach (Table 3.6).

Table 3.6: Correlation Coefficient of Post to Pre Monsoon

Year	IDW	Kriging	Kalman
Nov05-May05	0.93	0.52	0.93
Nov06-May06	0.66	0.27	0.72
Nov07-May07	0.79	0.23	0.82
Nov08-May08	0.77	0.35	0.81
Nov09-May09	0.99	0.26	0.93
Nov10-May10	0.21	0.16	0.34
Nov11-May11	0.26	0.45	0.52
Nov12-May12	0.12	0.19	0.30
Nov13-May13	0.54	0.29	0.65
Nov14-May14	0.89	0.31	0.90
Nov15-May15	0.92	0.54	0.92
Nov16-May16	0.91	0.45	0.88
Nov17-May17	0.94	0.54	0.95

The groundwater fluctuation maps of post-pre monsoon groundwater levels were created for every year, where the post monsoon groundwater levels of a year was subtracted from the pre monsoon groundwater levels of the same year (Fig. 3.16 a to m).
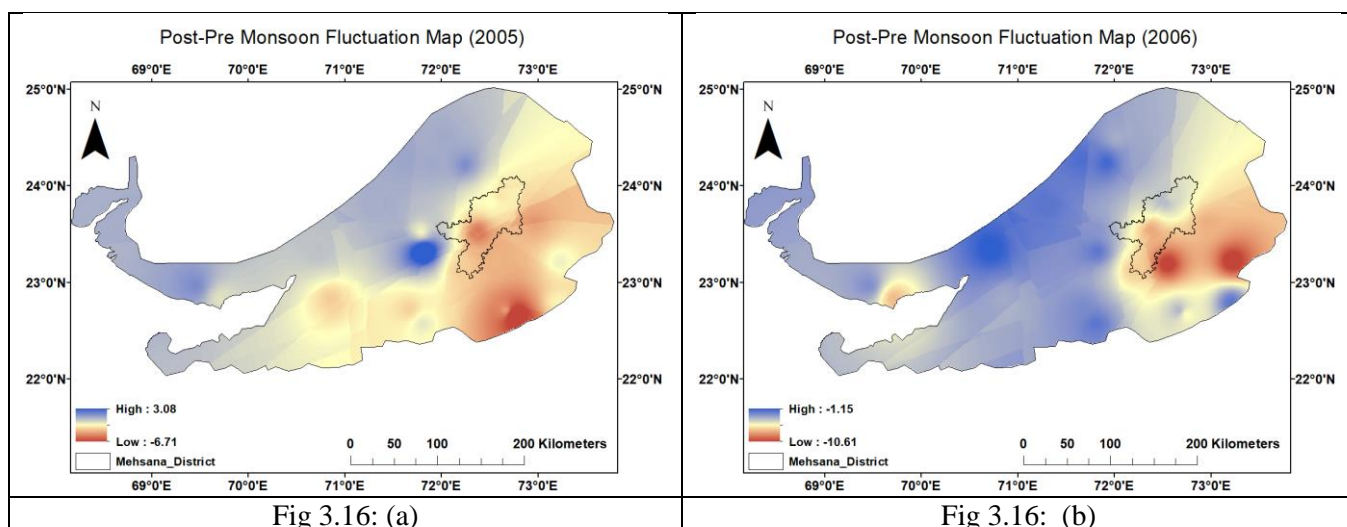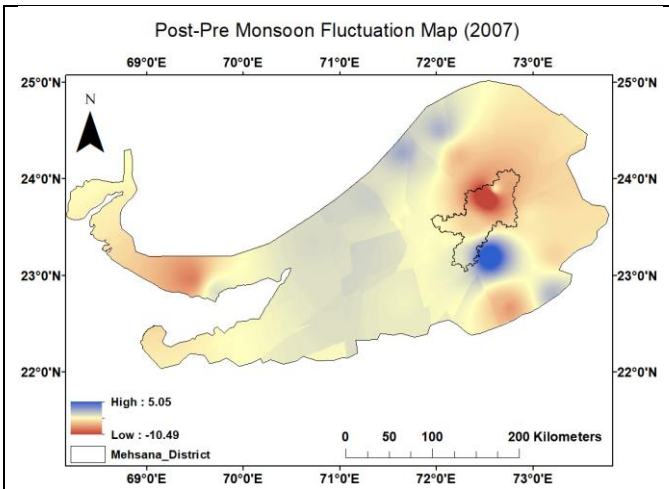
| Fig 3.16: (a) | Fig 3.16: (b) |
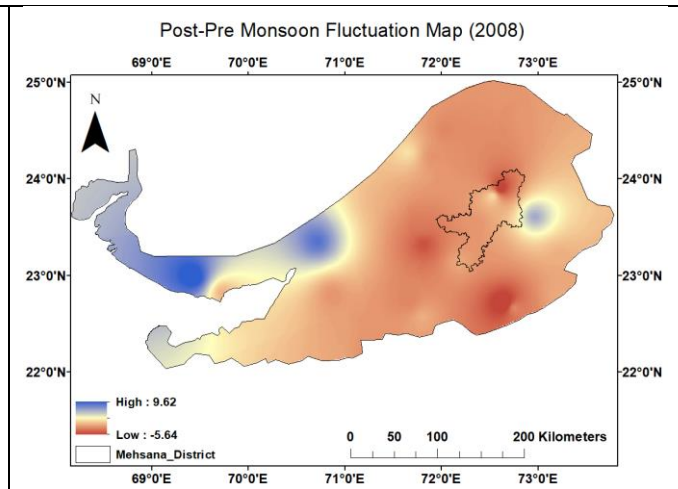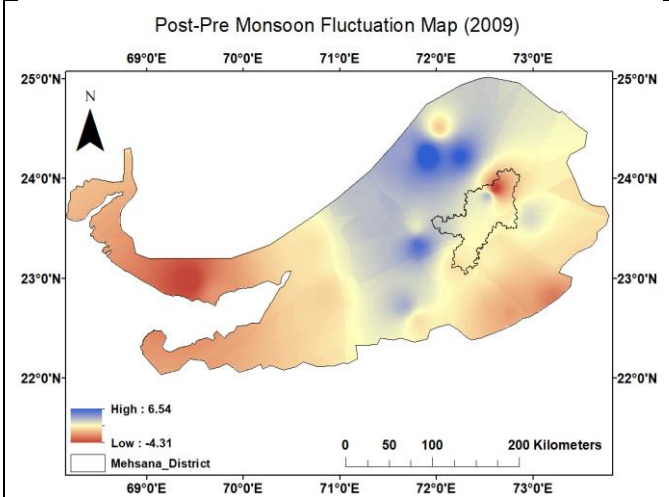
Fig 3.16: (c)

Fig 3.16: (d)

Fig 3.16: (e)
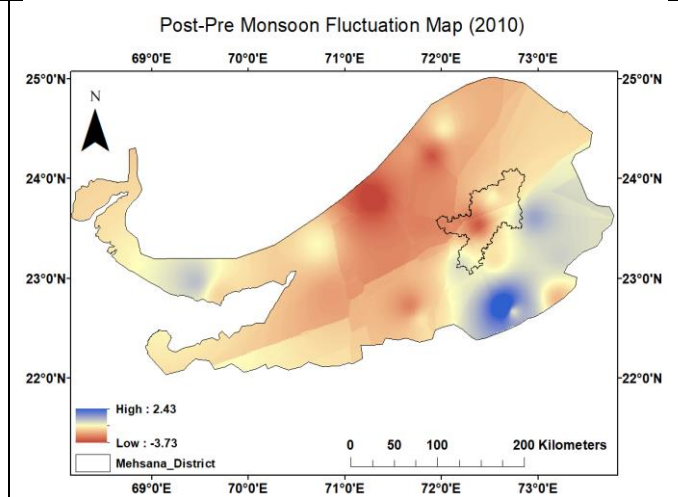
Fig 3.16: (f)

Fig 3.16: (g)

Fig 3.16: (h)

Fig 3.16: (i)
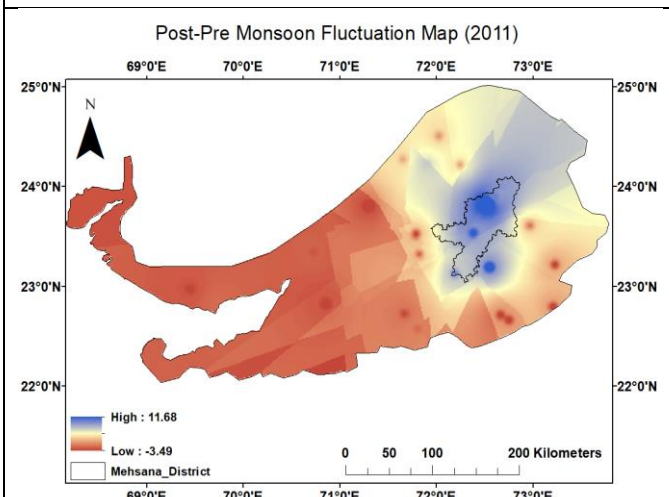
Fig 3.16: (j)
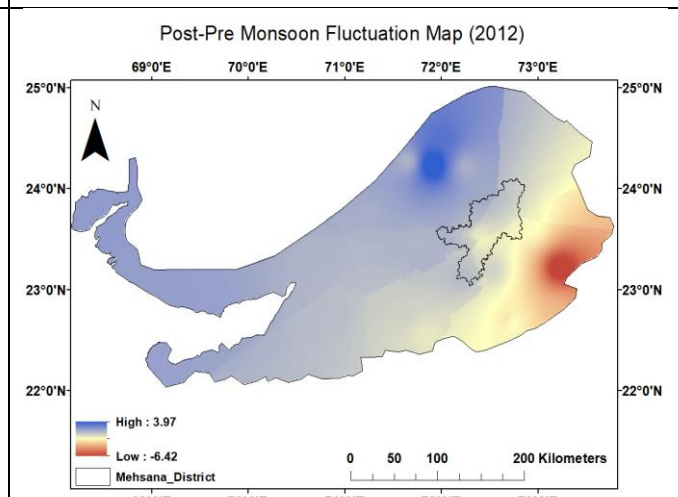
Fig 3.16: (k)
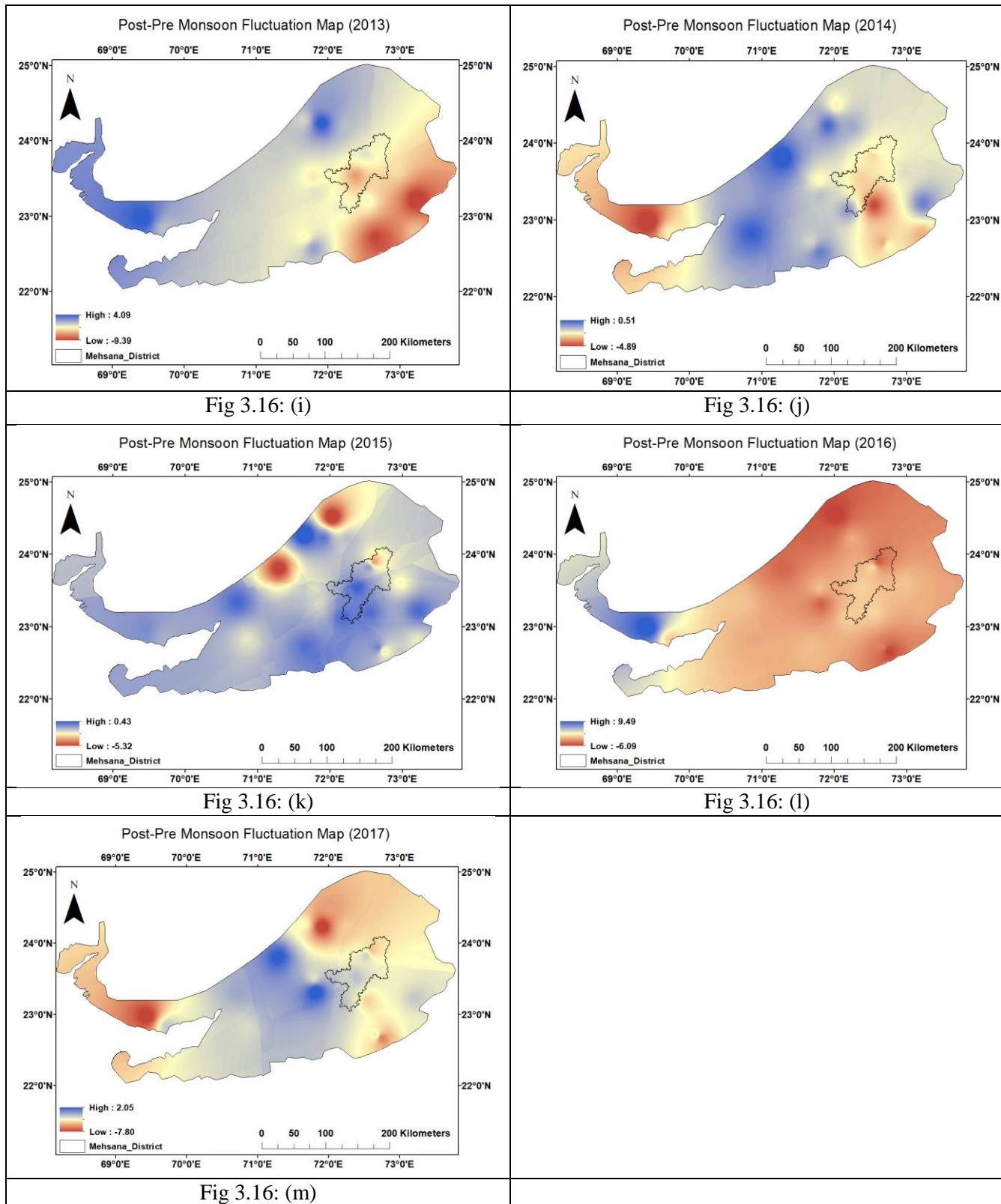
Fig 3.16: (l)

Fig 3.16: (m)

Fig 3.16 (a to m): Post-Pre Fluctuation Maps for Individual years (2005-2017)

The average post-pre fluctuation maps for 2005-2011, 2012-2017 and 2005-2017 are shown in Fig. 3.17 to 3.19 below. The standard deviation map for 2005-2017 is also shown in Fig. 3.20.
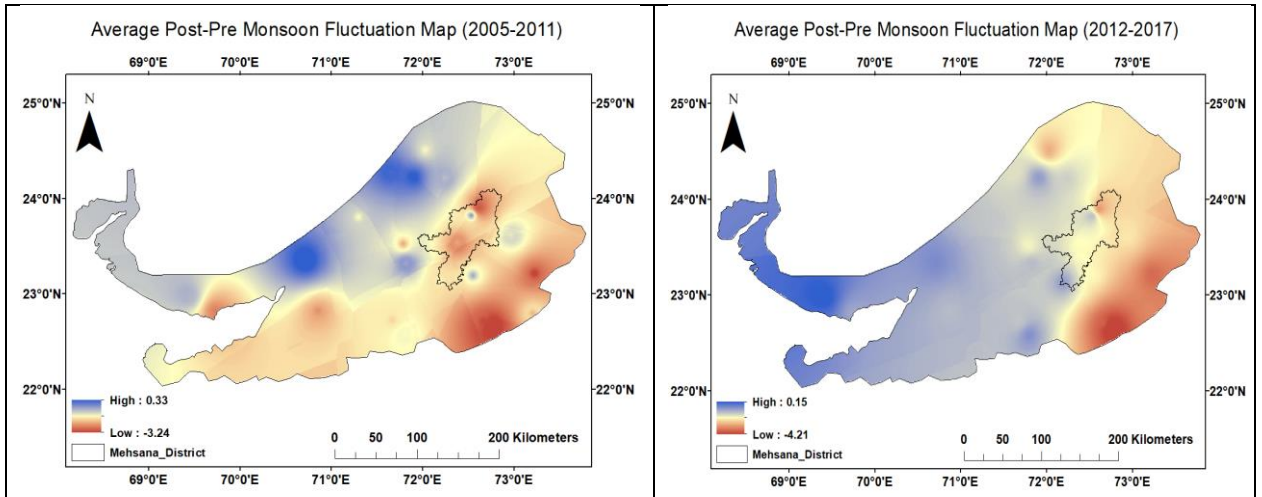
Fig 3.17 Average Map of Post-Pre Fluctuation (2005-2011)

Fig 3.18 Average Map of Post-Pre Fluctuation (2012-2017)
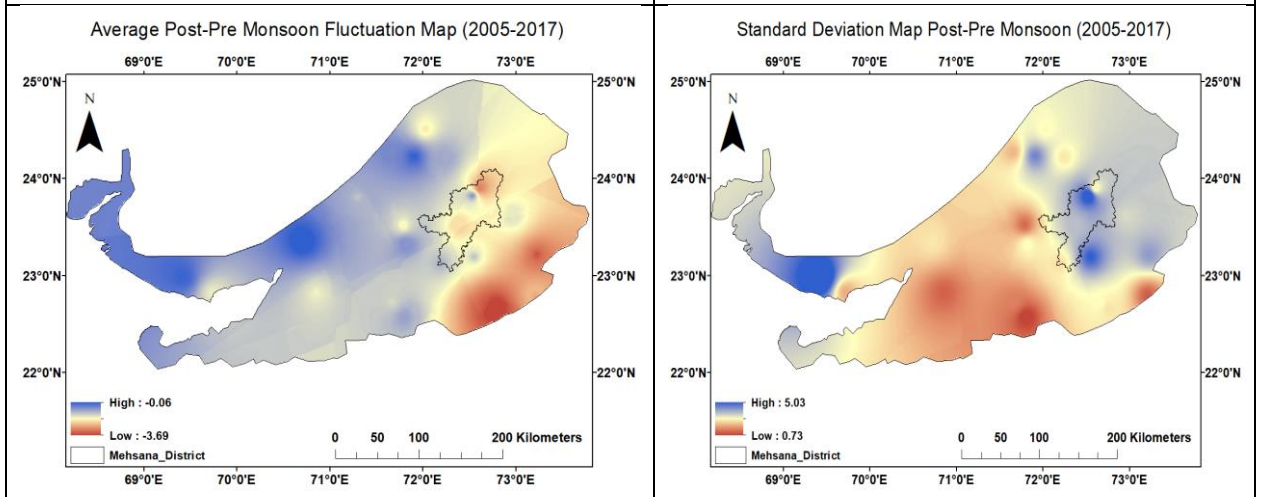
Fig 3.19: Average Map of Post-Pre Fluctuation (2005-2017)

Fig 3.20: Standard Deviation Map of Post-Pre Fluctuation (2005-2017)

The Depletion maps of Post Monsoon to Pre-Monsoon also show a high depletion trend like Pre-Pre Monsoon. It is inferred that areas in and around Mehsana had a higher rate of depletion in years prior to 2009 while there is gradual declining trend in depletion values as obtained from the piezometric head changes in and around Mehsana. The average map shows rate of depletion is moderate to high in and around Mehsana. The standard deviation map of Post-Pre monsoon also show high value of deviation from the average in around Mehsana District similar to pre-pre standard deviation map, which indicates that the groundwater head fluctuation is considerably more around Mehsana.

Since the Post-Pre fluctuations are also dependent on the rainfall falling in the monsoon period, linear regression analysis was done between Post-Pre water level fluctuations and rainfall to analyze the correlation between

105

rainfall and water table (Figure 3.21). The groundwater levels were segregated district wise as part of the composite Kutch-Sabarmati basin.
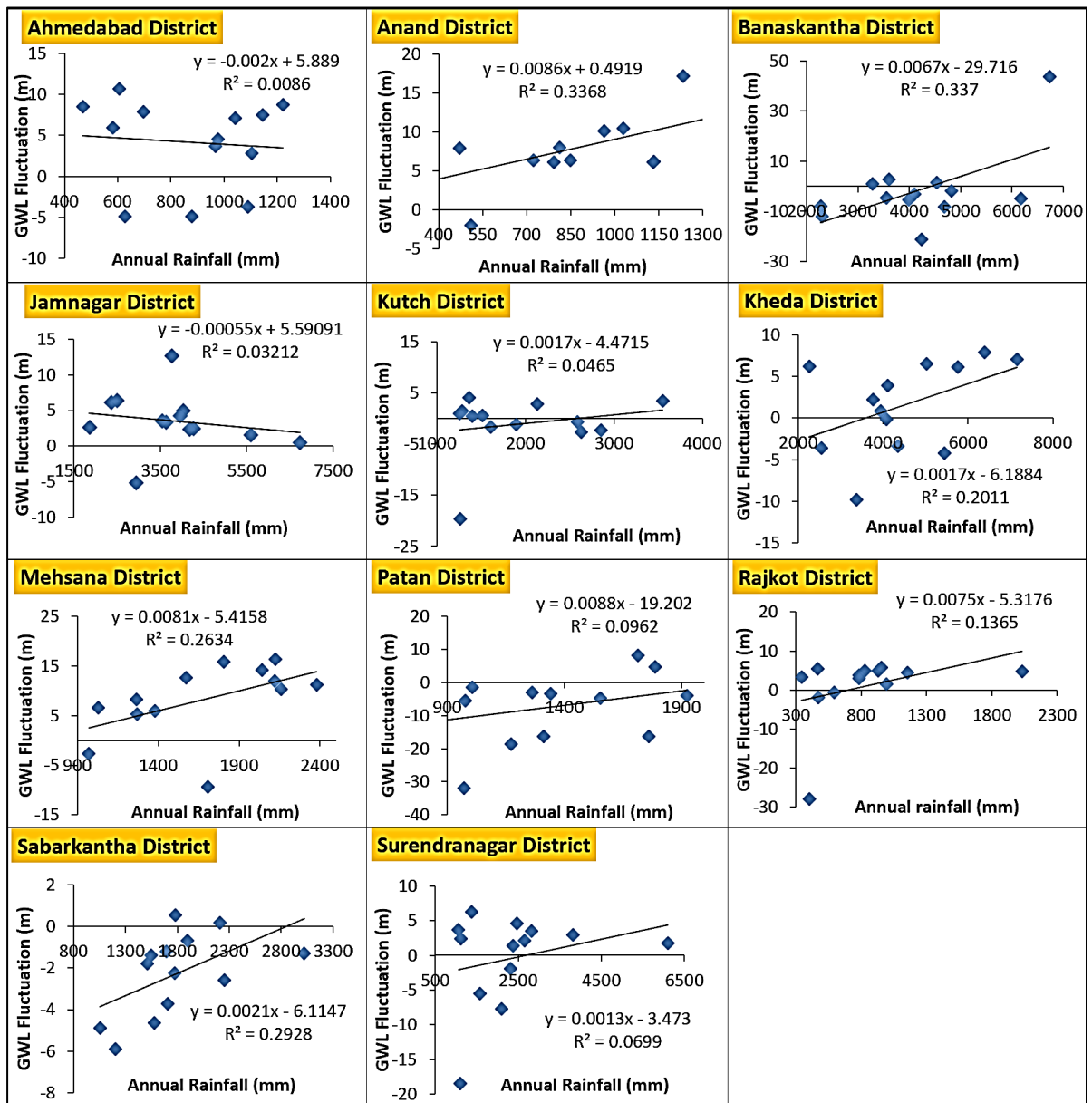
Fig 3.21: Correlation between fluctuations of Ground water depth and Annual rainfall

From Fig. 3.21, it is evident that during the period 2005-2017, rainfall rarely contributed towards the groundwater recharge as indicated by the lower R^2 values. The eastern and south east side of the basin Banaskantha, Anand, Sabarkantha and Mehsana districts showed comparatively higher R^2 values 0.33, 0.34, 0.29 and 0.26 which indicates that only towards the eastern side of the basin the rainfall contributes a little towards groundwater recharge but in other parts of the basin, rainfall plays a negligible role in recharging the groundwater system.

CHAPTER 4. PREDICTIVE MODELLING OF LAND SUBSIDENCE

4.1 Introduction

Since declining groundwater levels have been reported in many parts of Mehsana district of Gujarat, it is important to estimate the relative risk of land subsidence associated with groundwater withdrawal and aquifer compaction in the region. Land Subsidence is a consequence of Aquifer-System Compaction contributing to perpetual damage of aquifer system storage. The extent of land subsidence varies from season to season i.e. Pre-monsoon and post-monsoon. The depth of total aquifer system and the hydrogeological characteristics of the aquifer control the rate of subsidence of the area. Though the predictive modelling of aquifer compaction using hydrogeological characteristics can be used to estimate the subsidence, such methods are localized and are often restricted by the data availability issues. On the other hand, remote sensing based Differential Interferometric InSAR techniques can be used to investigate the spatial and temporal patterns of ground deformation over large areas. The present study estimates the land subsidence due to aquifer compaction and then correlates the subsidence rates obtained from aquifer compaction with the DInSAR derived deformation rates.

Aquifer compaction is controlled by several parameters, including the patterns of water level decline, as well as the aquifer compressibility, porosity, storage coefficient, and the thickness of the compacting layers. The rate of aquifer compaction relies on the subsurface soil properties and clay and mud compacts more as compared to sand and rock (Martínez et al., 2013). Initially the effective stress on the aquifer system is supported by the solid matrix of the aquifer and the pore water pressure within the system. With the pumping out of water from the aquifer there is a drop in the pore pressure and the porosity, thereby increasing the effective stress exerted

by the overlying solid matrix. Consequently, the matrix compresses, and aquifer compaction takes place. Conversely, if the water is pumped into the aquifer through natural or artificial methods, the fluid pressure is restored and the effective stress decreases (Lohman, 1961). Changes in aquifer compaction may be both elastic and inelastic. While elastic compactions are reversible and could be recovered after the induced stress is removed, inelastic compactions are irreversible or permanent and occur due to the decline in water levels in the confining layers of the aquifers having low vertical hydraulic conductivity and where regain of fluid pore pressures is slow due to the presence of clay or silty clay interbeds. Because of water over draft there is a fall in the piezometric pressure head between the aquifer and the overlying confining layers and the water is released from the confined layers into the aquifer below and undergoes inelastic compaction. Inelastic compaction plays a major role in land subsidence in comparison to elastic compaction due to its irreversible nature.

Secondary data sources including the detailed lithologic, hydrogeological and piezometric water-level data were used to assess potential risk of subsidence at the selected sites to perform groundwater development risk assessment in the study area. The elastic aquifer `compaction and inelastic compaction of confining layers were computed independently, and average cumulative rate of land subsidence was estimated.

The Differential SAR Interferometry (DInSAR) is one of the most commonly used interferometric technique used in deformation studies and exploits the phase differences between SAR acquisitions to make precise land subsidence and uplift measurements. Though DInSAR measurements provide highly precise deformation measurements, they also suffer from temporal and geometric decorrelations as well as atmospheric delays and produce better displacement products only in areas characterized by high coherence capable of providing reliable phase difference values. As such, to remove the DInSAR limiting factors and obtain precise displacement component associated only with the displacement all the decorrelating factors such as orbital, curvature or topographic factors that tend to delimit the correct measurement of phase difference and displacement were removed during DInSAR processing. Long

perpendicular baseline causes serious geometric decorrelation. As such InSAR pairs with large perpendicular baselines were not considered for further processing. Conventional DInSAR was employed in the present study where Interferogram flattening and topographic phase removal were done on single pair interferometric process. Interferogram flattening was done to get the phase values only due to the unevenness in the topography and obtain accurate topographic and deformation information in the phase values. The flattened data set was obtained by deducting the phase of this simulated interferogram from the interferometric phase. Topographic phase contributions were removed using a high resolution SRTM 1 arc second Digital elevation model. Filtering was carried out using Adaptive filter to reduce the phase noise. The interferometric phase is wrapped modulo 2π. To solve the 2π ambiguity and recover complete phase information phase unwrapping is performed. Minimum cost flow algorithm is preferred for phase unwrapping in areas limited by low coherence and where unwrapping is difficult. Displacement maps were then generated from the unwrapped phase. Whenever there is a displacement in the ground surface there is a change in the distance between the sensor and the point of observation and as such the phase value recorded by the sensor also changes. The change in signal phase ($\Delta\varphi$) is expressed by the eq. (24) below.

$$\Delta\varphi = \frac{4\pi}{\lambda} \Delta R + \alpha \qquad (24)$$

Where, λ is the wavelength of the sensor, ΔR is the displacement measured along the Line of Sight (LOS) and α is the phase shift due to different atmospheric conditions during two image acquisitions. The Line of sight (LOS) which is the direction from the sensor to the ground points can quantify the displacement with negative and positive values of LOS corresponding to regional subsidence or uplift in the LOS direction. The spatial and temporal movements of LOS motion rates can thus provide an insight into the subsidence patterns developing over time. Line of sight (LOS) can give measure of one-dimensional motion along the radar viewing geometry without information on the horizontal displacement which is considered negligible in case of land subsidence. Therefore, DInSAR-derived LOS measurements can be interpreted as vertical

deformation in land subsidence studies. If independent GNSS observations are available, such data can also be used to mathematically solve for the horizontal motion vector on a pixel-by-pixel basis. Since the GNSS observations are always at selective locations and cannot cover the whole area, the accuracy of GNSS velocities is limited with the proximity to the GNSS stations and the accuracy tend to decrease with distance (Fuhrmann et al., 2015, 2019).

4.2 AQUIFER SYSTEM COMPACTION

To model aquifer system compaction and inelastic compaction of aquitards, aquifer thickness, aquifer porosity, piezometric head, and bulk modulus were considered. Different approaches were used to calculate elastic and inelastic compaction and the total of both gave the total vertical shortening in the aquifer system. Due to high atmospheric and temporal decorrelations and pronounced vegetation in the area, the DInSAR based subsidence mapping was restricted to area near Mehsana city. As such the aquifer compaction calculations were also limited to the same area so that a proper comparison between Aquifer compaction rates and DInSAR deformations could be made. A total of four locations namely Mehsana-V, Mewad, Karalli-II and Modhera-II were selected in and around Mehsana city, where predictive modelling of aquifer compaction was carried out. In situ measurement of piezometric well recorded at different observation sites, were evaluated to calculate piezometric head variation, during two study periods 2006 to 2011 and 2012 to 2017 for both pre and post monsoon seasons years.

The datasets for both piezometric groundwater levels and the lithologs were obtained from CGWB (Central Groundwater Board, India). The study area maps were prepared in ArcGIS, and RockWorks 16 was used to create lithology striplogs and the cross sections to identify the primary aquifers and confining layers and calculate the thickness of the layers. Lohman's equation and Domenico's equation described in the literature review section earlier, were used to estimate the elastic and inelastic aquifer compaction at the observation wells. The total vertical shortening was calculated by summing both the elastic and inelastic components. The porosity values of the aquifer

materials were taken from the table values provided by Brassington, 1998. and the values of E$_s$ were taken from the tables as provided by Domenico and Mifflin, 1965. The thickness of the aquifers was inferred from the lithological strips and the information on the depth of the tapped zones as provided by the Central Ground water board. The piezometric head decline used to calculate the reduction in piezometric pressure Δp was calculated as the difference between the pre-monsoon and the post monsoon water levels. The methodology for predictive modelling of aquifer compaction is summarized in Fig. 4.1 below.
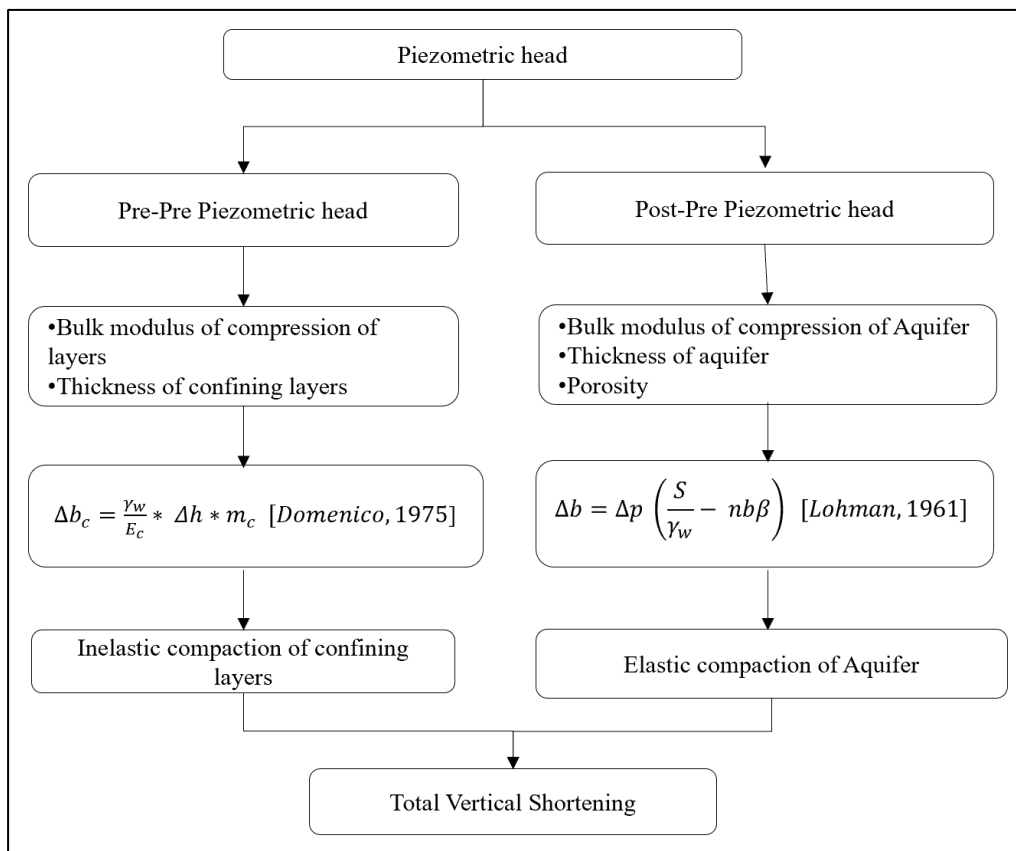
Fig 4.1: Flowchart for Predictive modelling of Aquifer compaction

The location of the observation wells as well as the boreholes are shown in Figure 4.2 below.
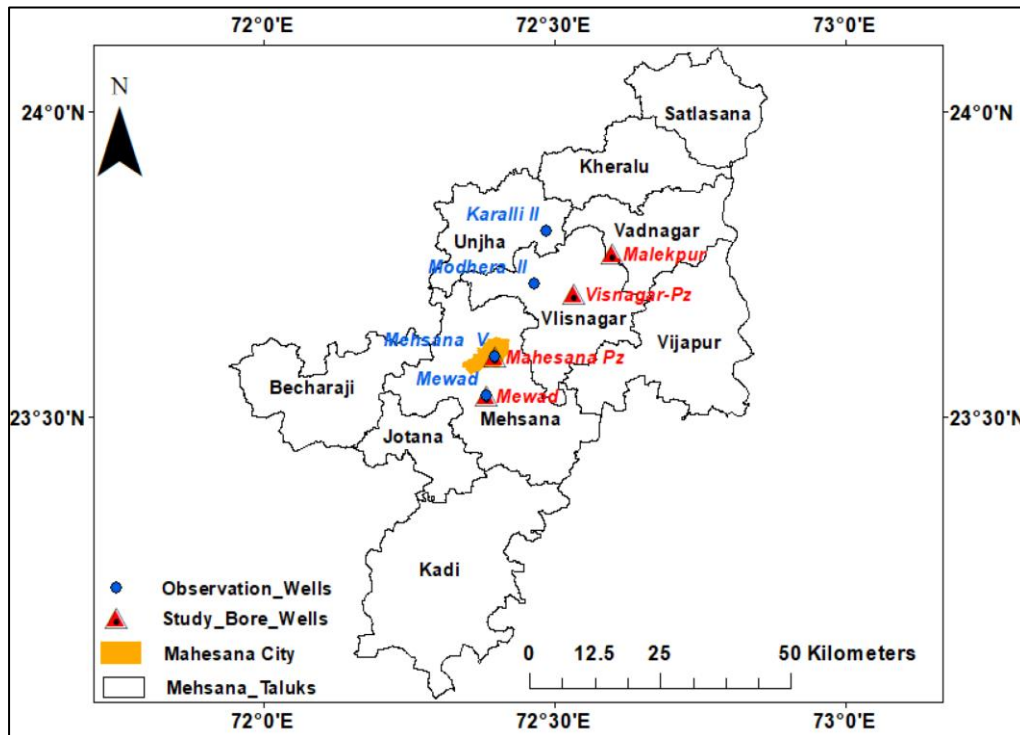
Fig 4.2: Location of Study Observation wells and Bore wells.

4.2.1 Results and Discussion

Elastic and Inelastic piezometric heads for calculation of land subsidence are shown in Table 4.1 and Table 4.2 respectively. From the analysis of pre and post monsoon piezometric head for elastic compaction it is observed that for Mehsana-V piezometric well, the maximum piezometric head for is 3.1 m in 2015 and the minimum is -8.66 m in 2012 with an average 0.15 m. Due to a relatively low rainfall recorded in Mehsana district in 2012 (Fig. 3.20) the post monsoon levels have gone down. In Mewad, the maximum head is 6.42 m in 2013 and the minimum is -0.41 m in 2009 and the average is 2.08 mbgl. In Karalli II, the maximum head is 4.93 m in 2009 and minimum is -2.64 m in 2016 with an average value of 1.75 mbgl. While for Modhera II, the maximum and minimum piezometric heads were 7.99 mbgl in 2009 and -3.38 mbgl in 2007 respectively and the average piezometric head is 1.73 mbgl (Table 4.1). The analysis of pre-pre monsoon seasons of consecutive years during the initial period of study time frame indicates water levels were declining with positive values for Mehsana-V, Mewad and Karalli wells (Table 4.2). The higher number of negative values post 2012 give an indication that there has been a

112

relative decline in groundwater levels after 2012 than during the period of 2007 to 2011. Combined analysis of both pre-post and pre-pre groundwater water levels thus indicates that Mehsana taluk is much more prone to groundwater decline and consequently more vulnerable to land subsidence as compared to the neighbouring taluk of Visnagar considered in the present study.

Table 4.1: Pre - Post Piezometric head (m)

Year	Mehsana V	Mewad	Karalli II	Modhera II
2007	2.17	2.92	0.35	-3.38
2008	1.2	1.05	3.49	0.18
2009	0.57	-0.41	4.93	7.99
2010	0.88	4.61	0.55	-0.52
2011	1.16	2.66	0.5	2.78
2012	-8.66	1.71	0.57	-1.47
2013	1.26	6.42	2.7	5.09
2014	0.19	2.74	3.75	0.86
2015	3.1	0.12	0.76	-0.14
2016	-2.05	0.09	-2.64	1.84
2017	1.87	0.98	4.24	5.82
Min	-8.66	-0.41	-2.64	-3.38
Max	3.1	6.42	4.93	7.99
Average	0.15	2.08	1.75	1.73

Table 4.2: Pre - Pre Piezometric head (m)

Year	Mehsana V	Mewad	Karalli II	Modhera II
2008-2007	-0.2	0.25	0.78	-3.38
2009-2008	1.29	3.67	-1.1	1.27
2010-2009	0.34	5	0.07	-3.45
2011-2010	0.24	-3.99	0.68	2.02
2012-2011	-0.02	-1.29	0.63	-2.09
2013-2012	-0.14	-1.24	1.02	4.81
2014-2013	-1.19	-6.18	-1.78	-5.55
2015-2014	-1.05	-1.94	-3.64	-1.38
2016-2015	1.04	-0.01	0.06	0.14
2017-2016	0.34	4.19	4.52	1.16
Min	-1.19	-6.18	-3.64	-5.55
Max	1.29	5	4.52	4.81
Average	0.06	-0.15	0.12	-0.65

The lithologs as received by CGWB have been plotted using rockworks 16. The lithologs consisted of fine to coarse gradations of soil with intervening confining beds of clay and sandy clay and act as leaky aquifers.

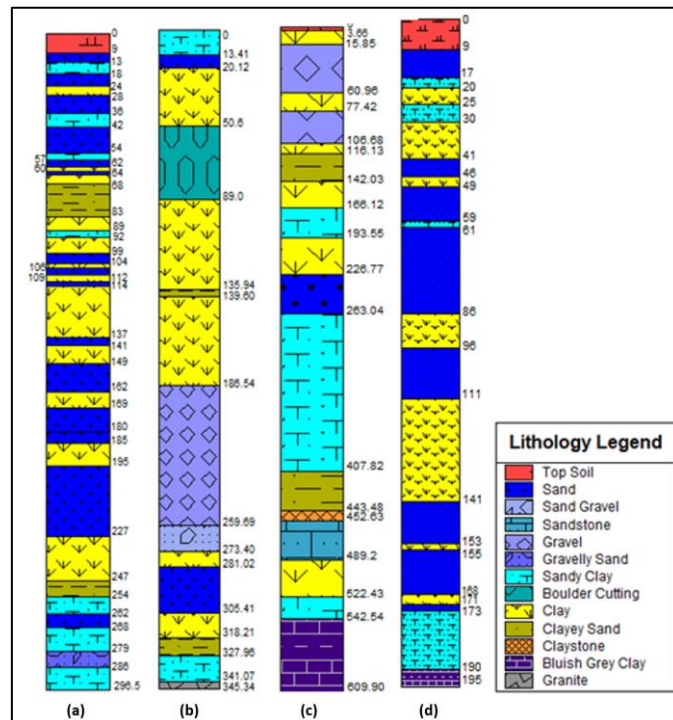**Fig 4.3**: Lithologs depicting the subsurface geology: (a) Mehsana-Pz (b) Malekpur
(c) Mewad (d) Visnagar-Pz. Source: CGWB, 2017

The cross sections Fig.4.4 blow, provides information regarding the lithology, depth of the boreholes and the depth at which the borehole encountered a reservoir rock.
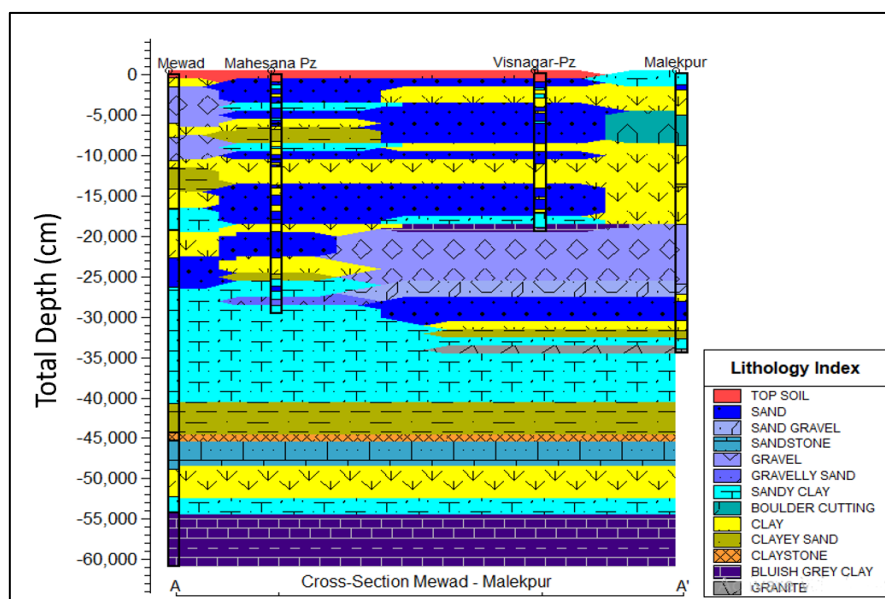
Fig 4.4: Cross section Mewad - Mehsana Pz- Visnagar-Pz and Malekpur showing the aquifers.

114

In Mehsana-Pz the major aquifer tapped zones by CGWB are from 169 mbgl to 185 mbgl and 195 mbgl to 227 mbgl. In Malekpur, the tapped aquifer zones lie between 281.02 mbgl and 305.41 mbgl. In Mewad, the tapped zone lies between 226.77 mbgl and 263.04 and in Visnagar-Pz, the zones have been tapped from 141 mbgl to 153 mbgl and 155 mbgl to 168 mbgl (Fig. 4.3).

The storage coefficient is dependent on the aquifer material and water compressibility's, and the total thickness of the aquifer and was calculated using the Jacob's equation (Table 4.3).

Table 4.3: Calculation of Storage Coefficient

Site Name	γ_w	b (m)	α (1 / E_s)	n	β	S
Mehsana	9810	48	1/7.65*10^7	0.39	1/2.1*10^9	0.00620
Mewad	9810	36.27	1/7.65*10^7	0.39	1/2.1*10^9	0.00495
Karalli-II	9810	24.39	1/7.65*10^7	0.39	1/2.1*10^9	0.00315
Modhera-II	9810	25	1/7.65*10^7	0.39	1/2.1*10^9	0.00323

The Inelastic subsidence of the confined aquifer which is based on pre-pre monsoon piezometric head, the hydrogeological properties and the total thickness of the confining layers of confined aquifer was calculated for 2007-2011 and 2012-2017 using the Domenico equation (1975). The results show that in most of the wells the inelastic compaction has been more during 2012 to 2017 as compared to 2007-2011. It is evident that a higher drop in piezometric head is controlling the rate of inelastic compaction which is more significant than the elastic compaction rates. Since Inelastic compactions are not recoverable, such compactions lead to land subsidence (Table 4.4).

Table 4.4: Calculation of Inelastic Compaction for different wells.

	Year	γw	Ec (N/m2)	Δh	m c	Δbc (cm)
MEHSANA-V	2007-2011	9810	7.65*10^6	0.18	39	0.90
	2012-2017	9810	7.65*10^6	0.48	39	2.40
	2007-2017	9810	7.65*10^6	0.54	39	2.70
MEWAD	Year	γw	Ec (N/m2)	Δh	m c	Δbc (cm)
	2007-2011	9810	7.65*10^6	-1.54	39	-7.70
	2012-2017	9810	7.65*10^6	5.43	39	27.16
	2007-2017	9810	7.65*10^6	3.94	39	19.70

	Year	γw	Ec (N/m2)	Δh	m c	Δbc (cm)
KARALLI	2007-2011	9810	7.65*10^6	-0.15	37	-0.71
	2012-2017	9810	7.65*10^6	3.50	37	16.61
	2007-2017	9810	7.65*10^6	3.74	37	17.75
MODHERA-II	Year	γw	Ec (N/m2)	Δh	m c	Δbc (cm)
	2007-2011	9810	7.65*10^6	1.29	37	6.12
	2012-2017	9810	7.65*10^6	-3.65	37	-17.32
	2007-2017	9810	7.65*10^6	4.54	37	21.54

The elastic compaction which is dependent on pre-post piezometric head, the water releasing capacity of the confined aquifer, hydro geological properties and the thickness of the aquifer also show a declining trend from 2007-2011 to 2012-2017 (Table 4.5). The elastic compactions rates are lower than the inelastic compaction rates since during pre-post monsoon season the effective stress on the aquifer framework gets balanced by the increased levels of groundwater after the monsoon period.

Table 4.5: Calculation of Elastic Compaction for different wells.

	Year	Δp(N/m2)		S	γw (N/m3)	n	b (m)	β N/m2)	Δb (cm)
		γw	Δh						
MEHSANA-V	2007-2011	9810	-1.01	0.00620	9810	0.39	48	1 / (2.1*10^9)	-0.62
	2012-2017	9810	10.53	0.00620	9810	0.39	48	1 / (2.1*10^9)	6.44
	2007-2017	9810	-0.3	0.00620	9810	0.39	48	1 / (2.1*10^9)	-0.18
	Year	Δp(N/m2)		S	γw (N/m3)	n	b (m)	β N/m2)	Δb (cm)
		γw	Δh						
MEWAD	2007-2011	9810	-0.26	0.00495	9810	0.39	36.27	1/(2.1*10^9)	-0.13
	2012-2017	9810	-0.73	0.00495	9810	0.39	36.27	1/(2.1*10^9)	-0.36
	2007-2017	9810	-1.94	0.00495	9810	0.39	36.27	1/(2.1*10^9)	-0.95
	Year	Δp(N/m2)		S	γw (N/m3)	n	b (m)	β N/m2)	Δb (cm)
		γw	Δh						
KARALLI	2007-2011	9810	0.15	0.00315	9810	0.39	24.39	1/(2.1*10^9)	0.05
	2012-2017	9810	3.67	0.00315	9810	0.39	24.39	1/(2.1*10^9)	1.14
	2007-2017	9810	3.89	0.00315	9810	0.39	24.39	1/(2.1*10^9)	1.21

MODHERA-II	Year	Δp(N/m2)		S	γw (N/m3)	n	b (m)	β N/m2)	Δb (cm)
		γw	Δh						
	2007-2011	9810	6.16	0.00323	9810	0.39	25	1/(2.1*10^9)	1.96
	2012-2017	9810	7.29	0.00323	9810	0.39	25	1/(2.1*10^9)	2.32
	2007-2017	9810	9.2	0.00323	9810	0.39	25	1/(2.1*10^9)	2.93

The total vertical shortening and the yearly subsidence rate which is the cumulative of elastic and inelastic compaction are shown in the table below (Table 4.6)

Table 4.6: Total Vertical Compaction for different wells.

Well	Period	Total Compaction (cm)	Yearly Rate (cm/yr.)
MEHSANA V	2007-2011	0.28	0.06
	2012-2017	8.84	1.47
	2007-2017	2.52	0.22
MEWAD	2007-2011	-7.83	-1.57
	2012-2017	26.8	4.47
	2007-2017	18.76	1.71
KARALLI	2007-2011	-0.67	-0.13
	2012-2017	17.75	2.96
	2007-2017	18.95	1.72
MODHERA II	2007-2011	8.08	1.62
	2012-2017	-15	-2.50
	2007-2017	24.47	2.22

The total compaction results show that the rate of compaction in the period 2012-2017 has significantly reduced than the earlier period of 2007 to 2011. The analysis from pre-pre and post-pre groundwater levels also indicated a relative decline in groundwater levels after 2012 than the preceding period. The agreement between both the results thus reveals that the piezometric head decline due to groundwater overdraft thus plays a very crucial role in aquifer compaction and consequent land subsidence.

4.3 DInSAR based monitoring and mapping of Land Subsidence

ALOS PALSAR 1 & 2 (L-Band) and RADARSAT-2 (C-Band) SAR data were used for DInSAR processing. The first step was estimating the spatial baseline and temporal baseline from Single Look Complex (SLC) data pairs. Data pairs with shorter spatial baselines were taken to reduce geometric decorrelation and topographic errors. Pairs with low Doppler difference are taken to prevent coherence loss. The coherence values were taken into consideration as they affect the quality of interferogram. The pairs with higher perpendicular baseline were not considered for further processing because of increased scope of noise in the anticipated Interferogram. Interferogram flattening and topographic phase removal was carried out during the interferometric process. A 30 m DEM from SRTM was used for topographic phase removal and obtain a flattened interferogram. Filtering was done to generate output with reduced noise phase and Goldstein filter was used for noise removal. Filtered scenes were subset to highlight the prominent subsiding areas. Filtering is followed by phase unwrapping. Minimum cost flow algorithm was used for Phase Unwrapping. Decomposition levels were set to 1 and coherence threshold lessened to 0.6. A coherence threshold of 0.6 was chosen to mask out less coherent features such as vegetation that are dynamic in nature and affect the interpretation of the results. Geocoded filtered Interferograms were used for fringe analysis. Prominent fringes were marked as possible land subsidence sites. The subsidence rates in the Line of Sight (LOS) were calculated from the unwrapped phase to get precise measurement of deformation rates. Time series analysis of deformation rates was done. The unwrapped produced were geocoded using Range Doppler terrain correction and were visualized in Google Earth for interpretation. The DInSAR processing is shown through a methodological flowchart in the Figure 4.5 below.
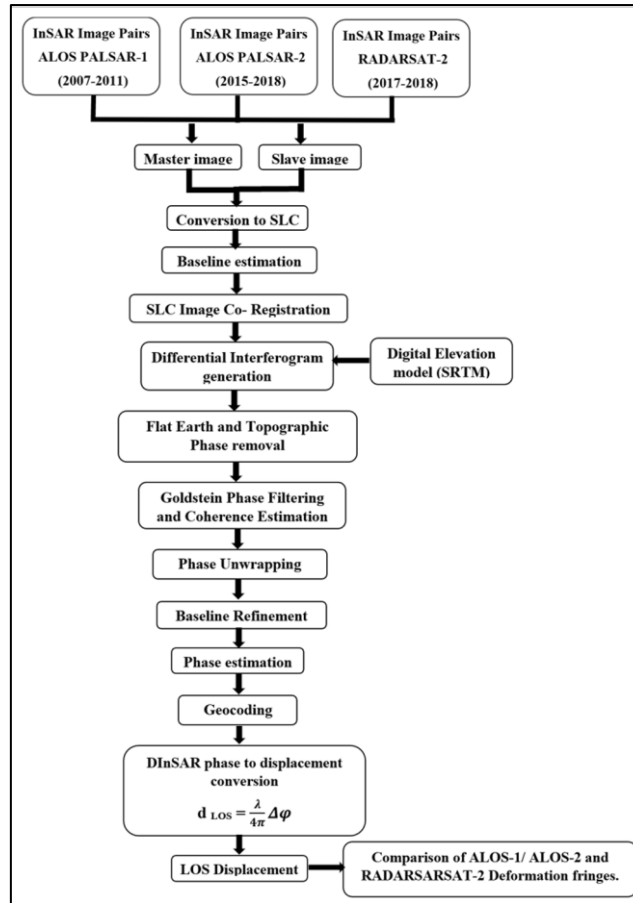
Fig 4.5: Flowchart for DInSAR modeling of land subsidence.

4.3.1 Results and Discussion

4 pairs of ALOS PALSAR-1 images between 2007 and 2011 were chosen from the available image pairs for further DInSAR processing. The selection of pairs was made based on the mean coherence values in the image pairs and where interferograms could be obtained. After the phase unwrapping, the areas with low coherence and having coherence values less than 0.6 were masked out to remove dynamic features like vegetation with low coherence. Masking the features with low coherence highlighted only those permanent scatterer's that had high coherence values and could provide reliable displacement values. Table 4.7 shows the parameters of the chosen ALOS PALSAR-1 pairs and figures 4.6 to 4.8 below show the different DInSAR derived products obtained during the whole process.

Table 4.7: Parameters of ALOS PALSAR-1 Image Pairs

| S No. | Data Pair | Date 1 | Date 2 | Baseline | | | Doppler | | | |
				Temporal (days)	Perpendicular	Critical	Centroid Diff.	Critical	Ambiguity height (m)	Mean Coherence
1	51590-118690	12-01-2007	16-04-2008	460	3785.9	13060	-17.09	2159.8	16.92	0.15
2	111980-273020	01-03-2008	10-03-2011	1104	693.6	13056	-3.68	2159.8	92.32	0.14
3	118690-273020	16-04-2008	10-03-2011	1058	495.2	13051	7.13	2159.8	129.28	0.14
4	165660-273020	04-03-2009	10-03-2011	736	2993.8	13053	-13.29	2159.8	21.38	0.14

119

4.3.1.1 ALOS PALSAR-1 Image Pair (51590-118690; Date: 12-01-2007 - 16-04-2008)

Fig 4.6: ALOS PALSAR-1 Image Pair: 51590-118690; Date 12-01-2007_16-04- 2008.
(a) Filtered Interferogram (b) Spatial Profile (c) Displacement over Mehsana city.

4.3.1.2 ALOS PALSAR -1 Image Pair (111980-273020;Date: 01-03-2008 - 10-03-2011)

Fig 4.7: ALOS PALSAR-1 Image Pair: 111980-273020; Date 01-03-2008_10-03- 2011.
(a) Filtered Interferogram (b) Spatial Profile (c) Displacement over Mehsana city.

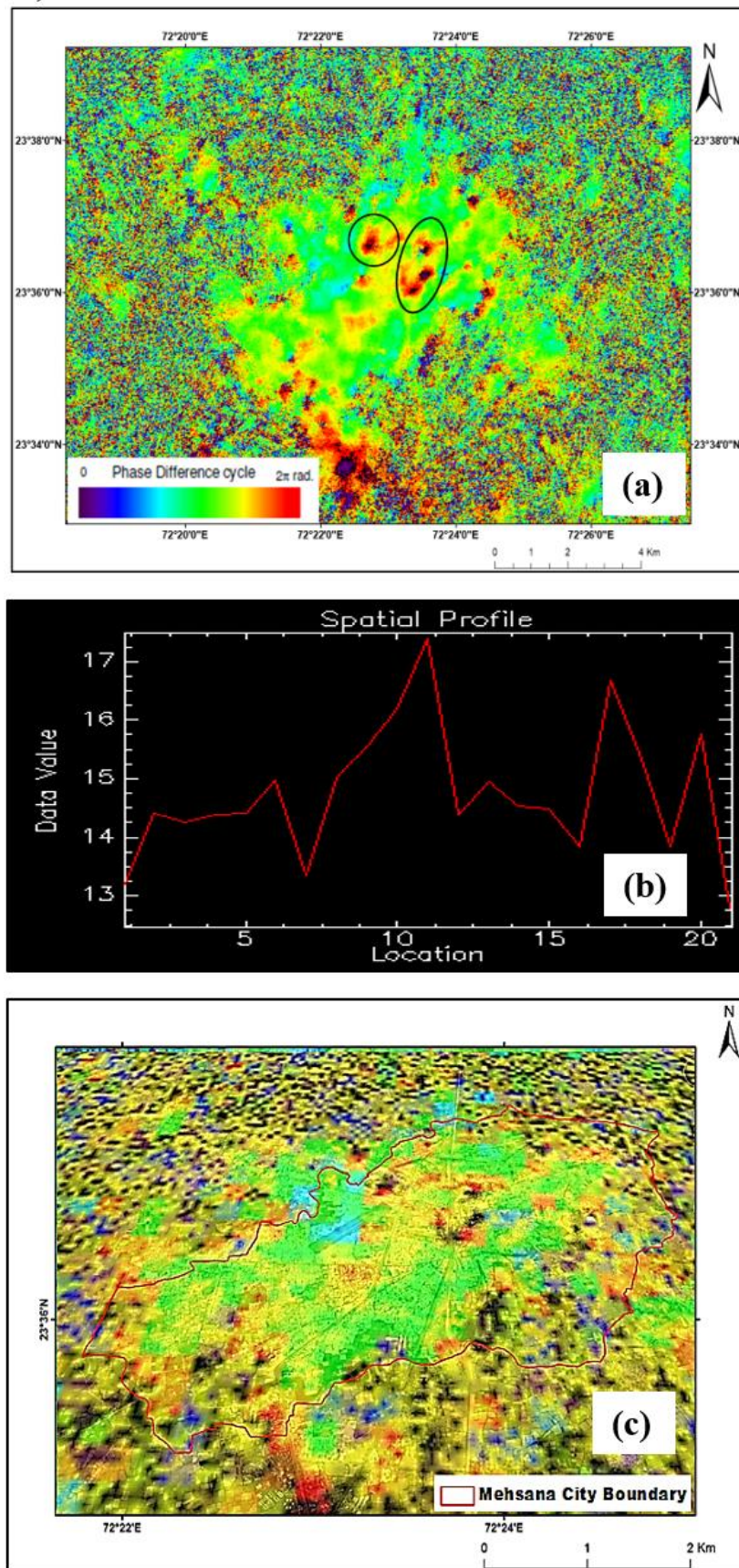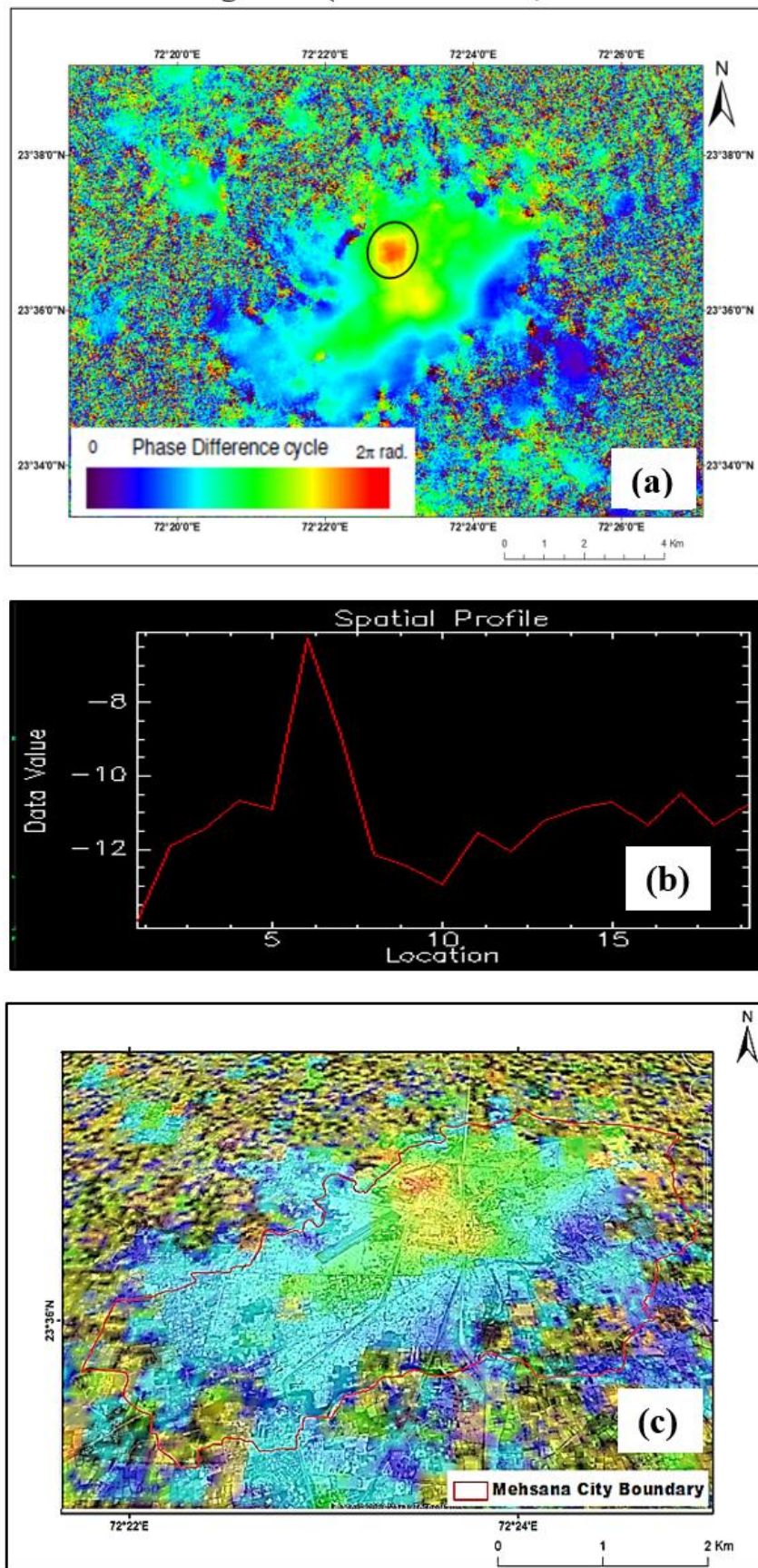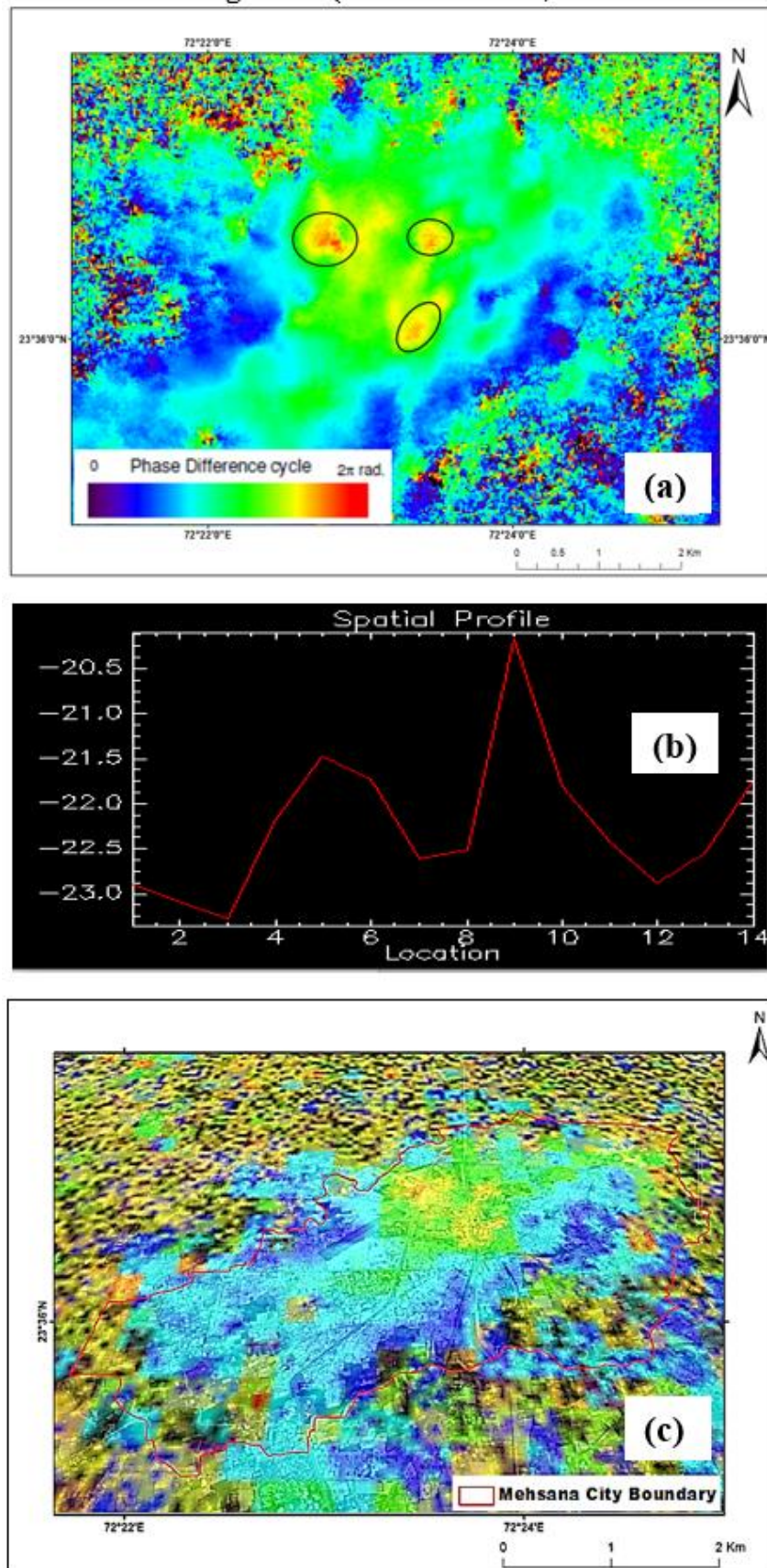### 4.3.1.3 ALOS PALSAR -1 Image Pair (165660-273020;Date: 04-03-2009 - 10-03-2011)

Fig 4.8: ALOS PALSAR-1 Image Pair: 165660-273020; Date 04-03-2009_10-03- 2011.
(a) Filtered Interferogram (b) Spatial Profile (c) Displacement over Mehsana city.

The Deformation was calculated by differencing the obtained maximum phase with the average phase values. The average phase values were computed from the values obtained from the spatial profile of the deformation fringes.

The deformation rate is calculated from the empirical formula given by eq.(25).

$$\Delta\rho = (\Delta\phi * \lambda)/ 4\pi \qquad (25)$$

Where $\Delta\rho$ is the Path Difference which is being calculated, $\Delta\phi$ is the Phase Difference λ is the sensor wavelength. From the path difference, the LOS rate is calculated from the eq. (26) below.

$$\text{LOS Rate} = (\Delta\rho * 365)/\Delta t \qquad (26)$$

The LOS values were calculated by dividing the product of deformation and the wavelength of ALOS PALSAR-1 Sensor which is 23 cm in our case by 4π. And then the Line of Sight (LOS) rate was determined by multiplying the LOS with number of days in the year and dividing by the temporal baseline of the image pair. The Line of Sight (LOS) gives the magnitude of deformation in the direction of the sensor. The mean weighted coherence which gave the overall subsidence during the period 2008 to 2011 was estimated by dividing the sum of mean coherence of individual pairs with the product of LOS rate and mean coherence. The calculations for ALOS PALSAR-1 data pairs are summarized in Table 4.8 below.

Table 4.8: Coherence weighted deformation rates from ALOS PALSAR-1 Image Pairs

Data Pair	Time Period	Temporal (days)	Deformation	LOS (cm)	LOS Rate cm/yr)	Mean Coherence	LOS Rate * Mean Coherence	Weighted Mean Coherence
51590-118690	12-01-2007 to 16-04-2008	460	2.83	5.32	4.22	0.15	0.63	
111980-273020	01-03-2008 to 10-03-2011	1104	1.76	3.30	1.09	0.14	0.15	2.49
118690-273020	16-04-2008 to 10-03-2011	1058	3.09	5.80	2.00	0.14	0.28	
165660-273020	04-03-2009 to 10-03-2011	736	2.73	5.12	2.54	0.14	0.36	
						∑=0.57	∑=1.42	

For ALOS PALSAR-2, 12 SAR images were available spanning the time period between 2014 to 2018. The 12 images resulted in 66 different pairwise combinations where Master image was the image from earlier period and Slave image belonging to the later time. The parameters of the 66 pairs

analyzed are shown in Table 4.9 below. All the image pairs were subjected through DInSAR processing steps and analyzed to select the best image pairs for subsidence calculations. Data pairs with shorter spatial baselines were taken to reduce geometric decorrelation and topographic errors. Pairs with low Doppler difference are taken to prevent coherence loss. The coherence values were taken into consideration as they affect the quality of interferogram. The pairs with higher perpendicular baseline were not considered for further processing because of increased scope of noise in the anticipated Interferogram.

Table 4.9: Parameters of pairwise combinations of ALOS PALSAR-2 Image Pairs

Sl. No.	Image Pair	Normal Baseline	Critical Baseline	Ambiguity height	Range Shift	Azimuth Shift	Doppler Critical	Temporal Baseline	Mean Coherence
1	141002 -141211	11.25	9700.66	4812.8	5.56	6.06	-0.04	70	0.34
2	141002 -150219	98.67	9700.66	548.54	29.51	-2.25	0.00	140	0.30
3	141002 -151210	116.10	1531.99	466.22	11.77	-0.28	-0.77	434	0.12
4	141002 -160218	202.57	18032.69	267.20	53.48	-3.63	-0.99	504	0.12
5	141002 -160721	121.14	18032.69	446.81	30.96	-6.63	-0.56	658	0.12
6	141002 -160929	103.57	18032.69	522.58	21.49	-3.37	-0.84	728	0.12
7	141002 -170216	-189.39	18032.69	285.79	-17.74	12.81	-1.01	868	0.12
8	141002 -170720	29.14	18032.69	1857.4	12.04	0.91	-0.88	1022	0.12
9	141002 -170928	138.04	-18032.69	392.11	40.66	-4.43	-1.15	1092	0.12
10	141002 -180201	-119.54	18032.69	452.78	-10.86	10.11	-0.77	1218	0.11
11	141002 -180301	-40.59	-18032.69	1333.5	1.92	8.05	-1.05	1246	0.12
12	141211 -150219	91.65	9702.40	590.66	23.95	-5.81	0.04	70	0.42
13	141211 -151210	107.26	18035.93	504.72	6.12	-3.84	0.73	364	0.12
14	141211 -160218	194.64	18035.93	278.12	47.92	-9.19	-0.95	434	0.12
15	141211 -160721	112.83	-18035.93	479.79	25.40	-12.19	-0.52	588	0.12
16	141211 -160929	94.45	18035.92	573.18	15.93	-6.93	-0.80	658	0.12
17	141211 -170216	197.82	18035.93	272.66	-23.30	9.25	-0.97	798	0.12
18	141211 -170720	20.03	18035.93	2702.5	6.48	-2.65	-0.84	952	0.12
19	141211 -170928	129.59	18035.93	417.74	35.10	-7.99	-1.11	1022	0.12
20	141211 -180201	-128.14	18035.93	422.46	-16.42	4.55	-0.73	1148	0.12
21	141211 -180301	-48.68	-18035.93	1111.9	3.64	4.49	1.01	1176	0.12
22	150219 -151210	32.80	18036.67	1650.6	-17.73	4.47	0.77	294	0.12
23	150219 -160218	104.18	18036.68	519.65	23.98	-0.88	-0.99	364	0.12
24	150219 -160721	26.32	-18036.68	2056.6	1.45	-3.88	-0.55	518	0.12
25	150219 -160929	28.86	18036.67	2015.1	-0.83	1.39	-0.83	588	0.12
26	150219 -170216	287.75	18036.67	188.15	-47.26	15.57	-1.01	728	0.12
27	150219 -170720	-72.80	18036.68	743.63	-17.47	3.66	-0.87	882	0.12
28	150219 -170928	44.42	18036.68	1218.8	11.15	0.32	-1.15	952	0.11
29	150219 -180201	-217.78	18036.68	248.58	40.38	12.86	-0.76	1078	0.12
30	150219 -180301	-139.50	-18036.68	388.09	27.59	10.80	-1.05	1106	0.12
31	151210 -160218	90.37	-9865.52	609.12	41.71	-2.84	-0.22	70	0.16
32	151210 -160721	12.97	-9865.52	4244.1	19.19	-5.85	0.21	224	0.24
33	151210 -160929	13.00	-9865.52	4233.7	9.72	0.58	0.07	294	0.21
34	151210 -170216	305.13	-9865.52	180.41	-29.52	13.59	0.24	434	0.20
35	151210 -170720	-87.02	-9865.52	632.63	0.27	1.69	0.11	588	0.18
36	151210 -170928	23.44	-9865.52	2348.2	28.89	-1.65	-0.38	658	0.17

Sl. No.	Image Pair	Normal Baseline	Critical Baseline	Ambiguity height	Range Shift	Azimuth Shift	Doppler Critical	Temporal Baseline	Mean Coherence
37	151210 -180201	-235.20	9865.52	234.05	22.64	10.89	0.00	784	0.18
38	151210 -180301	-155.91	9865.52	353.08	-9.85	8.83	0.28	812	0.18
39	160218 -160721	-83.28	-9869.06	661.21	-22.53	-1.01	0.44	154	0.25
40	160218 -160929	-105.11	-9869.06	523.85	-32.00	2.26	0.16	224	0.22
41	160218 -170216	-391.80	-9869.06	140.54	71.25	18.44	-0.02	364	0.22
42	160218 -170720	-174.93	-9869.06	314.78	-41.45	6.54	0.11	518	0.18
43	160218 -170928	-67.32	-9869.06	817.98	-12.83	1.19	-0.16	588	0.18
44	160218 -180201	-321.80	-9869.06	171.11	-64.37	15.74	0.23	714	0.18
45	160218 -180301	-243.09	-9869.06	226.52	-51.58	13.68	-0.06	742	0.12
46	160721 -160929	-23.13	-9867.65	2380.1	-9.47	5.26	-0.28	70	0.31
47	160721 -170216	-310.45	-9867.65	177.33	-48.71	21.44	0.46	210	0.25
48	160721 -170720	-92.95	9867.65	592.27	18.93	9.54	-0.32	364	0.22
49	160721 -170928	18.96	-9867.65	2903.8	9.70	4.20	-0.60	434	0.18
50	160721 -180201	-240.42	-9867.65	228.99	-41.84	18.74	0.21	560	0.19
51	160721 -180301	161.44	-9867.65	341.02	-29.05	16.68	-0.50	588	0.19
52	160929 -170216	-291.97	-9867.53	188.56	39.24	16.18	0.18	140	0.30
53	160929 -170720	74.19	-9867.53	742.12	-9.45	4.28	0.04	294	0.22
54	160929 -170928	36.00	9867.53	1529.3	19.17	0.93	-0.32	364	0.20
55	160929 -180201	-222.35	-9867.53	247.60	32.36	13.48	0.07	490	0.19
56	160929 -180301	-143.06	9867.53	384.85	-19.57	11.42	-0.22	518	0.20
57	170216 -170720	218.09	-9865.79	252.41	29.76	-11.90	0.14	154	0.24
58	170216 -170928	327.55	-9865.79	168.06	58.38	-15.24	-0.14	224	0.20
59	170216 -180201	69.99	-9865.79	786.50	6.87	-2.70	0.25	350	0.22
60	170216 -180301	149.14	-9865.79	369.10	19.65	-4.76	-0.04	378	0.22
61	170720 -170928	109.52	-9866.77	502.66	28.62	-2.84	0.28	70	0.28
62	170720 -180201	-148.17	-9866.77	371.55	22.90	9.70	0.11	196	0.24
63	170720 -180301	-68.71	-9866.77	801.25	-10.12	7.64	-0.17	224	0.24
64	170928 -180201	257.40	-9867.50	213.89	51.53	14.55	0.39	126	0.30
65	170928 -180301	-178.27	-9867.50	308.83	38.75	12.48	0.10	154	0.30
66	180201 -180301	79.53	-9867.61	692.26	12.78	-0.06	-0.29	28	0.56

The parameters of each of the pair including the baseline and mean coherence and the pairs that could reveal interferograms were taken into consideration to choose 5 pairs for further processing. A temporal baseline of one year or more which is used in slowly subsiding areas is considered. Table 4.10 shows the parameters of the chosen ALOS PALSAR-2 pairs and figures 4.9 to 4.13 below show the different DInSAR derived products obtained during the whole process.

Table 4.10: Parameters of ALOS PALSAR-2 Image Pairs

Data Pair	Date 1	Date 2	Baseline			Doppler Critical	Ambiguity height (m)	Mean Coherence
			Temporal (days)	Perpendicular	Critical			
2083640-2170580	10-12-2015	20-07-2017	588	-87.016	-9865.52	0.11	632.625	0.18
2083640-2199560	10-12-2015	01-02-2018	784	-235.201	9865.52	0.00	234.049	0.18
2093990-2170580	18-02-2016	20-07-2017	518	-174.926	-9869.06	0.11	314.78	0.18
2127110-2199560	29-09-2016	01-02-2018	490	-222.352	-9867.53	0.07	247.604	0.19
2147810-2199560	16-02-2017	01-02-2018	350	69.991	-9865.79	0.25	786.504	0.22

4.3.1.4 ALOS PALSAR -2 Image Pair (2083640-2170580;Date: 10-12-2015_20-07-2017)
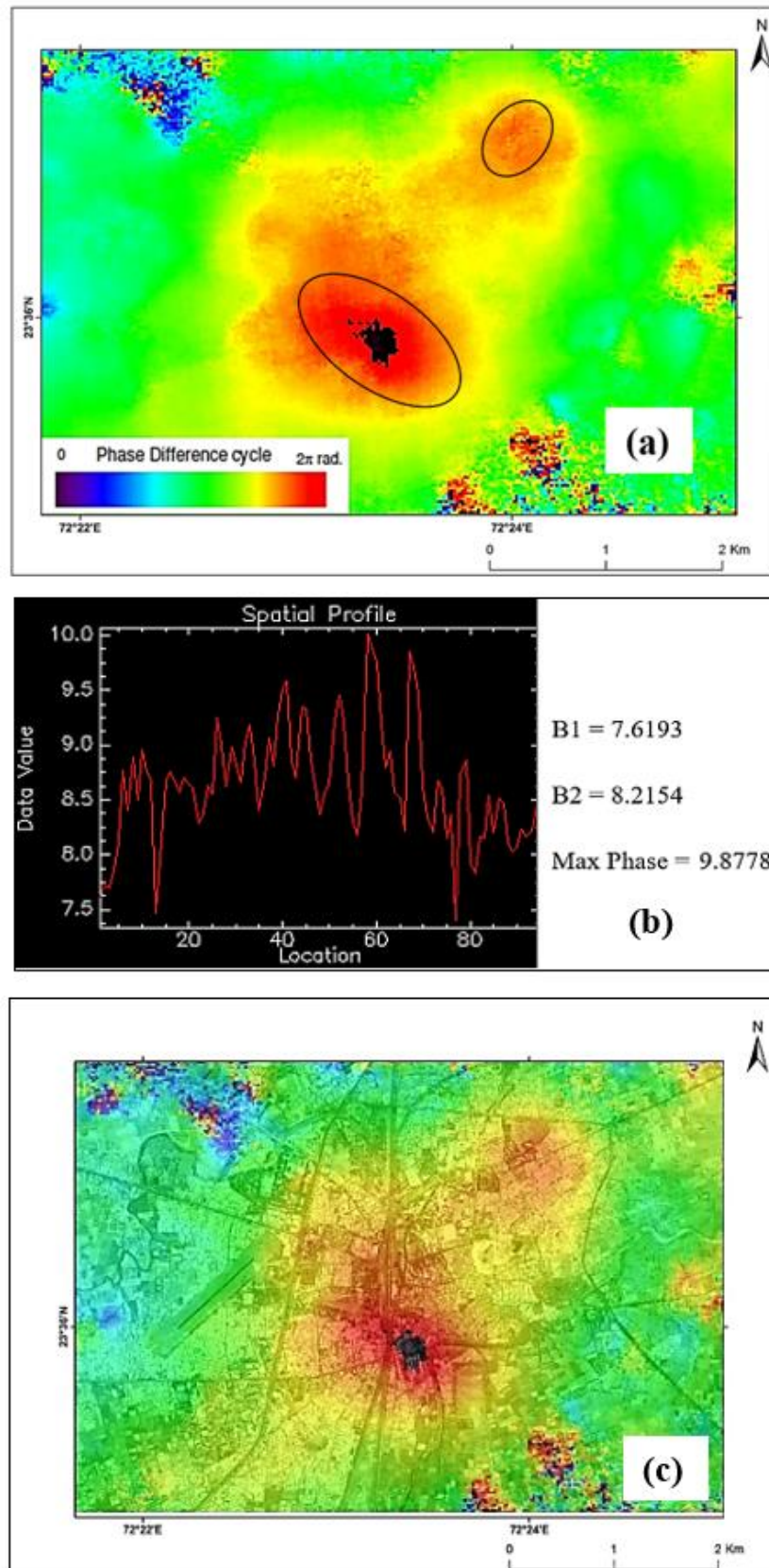

Fig 4.9: ALOS PALSAR -2 Image Pair: 2083640-2170580;Date: 10-12-2015_20-07-2017.
(a) Filtered Interferogram (b) Spatial Profile (c) Displacement over Mehsana city.

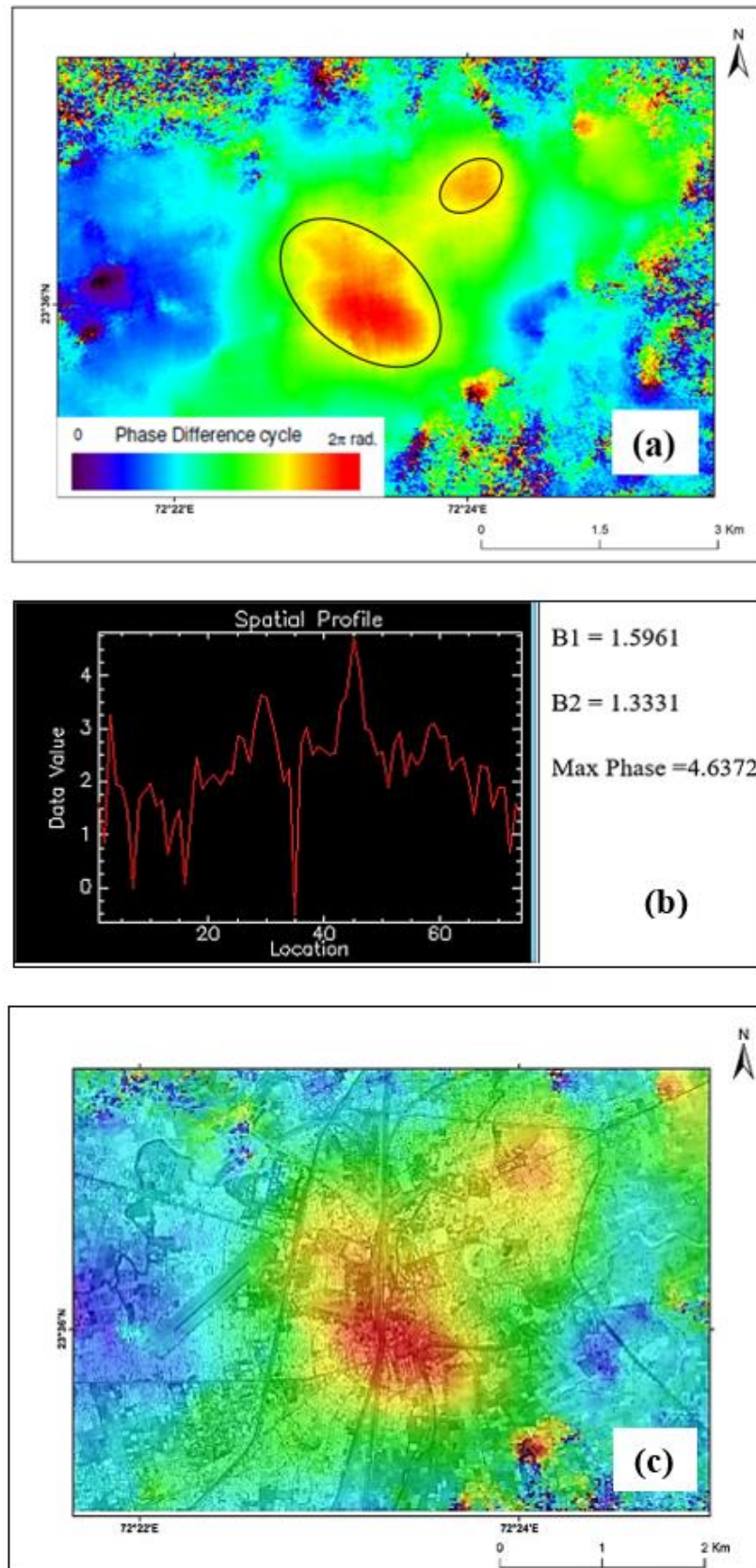**4.3.1.5   ALOS PALSAR -2 Image Pair (2083640-2199560;Date: 10-12-2015_01-02-2018)**

Fig 4.10: ALOS PALSAR -2 Image Pair: 2083640-2199560; Date: 10-12-2015_01-02-2018.
(a) Filtered Interferogram (b) Spatial Profile (c) Displacement over Mehsana city.

4.3.1.6 ALOS PALSAR -2 Image Pair (2093990-2147810;Date: 18-02-2016_20-07-2017)
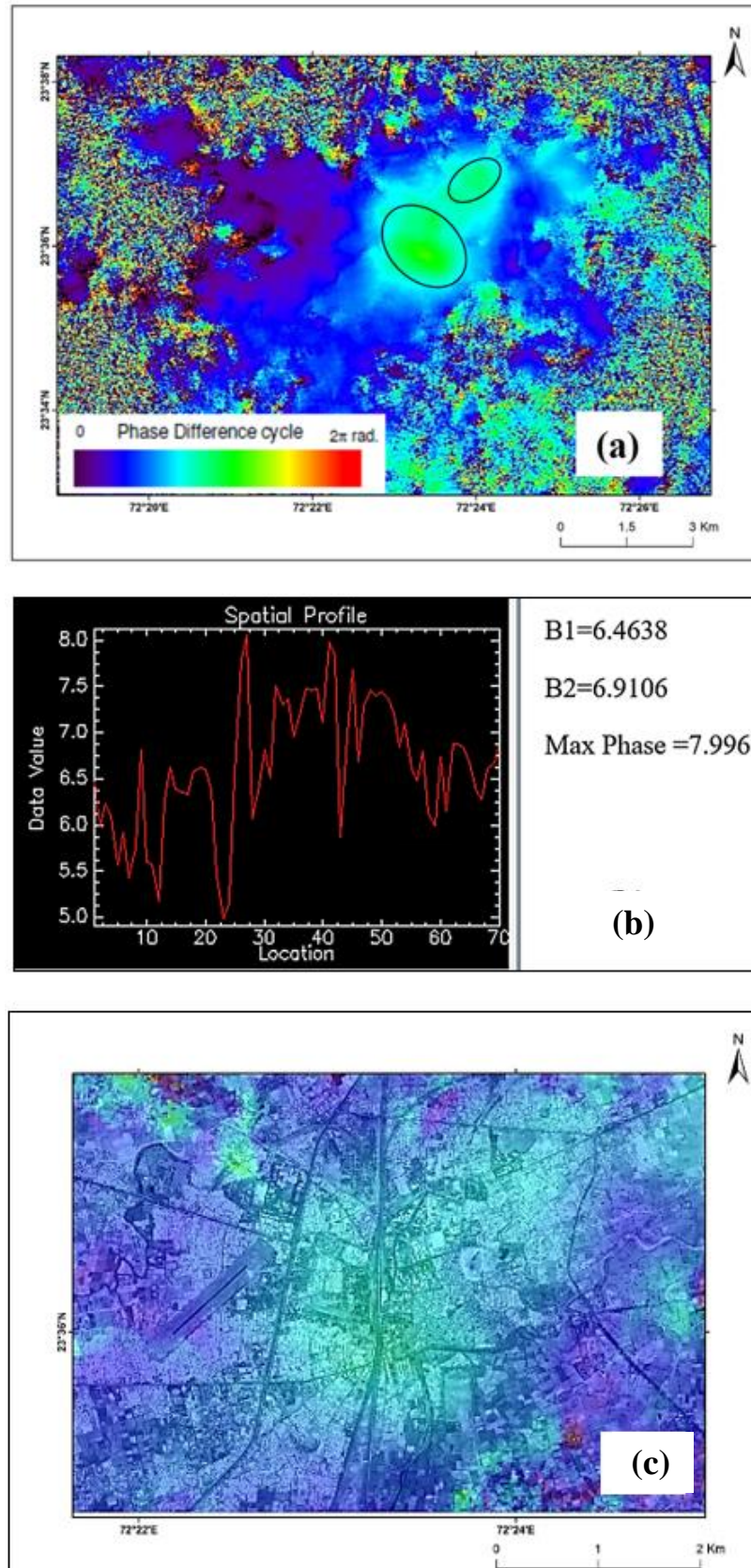

Fig 4.11: ALOS PALSAR -2 Image Pair: 2093990-2147810; Date: 18-02-2016_20-07-2017.
(a) Filtered Interferogram (b) Spatial Profile (c) Displacement over Mehsana city.

4.3.1.7 ALOS PALSAR-2 Image Pair (2093990-2199560; Date: 29-09-2016_01-02-2018)
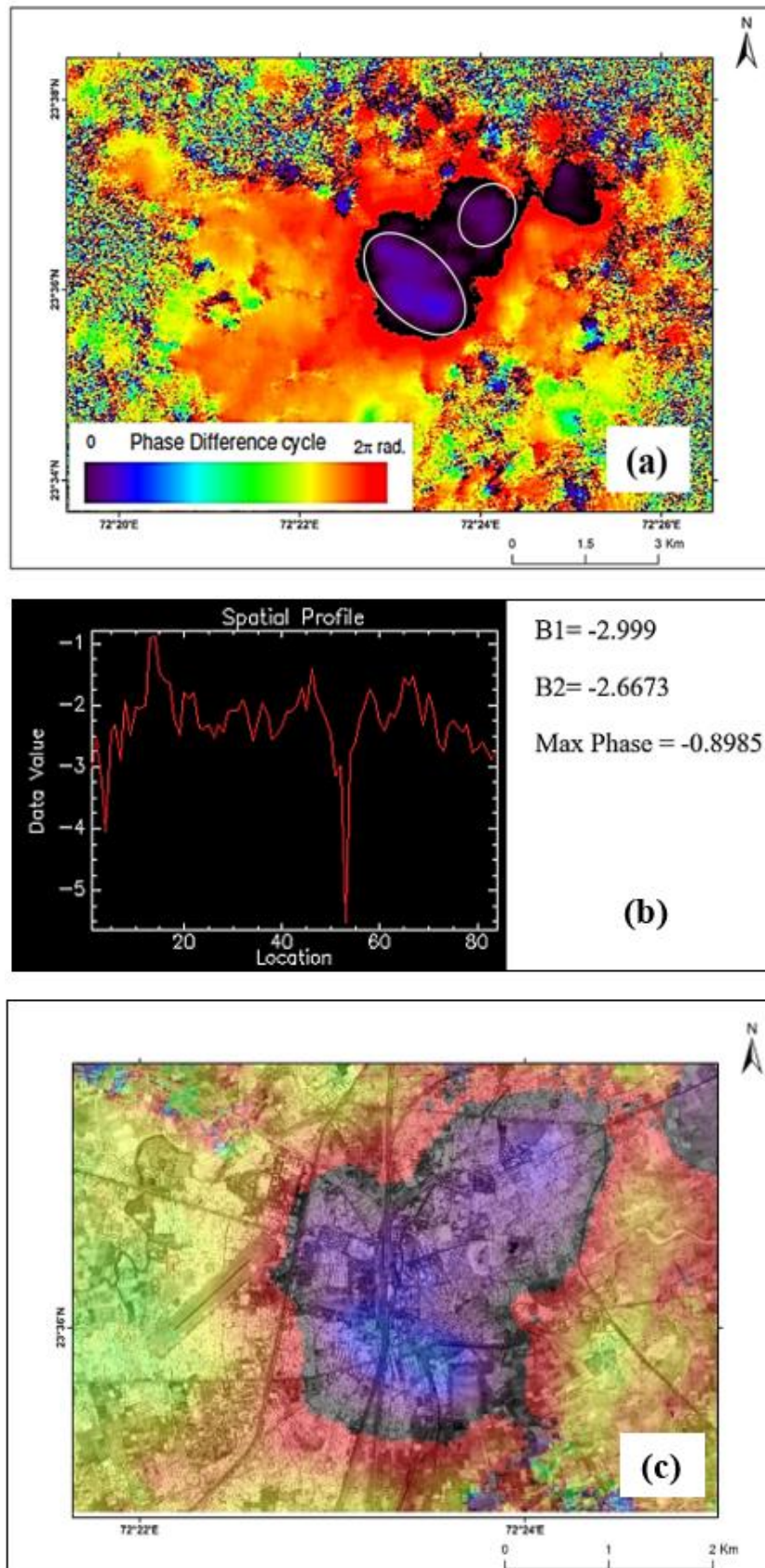

Fig 4.12: ALOS PALSAR -2 Image Pair: 2093990-2199560; Date: 29-09-2016_01-02-2018.
(a) Filtered Interferogram (b) Spatial Profile (c) Displacement over Mehsana city.

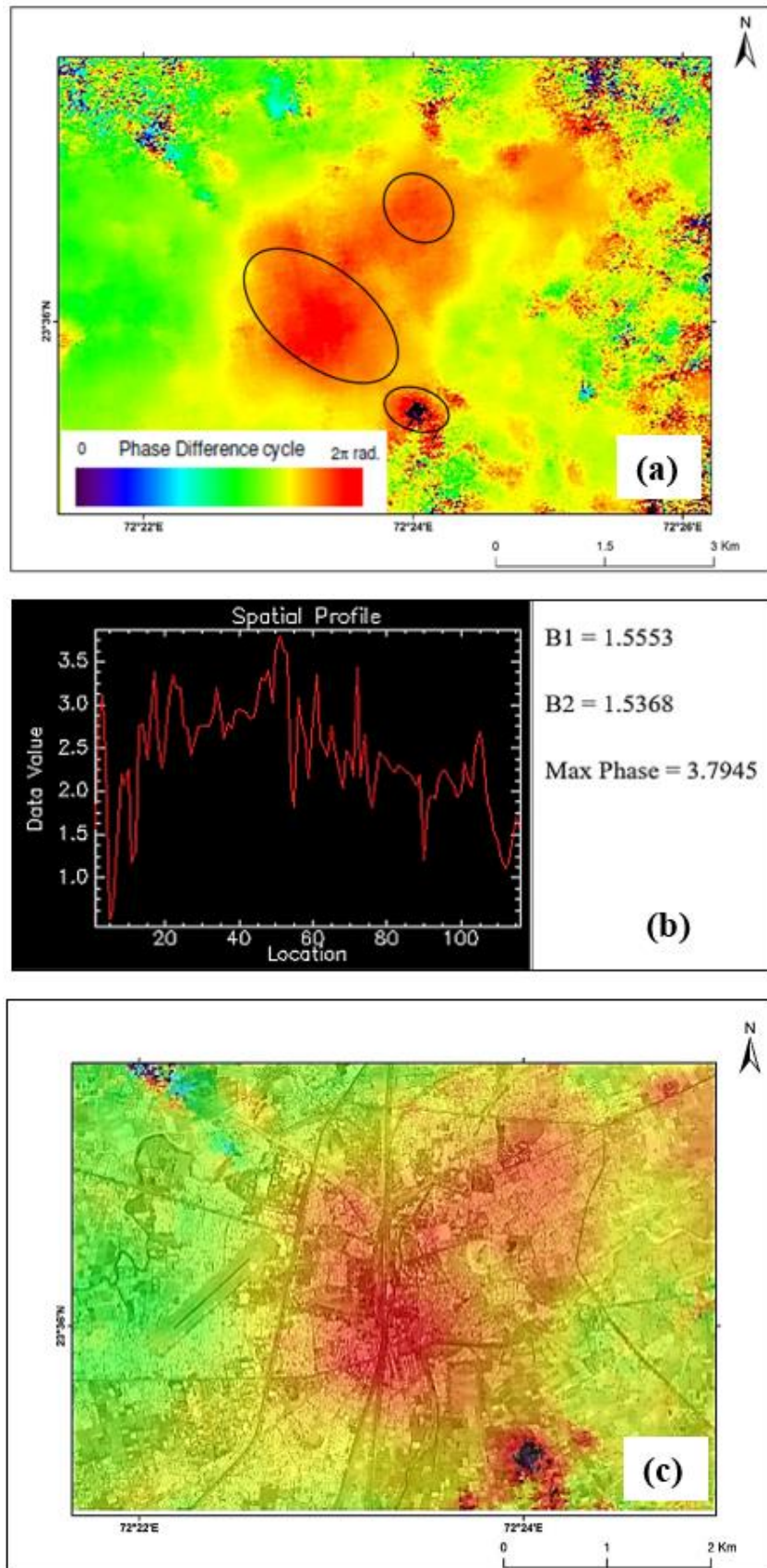### 4.3.1.8 ALOS PALSAR -2 Image Pair (2147810-2199560;Date: 16-02-2017_01-02-2018)

Fig 4.13: ALOS PALSAR -2 Image Pair: 2147810-2199560; Date: 16-02-2017_01-02-2018.
(a) Filtered Interferogram (b) Spatial Profile (c) Displacement over Mehsana city .

The Deformation was calculated by differencing the obtained maximum phase with the average phase values. The average phase values were computed from the values obtained from the spatial profile of the deformation fringes. The LOS values were calculated by dividing the product of deformation and the wavelength of ALOS PALSAR-2 Sensor which is 23 in our case by 4π. And then the LOS rate was determined by multiplying the LOS with number of days in the year and dividing by the temporal baseline. The mean weighted coherence which gave the overall subsidence during the period 2015 to 2018 was estimated by dividing the sum of mean coherence of individual pairs with the product of LOS rate and mean coherence. The calculations for ALOS PALSAR -2 data pairs are summarized in Table 4.11 below.

Table 4.11: Coherence weighted Deformation rates from ALOS PALSAR -2 Image Pairs

Time Period	Temporal Baseline	B1	B2	Max Phase	Average	Deformation	LOS (cm)	LOS Rate (cm/yr)	Mean Coherence	LOS Rate * Mean Coherence	Weighted Mean Coherence
10-12-2015 to 20-07-2017	588	7.619	8.215	9.8778	7.92	1.96	3.59	2.23	0.18	0.39	
10-12-2015 to 01-02-2018	784	1.596	1.333	4.6372	1.46	3.17	5.81	2.70	0.18	0.48	
18-02-2016 to 20-07-2017	518	6.464	6.911	7.996	6.69	1.31	2.40	1.69	0.18	0.30	2.78
29-09-2016 to 01-02-2018	490	-3.000	-2.667	-0.8985	-2.83	1.94	3.54	2.64	0.19	0.50	
16-02-2017 to 01-02-2018	350	1.555	1.537	3.7945	1.55	2.25	4.12	4.29	0.22	0.93	
									∑=0.94	∑=2.61	

From the DInSAR observations, it is evident that a subsidence fringe has developed around Mehsana and that there has been a progressive increase in land subsidence from 2007-2011 to 2015-2018. The area around Mehsana city airstrip is undergoing progressive subsidence as illustrated by the results above. The rate of land subsidence which was estimated to 2.49 cm/yr. during the period between 2007-2011 has increased to 2.78 cm/yr. during the latter half the decade between 2015-2018. The DInSAR derived trends in land subsidence are quite analogous to the aquifer compaction trends where the levels of rate of aquifer compaction increased during 2012-2017 than the earlier period of 2005-2011. To further compare and validate the results obtained from data pairs of ALOS PALSAR -1 and ALOS PALSAR -2 images, similar processing was carried out using RADARSAT-2 image pairs of 2017-2018 (Figure 4.14 to 4.16 below), which also concluded that similar deformation fringes have developed around the airstrip of Mehsana city.

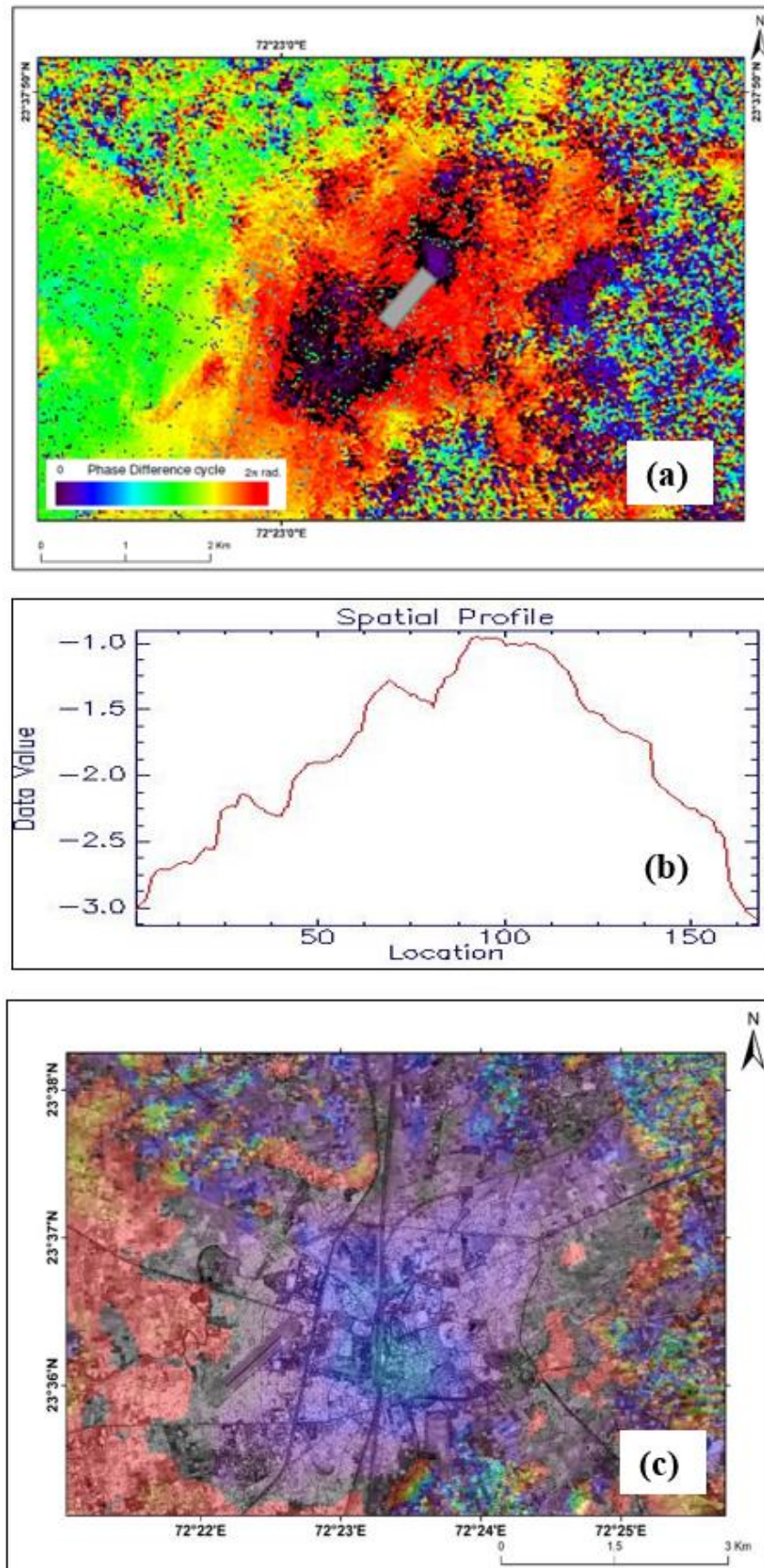**4.3.1.9   RADARSAT-2 Image Pair (Date: 09-12-2017_19-02-2018)**

Fig 4.14: RADARSAT-2 Image Pair: Date: 09-12-2017_19-02-2018. (a) Filtered Interferogram (b) Spatial Profile (c) Displacement over Mehsana city.

4.3.1.10 RADARSAT-2 Image Pair (Date: 09-12-2017_19-06-2018)

Fig 4.15: RADARSAT-2 Image Pair: Date: 09-12-2017_19-06-2018. (a) Filtered Interferogram (b)Spatial Profile (c) Displacement over Mehsana city.

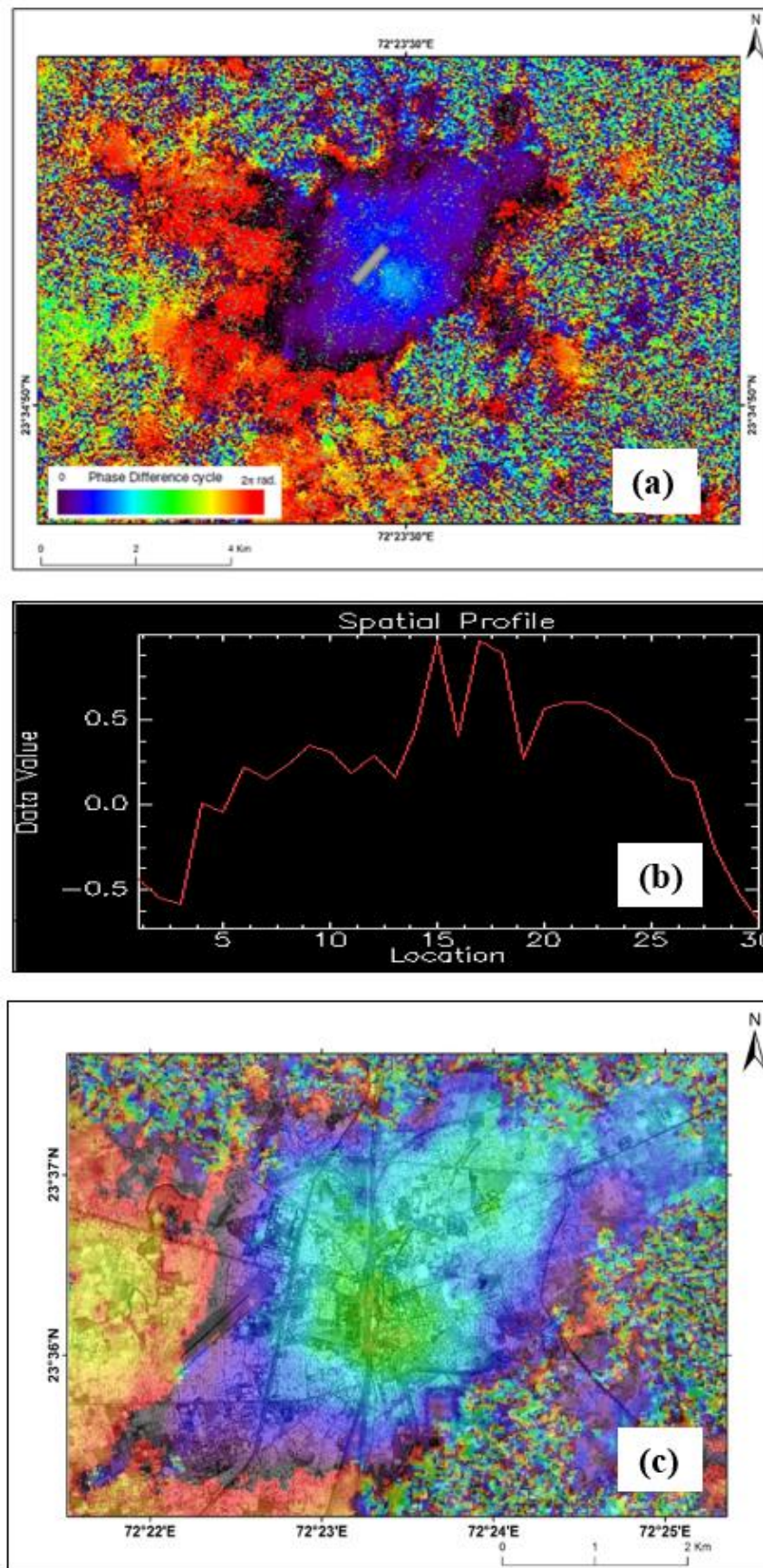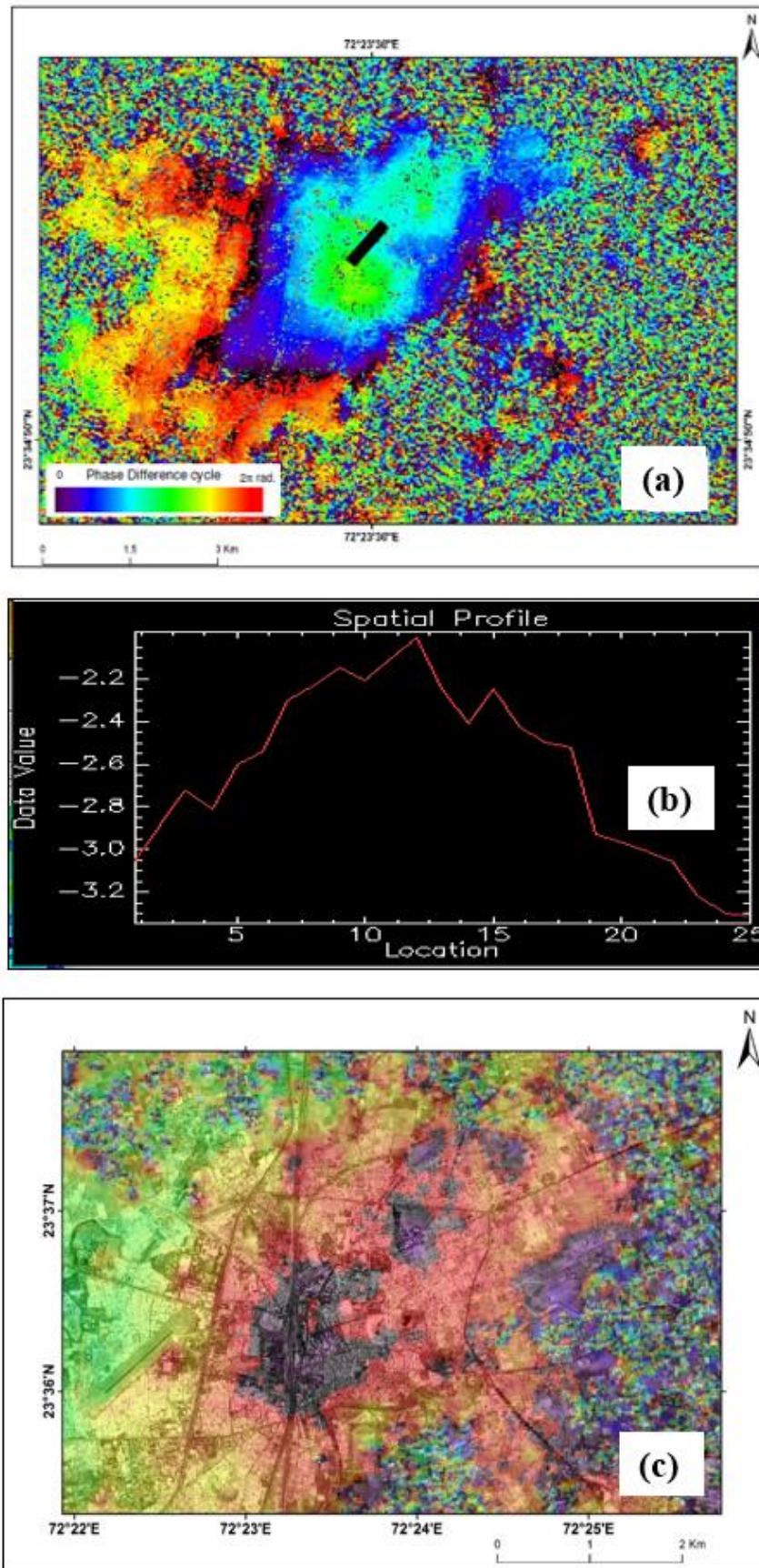### 4.3.1.11 RADARSAT-2 Image Pair (Date: 08-04-2018_19-06-2018)

Fig 4.16: RADARSAT-2 Image Pair: Date: 08-04-2018_19-06-2018. (a) Filtered Interferogram (b)Spatial Profile (c) Displacement over Mehsana city .

The results from DINSAR based observations show deformation fringes in both ALOS PALSAR-1 data FBD polarization data and ALOS PALSAR-2 FBS polarization data. The analysis from DInSAR reveals that the area in and around Mehsana is moderately subsiding. The average rate of subsidence in the area has increased slowly over the years. Though the ALOS PALSAR -1 data pairs were limited by low coherence values, the extraction of phase and displacement values could have an uncertainty in the derived results. A higher coherence threshold was chosen after phase unwrapping to remove the components with low coherence, therefore the results could still portray a good retrieval of land subsidence scenario in the region. The area around Mehsana is characterized by extensive vegetation which posed temporal decorrelation issues, but still we were able to estimate the land subsidence in urban areas of Mehsana by sub-setting the image around Mehsana city. The mean coherence in ALOS PALSAR-2 image pairs were relatively better, and phase values could be recovered better from them, and the coherence weighted land subsidence results could be obtained more reliably. The overall analysis showed slow progressive levels of land subsidence rates over the study period in and around Mehsana region. The area around Mehsana airstrip is seen to be undergoing progressive land subsidence during the study period. The deformation patterns from ALOS PALSAR-1 and ALOS PALSAR-2 images were compared with DInSAR results on RADARSAT-2 images and both ALOS PALSAR 1/2 and RADARSAT-2 images showed similar fringes around the Mehsana airstrip which confirmed our results that the area is showing signs of continued land deformation.

4.4   DInSAR based monitoring of Land Subsidence around Oil Fields

DInSAR processing was also carried out on ALOS PALSAR-1 and ALOS PALSAR-2 SAR image pairs to monitor deformation patterns around the oil fields in the vicinity of Mehsana. No deformation patterns were observed around the oil fields in both ALOS PALSAR-1 and ALOS PALSAR-2 data. The results suggest that there is no observed subsidence due to petroleum extraction and that the only signs of deformation are seen in the urban areas where the observed deformation patterns are mainly because of withdrawal of groundwater from underground aquifers. The petroleum reservoir compaction

could not be done due to paucity of the data on reservoir geotechnical parameters. Nevertheless, DInSAR modelling has been able to show that there is no subsidence happening around the oil fields during the study time period.
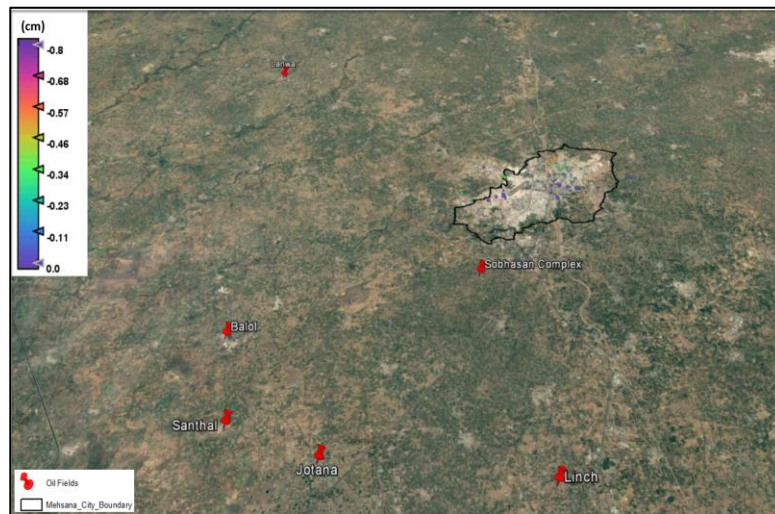

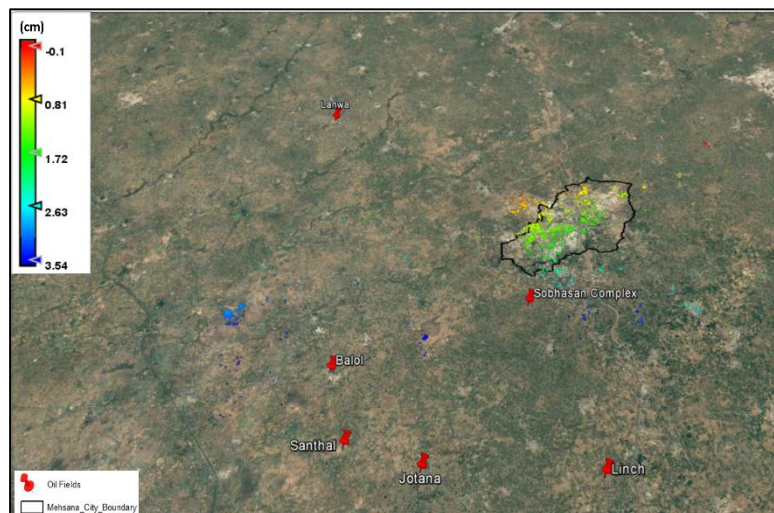**Fig 4.17**: Displacement around Mehsana Oil Fields. ALOS PALSAR-2 Pair:16-04-08_10-03-11

Fig 4.18: Displacement around Mehsana Oil Fields. ALOS PALSAR-2 Pair:21-07-16_28-09-17
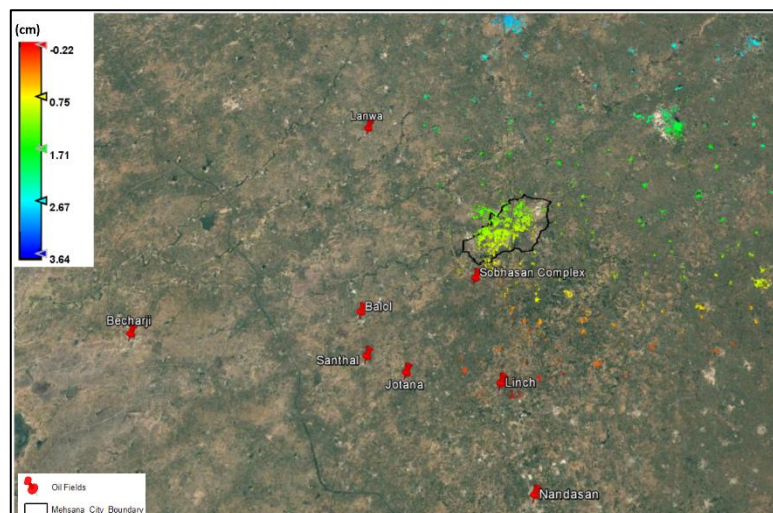

Fig 4.19: Displacement around Mehsana Oil Fields. ALOS PALSAR-2 Pair:28-09-17_01-03-18

CHAPTER 5.   RESULTS AND DISCUSSIONS

In this study an attempt has been made to characterize land subsidence in and around Mehsana through predictive modelling of aquifer compaction and DInSAR techniques. The impact of groundwater drawdown on incumbent land subsidence was analyzed. To understand the relationship between groundwater levels and the land subsidence a regional and local analysis of groundwater scenario in Kutch-Sabarmati basin was made. At a regional scale, groundwater trend analysis was conducted using Mann Kendall statistical test which was quantified using the Sen's slope estimator. The statistical trend test highlighted the areas in the basin facing a decline in the water levels during the pre and post monsoon seasons. The north east region of the basin specifically Banaskantha and Patan districts showed significant declining levels over the study period with a rate ranging between 0.4 to 3.6 m/yr. during the study period from 2005 to 2017. Elevation and high usage of groundwater for sustaining the increased agriculture practices in the districts were found to be a major reason for the depleting levels. Rainfall which is a major source of groundwater replenishment was not found showing any significant trend during our study period which infers the fact the declining pre monsoon groundwater levels was due to groundwater over-extraction between the post monsoon months of the preceding year and the pre monsoon months of the succeeding year. The results are quite synonymous with observations by various researchers from different parts of the world such as Calo et al. (2017), Othman and Abotalin (2019) wherein they concluded that agricultural practices were one of the major causes of groundwater depletion thus leading to land subsidence.

To study the fluctuation trends in the Kutch-Sabarmati basin and to identify the hotspots of recharge and depletion, statistical interpolation of seasonal groundwater levels namely the pre-pre and post-pre monsoon season

was carried out using the more robust Kalman filter algorithm, which provided better predicted values than the standard interpolation techniques. The results suggested that the Kutch and Saurashtra basin of the composite Kutch-Sabarmati basin are facing pronounced declining groundwater levels, while the depletion levels are improved on the west of the composite basin towards the Sabarmati basin. The Mehsana district along with some parts of Banaskantha and Patan district have shown an improvement in the declining levels post year 2009. Though there have been intermittent episodes of recharge and depletion in the area due to cyclic variations of rainfall patterns, but the results suggest that overall the groundwater levels have improved after 2009 in and around the vicinity of Mehsana district. The results are also supported by the fact that after the commissioning of Narmada canal in 2008, which passes through parts of South and North Gujarat, the dependence on groundwater for irrigation purposes have reduced thereby showing relative slowdown in the depletion scenario in the region. Also, the canal water recharges the underground aquifers which has also helped in the improvement of water levels. The Kutch Branch canal of Narmada Main canal that is supposed to supply water to the arid Kutch region is not fully functional as of now and it will take more time before we could see improvements in the groundwater levels of the Kutcha and Saurashtra regions. Large variations in piezometric heads as observed from the standard deviation maps were found in areas especially in and around Mehsana taluk of Mehsana district. These areas were later subjected to our further studies on land subsidence at a local scale through aquifer compaction modelling and DInSAR modelling to decipher the relationship between piezometric head variations and resulting land deformations.

For aquifer compaction modelling, both Inelastic and Elastic compactions were calculated which were aggregated to estimate the total compaction in the four observatory wells studied in and around Mehsana taluk. The total aquifer compaction is a measure of the land subsidence. The Inelastic and Elastic components were calculated using the one dimension consolidation equations given by Domenico and Lohman respectively. The piezometric heads were compiled from the observed groundwater level as recorded by the Central

Ground water board, India. The thickness of the aquifers was calculated from the lithologs and information on depth of tapped zones as provided by the CGWB. The results indicated that there had been a gradual increase in total aquifer compaction from the period 2005-2011 to 2012-2017. The average rate of aquifer compaction during 2005-2017 ranged from 0.22 to 1.71 cm/ yr. in Mehsana-V and Mewad wells of Mehsana taluk, while the rates were still higher Modhera-II and Karalli-II wells of Visnagar and Unjha taluks. The higher compaction rates especially in Modhera-II was because of large variations in piezometric heads recorded in the observation well. The analysis inferred that Inelastic compaction due to piezometric variations between pre monsoon months of two consecutive years, is the bigger and unrecoverable component of land subsidence and that the decline in pre-pre piezometric heads reveals an increased reliance and drawdown of groundwater resources in the region. The major role of Inelastic compaction in land subsidence as seen in our study wells was synonymous to the findings in similar studies done worldwide such as by Galloway and Burbey (2011), Chatterjee et al. (2013). Though the statistical interpolation showed a gradual recovery in depletion levels during the latter half of the study period post 2012 in North and South Gujarat regions of the basin, the localized studies at the observation wells indicated that land subsidence has been increasing at the local levels and that the areas with more groundwater head variations were more vulnerable to land subsidence.

Space borne DInSAR modelling was carried out to analyze the land subsidence scenario around the Mehsana region. ALOS PALSAR-I and ALOS PALSAR-2 InSAR data was utilized to study the deformation patterns in the area. The data of ALOS PALSAR-1 satellite that was decommissioned in 2011, was analyzed for the period 2007-2011, while ALOS PALSAR-2 data was examined for the period between 2015 and 2018. The DInSAR observations also reveal land subsidence in the area that have been gradually increasing over the years. The mean land subsidence rate was 2.49 cm/yr. from 2007 to 2011 which increased to 2.78 cm/yr. during 2015-2018. Though the ALOS PALSAR-1 data was limited by low coherence in the image pairs, and atmospheric and temporal decorrelations, especially in areas like Mehsana with large practices

of agriculture, the masking of phase results with higher threshold values helped retrieve coherent areas whose displacements could be estimated. ALOS PALSAR-2 data pairs showed considerably better coherence and selection of large temporal baseline of more than a year helped retrieve the phase differences and calculate the rates of deformation in the line of sight direction. The pairs of RADARSAT-2 images of 2017-2018 were also processed to compare our deformation results obtained from both ALOS PALSAR 1/2 images and both substantiated that deformation fringes have developed over the Mehsana city particularly in the vicinity of Mehsana airstrip.

The results of land subsidence achieved through DInSAR modelling are quite comparable to the ground based aquifer compaction results, with almost similar trends of land subsidence. The total aquifer compaction in Mehsana well increased from 0.06 cm/yr. in 2007-2011 to 1.47 cm/yr. in 2012-2017. The DInSAR subsidence results also moved up from 2.49 cm/yr. from 2007-2011 to 2.78 cm/yr. during 2015-2018. Though, the aquifer compaction results are localized and specific to a well, the DInSAR results are mean subsidence rates for the study period and could face uncertainties like overestimation owing to atmospheric and temporal decorrelations. Despite the differences in the scale and time period, the two modelling techniques showed a very good agreement in the results and validated the capabilities of space borne DInSAR techniques to effectively monitor land subsidence over a regional scale with a centimetre level of precision.

The investigation of deformation patterns in and around Mehsana city showed clear deformation fringes around the urban area. However, no deformation signatures could be identified from DInSAR around Mehsana oil fields. The deformation signatures around the oil fields are generally weaker in comparison to the groundwater based deformation signatures, owing to the deeper levels at which the compaction happens in a petroleum reservoir, no deformation patterns could be revealed in our study from the available ALOS PALSAR 1/2 and RADARSAT-2 satellite data.

CHAPTER 6. CONCLUSION

The present work was focussed on analysing the land subsidence patterns due to fluid withdrawal in Kutch-Sabarmati basin of Gujarat. The study investigated the relationship between groundwater extraction and land subsidence in the region through different modelling techniques. An estimation of local land subsidence induced by groundwater withdrawal in Mehsana was made through the satellite based DInSAR observations. Land deformations patterns around the petroleum fields surrounding Mehsana were also investigated through the DInSAR techniques. Aquifer modelling results which were based on ground recorded piezometric levels and the observed lithological and hydrogeological data were used to correlate and validate the space borne derived deformation rates. The piezometric data of 2005-2017 was used to evaluate the groundwater variability in Kutch-Sabarmati basin at a regional level through regional trend analysis and geostatistical techniques and was further used to estimate the aquifer system compaction at four chosen wells in and around Mehsana. A good consensus was observed between the land subsidence obtained from predictive modelling and DInSAR modelling.

The study tried to find plausible answers to the research questions put forward for the present work which are as follows:

- How far is groundwater depletion responsible for land subsidence?

The geostatistical analysis of regional groundwater levels showed high fluctuations in the Mehsana taluk in both pre-pre and post-pre monsoon seasons. The high fluctuating regions were found to be suffering more from aquifer compaction. The higher compaction rates in Mewad and Modhera-II was because of large variations in piezometric heads recorded in the observation well. The groundwater depletion maps reveal that there has been an increase in depletion levels in the second half of the study period especially after 2014. This

decline in the pre-pre piezometric heads that leads to Inelastic compaction, reveals an increased reliance and drawdown of groundwater resources in the region. The analysis from aquifer compaction results inferred that Inelastic compaction due to piezometric variations between pre monsoon months of two consecutive years, is the bigger and unrecoverable component of land subsidence. Land subsidence has been increasing at the local levels and the areas with more groundwater head variations were more vulnerable to land subsidence.

- Can time series analyses of advance DInSAR technique efficient enough to detect the trend of ground water depletion and how far are they comparable to the subsurface aquifer system compaction data ?

The time series analysis of DInSAR observations were quite comparable to the aquifer compaction results based on ground observed piezometric data. Areas susceptible to land subsidence as identified by DInSAR are in proximity to the potential subsidence areas revealed from the predictive modelling of aquifer compaction. The aquifer compaction rates during the period 2012-2017 increased from the preceding study period of 2005-2011. The DInSAR results also demonstrated similar increasing trends in the latter half of the study period. Though, the aquifer compaction results are localized and specific to a well, the DInSAR results are mean subsidence rates for the study period and could face uncertainties due to atmospheric and temporal decorrelations. Despite the differences in the scale and time period, the two modelling techniques showed a very good agreement in the results and validated the capabilities of space borne DInSAR techniques to effectively monitor land subsidence over a regional scale with a centimeter level of precision. Similar deformation patterns were obtained from ALOS PALSAR-1, ALOS PALSAR-2, and RADARSAT-2 data. The agreement between the results obtained from two different satellite data confirmed the applicability of DInSAR in monitoring land subsidence. However, precise GPS or levelling measurements in the subsiding areas can be used further to estimate and validate land subsidence at the local level.

▪ Can DInSAR based subsidence mapping detect deformations over the petroleum basins?

Though the DInSAR showed no specific land subsidence patterns around the Mehsana oil fields, but the applicability of the DInSAR technique to monitor land subsidence has been corroborated through the groundwater studies. The satellite data available suffered from low coherence and temporal decorrelations also posed a limitation on extracting precise deformation measurements in the area. Though we could not recover deformation signatures around oil fields from ALOS PALSAR 1/2 data, but the patterns could be further reinvestigated with satellite data having more precise orbital data in the future.

To conclude, the present work has been successful to characterize land subsidence in and around Mehsana. Subsidence in the area is due to groundwater over extraction. DInSAR observations that were validated with ground-based observations have been found to model the land subsidence quite effectively and can be used to map and quantify land subsidence at a regional scale.

6.1 Future Research Directions

Considering the present work done and the real context in which these techniques can be applied, we propose the following strategy for future research.

• From the present work, we were able to understand and analyze that land subsidence was taking place in Kutch-Sabarmati basin due to decline in pre-pre monsoon piezometric heads, which was mainly due to over extraction of groundwater for agriculture purposes. The unavailability of seasonal groundwater pumping and aquifer recharge data posed a limitation on correlating the ground observed water drawdown with the modelled land subsidence. In our future research work we would like to model the groundwater pumping and recharge data and use numerical groundwater flow models to simulate the hydrodynamic behavior of the aquifers and investigate their

relationship with the spatial and temporal changes in land subsidence.

- Microwave ALOS PALSAR 1/2 and RADARSAT-2 data that was available for the present study could not identify deformation signatures near Mehsana oil fields. However, in future we would like to integrate multi satellite InSAR data from Tandem-X, Cosmo SkyMed and open source SENTINEL-1 data and apply techniques of multi-temporal InSAR (MT-InSAR) using advanced algorithms such as Persistent Scatterer Interferometry (PSI), Small Baseline Subset (SBAS), QPS and SqueeSAR to reinvestigate deformation around the oil fields of Mehsana. The paucity of adequate hydrogeological and detailed petroleum reservoir compaction data posed a limitation in modelling hydrocarbon reservoir compaction and correlate it with satellite data, which would be an area of interest for our future studies.

- The NASA–ISRO SAR (NISAR) is another promising radar mission for investigating temporal and spatial land surface deformations. The NISAR mission can acquire global images of earth's surface and can monitor the phenomenon of land subsidence globally with deformation measurements having accuracies upto millimeter levels. The high-resolution capabilities of NISAR along with its wide swath, a 12-day repeat orbit cycle and dual-frequency (L- and S-band) modes can provide information on land deformations due to the withdrawal of groundwater and hydrocarbon resources. Such studies can thus help in understanding reservoir dynamics and for characterization and modelling of aquifers and hydrocarbon reservoirs. Land subsidence studies using the NISAR data can be an exciting research opportunity for future work.

- NASA's Ice, Cloud, and land Elevation Satellite-2 (ICESat-2) is also available since 2018 to measure changes in land elevation. The satellite uses lasers and very precise detection instruments to provide very precise altimetry data to aid in multi-temporal topographic measurements of oceans and land surfaces. Though the main objective of Geoscience Laser Altimeter System (GLAS) instrument onboard ICESat-2 satellite is to measure ice sheet elevations, but it can also be used for other applications such as bathymetry, height of vegetation canopy and land deformations. The altimetry data obtained

from ICESat can be used as ground control observations to significantly improve InSAR-derived DEMs to be used for deformation measurements. Some researchers have previously also investigated land subsidence due to groundwater extraction using GRACE-GLDAS derived groundwater depletion rates and ICESat derived elevation changes. Research work on similar lines could be explored in the near future.

- NASA's GEDI (Global Ecosystem Dynamics Investigation) mission launched in uses LIDAR equipment's to provide high-resolution global observations of vertical measurements. The satellite was launched primarily to provide information on forest vertical structure and to quantify and understand global biodiversity but can also gather information on land topography. The fusion of profile measurements from GEDI observations with radar measurements from pol-InSAR satellites such as ALOS PALSAR-2 and TanDEM-X can be explored in future.

6.2 Implications to Society

Such studies utilizing satellite-based techniques can thus help in understanding and mitigating the socio-economic impacts of land subsidence on human populations and would help in performing impact and vulnerability assessment of land subsidence especially in parts of the world having little in-situ geodetic measurements. The detrimental effects of land subsidence due to groundwater overdraft on society and environment such as damage to structures (roads, buildings, pipelines and sewage utilities, dams), loss of human life, deterioration of economic activities, increased vulnerability to landslides, increased exposure to flood and tidal risks due to lowering of ground surface levels especially in coastal areas, lowering of phreatic surface, changes in soil characteristics and geomorphology can be monitored and addressed in an effective way and steps can be taken to counteract the menace of land subsidence. Adequate and timely strategies can be formulated by decision makers to support groundwater administration and future infrastructural development plans.

REFERENCES

1. Agram P. S. and Simons M. (2015), "A noise model for InSAR time series", Journal of Geophysical Research, Solid Earth, Vol. 120, Issue 4 pp. 2752-2771.

2. Ahmad W., Choi M., Kim S. and Kim D. (2017), "Detection of Land Subsidence due to Excessive Groundwater Use Varying with Different Land Cover Types in Quetta valley, Pakistan Using ESA-Sentinel Satellite Data", Natural Hazards Earth System Science Discussions, doi: 10.5194/nhess-2017-234.

3. Alex Hay-Man Ng, Linlin Ge, Xiaojing Li (2015), "Assessments of land subsidence in the Gippsland Basin of Australia using ALOS PALSAR data", Remote Sensing of Environment, Vol. 159, pp. 86-101.

4. Allis R., Bromley C. and Currie S. (2009), "Update on subsidence at the Wairakei-Tauhara geothermal system, New Zealand", Geothermics, Vol. 38, Issue 1, pp.169–180.

5. Amelung F., Galloway D. L., Bell, J.W., Zebker H.A. and Laczniak, R.J. (1999), "Sensing the ups and downs of Las Vegas: InSAR reveals structural control of land subsidence and aquifer-system deformation", Geology, Vol. 27, No. 6, pp. 483-486.

6. ArcGIS Resources, Available online at https://desktop.arcgis.com/en/arcmap/10.6/extensions/geostatistical-analyst/deterministic-methods-for-spatial-interpolation.htm

7. Bell J.W., Amelung F. and Ferretti A. (2008), "Permanent scatterer InSAR reveals seasonal and long-term aquifer system response to groundwater pumping and artificial recharge", Water Resources Research, Vol. 44, W02407. doi:10.1029/2007WR006152.

8. Berardino P., Fornaro G., Lanari R. and Sansosti E. (2002), "A new algorithm for surface deformation monitoring based on small baseline

differential SAR interferograms", IEEE Transactions on Geoscience and Remote Sensing, Vol. 40, Issue 10, pp. 2375–2383.

9. Bernardo Lagos-Álvarez, Leonardo Padilla, Jorge Mateu, Guillermo Ferreira (2019), "A Kalman filter method for estimation and prediction of space–time data with an autoregressive structure", Journal of Statistical Planning and Inference, Vol. 203, pp. 117-130.

10. Bhatia B. (1992), "Lush Fields and Parched Throats: Political Economy of Groundwater in Gujarat", Economic and Political Weekly, XXVII (51-52): A 12- 170.

11. Bhattacharya A. K. (2011), "Land subsidence in Kolkata due to groundwater depletion", Electronic Journal of Geotechnical Engineering, Vol. 16, pp. 1415-1428.

12. Bhattacharya A.K. (2008), "Hydrogeology and land subsidence in Salt Lake City, Kolkata", Electronic Journal of Geotechnical Engineering, Vol.13, pp. 1-14.

13. Bhattacharya A.K. and Kumar D. (2012), "Land subsidence in East Calcutta", IOSR Journal of Engineering, Vol. 2, Issue 3, pp. 408-413.

14. Biot M.A. (1941) "General theory of three-dimensional consolidation, Journal of Applied Physics", Vol. 12, pp.155-164.

15. Bonì R., Cigna F., Bricker S., Meisina C. and McCormack H. (2016), "Characterisation of hydraulic head changes and aquifer properties in the London Basin using Persistent Scatterer Interferometry ground motion data", Journal of Hydrology, Vol. 540, pp. 835-849.

16. Bouwer H. (1977), "Land subsidence and cracking due to groundwater depletion, Ground Water" Vol. 15, Issue 5, pp. 358–364.

17. Brassington R. (1998), "Field Hydrogeology", 2nd Edition, John Wiley & Sons, Chichester, England.

18. Calò F., Abdikan S., Görüm T., Pepe A., Kiliç H. and Şanli F.B., (2015), "The Space-Borne SBAS-DInSAR Technique as a Supporting Tool for Sustainable Urban Policies: The Case of Istanbul Megacity, Turkey", Remote Sensing, Vol. 7, pp. 16519-16536, doi:10.3390/rs71215842

19. Calo F., Notti D., Galve J.P., Abdikan S., Gorum T., Pepe A. and Sanli F.B. (2017), "DInSAR-Based Detection of Land Subsidence and Correlation with

Groundwater Depletion in Konya Plain, Turkey", Remote Sens. 2017, Vo. 9(1), 83, 25 p.

20. Carpenter M.C., (1987), "Water-Level Declines, Land Subsidence, and Specific Compaction near Apache Junction, South-Central Arizona", U.S. Geological Survey, Water-Resources Investigations Report 86-4071, Available online at

https://pubs.usgs.gov/wri/1986/4071/report.pdf

21. Carrillo, N. (1947) "Influence of artesian wells in the sinking of Mexico City", In Carrillo V.N. (ed), Comision Impulsora y Coordinadora de la Investigacion Cientifica, Anuario 47. Secretaria de Hacienda y Credito Publico, Mexico City, pp 7–14, 1969.

22. Castellazzi P., Arroyo-Domínguez N., Martel R., Calderhead A.I., Normand J.C.L., Gárfias J., Rivera A. (2016) "Land subsidence in major cities of Central Mexico: Interpreting InSAR-derived land subsidence mapping with hydrogeological data", International Journal of Applied Earth Observation and Geoinformation, Vo. 47, pp. 102–111.

23. Chaabani A. and Deffontaines B. (2020), "Application of the SBAS-DInSAR technique for deformation monitoring in Tunis City and Mornag plain", Geomatics, Natural Hazards and Risk, Vol. 11, Issue 1, pp. 1346-1377.

24. Chatterjee R.S., Fruneau B., Rudant J.P., Roy P.S., Frison P.L., Lakhera R.C., Dadhwal V.K., and Saha R. (2006) "Subsidence of Kolkata (Calcutta) City, India during the 1990s as observed from space by differential synthetic aperture radar interferometry (D-InSAR) technique", Remote Sensing of Environment, 102-206: pp-176-185.

25. Chatterjee R.S., Syafiudin M.F. and Abidin H. (2013) "Land Subsidence Characteristics in Bandung City, Indonesia as Revealed by Spaceborne Geodetic Techniques and Hydrogeological Observations", Photogrammetric Engineering and Remote Sensing, Vol. 79, Issue 7, pp. 639-652.

26. Chaussard E., Amelung F., Abidin H., Hong S.H. (2013), " Sinking cities in Indonesia: ALOS PALSAR detects rapid subsidence due to groundwater and gas extraction", Remote Sensing of Environment, Vol.128, pp-150-161.

27. Chaussard E., Wdowinski S., Cabral-Cano, E., Amelung, F. (2014), "Land subsidence in Central Mexico detected by ALOS InSAR time-series", Remote Sensing of Environment, Vol. 140, pp-94–106.

28. Chen D., Lu Y. and Jia D. (2018), "Land deformation associated with exploitation of groundwater in Changzhou City measured by COSMO-SkyMed and Sentinel-1A SAR data", Open Geosciences, Vol. 10, Issue 1, pp. 678–68.

29. Colesanti C., Mouelic S. L., Bennani M., Raucoules D., Carnec C. and Ferretti A. (2005), "Detection of mining related ground instabilities using the permanent scatterers technique – a case study in the east of France", International Journal of Remote Sening, Vol. 26, Issue 1, pp.201–207.

30. Colesanti C., Ferreti A., Prati C., Rocca F. (2001), "Comparing GPS, optical leveling and permanent scatterers", Proceedings of IGARSS2001, Sydney, Australia, Vol. 6, pp. 2622–2624.

31. Coplin L.S. and Galloway D.L. (1999), "Houston-Galveston, Texas – Managing coastal subsidence" , Land subsidence in the United States, U.S. Geological Survey Circular 1182, pp. 35-48.

32. Crosetto M., Crippa B. and Biescas E. (2005), "Early detection and in-depth analysis of deformation phenomena by radar interferometry", Engineering Geology, Vol. 79, pp. 81-91.

33. Crosetto M., Monserrat O., Cuevas-Gonzalez M., Devanthery N. and Crippa B. (2016) "Persistent scatterer interferometry: A review", ISPRS Journal of Photogrammetry and Remote Sensing, Vol. 115, pp. 78–89.

34. Dinar A., Esteban E., Calvo E., Herrera G., Teatini P., Tomás R., Li Y., Albiac J. (2020) "Land Subsidence - The Forgotten Enigma of Groundwater (Over)Extraction", EAERE 2020, 25th Annual Conference of the European Association Environmental and Resource Economists, Berlin, Germany.

35. Dinesh M.K. (2000), "Institutional framework for managing groundwater: A case study of community organisations in Gujarat, India", Water Policy, ISSN: 1366-7017, Vol: 2(6), pp.423-432.

36. Ding X.L., Liu G.X., Li Z.W., Li Z.L and Chen Y.Q. (2004), "Ground subsidence monitoring in Hong Kong with satellite SAR interferometry", Photogrammetric Engineering and Remote Sensing, Vol. 70, Issue 10, pp-1151-1156.

37. Ding X.L., Li Z.W., Zhu J., Feng G. and Long J. (2008), "Atmospheric Effects on InSAR Measurements and Their Mitigation", Sensors, Vol. 8, pp. 5426-5448.

38. Domenico P.A. and M.D. Mifflin (1965), "Water from low-permeability sediments and land subsidence", Water Resources Research, Vol. 1, Issue 4, pp. 563-576.

39. Domenico P.A. (1972), "Concepts and models in groundwater hydrology", McGraw Hill Book Company, New York.

40. Edalat A., Khodaparast M.and Rajabi A.M. (2019), "Detecting Land Subsidence Due to Groundwater Withdrawal in Aliabad Plain, Iran, Using ESA Sentinel-1 Satellite Data", Natural Resources Research, Vol. 29, pp. 1935–1950.

41. Epstein V.J. (1987), "Hydrologic and geologic factors affecting land subsidence near Eloy, Arizona", U.S. Geological Survey Water-Resources Investigations Report, 87-4143, 28 p.

42. ESA Radar Courses (2019). Online MOOC course available at https://earth.esa.int/web/guest/missions/esa-operational-eo-missions/ers/instruments/sar/applications/radar-courses/content-2/-/asset_publisher/qIBc6NYRXfnG/content/radar-course-2-synthetic-aperture-radar

43. Ferretti A., Perissin D., Prati C., Rocca F. (2005), "On the physical nature of SAR permanent scatterers", in proceedings of URSI Commission F Symposium on Microwave Remote Sensing of the Earth, Oceans, Ice and Atmosphere, Ispra, Italy.

44. Ferretti A., Prati C. and Rocca F. (2000), "Non-linear subsidence rate estimation using permanent scatterers in differential SAR interferometry", IEEE Transactions on Geoscience and Remote Sensing, Vol.38, No. 5, pp-2202-2212.

45. Ferretti A., Prati C. and Rocca F. (2001), "Permanent Scatterers in SAR Interferometry", IEEE Transactions on Geoscience and Remote Sensing, Vol. 39, No. 1, pp-8-20.

46. Figueroa Vega, G. E. (1977), "Subsidence of the city of Mexico: a historical review", International Association of Hydrological Sciences, publication no. 121, pp. 35-38.

47. Finol A.S., Sancevic Z.A. (1995), "Subsidence in Venezuela", Developments in Petroleum Science, Chapter 7, Vol. 41, Pages 337-372.

48. Franceschetti, G. and Lanari, R. (1999), "Synthetic Aperture Radar Processing," CRS Press, New York, USA, pp.1-284.

49. Fruneau B., and Sarti F. (2000), "Detection of ground subsidence in the city of Paris using radar interferometry: isolation from atmospheric artefacts using correlation", Geophysical Research Letters, Vol. 27, Issue 24, pp-3981-3984.

50. Fryar A.E and Mukherjee A. (2019), "Groundwater Hydrology", in Reference Module in Earth Systems and Environmental Sciences.

51. Fuhrmann T., Cuenca M.C., Knöpfler A., Leijen F.J.V., Mayer M., Westerhaus M., Hanssen R.F. and Heck B. (2015), "Estimation of small surface displacements in the Upper Rhine Graben area from a combined analysis of PS-InSAR, levelling and GNSS data", Geophysical Journal International, Vol. 203, Issue 1, pp. 614–631.

52. Fuhrmann T. and Garthwaite M.C. (2019), "Resolving Three-Dimensional Surface Motion with InSAR: Constraints from Multi-Geometry Data Fusion", Remote Sensing, Vol. 11, Issue 2, 241, 21 p.

53. Gabriel A.K., Goldstein R.M., Zebker H.A. (1989), "Mapping small elevation changes over large areas: differential radar interferometry", Journal of Geophysical Research, Vo. 94, Issue B7, pp. 9183-9191.

54. Gabrysch R. K. (1984), "Ground-water withdrawals and land surface subsidence in the Houston Galveston region, Texas",1906-90, Texas Department of Water Resources, Report 287,64 p.

55. Galloway D. L., Hudnut K. W., Ingebritsen S. E., Phillips S. P., Peltzer G., Rogez F. (1998), "Detection of aquifer system compaction and land subsidence using interferometric synthetic aperture radar, Antelope Valley, Mojave Desert, California". Water Resources Research, Vol. 34, No. 10, pp-2573-2583.

56. Galloway D.L., Jones D.R. and Ingebritsen S.E. (1999), "Land subsidence in the United States", U.S. Geological Survey Circular 1182, Reston, VA, USA, 175 p., http://pubs.usgs.gov/circ/circ1182/

57. Galloway D.L. and Burbey T.J. (2011), "Review: Regional land subsidence accompanying groundwater extraction", Hydrogeology Journal, Vol. 19, pp.1459–1486.

58. Galloway D.L., Erkens G., Kuniansky E.L. and Rowland J.C. (2016), "Preface: land subsidence processes", Hydrogeology Journal, Vol. 24, pp. 547–550.

59. Gambolati G., P. Gatto, and G. Ricceri (1986). Land subsidence due to gas-oil removal in layered anisotropic soils by finite element model", in proceedings of the Third International Symposium on Land Subsidence Held at Venice, March 1984, IAHS Publ., 151, pp.29– 41.

60. Ganguly M. (2011), "Groundwater withdrawal and land subsidence: A study of Singur Block, West Bengal, India", International Journal of Geomatics and Geosciences, Vol. 2, Issue 2, pp. 465-470.

61. Gao M., Gong H., Li X., Chen B., Zhou C., Shi M., Guo L., Chen Z., Ni Z. and Duan G. (2019), "Land Subsidence and Ground Fissures in Beijing Capital International Airport (BCIA): Evidence from Quasi-PS InSAR Analysis", Remote Sensing, Vol. 11, issue 12, 1466, p. 17.

62. Ge S. and Gorelick S.M. (2015), "Groundwater and Surface Water", Encyclopedia of Atmospheric Sciences", 2nd Edition, Vol. 3, pp.209-216.

63. Ge L., Chang H.C and Rizos C. (2007), "Mine subsidence monitoring using multi-source satellite SAR images", Photogrammetric Engineering and Remote Sensing, Vol. 73, Issue 3, pp. 259-266.

64. Gilbert R.O. (1987), "Statistical Methods for Environmental Pollution Monitoring", Wiley, NY.

65. Gloe C. S. (1984), "Case History No. 9.1. Latrobe Valley, Victoria" in UNESCO Guidebook to studies of land subsidence due to Groundwater withdrawal.

http://wwwrcamnl.wr.usgs.gov/rgws/Unesco/PDF-Chapters/Chapter9-1.pdf

66. Goldstein R. (1995), "Atmospheric limitations to repeat-track radar interferometry", Geophysical Research Letters, Vol. 22, Issue 18, pp. 2517–2520.

67. Goldstein R.M., H. Engelhardt, B. Kamb and R.M. Frolich (1993), "Satellite radar interferometry for monitoring ice sheet motion: application to an

Antarctic ice stream", Science, Vol. 262, Issue 5139, pp.1525–1530.

68. Groundwater brochure Kachchh District, CGWB Report (2013). http://cgwb.gov.in/District_Profile/Gujarat/Kachchh.pdf

69. Gujarat State Environmental Information System (ENVIS) report [n.d.] http://www.gujenvis.nic.in/PDF/demo.pdf

70. Gupta A., Asopa U. and Bhattacharjee R. (2019), "Land Subsidence Monitoring in Jagadhri City Using Sentinel 1 Data and DInSAR Processing", 2nd International Electronic Conference on Geosciences, Vol. 2.

71. Hanssen R. F. (2001), "Radar Interferometry: Data Interpretation and Error Analysis", Vol. 2, Springer Science & Business Media.

72. Hanssen R.F. (2002), "Radar Interferometry", Kluwer Academic Publisher, New York.

73. Hanssen, R.F. (2005), "Satellite radar interferometry for deformation monitoring: a priori assessment of feasibility and accuracy", International Journal of Applied Earth Observation and Geoinformation, Vol. 6, pp. 253–260.

74. Hasan S.Z., Farooqui M. Y., Rao P.H., Ramachandran K., Tripathy P., Harinarayana T., (2013), "Petroliferous Basins and Shale Gas - An Unconventional Hydrocarbon Asset of India", Geosciences, Vol. 3, Issue 4, pp.108-118.

75. Helm D. C. (1994), "Horizontal aquifer movement in a Theis-Thiem confined system", Water Resources Research, Vol. 30, Issue 4, pp.953–964.

76. Helsel D.R and Hirsch R.M. (1992), "Statistical Methods in Water Resources," Elsevier Science, Vol.49, 1st edition, 546 p.

77. Hermansen H., Landa H.A., Sylte J.E. and Thomas L.K. (2000), "Experiences after 10 years of waterflooding the Ekofisk Field, Norway". Journal of Petroleum Science and Engineering, Vol. 26, pp. 11–18.

78. Hoffmann J. (2003), "The application of satellite radar interferometry to the study of land subsidence over developed aquifer systems", PhD thesis submitted to the department of geophysics and the committee on graduate studies of Stanford university. https://web.stanford.edu/group/radar/people/jhoffmann_2003small.pdf

79. Hooper A. (2008), "A multi-temporal InSAR method incorporating both persistent scatterer and small baseline approaches", Geophysical Research Letters, Vol. 35, Issue 16, 5 p.

80. Hooper A., Zebker H.A. (2007), "Phase unwrapping in three dimensions with application to InSAR time series", Journal of the Optical Society of America A., Optics, Image science and Vision, 24 (9), pp. 2737-2747.

81. Hu R.L., Yue Z.Q., Wang L.C. and Wang S.J. (2004), "Review on current status and challenging issues of land subsidence in China", Engineering Geology, Vol. 76, Issue 1-2, pp. 65-77.

82. Huang B., Shu L. and Yang Y. S. (2012), "Groundwater Overexploitation Causing Land Subsidence: Hazard Risk Assessment Using Field Observation and Spatial Modelling", Water Resources Management, Vol. 26, pp. 4225-4239.

83. Hung W., Hwang C., Liou J., Lin Y. and Yang H. (2012), "Modeling aquifer-system compaction and predicting land subsidence in central Taiwan", Engineering Geology, Vol. 147-148, pp. 78-90.

84. Hydrogeological Atlas of Rajasthan, Sabarmati River Basin (2013). https://phedwater.rajasthan.gov.in/content/dam/doitassets/water/Ground%2 0Water/Pdf/PublicReports/Groundwater_Atlas/Basinwise/Sabarmati%20Ri ver%20Basin.pdf

85. Jacob C.E. (1940), "On the flow of water in an elastic artesian aquifer". Transactions American Geophysical Union, Vol. 21, Issue 2, pp. 574–586.

86. Jacques W.D. (1999), "The handbook of groundwater engineering", CRC Press LLC, Indiana, USA.

87. Jain R.C., Shukla U.Z. and Bertone F. (2019), "Groundwater capacity beneath the Sabarmati river basin in Gujarat: an overexploited alluvial basin in Western India," Preprint submitted to Hydrogeology Journal October 5, 2019.

88. Wu J., Zhang L., Chen J. and Li T. (2012), "Monitoring ground subsidence in Shanghai maglev area using two kinds of SAR data", Journal of Applied Geodesy, Vol. 6, Issue 3-4, pp. 209-213.

89. Kadiyan N., Chatterjee R.S., Pranjal P., Agrawal P., Jain S. K., Angurala M. L., Biyani A. K., Sati M. S., Kumar D., Bhardwaj A. and Champati Ray P.

K. (2021), "Assessment of groundwater depletion–induced land subsidence and characterisation of damaging cracks on houses: a case study in Mohali-Chandigarh area, India", Bulletin of Engineering Geology and the Environment, Vol. 80, Issue 4, pp. 3217-3231.

90. Kendall M. G. (1975), "Rank Correlation Methods", 4th edition, Charles Griffin, London.

91. Khan, R., Li H., Afzal Z., Basir M., Arif M. and Hassan W. (2021), "Monitoring Subsidence in Urban Area by PSInSAR: A Case Study of Abbottabad City, Northern Pakistan", Remote Sensing, Vol. 13, Issue 9, p. 1651.

92. Khatri A., Chauhan P., Rao P.L.S, Rao P.H. (2015), "Hydrocarbon Prospectivity of Indian Sedimentary Basins-A Review", International Journal of Scientific Research, Vol. 4, Issue 2, pp. 82-86.

93. Khilyuk L.F., Chilingar G.V, J.O. Robertson Jr. and Endres B. (2000), "Interrelationships among Subsidence, Gas Migration, and Seismic Activity", in Gas Migration-Events Preceding Earthquakes, Chapter 21, pp. 309-313.

94. Khorrami M., Abrishami S., Maghsoudi Y., Alizadeh B. and Perissin D. (2020), "Extreme subsidence in a populated city (Mashhad) detected by PSInSAR considering groundwater withdrawal and geotechnical properties", Scientific Reports 10, Article No. 11357, 16 p.

95. Kocsis T, Kovács-Székely I and Anda A. (2017), "Comparison of parametric and non-parametric time-series analysis methods on a long-term meteorological data set", Central European Geology, Vol. 60, pp.316–332.

96. Krishnan P.V.S and Kim D.J (2018), "Subsidence Due to Groundwater Withdrawal in Kathmandu Basin Detected by Time-series PS-InSAR Analysis", Korean Journal of Remote Sensing, Vol. 34, No.4, pp.703-708.

97. Kumar N., Panchal C. C., Chandrawanshi S. K. and Thanki J. D. (2017), "Analysis of rainfall by using Mann-Kendall trend, Sen's slope and variability at five districts of south Gujarat, India", Mausam, Vol. 68(2), pp. 205-222.

98. Kumar M. D. (1995), "Over-exploitation and Approaches to Management: An Overview of Groundwater in Gujarat, Western India", Paper presented at

the 3rd South Asian NGO Summit, Kathmandu, Nepal, February 21-23.

99. Laurent F.F and Pottier E., (2016), "Microwave Remote Sensing of Land Surface, Techniques and Methods", ISTE Press Ltd. Published by Elsevier, pp.1-65.

100. Leake S.A. (2004), "Land subsidence from groundwater pumping", U.S. Geological Survey, USA. Available online at: http://geochange.er.usgs.gov/sw/changes/anthropogenic/subside/

101. Leal J. (1989), "Integration of GPS and Levelling in Subsidence Monitoring Studies at the Costa Bolivar Oil Fields". M.Sc. Thesis, Department of Surveying Engineering, University of New Brunswick, Fredericton, N.B.

102. Lohman S.W. (1961), "Compression of elastic artesian aquifers", in Short papers in the geologic and hydrologic sciences, U.S. Geol. Survey professional paper 424-B, pp. B47-B49.

103. M. N. Mayuga and D. R. Allen. (1969), "Subsidence in the Wilmington Oil Field, Long Beach, California, USA," Proceedings of the Tokyo Symposium on Land Subsidence, International Association of Scientific Hydrology, Gentbrugge, IASH-UNESCO, Paris, Vol. 1, No. 88, pp. 66-79.

104. Mair A. and Fares A. (2010), "Influence of groundwater pumping and rainfall spatio-temporal variation on streamflow", Journal of Hydrology, Vol. 393, Issue 3–4, Pages 287–308.

105. Malik K., Kumar D. and Perissin D. (2018), "Assessment of subsidence in Delhi NCR due to groundwater depletion using TerraSAR-X and persistent scatterers interferometry", The Imaging Science Journal, Vol. 67, Issue 1, pp. 1-7.

106. Mann H.B. (1945), "Nonparametric tests against trend", Econometrica, Vol. 13, pp. 245–259.

107. Marie-Pierre D., L.Q. Penelope, Tupin F., Briole P. and Nicolas J.M. (2009), "Time series analysis of Mexico City subsidence constrained by radar interferometry", Journal of Applied Geophysics, Vol. 69, Issue 1, pp. 1-15.

108. Martínez P. J., Hernandez-Marín M., Burbey T.J., González-Cervantes N., Ortíz-Lozano J.A., Zermeño-De-Leon M.E. and Solís-Pinto A. (2013), "Land subsidence and ground failure associated to groundwater exploitation in the Aguascalientes Valley, México", Engineering Geology, Vol. 164, pp. 172-186.

109. Massonnet D. and Feigl, K.L. (1998), "Radar interferometry and its application to changes in the earth's surface", Reviews of Geophysics, Vol. 36, pp. 441–500.

110. Maureen Feineman, Lecture Notes, Pennsylvania State University, https://www.e-education.psu.edu/earth111/node/931

111. Mora O., Mallorqui J.J. and Broquetas A. (2003), "Linear and nonlinear terrain deformation maps from a reduced set of interferometric SAR images", IEEE Transactions on Geoscience and Remote Sensing, Vol. 41, Issue 10, pp. 2243-2253.

112. Motagh M., Walter T.R., Sharifi M.A., Fielding E., Schenk, A., Anderssohn J. and Zschau J. (2008), "Land subsidence in Iran caused by widespread water reservoir overexploitation", Geophysical Research Letters, Vol. 35, Issue 16, 5 p.

113. Mukherjee P., Singh C.K. and Mukherjee S. (2012), "Delineation of Groundwater Potential Zones in Arid Region of India—A Remote Sensing and GIS Approach", Water Resources Management, Vol. 26, pp. 2643–2672.

114. Murthy V.N.S. (2002), "Geotechnical engineering: principles and practices of soil mechanics and foundation engineering", Marcel Dekker Inc., New York.

115. Narjary B., Kumar S., Kamra S. K., Bundela D. S. and Sharma D. K. (2014), "Impact of rainfall variability on groundwater resources and opportunities of artificial recharge structure to reduce its exploitation in fresh groundwater zones of Haryana", Current Science, Vol. 107, Issue 8, pp. 1305-1312.

116. NASA, 2019. https://www.nasa.gov/topics/earth/features/india_water.html

117. Okuyan M. N. (2000), "Modelling Land Subsidence Due to Groundwater Pumping/Re charging in the Las Vegas Valley", Master's Thesis, Department of Civil and Environmental Engineering, University of Nevada, Las Vegas.

118. Othman A. and Abotalib A.Z. (2019), " Land subsidence triggered by groundwater withdrawal under hyper-arid conditions: case study from Central Saudi Arabia", Vol. 78, Issue 7, 243, 8 p.

119. Pai D.S., Sridhar L., Rajeevan M., Sreejith O.P., Satbhai N.S. and Mukhopadhyay B. (2014), "Development of a new high spatial resolution

(0.25° X 0.25°) Long period (1901-2010) daily gridded rainfall data set over India and its comparison with existing data sets over the region", Mausam, Vol. 65, (1), pp1-18.

120. Panda D. K., Mishra A. and Kumar A. (2012), "Quantification of trends in groundwater levels of Gujarat in western India", Hydrological Sciences Journal, Vol.57, Issue 7, pp.1325-1336.

121. Pathak A.A and Dodamani B.M. (2019), "Trend Analysis of Groundwater Levels and Assessment of Regional Groundwater Drought: Ghataprabha River Basin, India", Natural Resources Research, Vol. 28 (3), pp.631–643.

122. Patle G.T., Singh D.K., Sarangi A., Rai Anil, Khanna Manoj and Sahoo R.N. (2015), "Time Series Analysis of Groundwater Levels and Projection of Future Trend", Journal of Geological Society of India, Vol. 85(2), pp. 232-242.

123. Pepe A. and Calo F. (2017), "A review of interferometric synthetic aperture RADAR (InSAR) multi-track approaches for the retrieval of Earth's surface displacements", Applied Sciences, Vol. 7, Issue 12, 39 p.

124. Phien-wej, N., Giao, P.H. and Nutalaya, P. (2006), "Land subsidence in Bangkok, Thailand", Engineering Geology, Vol. 82, pp.187-201.

125. Poland J. F. and B. E. Lofgren (1984), "Case History no. 9.13, San Joaquin valley, California, U.S.A.", in Guidebook to Studies of Land Subsidence Due to Groundwater Withdrawal, UNESCO, Paris, edited by J. F. Poland, pp. 263–277.

126. Poland J.F. and Davis G.H. (1969), "Land subsidence due to withdrawal of fluids", Reviews in Engineering Geology, Vol. II, edited by D.J. Varnes and Kiersch, G., Geological Society of America, pp. 187-269.

127. Poland J.F., Lofgren B.E., and Riley F.S. (1972), "Glossary of selected terms useful in studies of the mechanics of aquifer systems and land subsidence due to fluid withdrawal", U.S. Geological Survey Water-Supply Paper 2025.

128. Pratt W. E. and Johnson D. W. (1926), "Local subsidence of the Goose Creek oil field", Journal of Geology, XXXIV (7), Part 1, pp. 577–590.

129. Quanlong W. (2006), "Land subsidence and water management in Shanghai", Unpublished Master's thesis, TU Delft, Delft, the Netherlands.

130. Lanari R., Zeni G., Manunta M., Guarino S., Berardino P. and Sansosti E.

(2004), "An integrated SAR/GIS approach for investigating urban deformation phenomena: a case study of the city of Naples, Italy", International Journal of Remote Sensing, Vol. 25, Issue 14, pp. 2855-2867.

131. Liang H., Xu W., Ding X., Zhang L. and Wu S. (2021), "Urban Sensing with Spaceborne Interferometric Synthetic Aperture Radar", In: Shi W., Goodchild M.F., Batty M., Kwan MP., Zhang A. (eds), Urban Informatics. The Urban Book Series, Springer, Singapore.

132. Rajan N.M and Rajalakshmy P. (2014), "Estimation of Sensor Temperature Drift using Kalman Filter", International Journal of Engineering Research and Technology, Vol. 3, Issue 2, pp. 658-662.

133. Raucoules D., Colesanti C., and Carnec C. (2007), "Use of SAR interferometry for detecting and assessing ground subsidence", Comptes Rendus Geosciences, Vol. 339, Issue 5, pp. 289–302.

134. Raucoules D., Cozannet G.L., Woppelmann G., Michele M.D., Gravelle M., Daag A. and Marcos M. (2013), "High nonlinear urban ground motion in Manila (Philippines) from 1993 to 2010 observed by DIn-SAR: Implications for sea-level measurement", Remote Sensing of Environment, Vol. 139, pp. 386–397.

135. Renato G. and Zandaryaa S. (1998), "Environmental Engineering and Renewable Energy" 1st Edition, Elsevier Science Ltd.

136. Ribeiro L., Kretschmer N., Nascimento J., Buxo A., Rötting T., Soto G., Señoret M., Oyarzún J., Maturana H.and Oyarzún R. (2015), "Evaluating piezometric trends using the Mann-Kendall test on the alluvial aquifers of the Elqui River basin, Chile", Hydrological Sciences Journal, Vol. 60, Issue 10, pp. 1840-1852.

137. Rivard C., Vigneault H. and Pigott A.R. (2009), "Groundwater recharge trends in Canada", Canadian Journal of Earth Science, Vol. 46(11), pp. 841-854.

138. Rodriguez E. and Martin J.M. (1992), "Theory and design of interferometric synthetic aperture radars", IEE Proceedings F: Radar and Signal Processing, Vol.139, No. 2, pp. 147-159.

139. Rojas D.S, Cano E.C., Espriu A.H., Wdowinski S., DeMets C., Tlaczani L.S., Falorni G. and Bohane A. (2015), "Relation between terrane subsidence

InSAR-GPS and depression of the static level in Wells of the Mexico City metropolitan area", Boletín de la Sociedad Geológica Mexicana, Vol. 67, No. 2, pp. 273-283.

140. Rosen P., Hensley S., Joughin I., Li F., Madsen S.N., Rodriguez E. and Goldstein R. (2000), "Synthetic Aperture Radar Interferometry". Proceedings of the IEEE, Vol. 88, No. 3, pp. 333–382.

141. Saha D. and Ray R.K. (2019), "Groundwater Resources of India: Potential, Challenges and Management". Chapter 2, in Groundwater Development and Management. Springer, Cham., Editors Sikdar P.K., pp.19-42.

142. Sahu P. and Sikdar P. K. (2011), "Threat of land subsidence in and around Kolkata City and East Kolkata Wetlands, West Bengal, India" Journal of Earth System Science, Vol. 120 (3), pp. 435-446.

143. Scheiber R. and Moreira A. (2000), "Coregistration of Interferometric SAR Images Using Spectral Diversity", IEEE Transactions on Geoscience and Remote Sensing, Vol. 38(5), pp. 2179-2191.

144. Sefercik U. G. and Dana, I. (2011), "Crucial Points of Interferometric Processing for Dem Generation Using High Resolution Sar Data", International Archives of the Photogrammetry, Remote Sensing and Spatial Information Sciences, Vol. XXXVIII-4/W19, ISPRS Hannover Workshop.

145. Sen P. K. (1968), "Estimates of the regression coefficient based on Kendall's tau", Journal of the American Statistical Association, Vol. 63, pp.1379-1389.

146. Shahzad N., Ding X., Wu S. and Liang H. (2020), "Ground Deformation and Its Causes in Abbottabad City, Pakistan from Sentinel-1A Data and MT-InSAR", Remote Sensing, Vol. 12, Issue 20. 3442, 18 p.

147. Sikdar P.K., Biswas A.B. and Saha A.K. (1996), "A study on the possible land subsidence in Calcutta and Howrah cities due to groundwater overdraft", Indian Journal of Geology, Vol. 68(3) pp.193-200.

148. Sinha A. K (2014), "District groundwater brochure Mehsana district, Gujarat", Central ground water board, Ahmedabad. http://cgwb.gov.in/District_Profile/Gujarat/Mehsana.pdf

149. Stasik R., Korytowski M. and Liberacki D. (2016), "Trends in groundwater level changes in small forest catchments of Wielkopolska", Journal of Ecological Engineering, Vol. 17(4), pp.99–106.

150. Strozzi T., Wegmüller U., Tosi L., Bitelli G. and Spreckels V. (2001), "Land subsidence monitoring with differential SAR interferometry", Photogrammetric Engineering and Remote Sensing, Vol. 67, Issue 11, pp.1261-1270.

151. Subir Das, Singh H., Tiwari D. and Parulkar S.N. (2006), "Reservoir Classification and Geological Remodeling of Kalol Sands of Sobhasan Complex, North Cambay Basin, India", 6th International Conference & Exposition on Petroleum Geophysics, Kolkata, pp. 1062-1070. Available at https://spgindia.org/conference/6thconf_kolkata06/044.pdf

152. Suganthi S and Elango L. (2020), "Estimation of groundwater abstraction induced land subsidence by SBAS technique", Journal of Earth System Science, Vol. 129, Article No. 46, 13 p.

153. Suganthi S., Elango L. and Subramanian S. K. (2017), "Microwave D-InSAR technique for assessment of land subsidence in Kolkata City, India", Arabian Journal of Geosciences, Vol.10, Article No. 458, 10 p.

154. Sun H., Grandstaff D.E. and Shagam R. (1999), "Land subsidence due to groundwater withdrawal: potential damage of subsidence and sea level rise in southern New Jersey, USA", Environmental Geology, Vol. 37 (4), pp-290-296.

155. Tabari H., Nikbakht J. and Shifteh Some'e B. (2012), "Investigation of groundwater level fluctuations in the north of Iran", Environmental Earth Sciences, Vol. 66(1), pp.231–243.

156. Teatini P., Tosi L., Strozzi T., Carbognim L., Wegmuller U. and Rizzetto F. (2005), "Mapping regional land displacements in the Venice coastland by an integrated monitoring system", Remote Sensing of Environment, Vol. 98, Issue 4, pp. 403-413.

157. Teatini P., Tosi L. and Strozzi T. (2011), "Quantitative evidence that compaction of Holocene sediments drives the present land subsidence of the Po Delta, Italy", Journal of Geophysical Research, Vol. 116, Issue B8, doi:10.1029/2010JB008122.

158. Terzaghi K. (1925), "Principles of Soil Mechanics: I—Phenomena of Cohesion of Clay"s, Engineering News-Record, Vol. 95, No. 19, pp. 742-746.

159. Tiwari D., Sathe S., Kaushik K.C., Bhattacharya R.N. (2011), "Exploitation Strategy for BCS Sands in Sobhasan Complex, Mehsana, Gujarat, India", The 2nd south Asian Geoscience Conference and Exhibition, GEOIndia. Available online at https://apgindia.org/document/643.pdf

160. Tobler W. (1970), "A computer movie simulating urban growth in the Detroit region", Economic Geography, Vol. 46(2), pp.234-240.

161. Todd, D.K. and Mays L.W. (2005), "Groundwater Hydrology", Third Edition, John Wiley & Sons, Inc., New York.

162. Tripathi A. and Tiwari R.K (2019), "Spaceborne C-band DInSAR based urban subsidence mapping of Chandigarh area", Conference paper, 1st International Conference on Urban and Regional Planning, Bangladesh Institute of Planners.

163. Tripathi A., Maithani S., and Kumar S. (2018), "X-band persistent SAR interferometry for surface subsidence detection in Rudrapur City, India" Proc. SPIE 10793, Remote Sensing Technologies and Applications in Urban Environments III, 107930O, doi: 10.1117/12.2326267.

164. Tziachris P., Metaxa E., Papadopoulos F. and Papadopoulou M. (2017), "Spatial Modelling and Prediction Assessment of Soil Iron Using Kriging Interpolation with pH as Auxiliary Information", International Journal of Geo-Information, Vol. 6, Issue 9, 283.

165. UmaMageswari A., Ignatious J.J., Vinodha R. (2012), "A Comparative Study of Kalman Filter, Extended Kalman Filter And Unscented Kalman Filter For Harmonic Analysis Of The Non-Stationary Signals", International Journal of Scientific & Engineering Research, Vol. 3, Issue 7, 9 p.

166. Usai S (2001), "A new approach for long term monitoring of deformations by differential SAR interferometry", Doctor's Thesis, Delft University of Technology, Netherlands.

167. V.B.H Ketelaar (2009), "Subsidence Due to Hydrocarbon Production in the Netherlands," In: Satellite Radar Interferometry: Subsidence Monitoring Techniques, Springer, London, pp. 7-27. doi:10.1007/978-1-4020-9428-6_2.

168. Wei M. and Sandwell D.T. (2010), "Decorrelation of L-Band and C-Band Interferometry Over Vegetated Areas in California", IEEE Transactions on Geoscience and Remote Sensing, Vol. 48, Issue 7, pp. 2942 – 2952.

169. White W.A. and Morton R.A. (1997), "Wetland losses related to fault movement and hydrocarbon production, South eastern Texas Coast", Journal of Coastal research, Vol. 13, No. 4, pp.1305–1320.

170. White W. A., Calnan T.R., Morton R.A., Kimble R.S., Littleton T.G., McGowen J.H., Nance H.S. and Schmedes K.E. (1985), "Submerged Lands of Texas, Galveston-Houston Area: Sediments, Geochemistry, Benthic Macroinvertebrates, and Associated Wetlands", University of Texas, Austin, Bureau of Economic Geology, SL0005, 145 p.

171. Whittaker B. N. and Reddish D. J. (1989), "Subsidence: Occurrence, Prediction, and Control", In: Developments in Geotechnical engineering, Vol. 56, Elsevier Science, 528 p.

172. William Bleam (2017), "Soil and Environmental Chemistry", Second Edition, Academic Press, pp. 39-85.

173. Woodhouse I.H. (2006), "Introduction to microwave remote sensing", CRC Press, Boca Ranton, USA.

174. Xue Y.Q., Zhang Y., Ye S.J., Wu J.C. and Li Q.F (2005), "Land subsidence in China", Environmental Geology, Vol. 48(6), pp. 713-720.

175. Yastika P.E. and Shimizu N. (2016), "Applications of DInSAR for Ground Surface Deformation Measurements-Case Studies of Subsidence Measurements and Deformation Detections Due to an Earthquake", Conference paper, The 37th West Japan Symposium on Rock Engineering, Available at https://www.researchgate.net/publication/319876190

176. Yue S., Pilon P. and Phinney B. (2003), "Canadian streamflow trend detection: impacts of serial and cross-correlation," Hydrological Sciences Journal, Vol. 48 (1), pp.51–63.

177. Zaman M.M., Abdulraheem A. and Roegiers J.C. (1995), "Reservoir compaction and surface subsidence in the North Sea Ekofisk field", In: Subsidence Due to Fluid Withdrawal, edited by G. V. Chilingarian et al., Elsevier Science, Amsterdam, Netherlands, pp. 373–423.

178. Zcbker H. and R. M. Goldstein (1986), "Topographic mapping from interferometric synthetic aperture radar observations", Journal of Geophysical Research, Vol. 91, Issue B5, pp. 4993-4999.

179. Zebker H. A. and J. Villasenor (1992), "Decorrelation in interferometric

radar echoes", IEEE Transactions on Geoscience and Remote Sensing, Vol. 30, Issue 5, pp. 950-959.

180. Zebker H.A., P.A. Rosen and S. Hensley (1997), "Atmospheric Effects in Interferometric Synthetic Aperture RADAR Surface Deformation and Topographic Maps", Journal of Geophysical Research, Vol. 102, Issue B4, pp. 7547-7563.

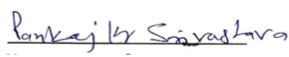181. Zhou X., Chang N.B and Li S. (2009), "Applications of SAR Interferometry in Earth and Environmental Science Research", Sensors, Vol. 9(3), pp.1876–1912.

APPENDICES

APPENDIX 1: THESIS PLAGIARISM CERTIFICATE
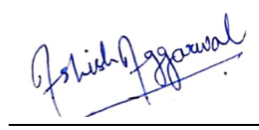
PLAGIARISM CERTIFICATE

1. We **Dr. Pankaj Kumar Srivastava** (Supervisor) and **Dr. Dharmendra Kumar Gupta** (Co-Supervisor) certify that the Thesis titled **"Predictive modelling and Characterization of Land Subsidence due to Groundwater and Petroleum extraction in and around Mehsana, Gujarat"** submitted by Scholar Mr. **Ashish Aggarwal** having SAP ID **500032953** has been run through a Plagiarism Check Software and the Plagiarism Percentage is reported to be ___2%___.

2. Plagiarism Report generated by the Plagiarism Software is attached.

Signature of the Supervisor   **Signature of Co-Supervisor**

Signature of the Scholar

APPENDIX 2: FIRST PAGE OF PLAGIARISM REPORT

UrKUND

Document Information

Analyzed document	Thesis-For Plagiarism Check.pdf (D90577355)
Submitted	12/24/2020 3:54:00 AM
Submitted by	Ashish
Submitter email	aaggarwal@ddn.upes.ac.in
Similarity	2%
Analysis address	aaggarwal.upes@analysis.urkund.com

Sources included in the report

W	URL: https://www.indiascienceandtechnology.gov.in/research/predictive-modelling-and-cha ... Fetched: 12/24/2020 3:55:00 AM	3
W	URL: https://www.researchgate.net/publication/276486005_Land_Subsidence_due_to_groundwa ... Fetched: 11/29/2019 4:28:29 AM	6
W	URL: https://www.usgs.gov/mission-areas/water-resources/science/land-subsidence Fetched: 12/24/2020 3:55:00 AM	1
W	URL: https://www.science.gov/topicpages/l/land%2Bsubsidence%2Bresulting Fetched: 11/26/2020 6:11:49 AM	1
W	URL: https://www.researchgate.net/publication/228605254_Detection_of_aquifer_system_com ... Fetched: 10/11/2019 3:20:38 PM	1
W	URL: https://www.researchgate.net/publication/227103174_Monitoring_severe_aquifer-syste ... Fetched: 12/24/2020 3:55:00 AM	3
W	URL: https://www.researchgate.net/publication/226363459_Threat_of_land_subsidence_in_an ... Fetched: 1/31/2020 11:23:25 AM	2
W	URL: https://www.researchgate.net/publication/256699800_Modeling_aquifer-system_compact ... Fetched: 12/24/2020 3:55:00 AM	3
J	**Determining hydrogeological parameters of an aquifer in Sirjan Basin using Envisat ASAR interferometry and groundwater modelling** URL: c50fbb67-18bf-4725-99cb-d37e643a5fce Fetched: 12/11/2019 4:18:48 PM	2
W	URL: https://core.ac.uk/download/pdf/230462951.pdf Fetched: 12/24/2020 3:55:00 AM	1
W	URL: https://www.researchgate.net/publication/235644398_Land_subsidence_induced_by_grou ... Fetched: 11/29/2019 4:27:42 AM	2

1/53

166

Curriculum-Vitae

Ashish Aggarwal, Dept. of Petroleum and Earth Sciences,
University of Petroleum and Earth Sciences, Dehradun

━━━━━━━━━━━━━━━━━━━━━━━

Present Position: Assistant Professor (Selection Grade), Dept. of Petroleum
and Earth Sciences
Address: University of Petroleum and Energy Studies, Bidholi Campus,
Dehradun-248007
Mob: 09557654253
Email: aaggarwal@ddn.upes.ac.in
Date of Birth: February 28, 1978

Educational Qualifications

Degree	Subject	University/Board	Year of Passing
Pursuing PhD		Univ of Petroleum and Energy Studies, Dehradun	
M.Sc Tech (GIS)	GIS, Remote Sensing	Univ of New South Wales, Sydney, Australia	2004
M.Sc(Honors)	Geology	Punjab University	2001
B.Sc.(Honors)	Geology	Punjab University	1999
Intermediate	Science , Biology	HP Board	1995
High School	General Science	CBSE Board	1993

Experience

- Assistant Professor (Selection Grade), UPES Dehradun

  (Jan 2017 - Present)

- Assistant Professor (Senior Scale), UPES Dehradun

  (July 2013 - Jan 2017)

- GIS Consultancy, Bengaluru

  (Aug 2009 - June 2013)

- GIS Specialist, TAK Services and Assets, Amman, Jordan

  (July 2008 - July 2009)

- SAP Functional Consultant E-Matrix Technologies, Bangalore

  (July 2007 – June 2008)

- Digital Cartographer, Infotech Enterprises Ltd., Noida

  (Nov. 2005 - July 2006)

- GIS Engineer, RMSI Pvt. Limited, Noida

(Mar. 2005 - Nov. 2005)

- GIS Project Trainee, Systems Research Institute, Pune

(Oct. 2004 – Mar. 2005)

Research Interests:

Spatial modelling in GIS for user-specific applications, Urban change detection, Land use and land cover mapping, and Natural hazard analysis and mitigation. My current research activity is based on Radar remote sensing where my work focusses on monitoring and characterization of Land Subsidence due to Groundwater Depletion and Petroleum Extraction in and around Mehsana, Gujarat.

Awards/Recognition:

Qualified GRE, TOEFL & IELTS for admission to M.Tech program at University of New South Wales, Sydney, Australia

Courses Teaching at UPES:
- Introduction to GeoInformatics
- Photogrammetry , Remote Sensing, GIS and GPS
- GPS and Satellite Navigation Systems
- Applications of GeoInformatics
- Geothermal Science
- GIS Image Processing for Petroleum Industry

Research Projects during M.Tech
- Sensitivity Analysis of Window size for predicting groundwater discharge using FLAG model in Monavale agricultural catchment, New South Wales, Australia.
- Multi Criteria Approach to Construction Site Spatial Analysis in Pulaski County, Missouri, University of Arkansas, Fayetteville, USA.
- Determining appropriate development sites and land use allocation using Multi-Objective Linear Analysis in GIS at the Edith and Joy Foundation, Kioloa, New South Wales, Australia.
- Explicit spatial analysis for serrated tussock (weed) management in New South Wales.
- Mineral Mapping in Cuprite Nevada, USA using Hyperspectral tools.
- Geologic mapping of Ningaloo reef, Western Australia using Hyperspectral tools.
- Determination of the alignment (route) for new railway corridors (extensions) in existing railway routes in Sydney using TRANSCAD.
- GIS database implementation using ARC/INFO and ARCVIEW.

Seminars/Trainings

- 2016 Attended one-month training on Advances in GIS conducted by National Remote Sensing Centre, ISRO, India.
- 2014 Attended a two-day workshop on ArcGIS 10.1 by ESRI India, at UPES, Dehradun.
- 2013 Attended a four day "Proficiency Course on Modern Practices in Petroleum Exploration" organized by Petrotech chapter, at ONGC Dehradun.
- 2006 Gave a presentation on Multi Criteria Approach to Construction Site Spatial Analysis in Pulaski County, Missouri; University of Arkansas, Fayetteville.
- 2004 Gave a presentation on Use of Hyperspectral Remote sensing for mineral mapping at Ningaloo Reef, Western Australia; University of New South Wales, Sydney.
- 2003 Gave a Presentation on Mineral Mapping in Cuprite, Mining district, Nevada, U.S.A, using Hyperspectral tools, University of New South Wales, Sydney.
- 2001 Presented the seminar on Petroleum Geology at Panjab University Geology Department.
- 2001 Attended three weeks Field Training at Jaipur, Jodhpur, Degana, Jaisalmer & Bikaner.
- 2000 Attended three weeks Field Training at Pune, Gokak, Goa.
- 2000 Attended a Field Workshop of Krol-Tal formation at Mussourie.
- 1999 Presented seminar on Geomagnetism & Its Role in Mineral Exploration at Geology department, Punjab University.
- 1999 Attended three weeks Field Training at Jaipur, Udaipur, Zawar Mines, Jodhpur & Mt. Abu.
- 1998 Presented the seminar on reasons of Earthquake of India in Geology department, Punjab University, Chandigarh
- 1998 Attended two weeks Field Training of Subathu, Solan, Dharampur, Saketri.

APPENDIX 4: LIST OF PUBLICATIONS

1.   **Aggarwal Ashish**, Srivastava P.K., Tiwari Aman, Chatterjee R.S. and Gupta D.K., "ArcSwat based Geospatial modeling of Rainfall-runoff processes in Rupen basin, Mehsana district, Gujarat", *Disaster Advances*, Vol. 12(10), October 2019.

2.   **Aggarwal Ashish**, Srivastava P.K., Gupta D.K., Chatterjee R.S. , " GIS based Statistical Analysis of Seasonal Groundwater Trends and Rainfall Correlations in Kutch-Sabarmati Basin, Gujarat, India", *Test Engineering and Management*, Vol. 83, June 2020, pp. 23709-23719.

3.   **Aggarwal Ashish**, Srivastava P.K., Gupta D.K., Chatterjee R.S., "Estimating Regional Land Subsidence in Mehsana Urban Block, Gujarat: Effect of Groundwater Induced Aquifer Compaction", Paper under Review in *Materials Today: Proceedings*, Manuscript Number: MATPR-D-21-03195, Article Type:SCPINM-2021.